(NASA-CR-135211) SMALL, HIGH-PRESSURE LIQUID OXYGEN TURBOPUMP Interim Report, Aug. 1973 - Apr. 1976 (Rocketdyne) 289 p HC A13/MF A01 CSCL 13K

N77-27403

Unclas
G3/37 36843

NASA CR-135211
R76-178

INTERIM REPORT

SMALL, HIGH-PRESSURE LIQUID OXYGEN TURBOPUMP

by

A. Csomor, and R. Sutton

Rockwell International

Rocketdyne Division

prepared for

NATIONAL AERONAUTICS AND SPACE ADMINISTRATION

NASA-Lewis Research Center

Contract NAS3-17800

R. E. Connelly, Project Manager

1. Report No. NASA CR-135211	2. Government Accession No.	3. Recipient's Catalog No.
4. Title and Subtitle SMALL, HIGH-PRESSURE, LIQUID OXYGEN TURBOPUMP INTERIM REPORT		5. Report Date July 1977
		6. Performing Organization Code
7. Author(s) A. Csomor and R. Sutton		8. Performing Organization Report No. R76-178
		10. Work Unit No.
9. Performing Organization Name and Address Rocketdyne Division of Rockwell International, 6633 Canoga Avenue, Canoga Park, California 91304		11. Contract or Grant No. NAS3-17800
		13. Type of Report and Period Covered Interim (August 1973 - April 1976)
12. Sponsoring Agency Name and Address National Aeronautics and Space Administration, Washington, D.C. 20546		14. Sponsoring Agency Code
15. Supplementary Notes Project Manager, R. E. Connelly, NASA-Lewis Research Center, Cleveland, Ohio 44135		

16. Abstract

A small, high-pressure, liquid oxygen turbopump was designed, fabricated, and tested. The pump was of a single-stage, centrifugal type; power to the pump was supplied by a single-stage, partial-emission, axial-impulse turbine. Design conditions included an operating speed of 70,000 rpm, pump discharge pressure of 2977 N/cm^2 (4318 psia), and a pump flowrate of 16.4 kg/s (36.21 lb/sec). The turbine was propelled by LO_2/LH_2 combustion products at 1041 K (1874 R) inlet temperature, and at a design pressure ratio of 1.424. The approaches used in the detail analysis and design of the turbopump are described, and fabrication methods are discussed. Data obtained from gas generator tests, turbine performance calibration, and turbopump testing are presented.

17. Key Words (Suggested by Author(s))	18. Distribution Statement
Turbopump Centrifugal pump Partial-emission turbine Gas generator	

19. Security Classif. (of this report)	20. Security Classif. (of this page)	21. No. of Pages	22. Price*
Unclassified	Unclassified	300	

* For sale by the National Technical Information Service, Springfield, Virginia 22151

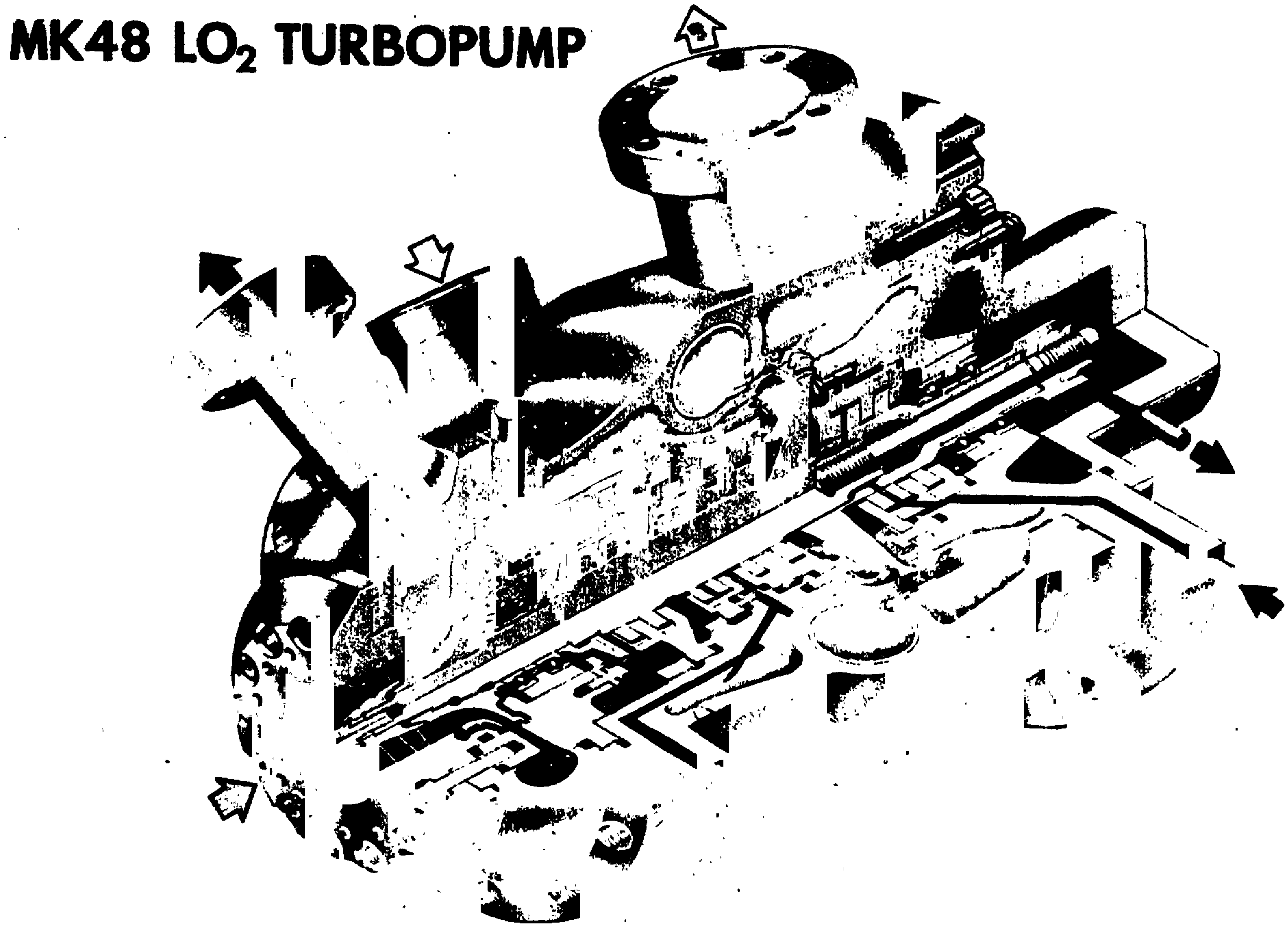

Mark 48-0 LO_2 Turbopump

FOREWORD

The work herein was conducted by the Advanced and Propulsion Engineering and the Engineering Test personnel of Rocketdyne, a division of Rockwell International, under Contract NAS3-17800 from August 1973 to April 1976. Mr. R. Connelly, Lewis Research Center, was NASA Project Manager. At Rocketdyne, Mr. H. Diem as Program Manager, Mr. A. Zachary as Rocketdyne Project Manager, and Mr. A. Csomor as Project Engineer were responsible for the technical direction of the program.

Important contributions to the conduct of the program and to the preparation of this report were made by the following persons:

Turbomachinery:	Dr. E. D. Jackson
Turbomachinery:	S. B. Macaluso
Stress:	F. P. Nitz
Consultant:	Dr. K. Rothe

CONTENTS

ILLUSTRATIONS

TABLES

SUMMARY

The objective of this program was to establish the technology for small, high-pressure liquid oxygen (LOX) pumping capability. Turbopumps in this category are needed for applications in small, high-performance, reusable, versatile, staged-combustion rocket engines. To accomplish this objective, analysis and design effort was expended to produce specifications and shop drawings in sufficient detail to permit fabrication of test hardware.

To obtain high performance and minimize weight, the rotor speed was established at 7330 rad/s (70,000 rpm). The pump design included a single-stage centrifugal impeller preceded by an axial-flow inducer to reduce the net positive suction head (NPSH) requirements. Rotor axial thrust control was provided by incorporating a self-compensating, double-acting balance piston as an integral part of the impeller rear shroud. Power for the pump was developed by a single-stage, partial-admission turbine using the combustion products of liquid hydrogen (LH_2) and LOX as the propellant. The rotor was supported on two ball bearings at each end. The pump end bearings were cooled by recirculating LOX. The turbine end bearings, located outboard of the turbine disk to provide auxiliary power takeoff capability, were cooled by LH_2. Controlled gap seals were used to accomplish sealing along the rotor.

Hardware was fabricated for two complete turbopump assemblies. To provide a hot-gas source for the turbine, a gas generator was designed, fabricated, and tested.

The turbine was calibrated at Wyle Laboratories with gaseous nitrogen as the driving fluid and a torquemeter was used to measure output. The turbine efficiency was measured at 51%, 9% below the predicted value at the design point.

The turbopump assembly was tested at Lima stand of Rocketdyne's Propulsion Research Area (PRA). Eighteen tests were conducted on one turbopump assembly, with LOX as the pump fluid on all but three tests. (Liquid nitrogen (LN_2) was initially used to verify integrity.) The turbine was propelled by ambient-temperature gaseous hydrogen on seven tests, and by hot gas on the remaining tests. Speeds in excess of the design level, up to 7765 rad/s (74,191 rpm) were explored. Pump discharge pressures ranging up to 3175 N/m (4604 psia) were generated with flowrates up to 0.013 m^3/s (193 gpm). The turbine was exposed to a maximum inlet temperature of 1133 C (2040 F).

Analysis of the fluid dynamic performance of the pump revealed a need for additional development effort in the following areas: the data indicated a low suction performance either because the inducer generated insufficient head or because of blockage at the impeller inlet. The diffuser through-flow area was smaller than required for good diffuser performance. Finally, the resistance of the passages for the balance piston return flow was too high, resulting in a reduced balance range for the piston.

To resolve the first problem, a modified inducer configuration or rework of the leading edges of the impeller will be necessary. The diffuser and balance piston deficiencies should be resolved by minor changes to the appropriate hardware.

In terms of the mechanical operation of the turbopump, only two discrepancies were noted. The front bearings were discolored due to overheating, and a section had split off from one ball. It could not be ascertained whether the bearing overheating was caused by high bearing axial loads or by metal damage incurred during operation in LN_2. The other discrepancy was flaking and blistering of the rotor chrome plating under the primary hot-gas seal. Increased radial clearance and improved quality control over the chrome plating process are expected to resolve this problem. The other components of the turbopump were in good condition.

INTRODUCTION

System studies have been conducted to determine the feasibility of developing a reusable vehicle for performing future Air Force and NASA space maneuvering missions. These studies have shown that, over the thrust range of interest, high-pressure, staged-combustion-cycle engines offer the highest specific impulse and payload capability. A review of the vehicle and engine system study results indicates that a single-bell-nozzle, staged-combustion-cycle engine at 88,964 N (20,000 pounds) thrust level is near optimum for the DOD and NASA mission requirements.

This program was initiated to provide the required LOX turbopump technology base for subsequent development of a high-performance, staged-combustion rocket engine.

Technology items of particular interest during the course of this program included establishing the fluid dynamic parameters and design details for a small-capacity, high-pressure LOX pump, and low-pressure-ratio, partial-admission turbine; operation of a balance piston with no axial rubbing features; balance and operation of a high-speed rotor; high DN bearings in LOX; hydrogen-environment embrittlement protection; and fabrication of small components with limited accessibility for generating internal passages. To provide a hot-gas source for the turbine, work was also performed on high-pressure, concentric-element, O_2/H_2 injector gas generators.

The objectives of this program were to design, fabricate, and test a high-pressure LOX turbopump capable of meeting the performance requirements of the 88,964 N (20,000 pounds) thrust, staged-combustion-cycle engine, demonstrate its basic capability, and identify any areas where additional effort due to technology limitations is required to place a future engine program on a solid basis.

Rocketdyne has assigned the designation "Mark 48-0 Turbopump" to the small, high-pressure, liquid oxygen turbopump design generated under this contract. The two terms will be used interchangeably throughout this report.

DISCUSSION

ANALYSIS AND DESIGN

ASE Engine Configuration

The objective of this program was to establish the technology base for small, high-pressure, liquid oxygen pumping capability for application on the Advanced Space Engine (ASE). The basic performance parameters for the ASE have been established in a preliminary design task, the results of which are reported in Ref. 1.

A schematic of the Advanced Space Engine is presented in Fig. 1. It is a staged-combustion-cycle engine using liquid hydrogen and liquid oxygen as propellants. The major components comprising the engine are two low-pressure, gas-driven boost pumps; two high-pressure pumps; a preburner; a regeneratively cooled combustion chamber and nozzle; dump-cooled nozzle extension; and valves.

The small, high-pressure, liquid oxygen turbopump effort performed under this contract was directed toward establishing the technology for the main oxygen turbopump.

Turbopump Requirements

The performance requirements for the Mark 48-0 turbopump are listed in Table 1. The pump is required to deliver 16.4 kg/s (36.21 lb/sec) of liquid oxygen starting with an inlet pressure of 68.9 N/cm^2 (100 psia) provided by the low-pressure pump, to a discharge pressure of 2977 N/cm^2 (4318 psia). The propellant gas for the turbine is a mixture of free hydrogen and steam resulting from the combustion of liquid hydrogen and liquid oxygen. The gas is provided at a temperature of 1041 K (187[illegible] R) and an inlet pressure of 2320 N/cm^2 (3366 psia). The total gas flowrate available is 1.34 kg/s (2.92 lb/sec). The horsepower requirement of the pump is matched by adjusting the pressure ratio across the turbine. Since turbine pressure ratio has a strong influence on the attainable engine combustion pressure in a staged combustion cycle, it is to be maintained at the lowest possible level. As noted in Table 1, the mechanical operating requirements included multiple starts with long operating durations and potentially long coast times between operations.

The values noted in Table 1 deviate slightly from the requirements expressed in the original contract work statement. Refined computer runs of the engine balance indicated minor shifts in the required pump discharge pressure, turbine inlet temperature and pressure, and turbine hot-gas flowrate. The revised values were incorporated in the requirements with the NASA Project Manager's approval.

In the area of the pump, the combination of low flowrate and high discharge pressure imposed a difficult impeller fabrication task because of the relatively narrow passages required compared with the outer diameter. The desire for high efficiency, compact packaging, and light weight placed the rotor speed into the 6282 to 9423 rad/s (60,000-to 90,000-rpm) range, pushing bearing DN value to the 1.5×10^6 mm rpm limit noted in the Design Ground Rules (Appendix A). The bearing

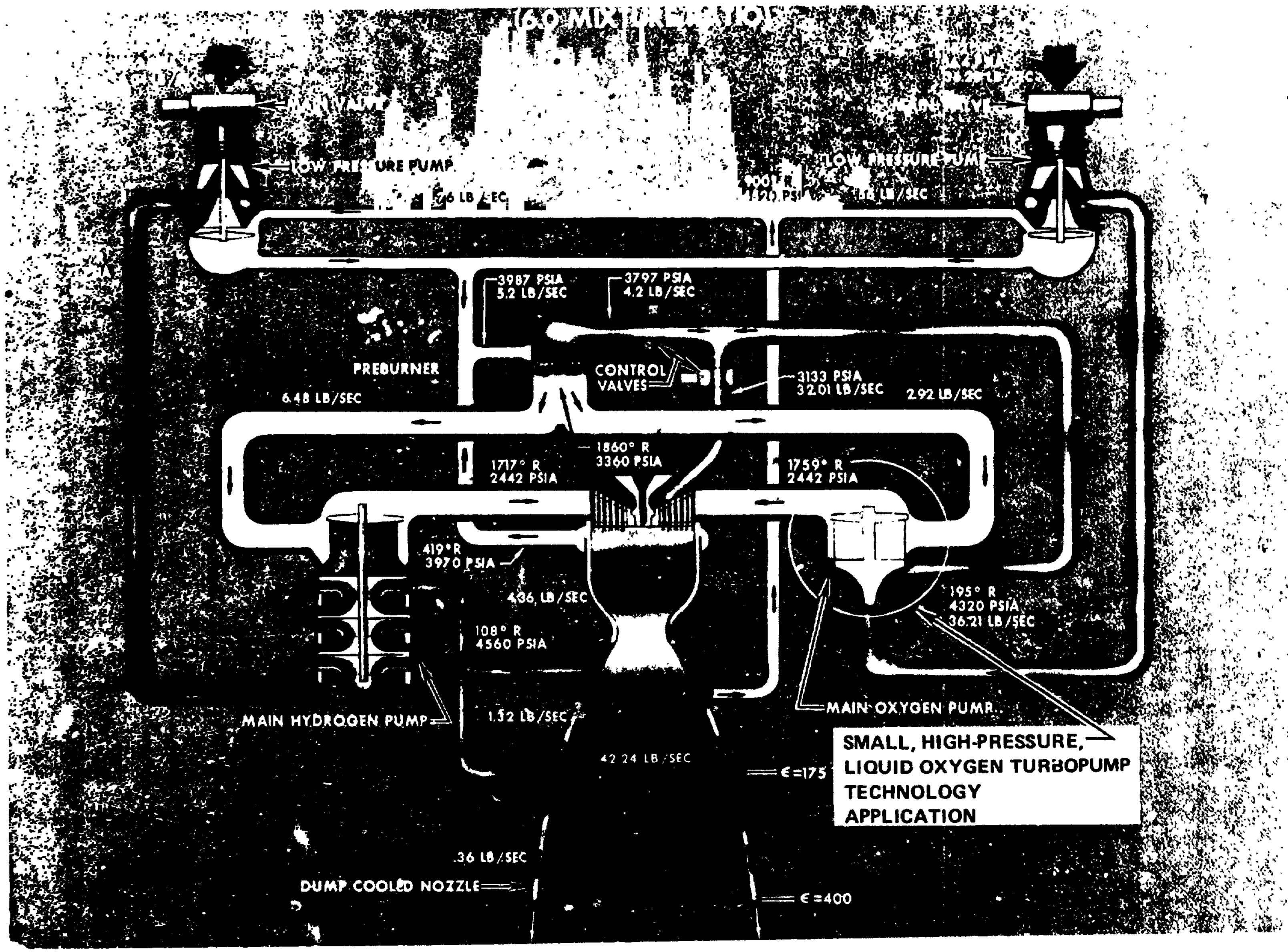

Figure 1. Engine System Schematic

TABLE 1. LIQUID OXYGEN TURBOPUMP NOMINAL DESIGN CONDITION

	Metric Units	English Units
Turbopump		
Capable of operation at pumped-idle conditions (5 to 10 of full thrust)		
Off-design operation	±20% Q/N at full thrust down to 30% Q/N at 20% N	
Number of start-stop cycles	300	
Time between overhaul	10 hours	
Pump		
Type	Centrifugal	
Propellant	Liquid oxygen	
Inlet pressure	68.9 N/cm^2	100 psia
Inlet temperature	90-95.5K	162 to 172 R
Discharge pressure	2977 N/cm^2	4318 psia
Mass flow	16.4 kg/s	36.21 lb/sec
Number of stages	One	
Turbine		
Working fluid	H_2-O_2 combustion products (H_2 x H_2O)	
Inlet temperature	1041	1874 R
Inlet pressure	3220 N/cm^2	3366 psia
Pressure ratio	Minimum necessary to develop pump horsepower requirements.	
Flowrate	1 34 kg/s	2.92 lb/sec
Number of stages	One	
Type	Partial admission	
Service life between overhauls:	*300 Thermal cycles or 10 hours accumulated run time	
Service-free life	*60 Thermal cycles or 2 hours accumulated run time	
Maximum Single Run Duration:	2000 s	
Maximum time between firings during mission:	14 days	
Maximum time between firings during mission:	1 minute	
Maximum storage time in orbit (dry):	52 weeks	
Thermal cycle defined as engine start (to any thrust level) and shutdown		

operation at high DN values in a turbopump installation as well as the dynamic behavior of the rotor at high speeds needed to be demonstrated. Because of the high operating speed involved, the bearings would not be able to take an appreciable axial thrust load. This condition dictated that an axial thrust balance device be employed which, in liquid oxygen, would have to be of the nonrubbing type. The operating characteristics of such a device also required evaluation.

In the turbine, the low-pressure ratio (approximately 1.4) and low arc of admission (28%) presented a combination for which no empirical data were available. Performance predictions based on calculations needed to be validated or modified by measured performance data.

From a structural consideration, the requirement for 300 thermal cycles was significant in that it established low-cycle-fatigue criteria and eventually necessitated incorporating a liner in the turbine manifold to limit the maximum thermal gradients in structural walls.

In addition to the performance criteria noted in Table 1 , the contract work statement included certain ground rules relating primarily to the structural analysis and mechanical design of the turbopump. These ground rules are enclosed in Appendix A.

Turbopump Description

The mechanical configuration of the small, high-pressure, liquid oxygen turbopump is illustrated in Fig. 2 , with the significant parts identified. The top assembly requirements are established on Rocketdyne drawing number RS009820E, which is included in Appendix B. The design was given the Rocketdyne internal designation of Mark 48-0.

Liquid oxygen is introduced to the pump through the axial-flow inlet of 4.214 cm (1.659 inch) diameter and passes through a four-bladed, constant-outer-diameter, tapered-hub inducer which raises the pressure to an intermediate level. From the inducer the liquid proceeds into a centrifugal impeller containing four partial and four full blades. Subsequently, it is diffused in a radial diffuser which incorporates 13 guide vanes. Downstream of the diffuser, liquid oxygen is collected, further diffused in a volute section, and delivered through a single 2.54 cm (1.00 inch) diameter duct.

Hot gas to the turbine is admitted through a scroll-shaped, constant-velocity inlet, lined with a 1.57 mm (0.062 inch) metal liner to maintain the thermal gradients across the structural walls at an acceptable level. The inlet duct diameter is 3.1 cm (1.22 inch). The active arc of the partial-admission nozzle extends over 1.8 rad (103 degrees) or 28.6% of the circumference, and it includes seven flow passages. The gas is fully expanded through the nozzle, after which it passes through a single row of unshrouded impulse-type blades (79 blades) of the rotor. The exhaust gas is directed through a row of stationary vanes which guide the gas toward a single radial exit duct of 3.81 cm (1.50 inch) diameter.

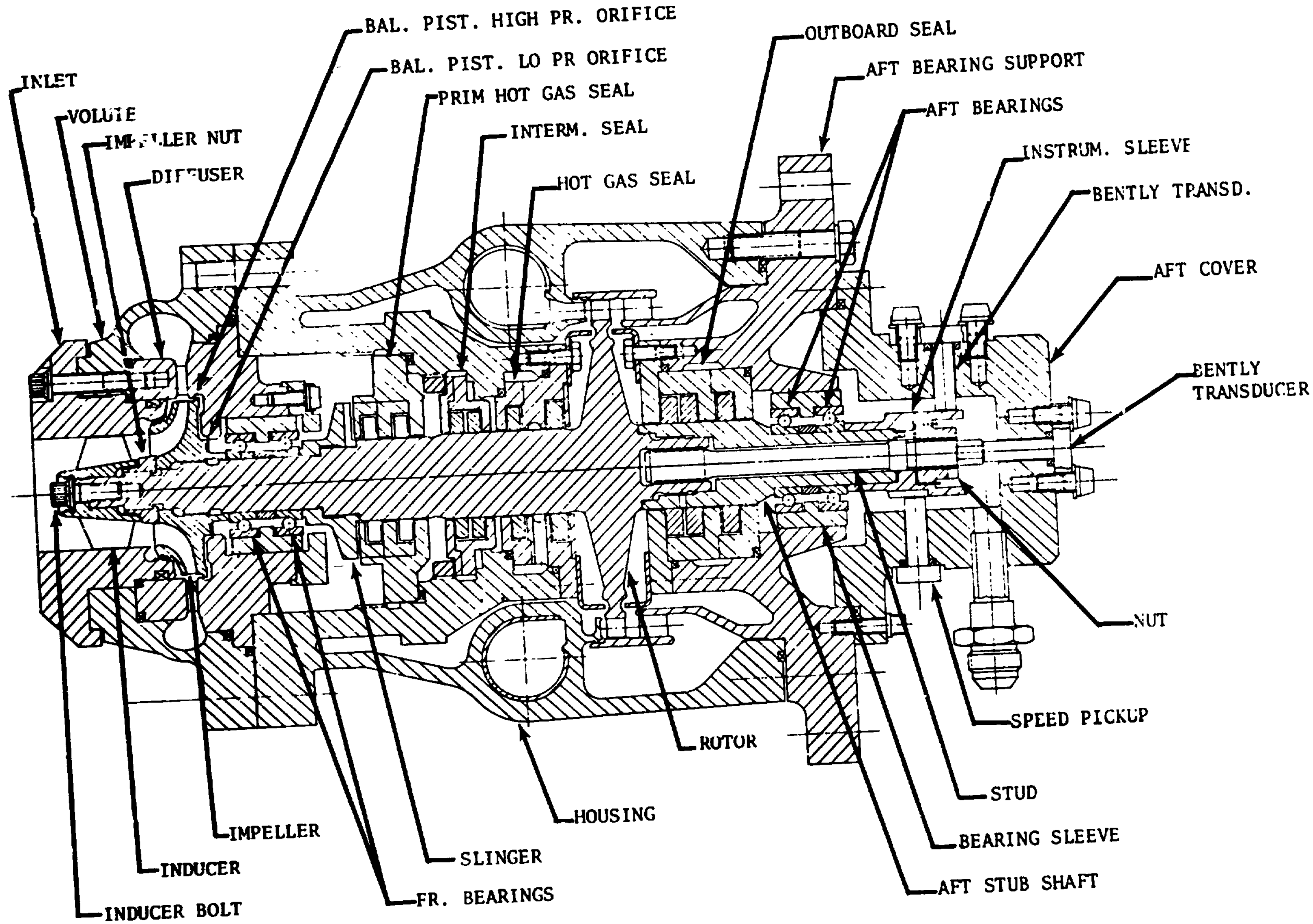

Figure 2. Mark 48-0 Turbopump

The pump shaft and the turbine disk are designed as an integral part. On the outboard end, a stub shaft is used with a stud and nut to extend the rotor. Two pairs of angular-contact, 20 mm ball bearings are used to support the rotor. The pump-end bearings are cooled by recirculating liquid oxygen through them. The outboard shaft seal is pressurized with liquid hydrogen, and the leakage toward the outboard side is used as bearing coolant. A small amount of liquid hydrogen is bypassed around the seal and introduced to the bearing directly as a redundant source of coolant. The bearings in each pair are axially preloaded against each other with Belville springs to prevent ball skidding. The turbine-end bearings are free of other axial loads. The outer-race sleeve of the pump-end bearings is axially retained so that the bearings absorb rotor axial thrust during transient periods when the balance piston does not control the rotor axial position.

Under conditions other than early transient stage during startup or at the end of shutdown, the rotor axial thrust is neutralized by a self-compensating balance piston. The rotating member of the piston is the rear shroud of the impeller. To operate the piston, high-pressure liquid oxygen from the impeller discharge passes through a high-pressure orifice located at the outer diameter of the impeller into the balance cavity. From the cavity, the liquid passes through a low-pressure orifice near the impeller hub into the sump. From there the liquid oxygen is returned to the eye of the impeller through axial passages in the diffuser vanes and radial holes in the diffuser and inlet. Thrust-compensating effect is achieved by virtue of the fact that the high- and low-pressure orifice openings vary with the axial position of the rotor, and the pressure force on the rear shroud of the impeller varies correspondingly; e.g., an unbalanced load toward the pump inlet causes a reduction in the high-pressure orifice gap and an increase in the low-pressure orifice gap. This, in turn, causes a reduction in the pressure force of the impeller rear shroud, introducing a compensating load change.

Because of the danger of explosion when rubbing in liquid oxygen, the balance piston orifices were designed as noncontacting type, formed by the axial proximity of close clearance, 0.038 mm (0.0015-inch) average, diametral, cylindrical surfaces.

To preclude mixing liquid oxygen from the pump with the combustion products from the turbine, the two regions are separated by three dynamic seals. All three seals are of the controlled-gap type, with two seal rings in each. The controlled-gap concept was selected for this application primarily because it has low drag torque, a "must" for idle-mode starts. This concept also minimizes power absorption during steady-state operation, and permits very long service life. Pump fluid is contained by the primary LOX seal. The oxygen which flows past this seal is drained overboard from the cavity formed by the primary and intermediate seals. A slinger containing pumping ribs was included upstream of the primary LOX seal to reduce the pressure at the seal gap to a level that will vaporize the fluid. The objective was to reduce the mass flowrate through the seal with this technique.

On the turbine side, because of the high pressure involved, sealing and drainage was accomplished in two steps. An overboard drain was included downstream of the first ring, which reduces the pressure between the two rings to 79 N/cm^2 (115 psia). The small amount of turbine gas which leaks past the second ring is drained overboard with a drain cavity pressure of approximately 14 N/cm (20 psia).

To provide separation of the pump and turbine fluids, an intermediate seal was incorporated between the two drain areas with a GHe purge which maintains the cavity between the two rings at 35 N/cm^2 (50 psia).

Turbopump Configuration Selection

The statement of work defined the configuration of the turbopump as a centrifugal pump powered by a single-stage, partial-admission turbine. These guidelines were established based on the result of a prior effort conducted under NASA-Lewis Research Center contract in which the basic parameters of the Advanced Space Engine were defined (Ref. 1). In addition, the speed of the LOX turbopump rotor was limited to the range of 6282 to 9423 rad/s (60,000 to 90,000 rpm) to achieve reasonable efficiency and weight, while maintaining a maximum bearing DN limit of 1.5 million.

Within the above-specified limits, the most important options which had to be considered were those relating to the type of axial thrust control concept and type of impeller and diffuser to be used, and whether an inducer was necessary at the pump inlet. Each of these features was studied with respect to advantages and disadvantages, and the conclusions are discussed below. A summary is enclosed in Fig. 3 .

Impeller With or Without Inducer. The higher the pump speed that can be selected, the higher the obtainable performance and the smaller the pump envelope and weight will be. Therefore, the speed was selected based on the given bearing DN value limitation as well as axial thrust control considerations, which limit the minimum impeller diameter that can be used to achieve thrust balance. If we assume a speed of 7853 rad/s (75,000 rpm), which corresponds to a DN value of 1.5 x 10^6 for a 20 mm bearing a pump suction specific speed of 24,000 would be required (available NPSH 170 feet). This suction specific speed, however, can be obtained only by using an inducer. It is for this reason that the inducer-impeller combination was selected.

Open-Faced or Shrouded Impeller. Experience shows that a shrouded impeller results in a higher performance than an unshrouded. In addition, its performance is independent of the axial rotor position, and allows a generous clearance between rotor and housing, thus eliminating an explosion hazard. The shroud also adds rigidity to the impeller, which is desirable when an integral impeller-balance piston system is used. Although more difficult to manufacture, the above factors dictate a shrouded impeller.

Axial Thrust Control, Integral versus Separate Balance Piston. The advantage of the separate balance piston is that its size can be selected such that any axial thrust condition can be controlled. The disadvantages, however, outweigh this advantage: pump length and weight increase, and pump performance decreases since balance piston leakage losses and disk friction increase. Using an integral impeller-balance piston system reverses the advantages and disadvantages of the separate pistons: Weight, length, and performance losses are minimized; however, the thrust balancing range is limited, being a function of the impeller size.

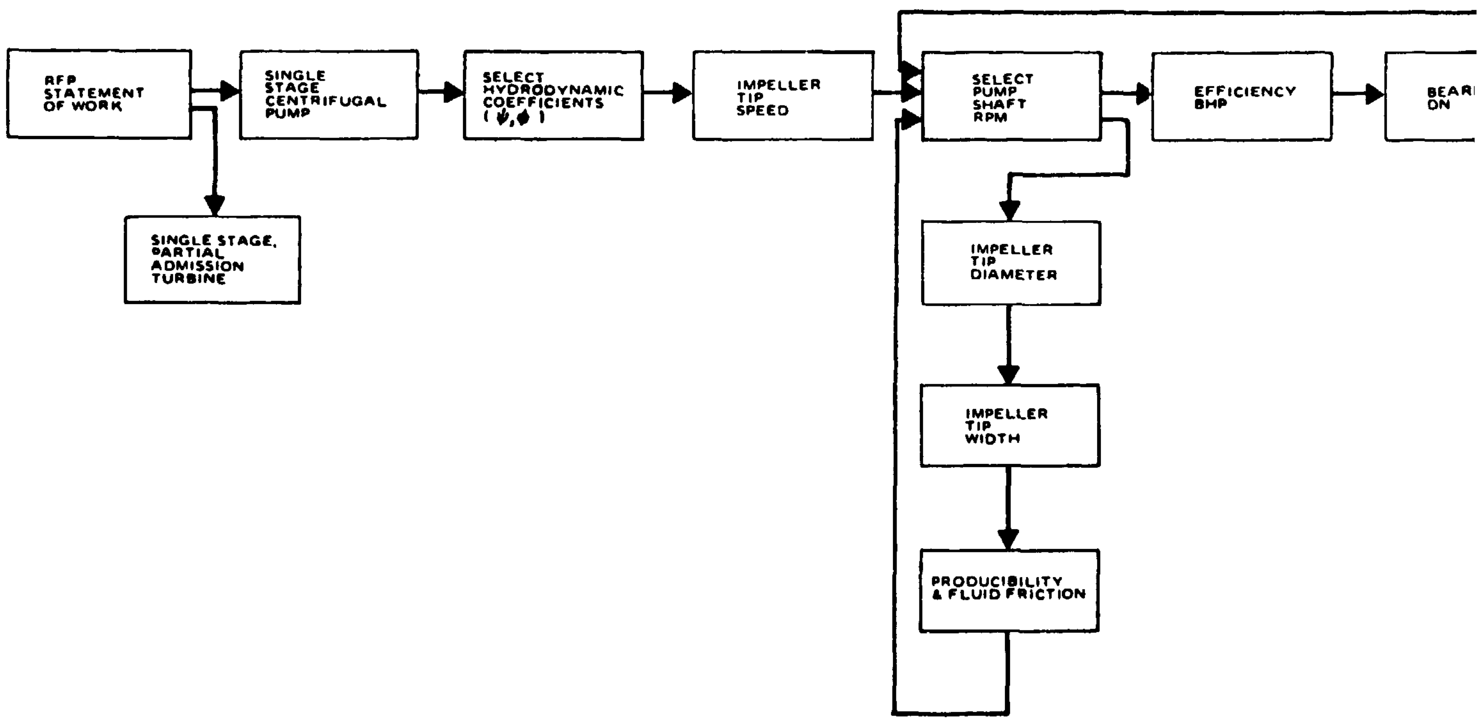

FOLDOUT FRAME 1

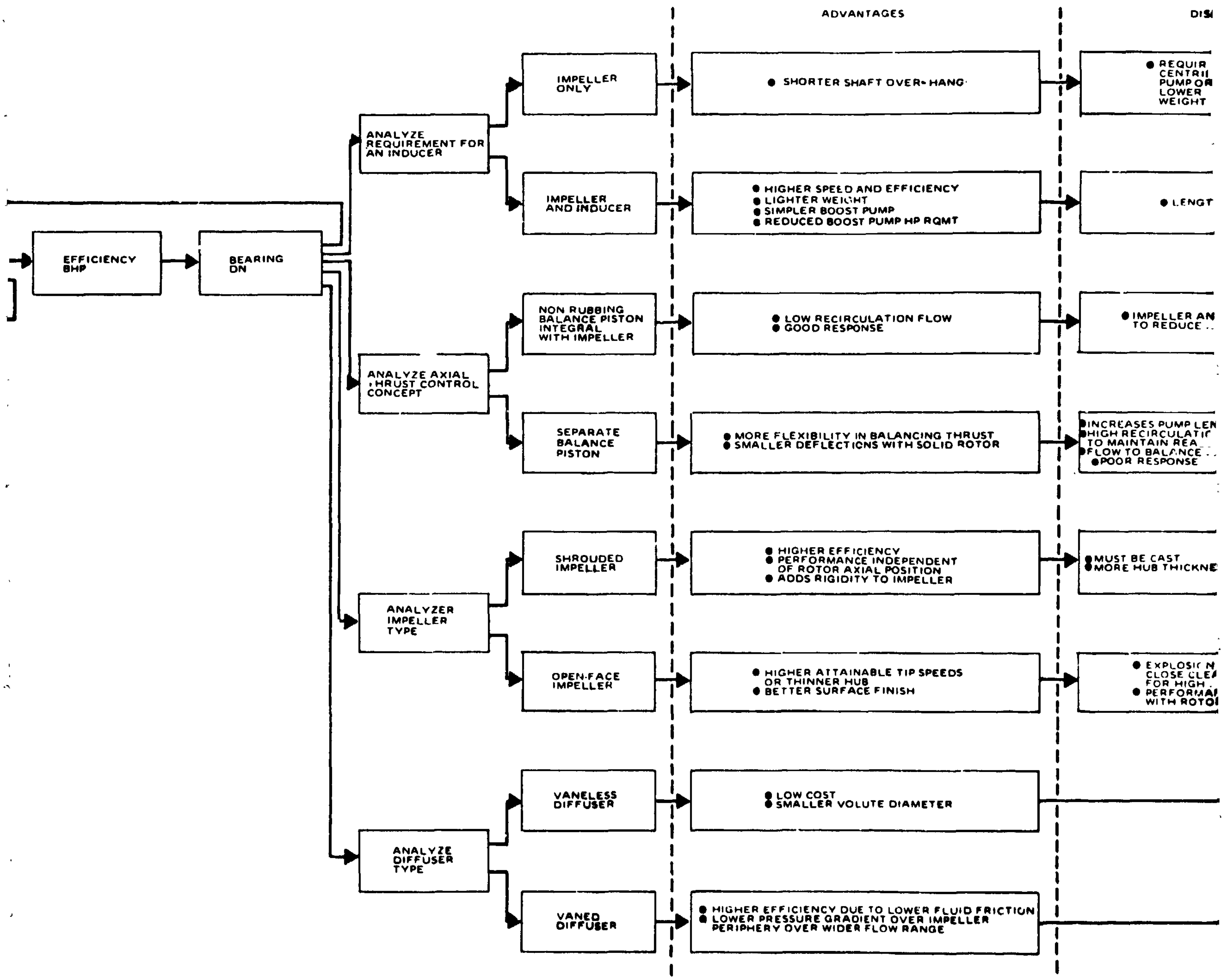

FOLDOUT FRAME 2

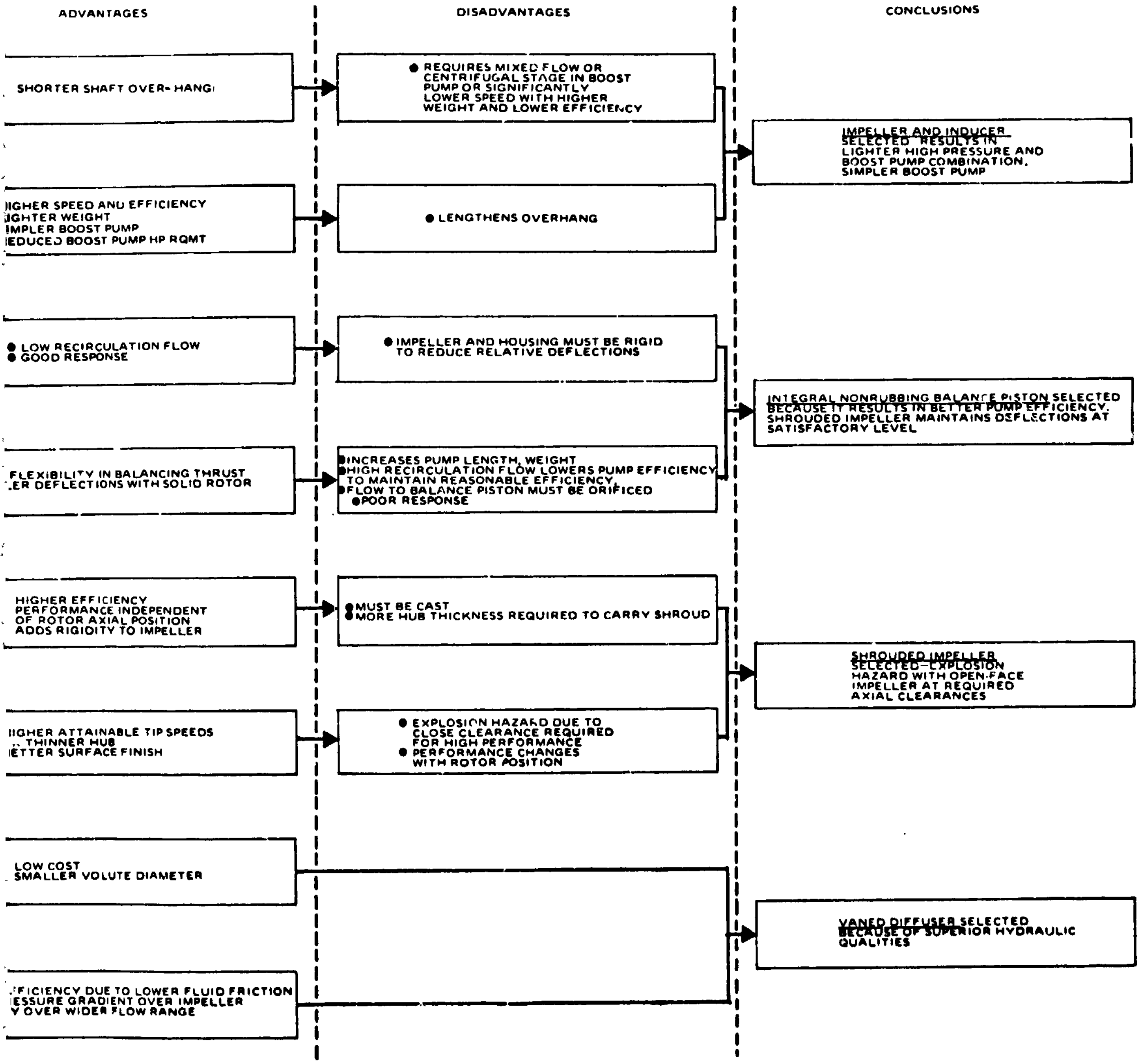

Figure 3. Configuration Selection Logic Diagram

FOLDOUT FRAME 2

To ensure that sufficient thrust control could be achieved with the integral system, a parametric trade study was made. The results of this study, summarized in Fig. 4 , showed that axial thrust control could be achieved if the impeller diameter was maintained above 5.8 cm (2.3 inch). Based on this, the integral impeller balance system was selected.

Vaneless or Vaned Diffuser. This option was considered only because a vaneless diffuser is easier to manufacture. The pump efficiency, however, increases when a vaned diffuser is used. A vaned diffuser reduces the velocity in a short length, the flow path length is reduced and, therefore, the friction losses. (For experimental results see Ref. 2 , page 17, Fig. 6). A second advantage of the vaned diffuser is that the pressure around the periphery of the impeller is more uniform, resulting in reduced radial loads. For these reasons, the vaned diffuser configuration was selected.

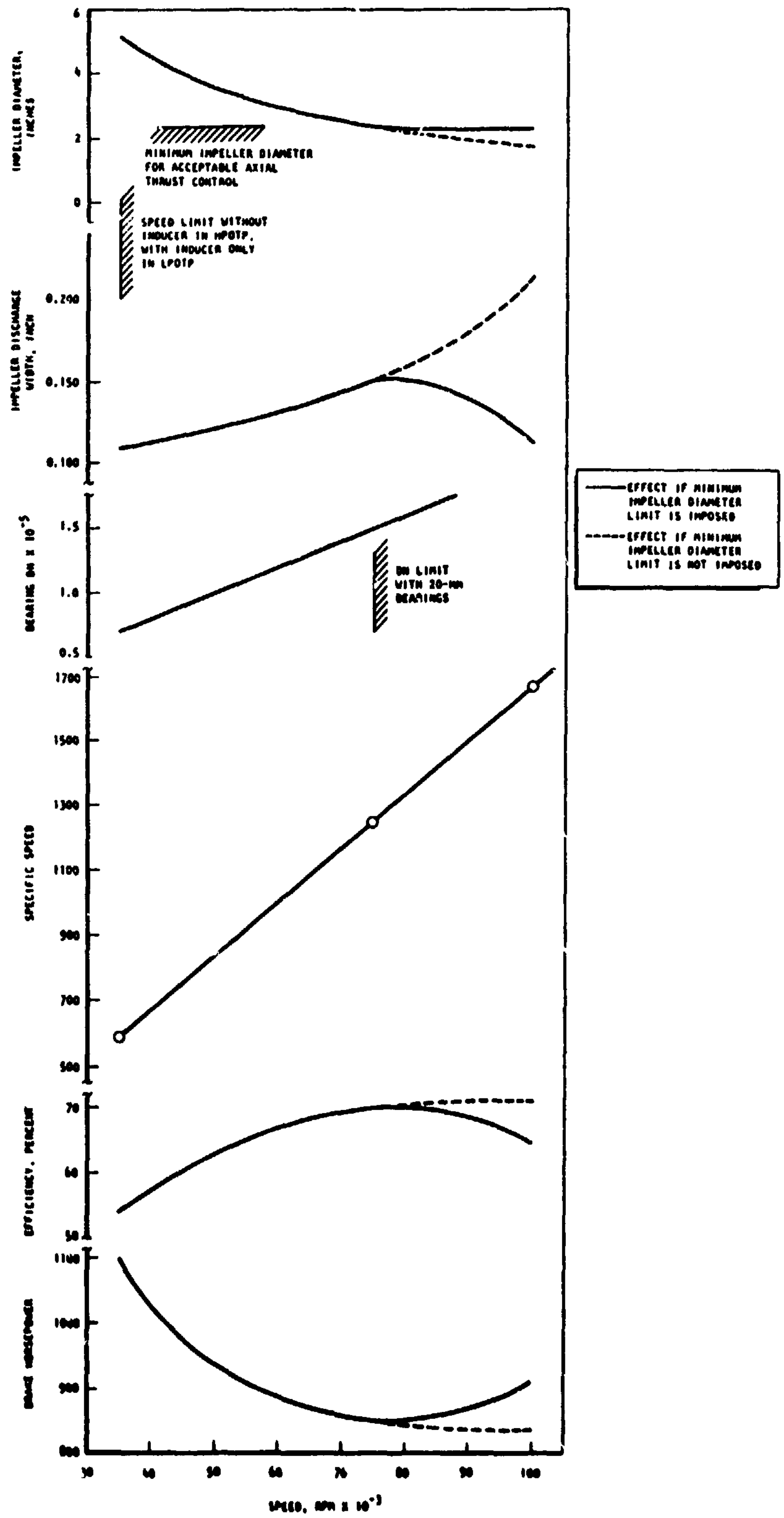

Figure 4. Speed Effects

Hydrodynamic Analysis of the Pump

Pump Speed Selection. The speed selection involved a compromise between several considerations. It included a design study, critical speed analyses as a function of bearing stiffness, axial thrust control calculations, the bearing DN value, and the effect of speed on pump performance. From the design study and critical speed analyses, the use of a 20 mm bearing resulted which, in turn, fixed the maximum speed at 7850 rad/s (75,000 rpm) based on the 1.5 × 10^6 DN limit imposed in the Design Ground Rules (see Appendix A). At an estimated bearing stiffness of 35,000 N/mm (2 x 10^5 lb/in.)/bearing, the second critical is located at 5550 rad/s (53,000 rpm); meanwhile, the third is located at 10,500 rad/s (100,000 rpm). Thus, from the standpoint of critical rotor frequencies, the speed range of 6912 rad/s (66,000 rpm) to 8376 rad/s (80,000 rpm) was acceptable after a 20% allowance was made for margin. Another criterion to be considered was the axial thrust control. With a selected impeller head coefficient of 0.47 (see Impeller Design) an impeller diameter of 6.05 cm (2.38 inches) would result in a speed of 7850 rad/s (75,000 rpm). This diameter was only slightly larger than the 5.84 cm (2.3 inches) impeller diameter thrust capability limit established by the parametric study (Fig. 4). To ensure that enough axial thrust capability margin was incorporated, the impeller diameter was established at 6.48 cm (2.55 inches), resulting in an operating speed of 7330 rad/s (70,000 rpm).

Inducer Inlet Flow Coefficient. The available nominal inlet pressure to the pump is presently established at 68.94 N/cm^2 (100 psi). Initially in the program, this value was 52.91 N/cm^2 (76.75 psia) minimum, and the presented inducer analysis was based on the latter pressure level. The NPSH available at the inducer inlet at 52.91 N/cm^2 (76.75 psi) inlet pressure and 95.5 K (172 R) inlet temperature is 320 J/kg (107 feet), which corresponds to a suction specific speed of 111.5 rpm $(m^3/s)^{1/2}(J/kg)^{3/4}$ [31,867 rpm $(gpm)^{1/2}$ $(ft)^{3/4}$] at 7320 rad/s (70,000 rpm). To obtain the maximum margin on suction performance, particularly in view of the degradation of obtainable suction specific speed due to the small-size inducer, an inlet flow coefficient ϕ = 0.085 was selected. With this flow coefficient, larger-size inducers have the potential of reaching a corrected suction specific speed of 192.5 rpm $(m^3/s)^{1/2}/(J/kg)^{3/4}$ [55,000 rpm $(gpm)^{1/2}$ $(ft)^{3/4}$, see Fig. 4, page 12 of NASA Report SP8109]. A second consideration in selecting 0.085 as the flow coefficient was the limitation imposed by the inducer blade angle. With inducer tip and hub diameters of 4.19 cm (1.65 inches) and 1.78 cm (0.7 inch), respectively, the inlet blade angle of the tip becomes 0.15 rad (8.5 degrees). A lower flow coefficient, which theoretically yields higher suction specific speeds and therefore a larger design margin, would require even smaller blade angles. To provide sufficient flow passage area, the inducer tip diameter would have to be increased and the blades made thinner. As a consequence, the blades would be higher stressed, and fabrication would become more difficult. Furthermore, the diameter ratio of the impeller would be unfavorably affected and, as a result, the pump efficiency would drop. Therefore, the selected flow coefficient of 0.085 represents the lower limit and, hence, the optimum choice for this application.

Inducer Inlet Blade Angles. The blade centerline was canted forward 0.16 rad (9 degrees) from the radial direction to counteract the hydraulic loads by centrifugal forces. A 2.09 rad (120 degrees) sweep was used to ease the blade stress conditions.

As noted above, the blade angle at the inlet tip was established at 0.15 rad (8.5 degrees) in conjunction with the selection of the flow coefficient and tip diameter. Angles at other radii were determined by the relationship

$$\frac{r \tan \beta}{\cos (0.16 \text{ rad})} = \text{constant}$$

where

r	=	radius
β	=	blade angle from tangential
cos (0.16 rad)	=	cant angle correction

The resulting blade angle at the hub is 0.339 rad (19.4 degrees).

Inducer Discharge Blade Angles. The inducer discharge blade angles were determined by the impeller suction capability, which was selected as S_s = 2.569 rad/s $(m^3/s)^{1/2}/(J/kg)^{3/4}$ (7000 rpm $(gpm)^{1/2}$ $(ft)^{3/4}$). Since the impeller front wear-ring flow as well as the balance piston flow is returned to the inlet of the impeller, downstream of the inducer, the following impeller flow was used:

	kg/s	lb/sec	
Through flow	16.44	36.21	
Front wear-ring flow	0.74	1.62	
Balance-piston flow	2.19	4.83	
Impeller flow	19.37	42.66	= 270 gpm

The value of the balance piston flow used in the impeller analysis was derived from a preliminary analysis. It is larger than the flow which results when the final tolerances are used. (See Axial Thrust Analysis section of this report)

Based on this impeller flowrate and S_s, the required impeller inlet NPSH is 2690 J/kg (900 feet). Assuming an available inducer inlet head of 52.9 N/cm (76.75 psia) results in a minimum inducer required headrise of 2346 J/kg (785 feet).

The inducer discharge angles were determined by using a head rise requirement of 301 J/kg (900 feet). This was done to account for the size effect. The discharge blade angles from hub to tip are determined by the relation

$$r \tan \beta = \text{constant}$$

This does not produce an ideal constant head output from hub to tip, but eases the fabrication considerably. First the angle at inducer discharge rms is calculated:

$$\text{Euler Head} = \frac{u_{rms} \left(c_u\right)_{rms}}{g} = \frac{\Delta H}{\eta_{hydr}}$$

$$\left(C_u\right)_{rms} = \frac{\Delta H \quad g}{\eta_{hydr} \quad u_{rms}}$$

$$= \frac{(2690)}{(0.8)(124)} = 27.1 \text{ m/s (SI)}$$

$$= \frac{(900)\cdot(32.2)}{(0.8)\ (407)} = 89.1 \text{ ft/sec (English)}$$

The exit area is

$$A_2 = \frac{\pi}{4} \left(D_T^2 - D_H^2\right)$$

$$= \frac{\pi}{4} \left(4.19^2 - 2.29^2\right) = 9.67 \text{ cm}^2 \text{ (SI)}$$

$$= \frac{\pi}{4} \left(1.65^2 - 0.9^2\right) = 1.5 \text{ in.}^2 \text{ (English)}$$

where D_T and D_H are the inducer tip and discharge hub diameters, respectively. If the blockage is assumed to be 0.8,

$$C_m = \frac{Q}{(A)\ (0.8)}$$

$$= \frac{(0.0144)}{(9.67 \times 10^{-4})\ (0.8)} = 18.6 \text{ m/s (SI)}$$

$$= \frac{(229)\ (144)}{(449)\ (1.5)\ (0.8)} = 61.2 \text{ ft/sec (English)}$$

with that, the relative flow angle at rms is

$$\alpha_{2\ rms} = \text{arc tan } \frac{C_{m_2}}{u_{rms} - c_{u_{2_{rms}}}}$$

$$= \text{arc tan } \frac{18.6}{124 - 27.1} = 0.19 \text{ radian (SI)}$$

$$= \text{arc tan } \frac{61.2}{407 - 89.1} = 10.9 \text{ degrees (English)}$$

The total turning at the rms radius is 0.107 radian (6.16 degrees). Assuming a deviation angle of 0.044 rad (2.5 degrees) results in a blade discharge angle of 0.24 radian (13.5 degrees) and, therefore, a blade tip angle, β_2, of 0.19 radian (10.95 degrees). Based on this, it was decided to use 0.19 radian (11 degrees) at the tip of the inducer discharge, which results in an angle of 0.34 radian (19.4 degrees) at the hub of the discharge.

Figure 5 shows the blade angle distribution as a function of the axial length, and Fig. 6, the blade loading, which was calculated using Rocketdyne's VELDIS computer program.

Impeller Design. With the inducer design established, the inlet eye diameter of the impeller is also fixed (4.19 cm; 1.65 inches). The required pump head rise is 25,974 J/kg (8690 feet) which, at 7330 rad/s (70,000 rpm), corresponds to a stage specific speed of 4.1 rpm $(m^3/s)^{1/2}/(J/kg)^{3/4}$ (1174 rpm $(gpm)^{1/2}/(ft)^{3/4}$). From this, using the available experience documented in Fig. 5 of NASA Report SP 8109, an impeller diameter ratio of about 0.65 has to be selected to obtain a high pump efficiency. Therefore, the impeller tip diameter is set to 6.48 cm (2.55 inches) which, with the selected speed of 7330 rad/s (70,000 rpm), results in a required head coefficient of $\psi = 0.4725$. From Fig 16 of NASA Report SP 8109, the minimum number of blades required to obtain $\psi = 0.4725$ is found to be between five and six,

Since a four-bladed inducer has been selected, it is desirable to also have four blades at the impeller inlet. This will ensure minimum impeller inlet blockage and, at the same time, ease producibility. However, an impeller with only four full blades results in blade surface velocity gradients exceeding the limits. Therefore, four partial blades were added.

The final determination of the blade angles and shape is a function of blade loading, stress, and producibility, all of which are also affected by the shroud contour. Its curvature, therefore, was made moderate to avoid separation. The shroud shape also has to be coordinated with the blade thickness required by stress.

After several iterations, hydrodynamics, stress, and fabrication could be satisfied using an impeller blade discharge angle of 0.454, 0.489, and 0.524 rad (26, 28, and 30 degrees) at the shroud, mean stream line and hub, respectively.

The tip width was established as 3.81 mm (0.15 inch) which corresponds to an impeller discharge flow coefficient of $\psi = 0.151$.

The assumptions used to arrive at these dimensions are as follows:

Total head to be generated:

$$H_{TOT} = H \text{ pump} + \text{losses}$$

The losses are:

1. Friction in impeller
2. Impeller incidence loss
3. Friction in diffuser
4. Diffuser incidence loss
5. Volute loss

For the design point, the incidence losses are assumed to be zero.

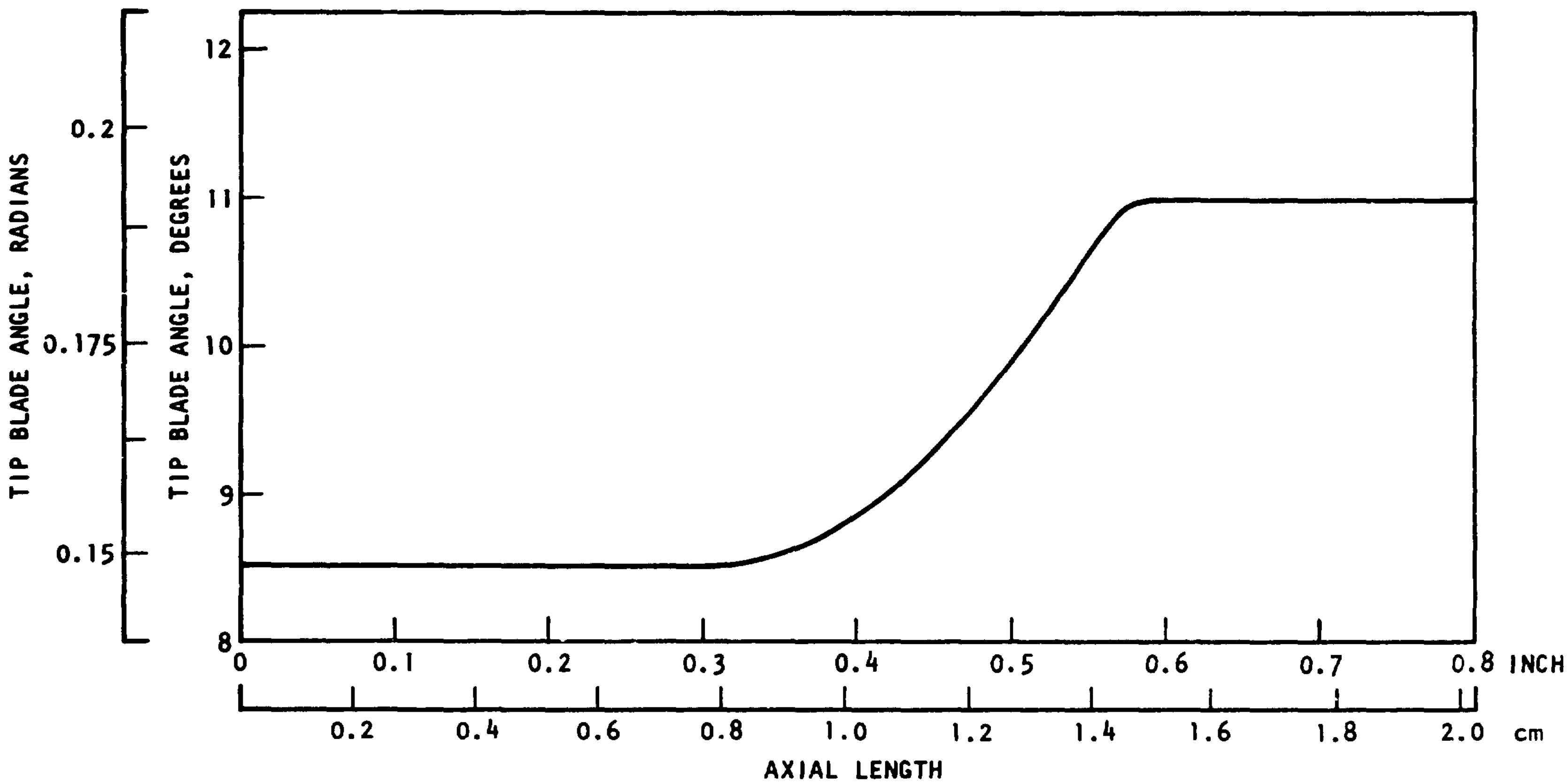

Figure 5. Mark 48-0 Inducer Blade Angle Distribution

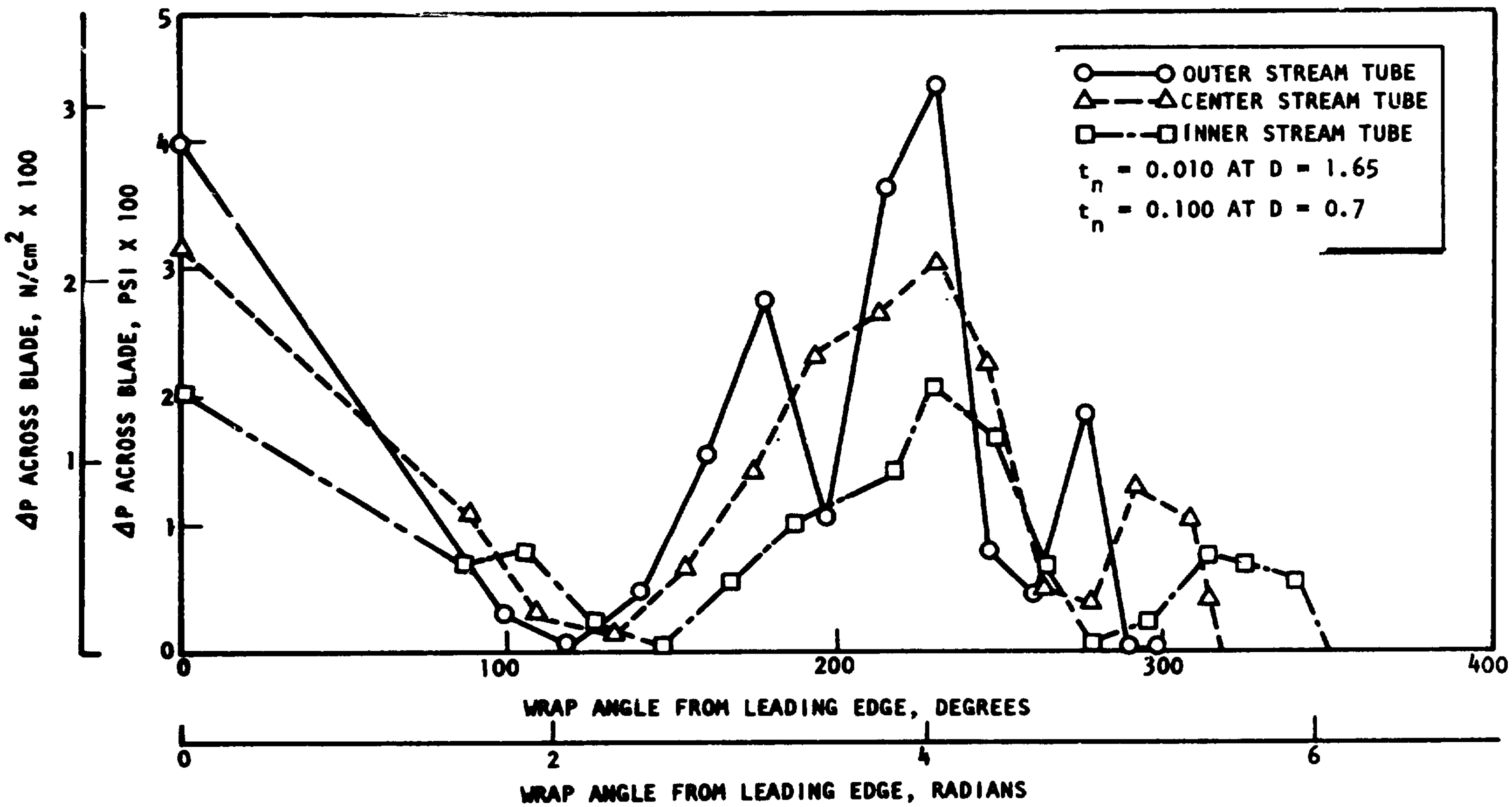

Figure 6. Mark 48-0 Inducer Blade Loading

The loss values for the pump design point performance calculation are shown in Table 2 . These values are selected based on Rocketdyne's experience. For the calculation of off-design performance, the loss coefficients were varied.

TABLE 2. LOSS VALUES FOR PUMP DESIGN POINT PERFORMANCE CALCULATIONS
(Q = 232 gpm, N = 70,000 rpm)

	Inducer	Impeller	Vaneless Space	Diffuser	Volute
Roughness	0.000064	0.000064	0.000064	0.000064	0.00125
Momentum Loss Coefficient	--	--	--	--	0.00206
Incidence Loss Coefficient	0.00426	0.00073	--	0.0007	--
Skin Friction Loss Coefficient	0.00947	0.00578	0.005438	0.01082	0.00609
Diffusion Loss Coefficient	0.00121	0.00004	--	0.01761	--
Exit Diffuser Loss Coefficient	--	--	--	--	0.00144

The blade angle distribution is shown in Fig. 7, and the results of the blade loading analysis, calculated using Rocketdyne's two-dimensional axisymmetric blade-loading analysis computer program, are shown in Fig. 8 and 9. Figure 10 shows the predicted pump performance map, which is calculated using Rocketdyne's loss isolation computer program.

Vaned Diffuser Design. The impeller is followed by a radial vaned diffuser. This type is selected to provide maximum efficiency and, with proper volute design, a more nearly constant static pressure around the periphery of the impeller, thus minimizing radial bearing loads.

The radial clearance between the impeller discharge and diffuser inlet is set at 0.1 inch, which corresponds to approximately 4% of the impeller diameter. Thus, the diffuser inlet diameter is 2.75 inches. The diffuser exit diameter is set at 3.65 inches, or 1.43 times the impeller diameter. The diffusion is produced by 13 vanes. Hydrodynamic loads are insignificant compared to the tensile load. The cross-sectional area, therefore, must be selected to carry this load. Rocketdyne's diffuser computer program was used to determine the vane shape (Fig. 11).

Volute. The diffuser discharges into a volute folded over toward the pump inlet. This type is used to minimize the outside diameter and to create a stable secondary flow pattern, which reduces volute losses.

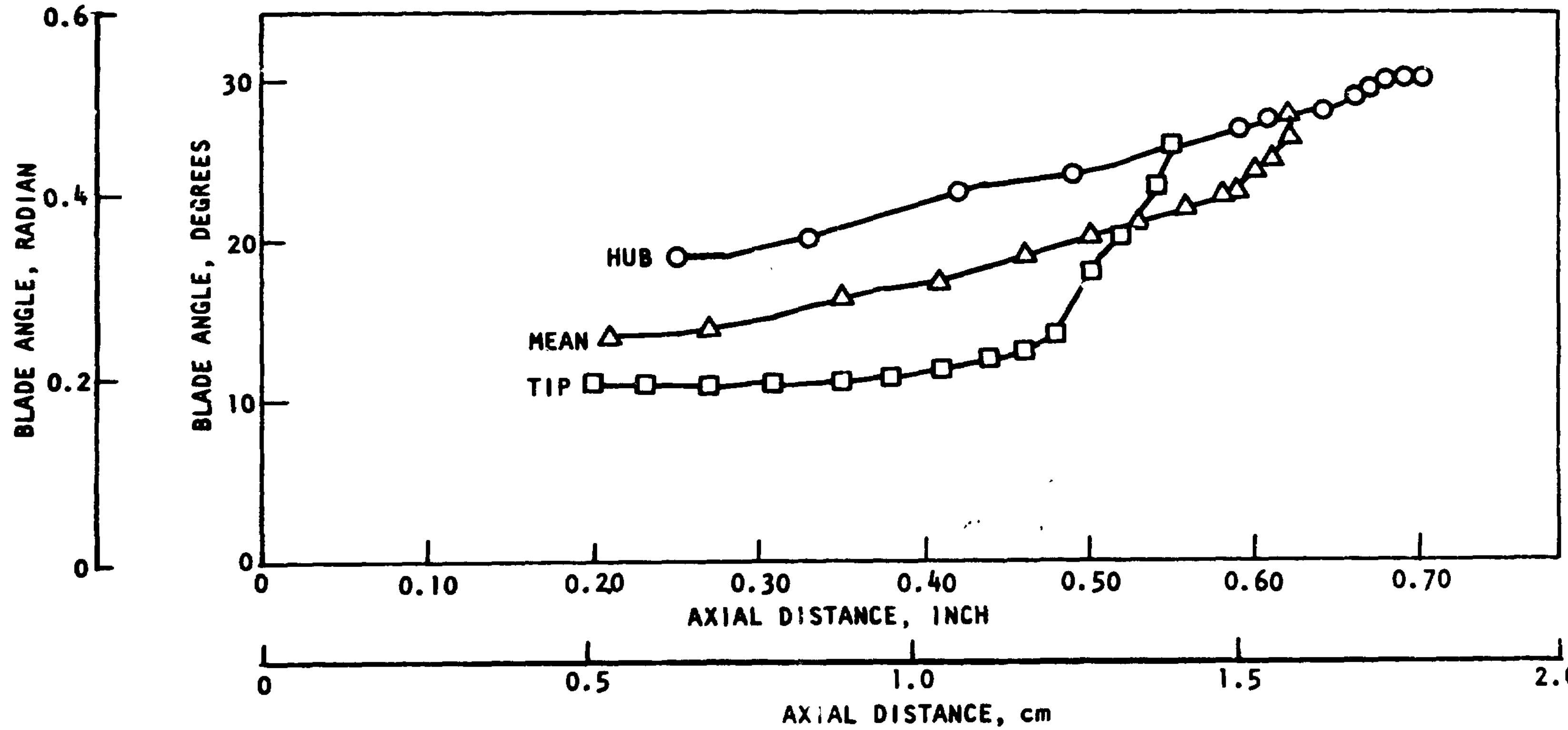

Figure 7. Mark 48-0 Impeller Blade Angle Distribution
(Angles Measured From Tangential)

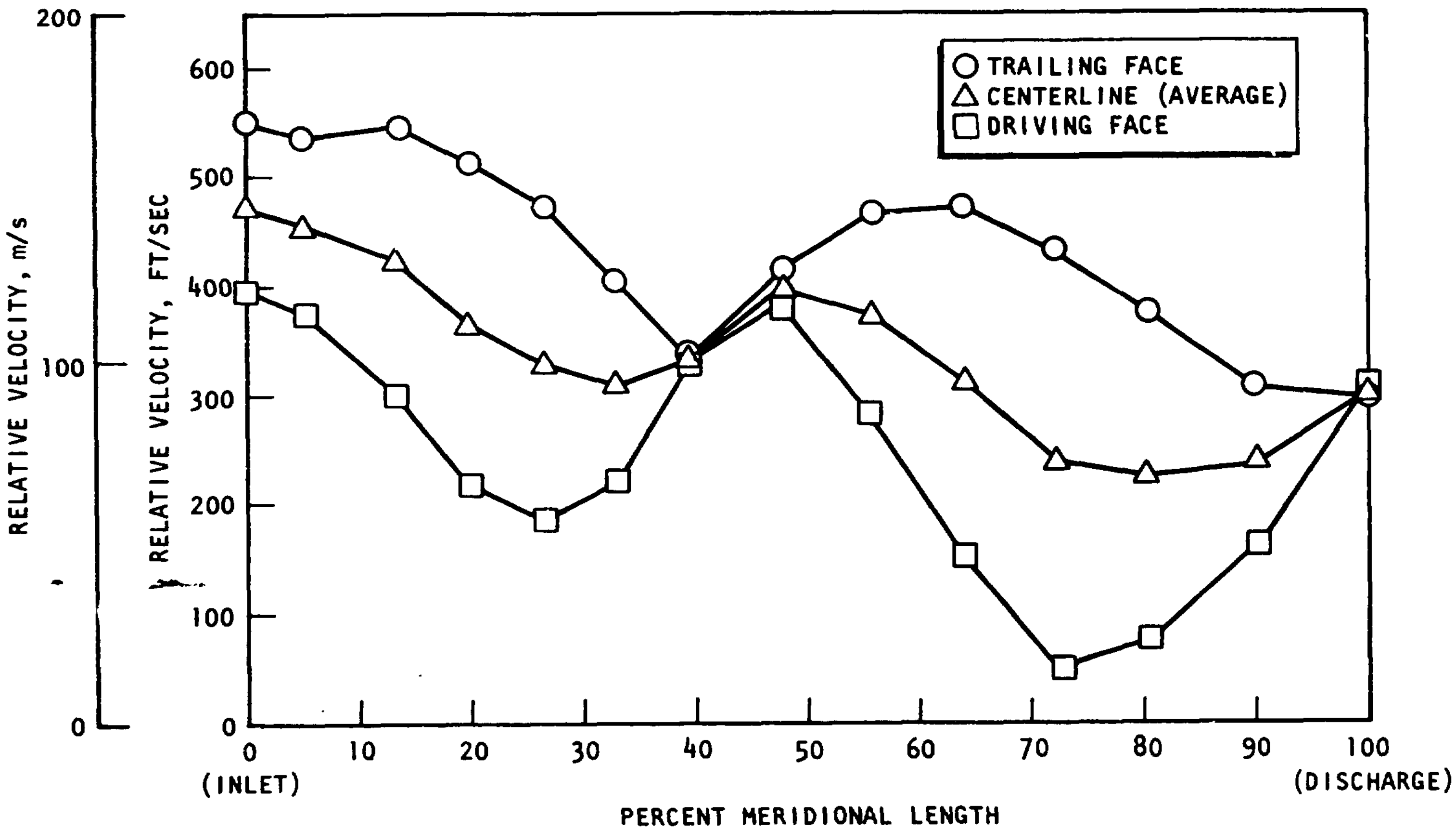

Figure 8. Mark 48-0 Impeller Relative Velocities, Outer Stream Tube

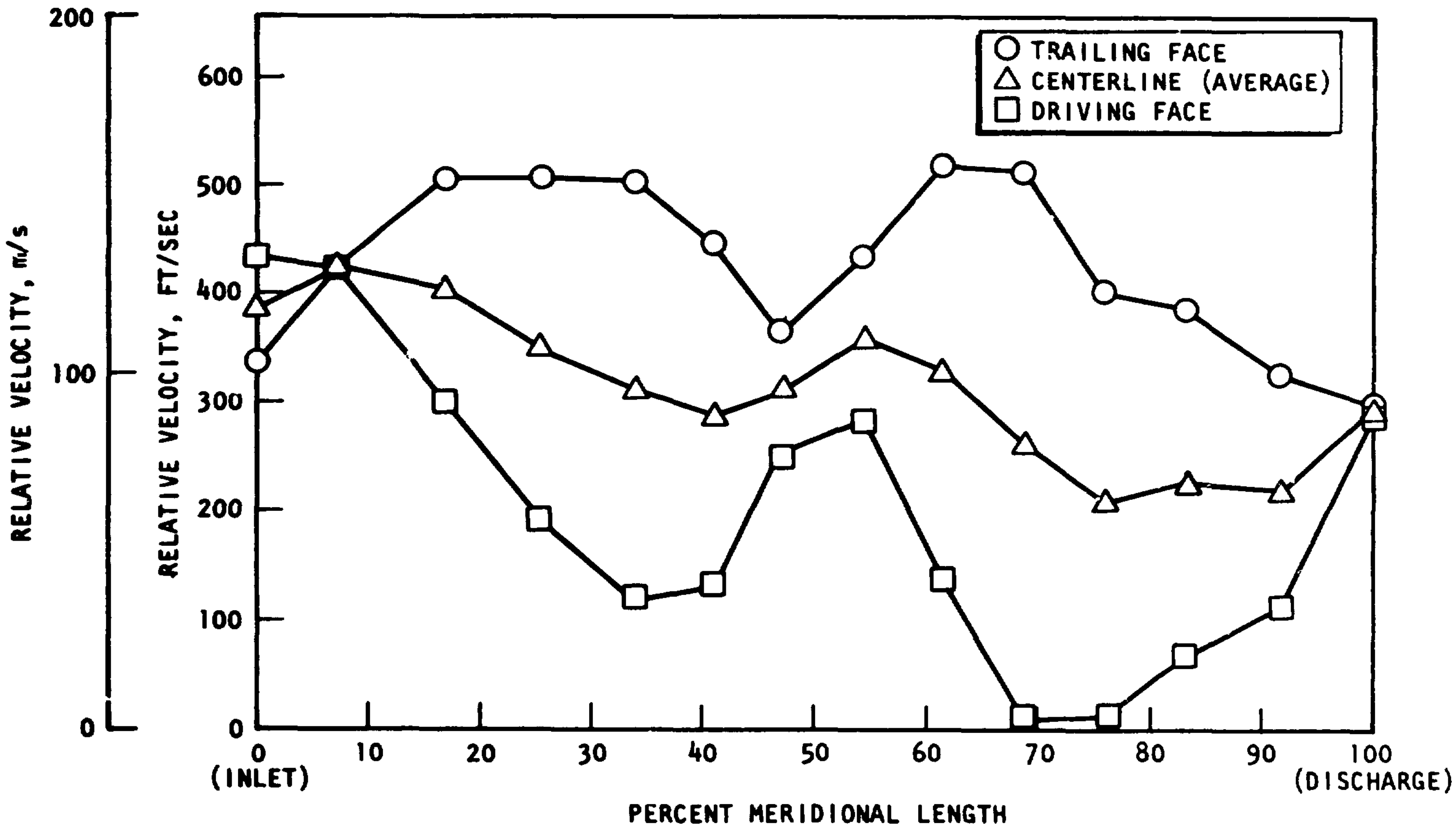

Figure 9. Mark 48 LO_2 Impeller Relative Velocities Inner Stream Tubes

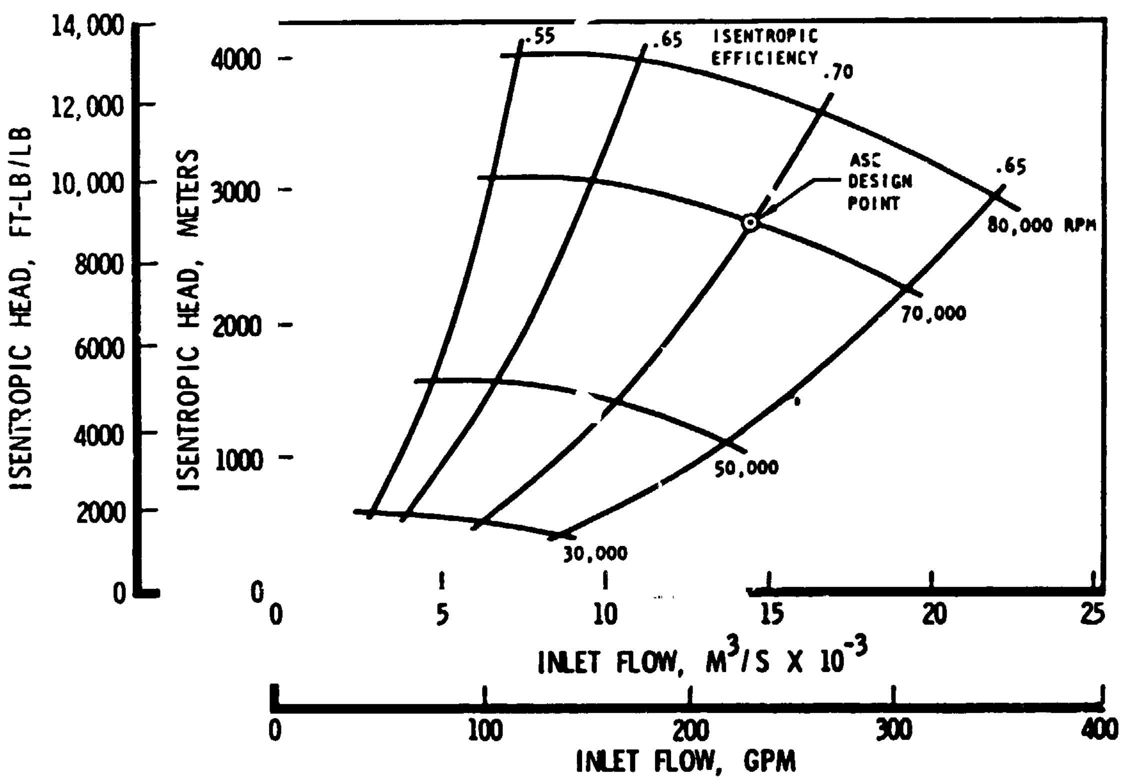

Figure 10. Mark 48 Oxidizer Pump Performance

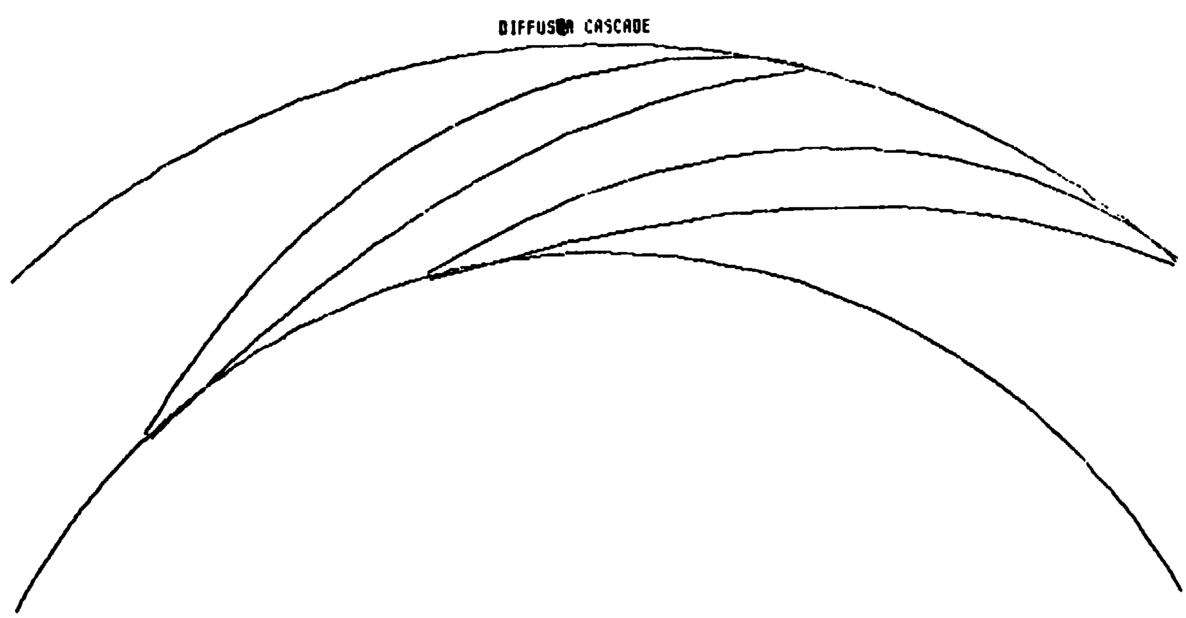

Figure 11. Mark 48-0 Diffuser Vane Profile

The volute area distribution and location of each area with respect to the tongue is calculated as a function of wrap angle, θ.

$$\theta = \frac{360 \times r_{in.} \, cu_{in.}}{W \, 0.144} \quad \frac{bdr}{r}$$

The total wrap angle is 6.28 radians (360 degrees) and Q, the flowrate, is expressed in ft^3/sec. The coefficient makes allowance for blockage to boundary layer buildup. Figure 12 shows the resulting area distribution as a function of the wrap angle.

Turbine Aerothermodynamic Analysis

Preliminary Analysis. The turbine aerothermodynamic analysis was based on the design parameters stated in Table 3. The developed power and operating speed were established at 638 kW (856 hp) and 7330 rad/s (70,000 rpm) by pump requirements.

A preliminary analysis was conducted under a prior program (Ref. 1) to determine the basic configuration of the turbine. This study indicated that a single-stage, partial-admission, impulse turbine would best meet the design requirements.

Turbine Aerothermodynamic Design. The turbine mean diameter of 11.94 cm (4.70 inches) was selected based on the results of a study to optimize turbine efficiency as shown in Fig. 13. The analysis used the design requirements data, a maximum hub-to-tip diameter ratio of 0.9 for partial admission, and efficiency trends with velocity ratio and partial admission from Ref. 3. Turbine blade speed was maintained within structural limits. The trade study compared the increase in performance from increased blade speed (larger diameter) to the reduction in performance due to reduced arc of admission. The smallest diameter was desirable to minimize turbopump weight. The 11.94 cm (4.70 inch) diameter resulted in a mean blade speed of 437 m/s (1435 ft/sec) at 7330 rad/s (70,000 rpm).

The design analysis was conducted utilizing Rocketdyne's turbine design computer programs which have been developed and verified with rocket engine turbine operational data and experimental turbine test data. The gas path element wall friction and turbulence losses were established from the expansion and kinetic energy coefficients, which are a function of the blade deflection angles and blade size. The program establishes gas path energy distribution and exit energy losses, and adjusts the turbine diagram efficiency. Table 3 presents a summary of the turbine design data, including the design requirements. Table 4 is a summary of the energy balance for the turbine design, and Table 5 presents the turbine blade path summary.

The turbine manifold was designed to minimize the inlet flange velocity head energy loss. Inlet flange velocity head energy is a significant part of the available energy in a low-pressure-ratio turbine. The manifold torus was sized to maintain the inlet flange velocity constant over the single arc of admission. The nozzle inlet was designed for minimum incidence within the structural constraints.

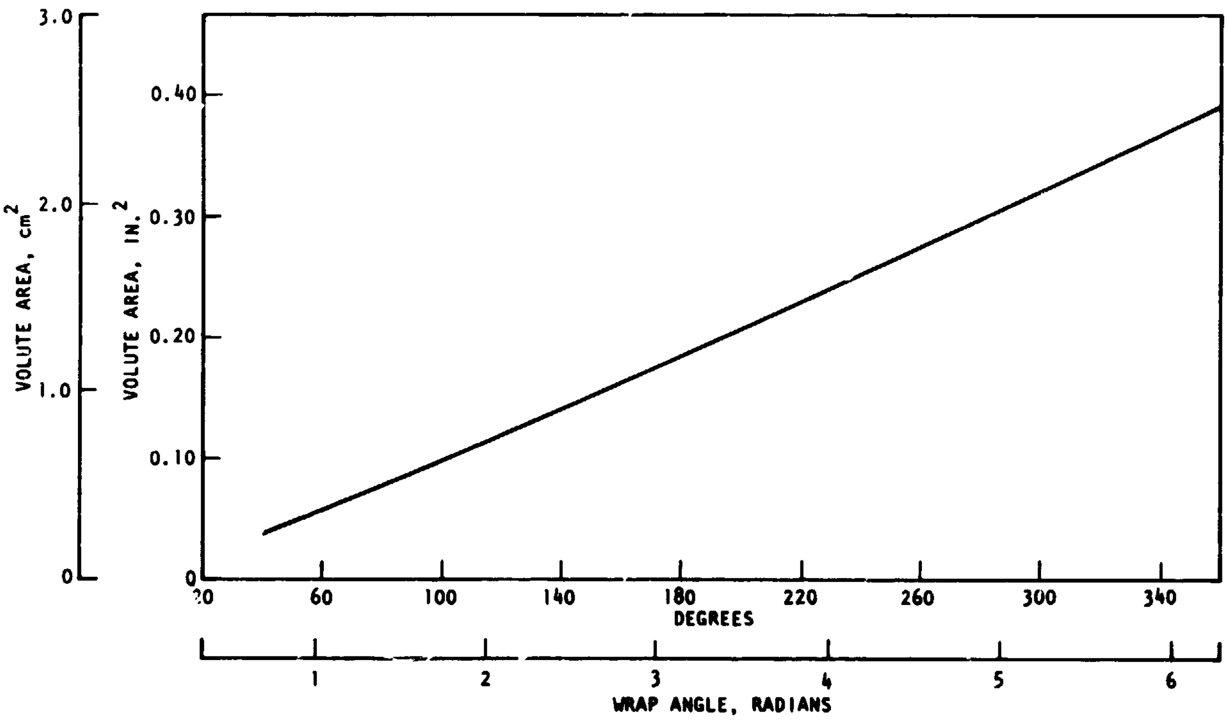

Figure 12. Mark 48-0 Volute Area Distribution

TABLE 3. MARK 48-0 HIGH-PRESSURE OXIDIZER TURBINE DESIGN SUMMARY

	Metric Units	English Units
Type - Single-Row Impulse, Partial-Admission Stage		
Working Fluid - LO_2/LH_2 (JANNAF Data)		
Turbine Mean Diameter, D_m	11.94 cm	4.70 inches
Speed, N	7330 rad/s	70,000 rpm
Total Turbine Inlet Temperature, T_{t_1}	1041 K	1874 R
Total Turbine Inlet Pressure, P_{t_1}	2321 N/cm^2	3366 psia
Static Turbine Exhaust Pressure, P_{s_2}	1630 N/cm^2	2364 psia
Pressure Ratio, PR (Total to Static)	1.424	1.424
Turbine Mass Flowrate, W_t	1.33 kg/s	2.92 lb/sec
Turbine Horsepower, hp_t	638 kW	856 hp
Pitch Line Velocity, U_m	437 m/s	1435 ft/sec
Nozzle Arc of Admission	28.5% 1.8 rad	28.5 103 degrees
Turbine Velocity Ratio, U/C_o (Total to Static)	0.343	0.343
Turbine Efficiency, η_t, (Total to Static)	0.598	0.598
Turbine Available Energy (Total to Static Δhat-S)	0.813×10^6 J/kg	348.9 Btu/lb
Turbine Specific Work, Δhw	0.485×10^6 J/kg	208.6 Btu/lb
Aerodynamic Mean Radius Loading, $(gJ\Delta h_w/2\Sigma U_m^2)$		1.26

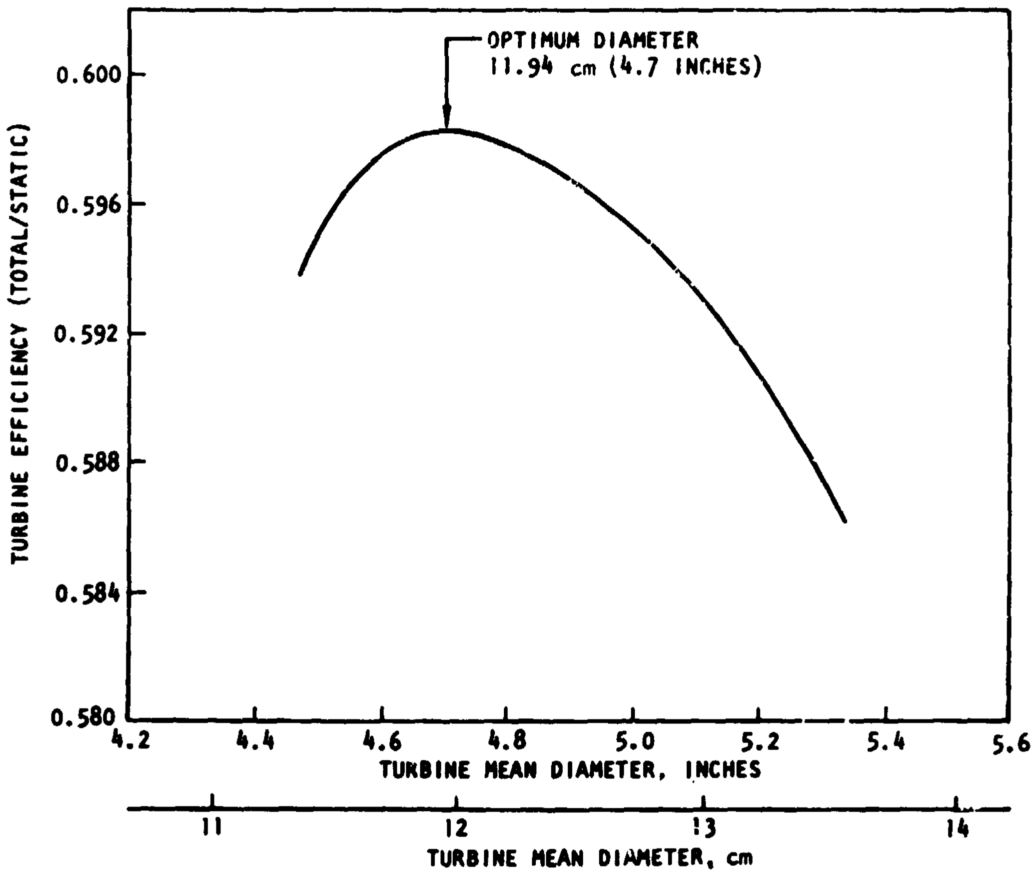

Figure 13. Mean Diameter Optimization

TABLE 4. TURBINE ENERGY DISTRIBUTION

	Energy		Available Energy, %
	kJ/kg	Btu/lbm	
Flow Passage Losses			
Nozzle Expansion Energy Loss	67.7	29.1	8.3
Rotor Kinetic Energy Loss	134.4	57.8	16.6
Turbine Leaving Loss	42.3	18.2	5.2
Additional Losses			
Tip Clearance Loss	17.4	7.5	2.1
Partial-Admission Losses			
Rotor Windage, Inactive Arc	44.4	19.1	5.6
Jet Expansion Loss in Rotor	4.2	1.8	0.5
End of Sector Pumping Loss	15.8	6.8	1.9
Turbine Specific Work	485.1	208.6	59.8
Turbine Available Energy	811.3	348.9	100.0

TABLE 5. MARK 48 LO_2 TURBINE BLADE PATH SUMMARY

(METRIC UNITS)

TURBINE GAS PATH

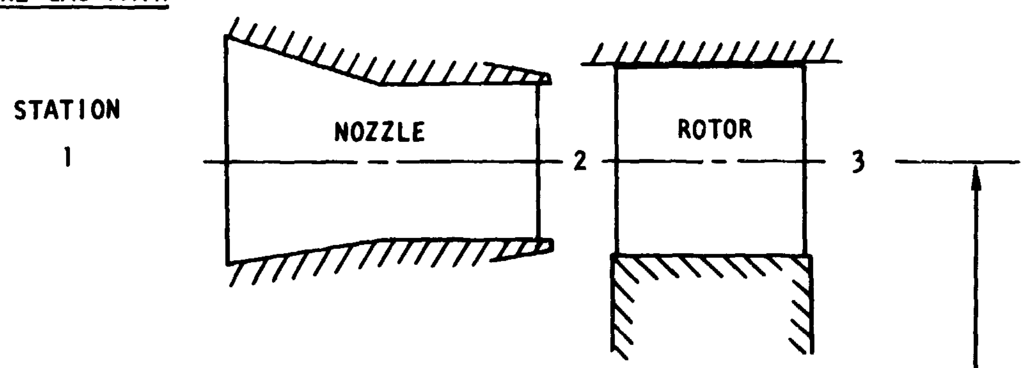

Working Fluid - LO_2/LH_2			
Speed, rad/s			7330
Power, kW			638
Gas Path Element	N-1		I-R
Number (Vanes, Blades)	7		79
Height, cm	0.61		0.72
Axial Width, cm	1.27	0.318	0.762
Inlet Angle, rad	0.79		0.44
Exit Vector Angle, rad	0.28*		0.44
Outlet Area, cm^2	1.51		3.00
Station	1	2	3
Pressure, Total, N/cm^2	2321		
Pressure, Static, N/cm^2		1630	1630
Temperature, K	1041	994	977
Specific Volume, m^3/kg		0.134	0.136

*0.017 radian deviation from blade angle

TABLE 5. (Concluded)

(ENGLISH UNITS)

TURBINE GAS PATH

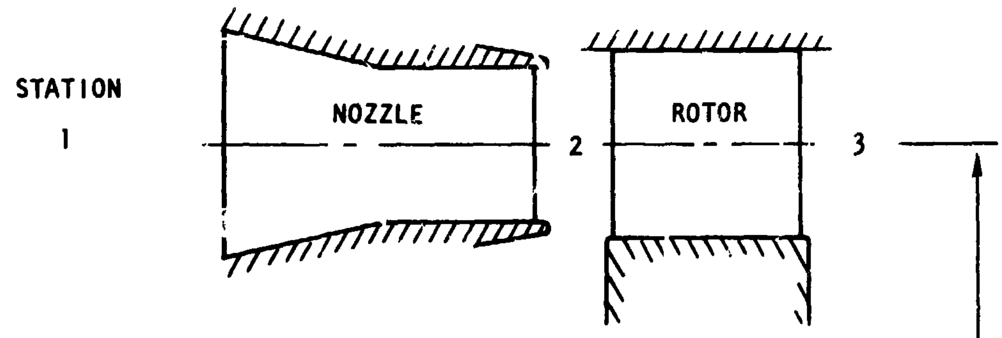

Working Fluid - LO_2/LH_2			
Speed, rpm	70,000		
Horsepower, hp	856		
Gas Path Element	N-1		1-R
Number (Vanes, Blades)	7		79
Height, inch	0.24		0.285
Axial Width, inch	0.50	0.125	0.300
Inlet Angle, degrees	45		25
Exit Angle, degrees	16 (vector angle)*		25 (vector angle)
Outlet Area, in.^{2}	0.2333		0.4658
Station	1	2	3
Pressure, Total, psia	3366		
Pressure, Static, psia		2364	2364
Temperature, R	1874	1798	1759
Specific Volume, ft^3/lb		2.156	2.189

*1 degree deviation from blade angle

The turbine isentropic available energy was 0.813×10^6 J/kg (348.9 Btu/lb) from the nozzle inlet plane to the rotor exit plane for the inlet temperature and pressure and outlet pressure noted in Table 3. The entire pressure drop occurs across the nozzle for the partial-admission, impulse design. The nozzle inlet angle of 0.79 radian (45 degrees; angle from the tangential) was selected for minimum incidence with adequate vane structural section. The nozzle outlet angle of 0.25 radian (15 degrees) was selected to provide high performance within the blade height limitations. The nozzle expansion energy coefficient was 0.916 per Ref. 4 for a total nozzle loss of 0.0676×10^6 J/kg (29.1 Btu/lb). The nozzle outlet velocity of 1221 m/s (4006 ft/sec) is shown in the velocity vector diagram in Fig. 14 and 15. The kinetic energy available to the rotor to produce work is presented by W_1 in Fig. 14 and 15.

The rotor blade inlet angle was set for zero incidence. The rotor outlet angle of 25 degrees was selected for high work output and low leaving loss. For the selected rotor axial width of 0.76 cm (0.300 inch), the rotor kenitic energy coefficient was 0.589 per Ref. 4. Rotor outlet kinetic energy is represented by W_2 in Fig. 14 and 15. The rotor leaving loss velocity is represented by C_2 of 291 m/s (955 ft/sec). Rotor kinetic energy loss was 0.123×10^6 J/kg (57.8 Btu/lb).

The vector diagram specific work shown in Fig. 14 and 15 was 0.567×10^6 J/kg (244 Btu/lb) for the flow through the nozzle and rotor passages. Additional losses exterior to the flow passages reduce the turbine work output. These additional losses, summarized in Table 4, include tip clearance losses and partial-admission losses.

Tip clearance loss was determined using the empirically established efficiency ratio data reported by Cordes in Ref. 5 for an unshrouded impulse turbine as a function of tip clearance/blade height ratio. The radial tip clearance established by mechnaical design considerations was 0.127 mm (0.005 inch) which resulted in clearance/blade height ratio of 0.0175. Tip clearance losses are significant for unshrouded, high-turning rotating blades. Any increase in operating tip clearance will result in significant efficiency degradation.

Partial-admission losses were minimized in this design by maintaining the arc of admission greater than 25% of the circumference and by grouping the nozzles in one sector of admission. Partial-admission losses of blade windage in the inactive section of the rotor, nozzle jet expansion through the rotor, and pumping loss at the end of the sector were determined using correlations by Traupel and Suter, and by Stenning reported by Horlock (Ref 6).

The summation of the gas path losses, tip clearance losses, and partial-admission losses resulted in a turbine output specific work of 0.485×10^6 J/kg (208.6 Btu/lb as listed in Table 4.

Nozzle Vane Profile. The nozzle profile was designed to accelerate and direct the turbine flow correctly to achieve design performance. The low-turning, radially convergent design was selected for use with the tangential inlet, constant-velocity, low-pressure-loss, turbine inlet manifold. The 0.79 radian (45 degree) nozzle inlet angle was selected as a structural and performance compromise.

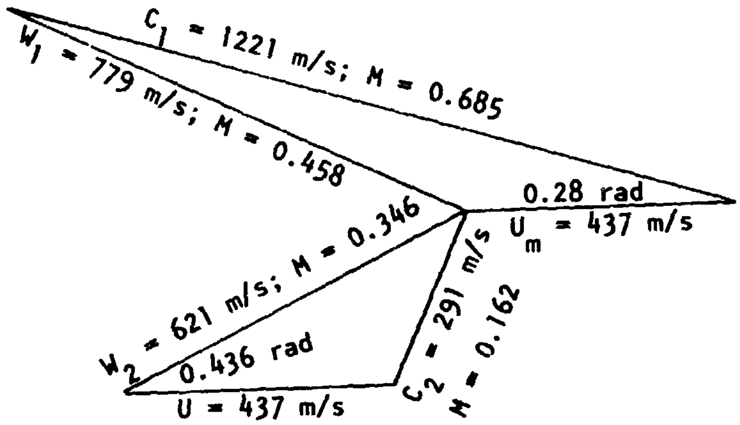

FLOW PASSAGE SPECIFIC WORK

$= U_m \ \Delta \ C_u$

$= U_m \ (C_1 \cos \alpha_1 + W_2 \cos \beta_2 - U_m)$

$= 437 \ (1221 \cos 0.28 + 621 \cos 436 - 437)$

$= 0.567 \times 10^6$ J/kg

Figure 14. Turbine Gas Path Calculation Velocity Vector Diagram (Metric Units)

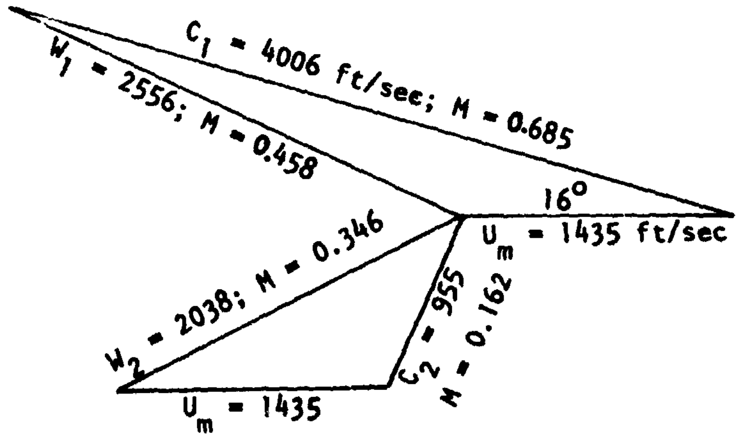

FLOW PASSAGE SPECIFIC WORK

$$= \frac{U_m \ \Delta \ C_u}{g \ J}$$

$$= \frac{U_m \ (C_1 \cos \alpha_1 + W_2 \cos \beta_2 - U_m)}{g \ J}$$

$$= \frac{1435 \ (4006 \cos 16^\circ + 2038 \cos 25^\circ - 1435)}{32.17 \times 778.2}$$

= 224 Btu/lbm

Figure 15. Turbine Gas Path Calculation Velocity Vector Diagram (English Units)

Seven nozzle passages, grouped together, were used to provide a low prime number with an acceptable throat aspect ratio near 2 with the low-turning nozzle. Seven nozzles result in passage dimensions that can be fabricated. The axial width of 1.27 cm (0.5 inch) provided adequate passage length for gradual radial convergence and a rectangular outlet throat section. Leading and trailing edges are radial.

The nozzle outlet throat area was determined from the gas path calculation throat flow area and the passage fillet area. The gas path flow area includes the effects of the nonideal gas characteristics and compressibility for the high-pressure hydrogen/oxygen combustion products.

The nozzle profile is shown in the turbopump housing drawing in Fig. 16. The profile has a straight back suction surface from the throat to the trailing edge. The trailing edge has a 0.195 mm (0.0075 inch) radius to minimize nozzle wake intensity. The straight back suction surface angle was set at 0.25 radian (15 degrees). The pressure and suction surfaces upstream of the throat are defined by circular arcs. The profile section is adequate to carry the structural loads resulting from the high pressure in the torus. The nozzle inlet was sized to accept the manifold torus velocity with minimum losses and blockage.

The profile surface velocity distribution was calculated for the pitch diameter section assuming constant blade height using the Douglas-Neumann analysis program reported in Ref. 7. The suction and pressure surface velocity distribution are shown in Fig. 17. The velocity distribution showns gradual acceleration, with maximum overspeed of 1.1 of the exit velocity. The analysis confirms the fluid turning required of the flow passage. The actual inlet/outlet velocity ratio would be lower than indicated because the nozzle inlet height is larger than assumed.

Rotor Blade Profile. Maximum axial width was used for low weight, consistent with minimum manufacturable throat opening. Blade spacing was set to give a prime blade number for an aerodynamic loading coefficient (Zweifel number) consistent with previous rocket engine turbine practice.

Rotor blade throat area was determined from the required gas path throat flow area ratioed by the actual arc of admission to equivalent full-admission flow area plus the rotor root fillet area. Throat opening at the mean diameter was determined from the rotor total throat area divided by the number of blades and the blade height.

The rotor blade profile at the mean diameter is shown in Fig. 18. The profile was designed in accordance with Rocketdyne's established practice for this type of inpulse blading. This procedure calls for zero incidence angle according to the gas path calculation and a slightly convergent passage to provide a smooth velocity pattern. The velocity distribution for the rotor blade is presented in Fig. 19.

The rotor blade height overlaps the nozzle outlet height by 1.143 mm (0.045 inch) or 19%, as indicated in Table 5. Nozzle/rotor blade axial spacing was set at 3.175 mm (0.125 inch) to minimize nozzle wake effects at the rotor inlet. Rotor blades are unshrouded for ease of fabrication and structural reasons.

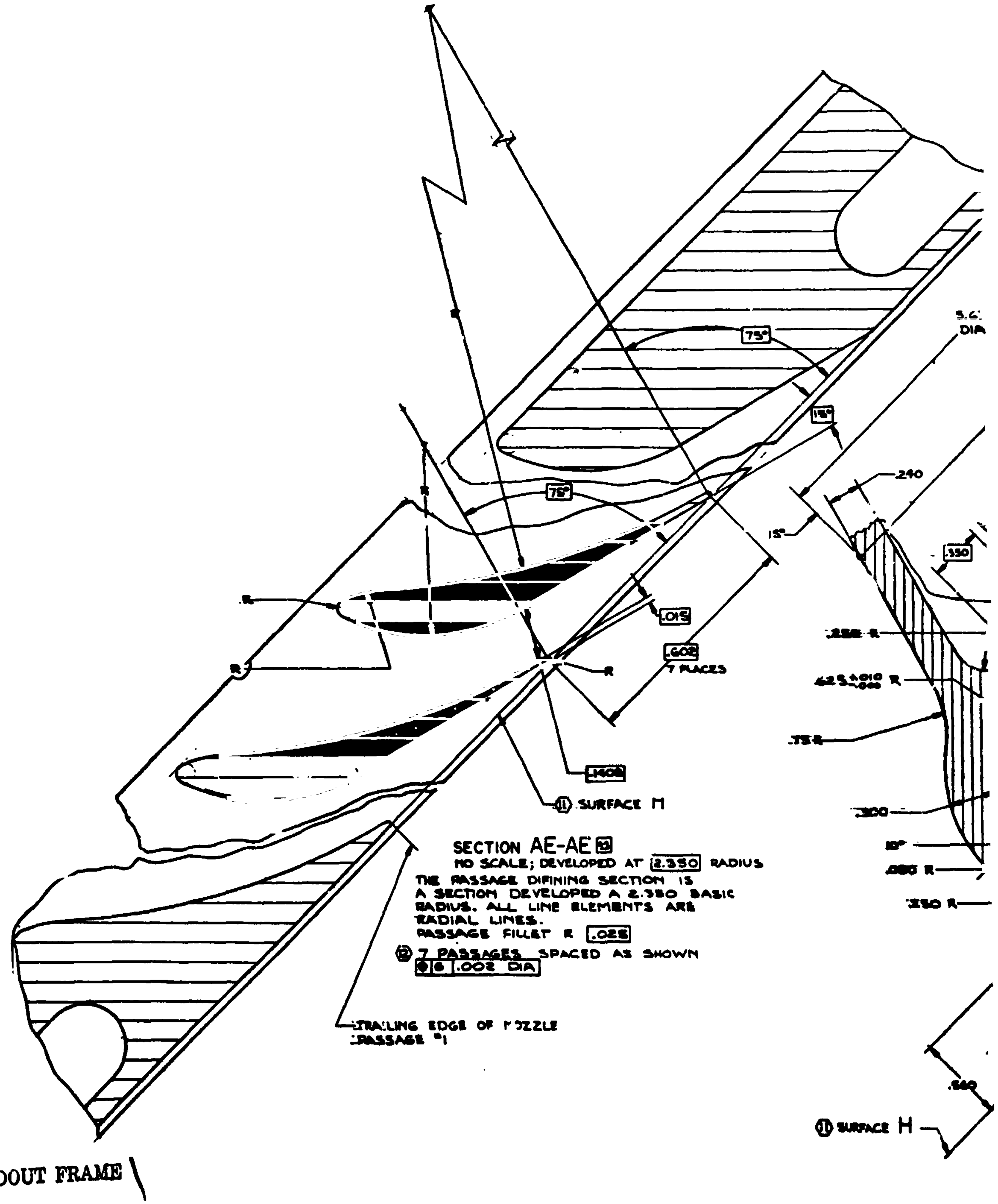

FOLDOUT FRAME

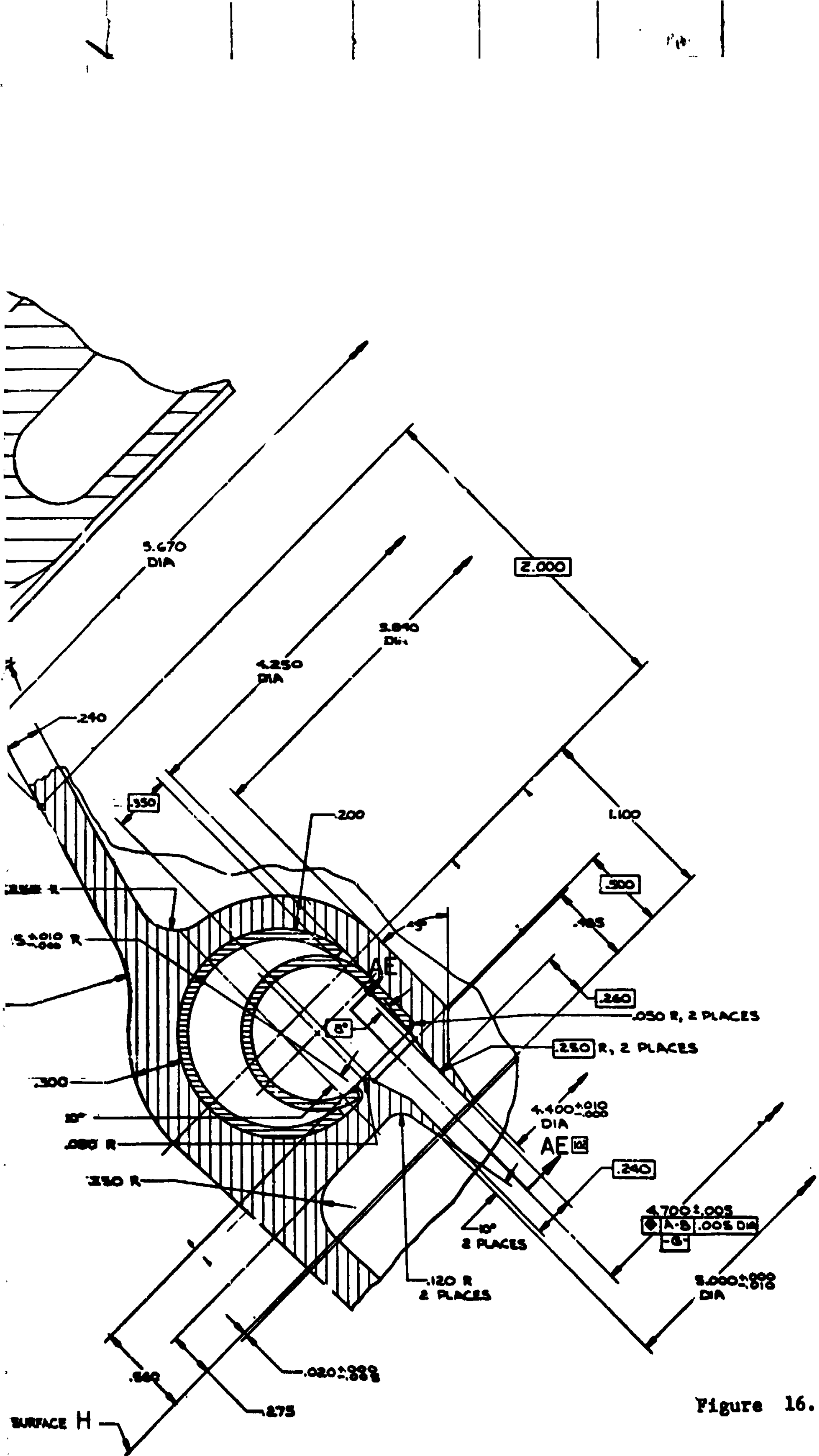

Figure 16. LO_2 Turbopump Turbine Nozzle

FOLDOUT FRAME 2

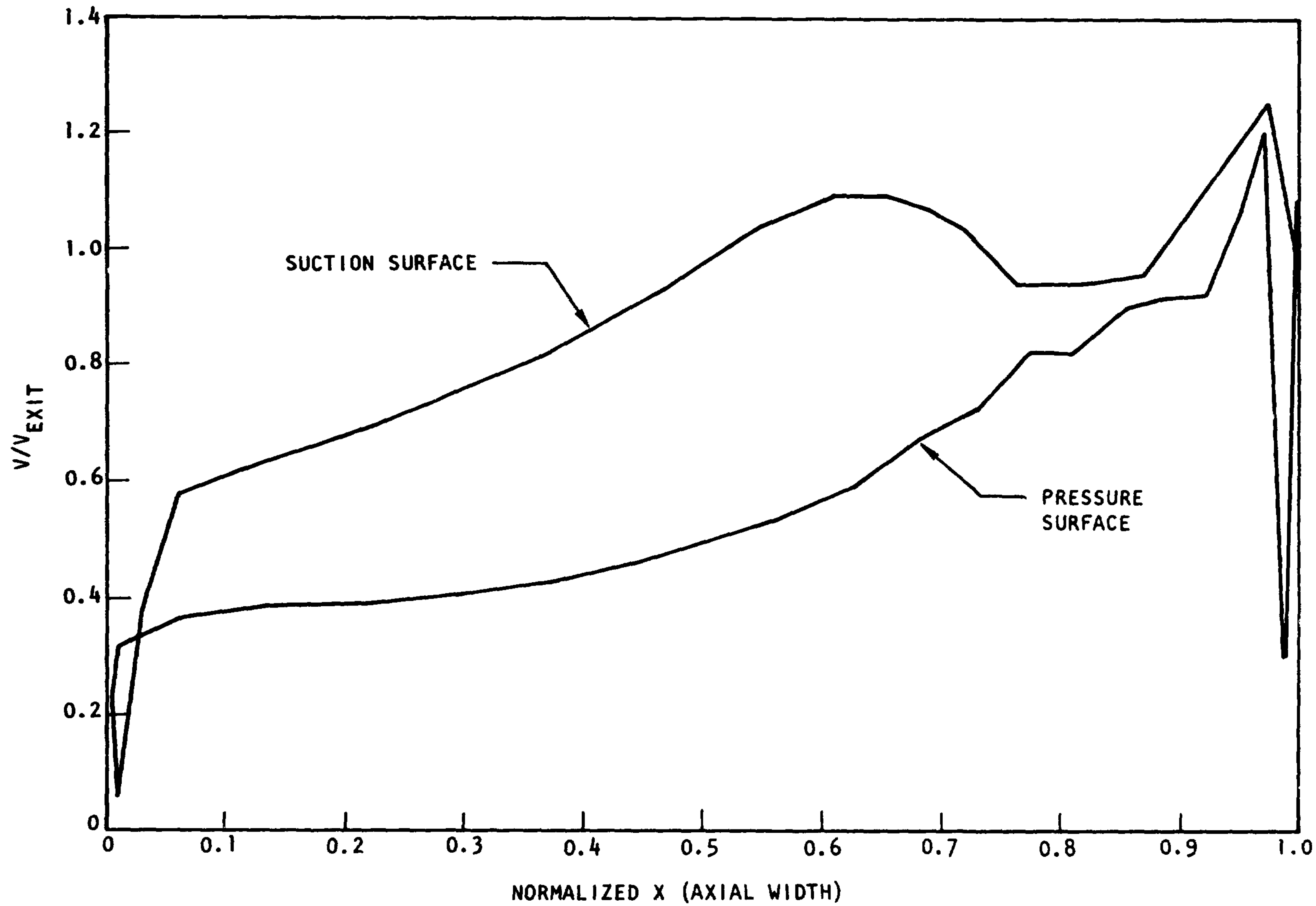

Figure 17. Mark 48-0 Nozzle Normalized Douglas-Neumann Output

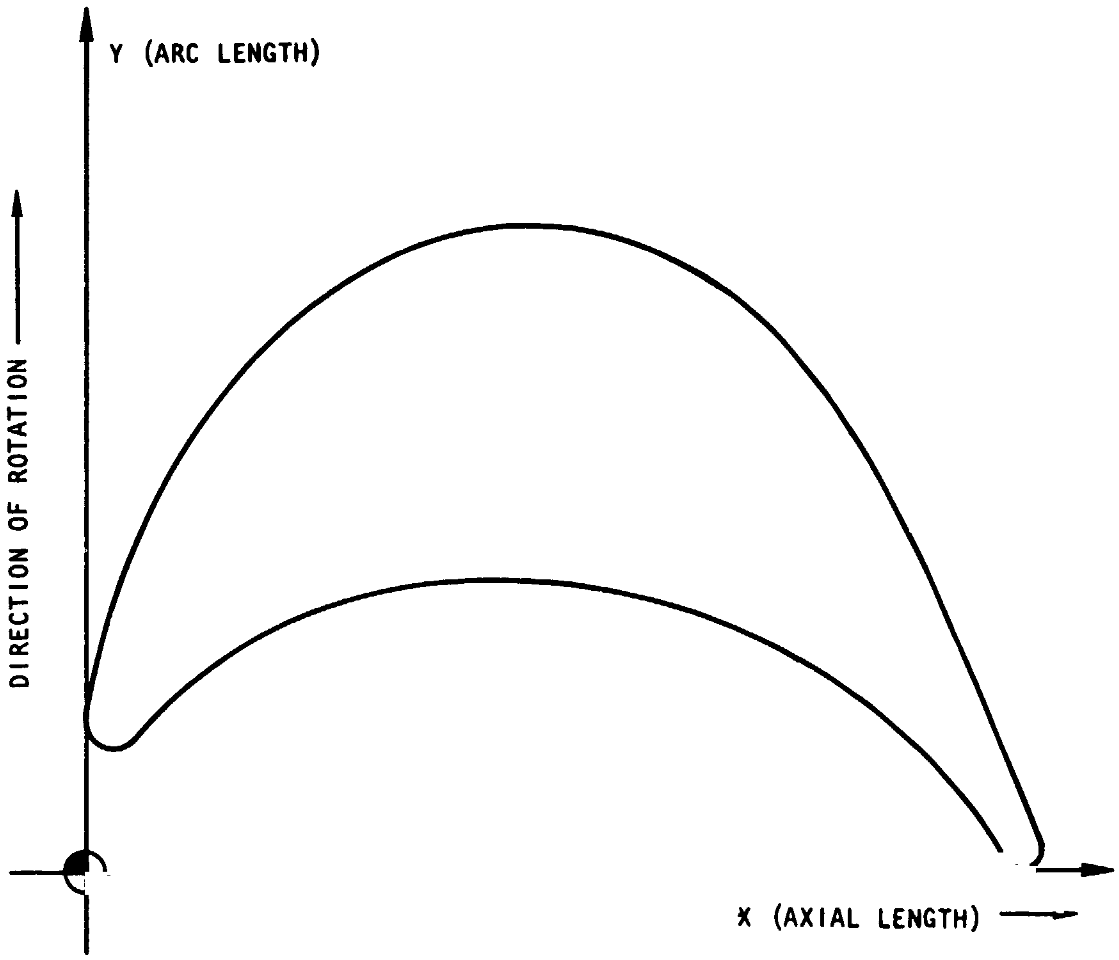

Figure 18. Blade Cross Section on Developed Cylinders
Radius = 2.35)

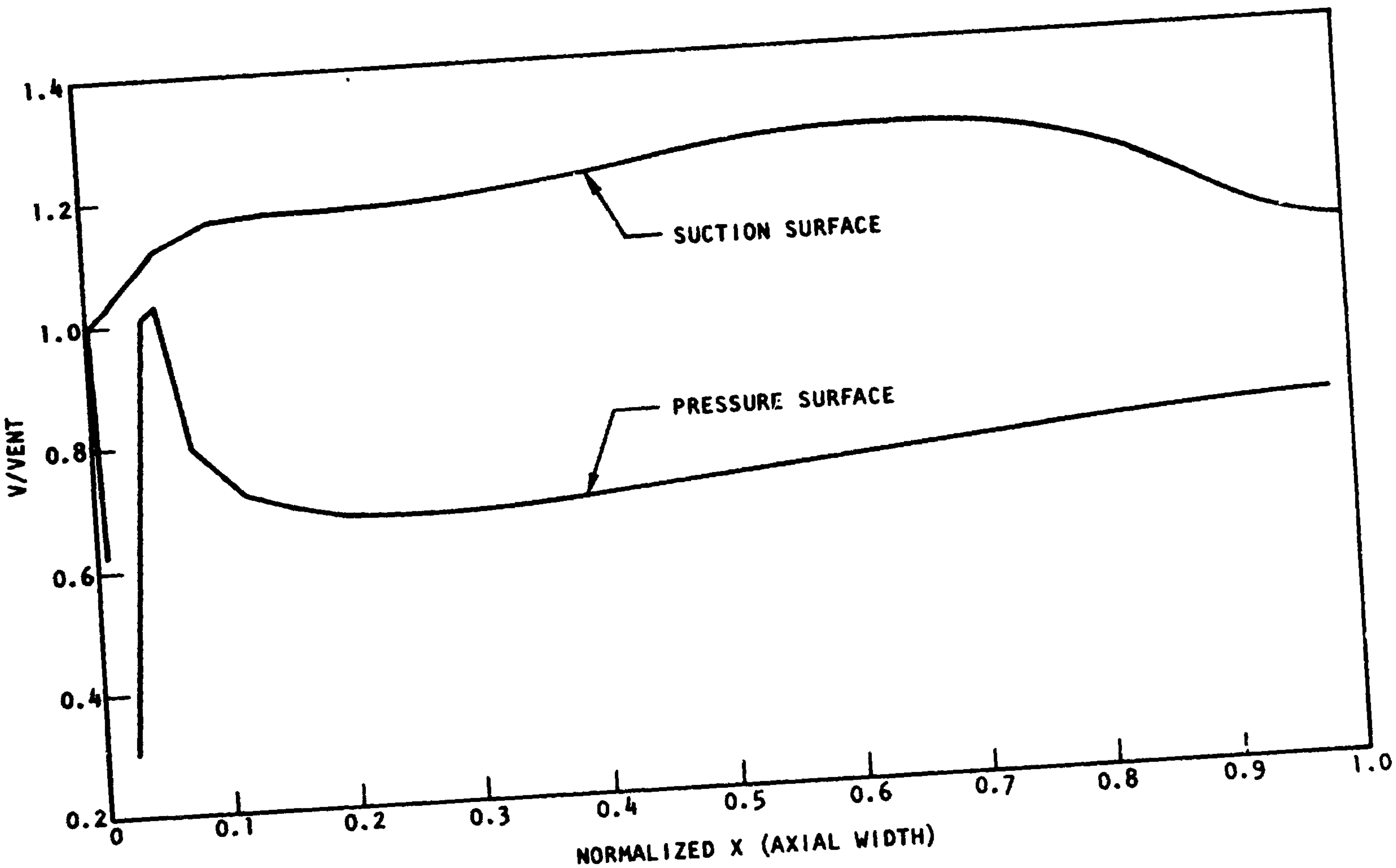

Figure 19. Mark 48-0 Rotor Normalized Douglas-Neumann Output Surface Velocity Distribution

Turbine Predicted Performance. The predicted turbine efficiency as a function of mean velocity ratio is shown in Fig. 20. A design efficiency of 0.598 at a mean velocity ratio of 0.343 is shown in Fig. 20. The off-design performance characteristic was established using the test results from Ref. 3 for a turbine of similar size and arc of admission. Crossplots of Ref. 3 test data indicated near liner torque-speed characteristics. The characteristic slope for the Mark 48-0 turbine arc of admission was plotted through the design point to establish the turbine off-design performance.

The predicted turbine flow parameter characteristics are shown in Fig. 21 The flow parameter as defined in Fig. 21 is a function of turbine pressure ratio and rotational speed over the square root of inlet temperature ratio. The flow parameter characteristics were determined from an iterative computer calculation matching flow element areas with turbine operating conditions.

It should be noted that Fig. 21 is constructed for gaseous hydrogen as the working fluid; however, it can be used also for LO_2/LH_2 combustion products by applying proper corrections for fluid properties.

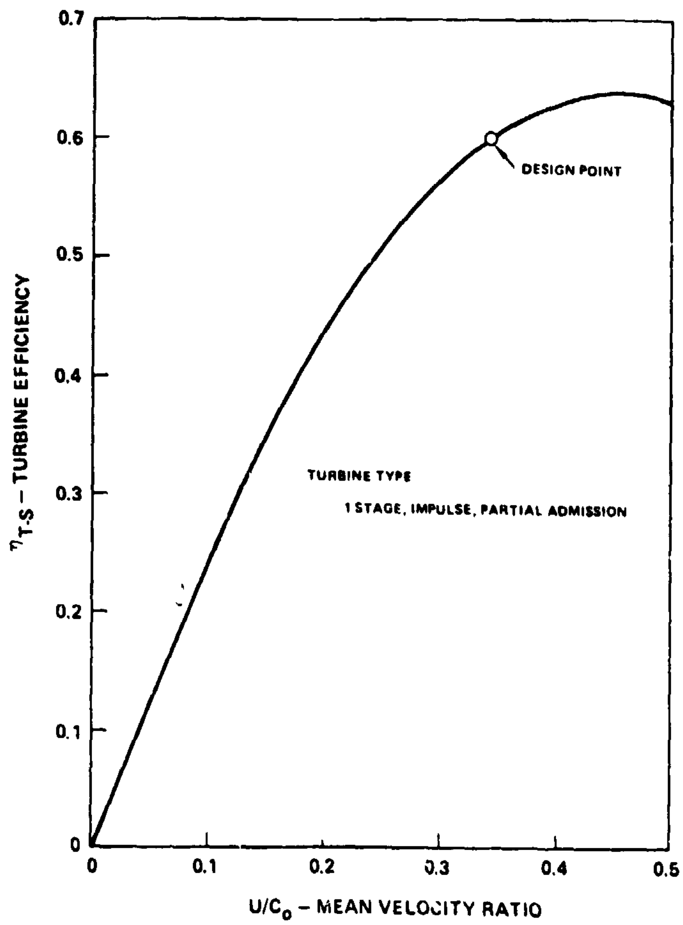

Figure 20. Small High Pressure LOX Turbopump Predicted Turbine Performance Map

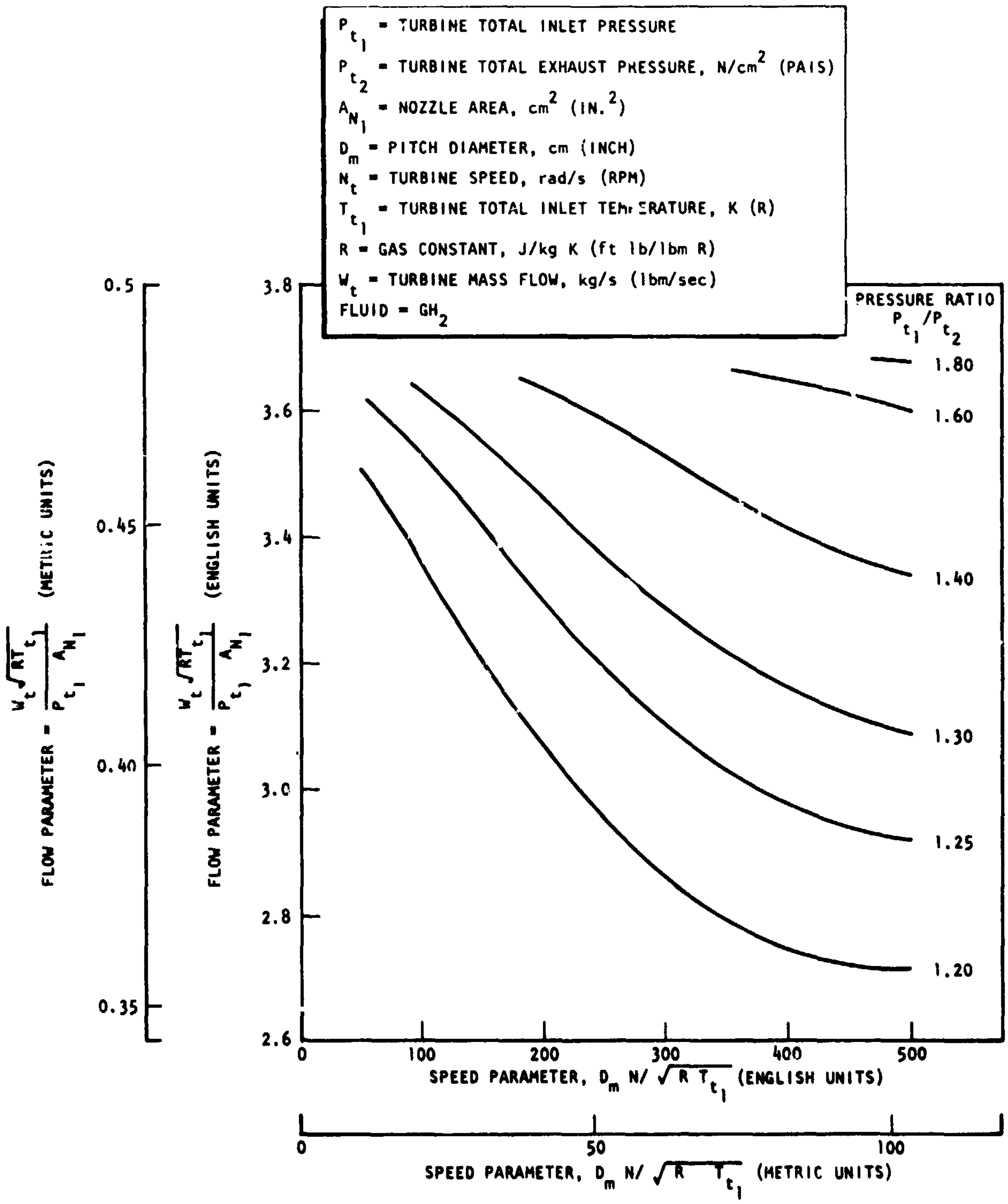

Figure 21. Mark 48-O Turbine Flow-Speed Parameters

Axial Thrust Control

The unbalanced axial thrust forces generated by the inducer-impeller, the slinger mounted between pump bearing and seals, and the turbine are balanced by a thrust balance piston machined integral with the impeller. A number of different axial thrust systems were investigated. They include impellers with different wear ring diameters, inboard pump and turbine bearing arrangement, inboard pump and outboard turbine bearing arrangement, turbine disk with and without wear rings, as well as with and without a slinger between bearing and seals.

The configuration finally selected is shown in Fig. 22. The forces acting on turbine, impeller, and slinger are calculated for nominal design conditions using the pump map shown in Fig. 23. For the forces acting on the slinger, it is assumed that vapor is generated on the slotted slinger side.

The total balance piston travel is set to 2.54 mm (0.010 inch). Both the high- and low-pressure orifices are of the nonrubbing type. The diametral orifice clearance is set to 0.066 and 0.0178 mm (0.0026 and 0.0007 inch), respectively. Figure 24 shows the pressure behind the impeller and slinger as they are affected by the different balance piston positions. In Fig. 25 the net balance piston restoring force is shown as a function of the balance piston travel.

Bearing Design

The Mark 48-0 bearings are 20 mm bore, angular-contact ball bearings arranged in two spring-preload pairs. The forward pair is located immediately behind the pump impeller and is cooled by LOX. The aft pair is located on the downstream side of the turbine disc and is cooled by LH_2.

The Mark 48-0 bearings are identical to those designed earlier for the Mark 48-F turbopump. Dual use of the same bearing is technically feasible because the design speed of the fuel pump is higher, 9948 rad/s (95,000 rpm) than that of the LOX pump, 7330 rad/s (70,000 rpm). Economy in procurement was also effected by purchasing only one type of specially designed bearing.

The internal geometry of the bearing was optimized for 9948 rad/s (95,000 rpm) and formalized into the Rocketdyne Source Control Drawing, RES1174 (Fig. 26). There was no existing bearing with satisfactory features, so a special bearing was designed and fabricated with the following features:

1. Bearing Size. The dimensions of the dynamic components were minimized to reduce the inertial forces due to speed as far as possible. At the time of selection, the LOX pump's bearing DN value of 1.4×10^6 was within the state of technology for LH_2-cooled bearings, but was beyond the 1.1×10^6 established in Rocketdyne IR&D testing for LOX-cooled bearings. In subsequent testing, a 7.5-hour life at 1.8×10^6 DN was achieved for the SSME LOX pump bearings.

   The pitch diameter and outer race outer diameter were made different than those existing for a standard metric envelope to accommodate, at minimum size, the thicker inner race cross section required to

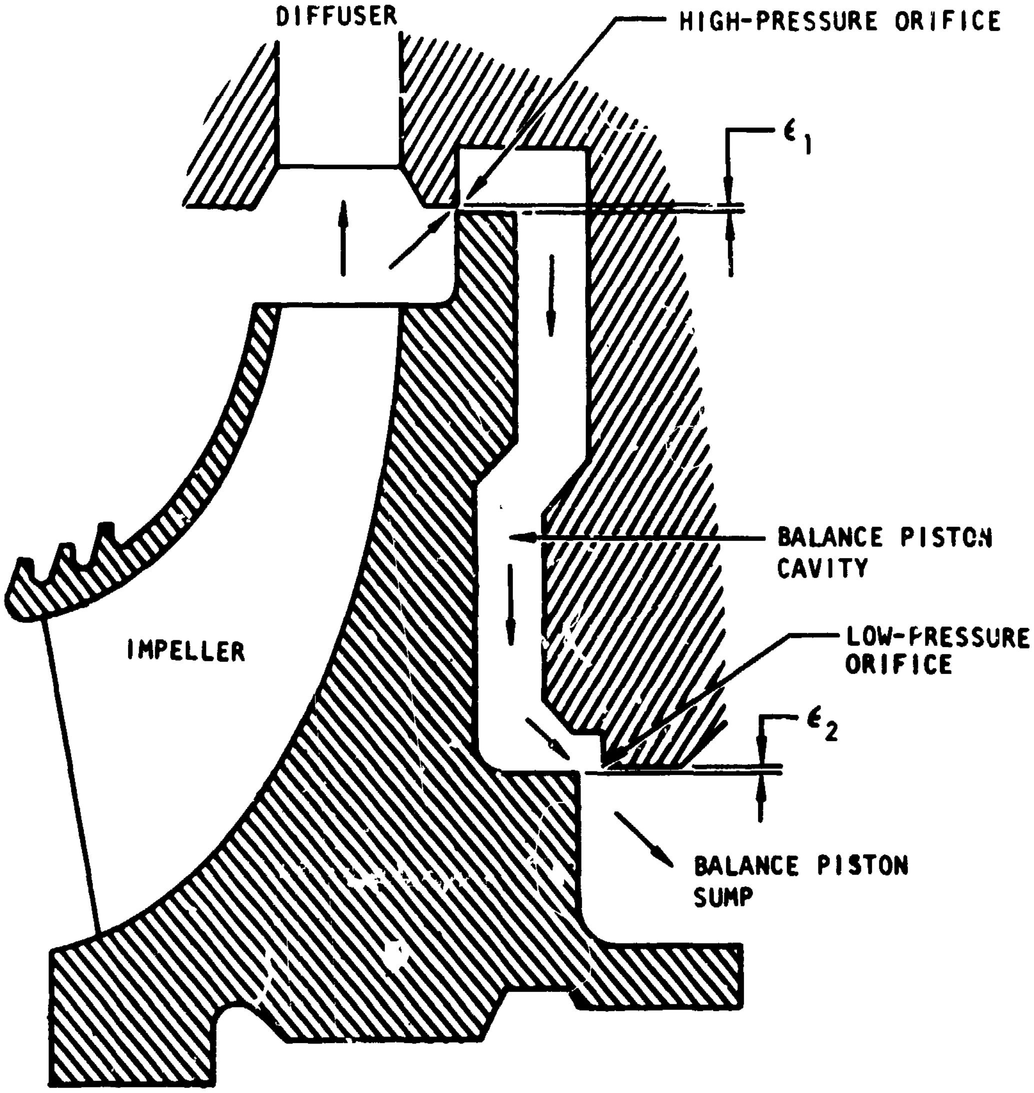

Figure 22. Mark 48-0 Balance Piston

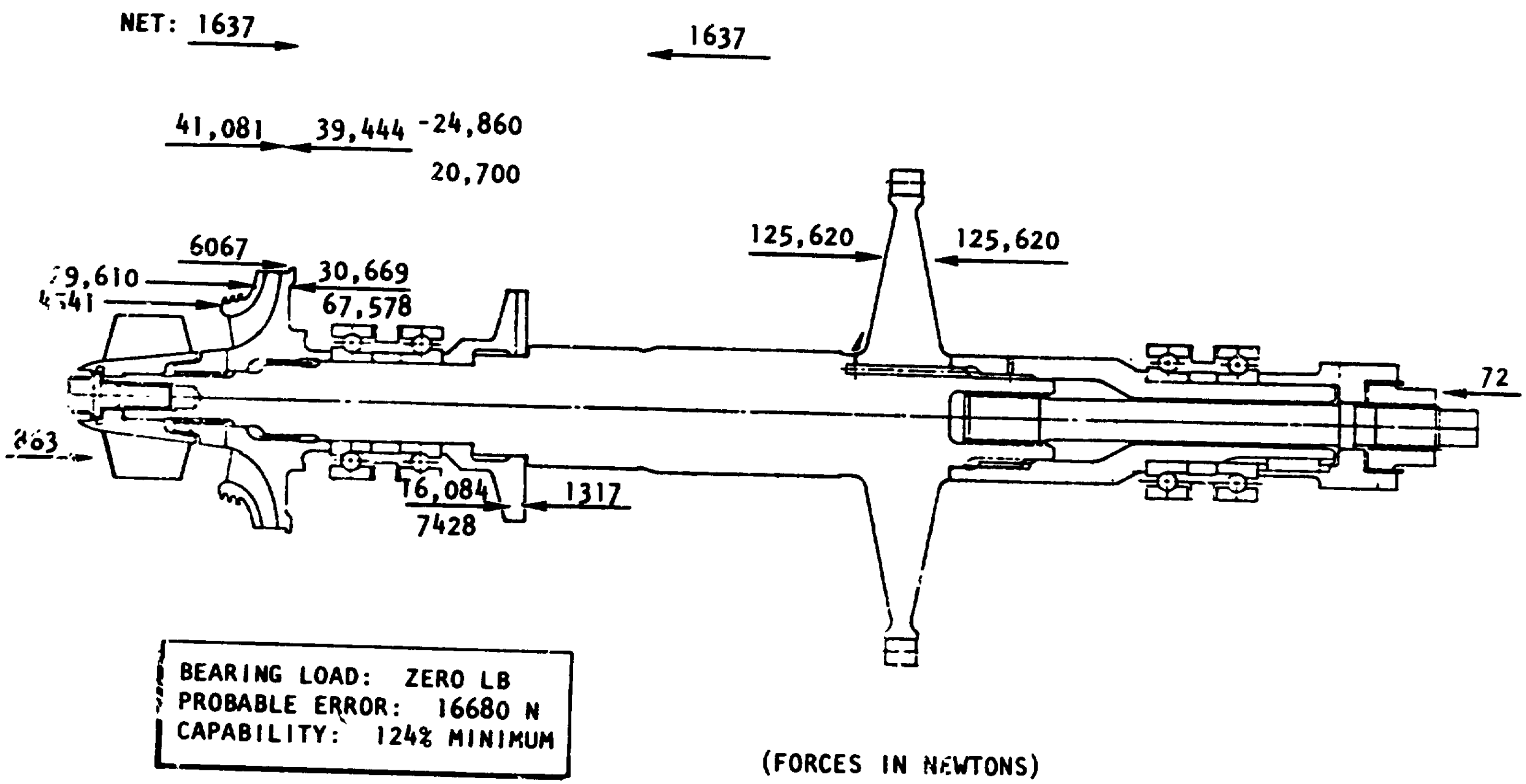

Figure 23. High-Pressure Oxidizer Turbopump Axial Forces

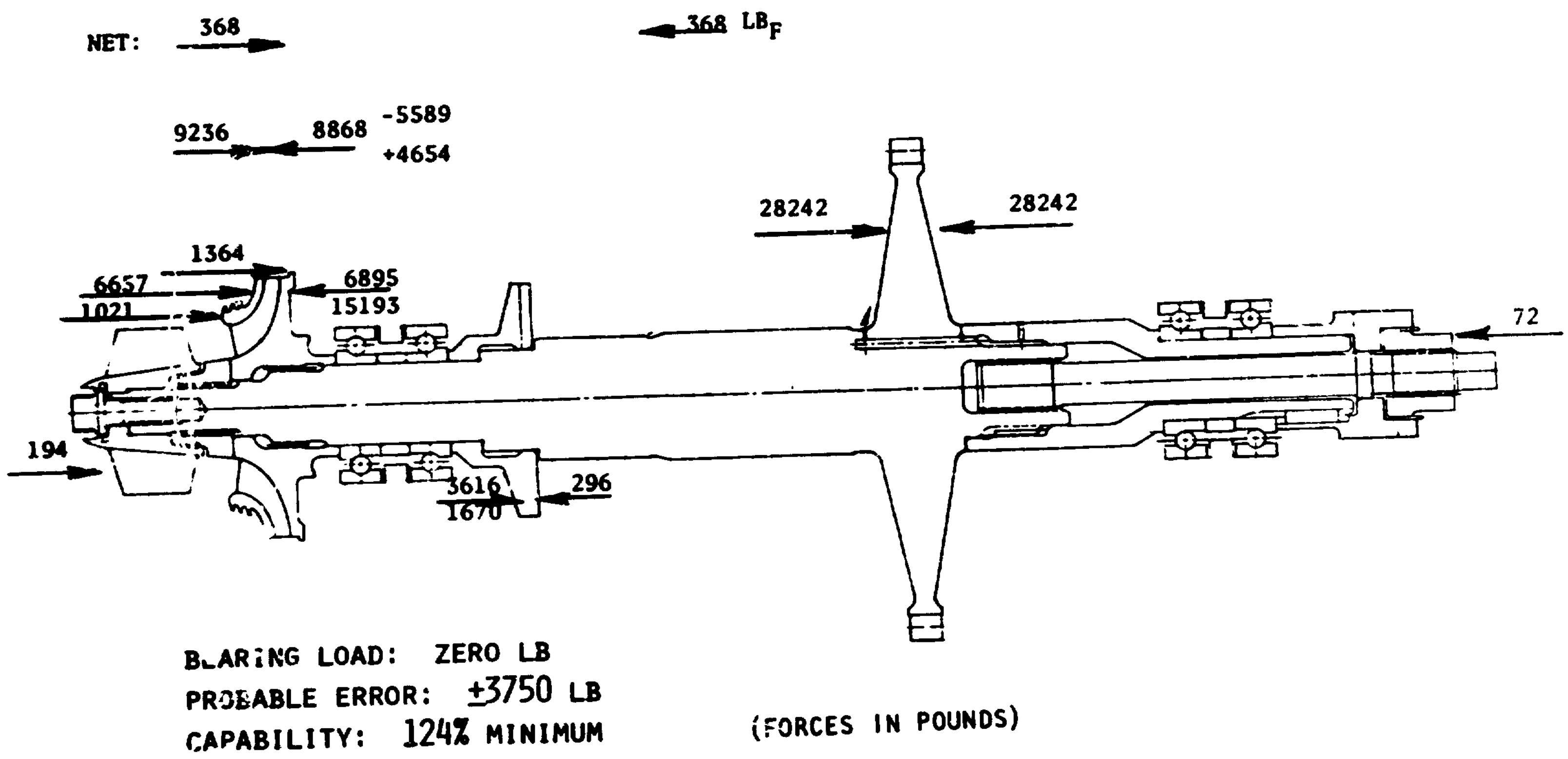

Figure 23. (Concluded)

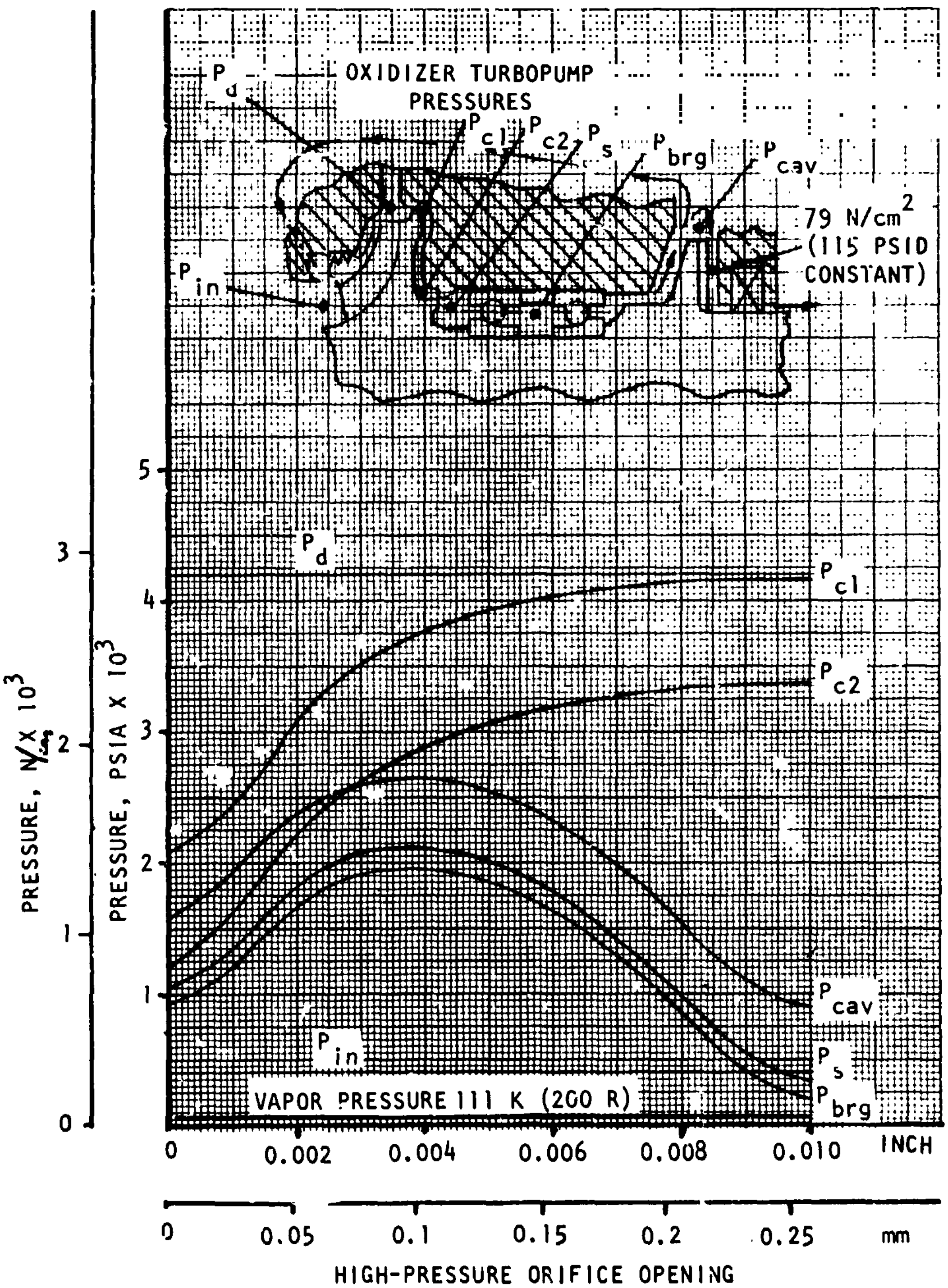

Figure 24. Mark 48-0 Turbopump Balance Piston Pressure Levels

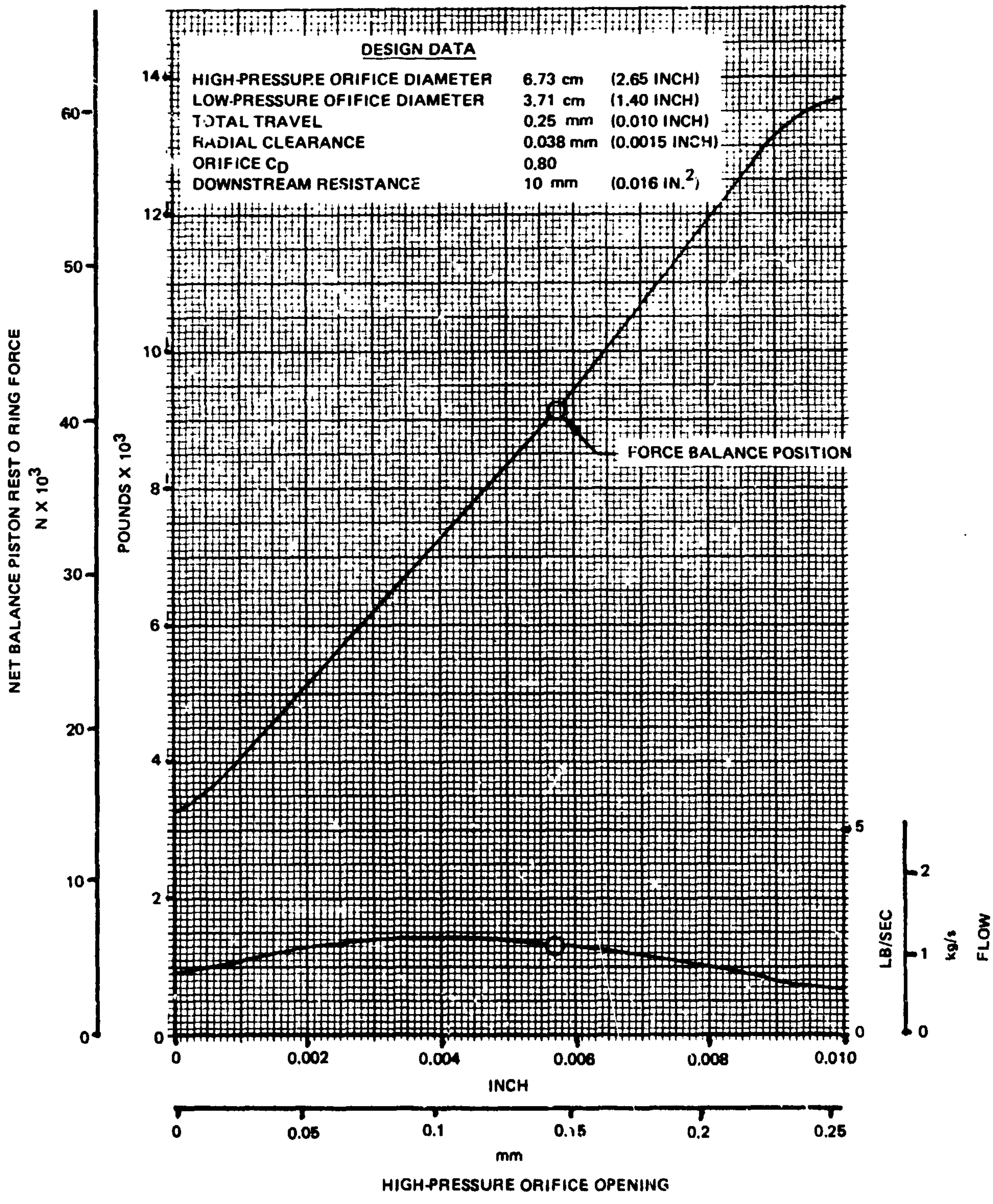

Figure 25. Mark 48-0 Turbopump Balance Piston Performance

CHARACTERISTIC	ENGLISH UNITS	SI UNITS
ENVELOPE DIMS. -		
BORE	.78725 $^{+.00015}_{-.00000}$ DIA.	20 mm
OUTER DIA.	1.5354 $^{+.0000}_{-.0002}$ DIA.	39 mm
WIDTH (INDIVIDUAL RINGS)	.3937 $^{+.0000}_{-.0100}$	10 mm
(ACROSS BEARING)	.393 $^{+}_{-}$.002 10 m	
INTERNAL GEOMETRY -		
PITCH DIA.	1.175 DIA. (REF.)	29.8 mm
RACE RADII (OUTER RACE)	52% OF BALL DIA. (REF.)	
(INNER RACE)	53% OF BALL DIA. (REF.)	
DIAMETRAL CLEARANCE (UNFITTED)	.0020 TO .0023 IN.	0.051 TO 0.058 mm
(OPERATING)	.0011 TO .0014 IN. (REF.)	0.028 TO 0.036 mm
BALL COMPLEMENT (NUMBER)	TEN	
(DIAMETER)	.1875 DIA. (NOMINAL)	4.76 mm
SHOULDER HEIGHTS (OUTER RACE)	20% OF BALL DIA. (REF.)	
(INNER RACE)	23% OF BALL DIA. (REF.)	
CAGE CLEARANCES (BALL POCKET)	.020 TO .025 IN.	0.51 TO 0.64 mm
(GUIDING LAND)	.003 TO .009 IN.	0.08 TO 0.22 mm
MATERIALS -		
RACES	CEVM 440-C R_c 58-62	
BALLS	CEVM 440-C R_c 60-64	
CAGE	GLASS FABRIC SUPPORTED TEFLON (ARMALON)	
CAGE WEB THICKNESS (AT PITCH DIA.)	.156 IN. (REF.)	3.96 mm

8. IDENTIFY FACES "A"&"B"
7. BALLS SHALL BE AFBMA GRADE 5
6. BEARING TOLERANCES NOT SHOWN SHALL BE PER ABEC 7.
5. CLEAN & PACKAGE FOR LIQUID HYDROGEN SERVICE. (CLEAN & [
4. THE ARMALON CAGE SHALL MEET REQUIRMENTS OF RB0130-01.
3. ONLY THE ITEM DESCRIBED ON THIS DWG WHEN PROCURED FR SUPPLIER LISTED, IS APPROVED BY ROCKETDYNE, CANOGA PARK, C IN THE APPLICATION SPECIFIED HEREON. A SUBSTITUTE ITEM SHA USED WITHOUT PRIOR TESTING & APPROVAL BY ROCKETDYNE.
2. THE ITEM SHALL BE DURABLY & LEGIBLY MARKED PER MIL-STD-1 ADDITION THE ROCKETDYNE CONTROL DWG NO. SHALL BE MARKED C
1. MFG. SHALL PREPARE ANY NEW DWGS REQD & ASSIGN PART NO. F & SHALL OBTAIN ROCKETDYNE ENGRNG. REVIEW OF PROPOSED CH

FOLDOUT FRAME 1

SI UNITS
20 mm
39 mm
10 mm
29.8 mm
.051 TO 0.058 mm
.028 TO 0.036 mm
4.76 mm
.51 TO 0.64 mm
.08 TO 0.22 mm
3.96 mm

REVISIONS

LTR	DESCRIPTION		DATE	APPROVED
	1. MAY BE REWORKED 2. CANNOT BE REWORKED 3. RECORD CHANGE 4. NOW SHOP PRACTICE 5. PARTS MADE OK			

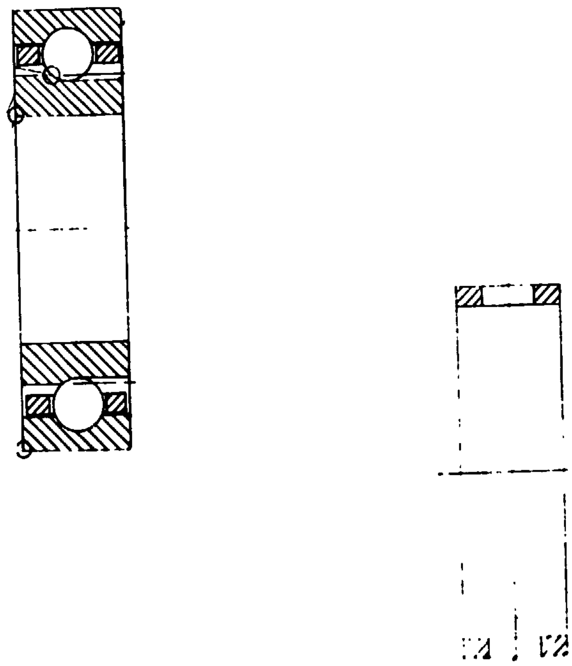

5
SHALL BE PER ABEC 7.
YDROGEN SERVICE. (CLEAN & DRY)
REQUIRMENTS OF RB0130-013
HIS DWG WHEN PROCURED FROM THE
ROCKETDYNE, CANOGA PARK, CALIF. FOR USE
HEON. A SUBSTITUTE ITEM SHALL NOT BE
APPROVAL BY ROCKETDYNE.
GIBLY MARKED PER MIL-STD-130. IN
DWG NO. SHALL BE MARKED ON THE ITEM.
REQD & ASSIGN PART NO. PER MIL-D-1000
RNG. REVIEW OF PROPOSED CHANGES.

ROCKETDYNE CONTROL NO. & SUFFIX NO.	APPROVED SOURCE OF SUPPLY MFR. NAME AND ADDRESS	CODE IDENT.	MFR. PART NO.
-01 ( )			

Figure 26. Bearing Design

SOURCE CONTROL DRAWING

UNLESS OTHERWISE SPECIFIED DIMENSIONS ARE IN INCHES AND APPLY PRIOR TO FINISH

DO NOT SCALE PRINT

DRN F. BERNARD

Rocketdyne
North American Rockwell

BEARING, BALL -
ANGULAR CONTACT

D 02602 RES1174

SCALE 4/1

RES1174

FOLDOUT FRAME 2

withstand the bolt tension load in the Mark 48 LH_2 turbopump. The thicker inner race is also less prone to brittle fracture from tensile and thermal stresses.

2. Ball Complement. A ball diameter of 4.7625 mm (0.1875 inch) was selected in preference to the off-the-shelf bearing size of 5.556 mm (0.21875 inch) to reduce the centrifugal force and extend the fatigue life of the outer race. The number of balls was set at 10 to maintain a web thickness in the cage of over 3.81 mm (0.150 inch) to provide adequate wear life and cage strength.

3. Race Radii. The race radii, which are expressed as curvature (percent of ball diameter), were selected to obtain maximum fatigue life consistent with practical manufacturing limitations. The outer race conforms closely to the ball surface with a 52% curvature. Lower curvatures closer conformity) is avoided because excessive nonrolling action will occur in the ball-race contact. In addition, contact angle will vary rapidly for small changes in bearing internal clearance due to manufacturing tolerances, press fits, and thermal expansion.

   The bearing fatigue life is maximized if the lives of the inner and outer races are equal. Therefore, the inner race curvature of 53% was selected to balance the race lives. Use of a higher (less conforming) curvature on the inner race is a reversal of commercial practice for low-speed bearings. It was done here to maintain reasonable life, contact angle, and clearance for the overall bearing while maximizing the fagitue life of the outer race, which is adversely affected by ball centrifugal forces at high speeds.

4. Race Shoulder Heights. The race shoulders were made deep enough to contain the ball contact "prints" at the contact stress-limited axial load. This configuration takes full advantage of the bearing's potential capacity and at the same time does not excessively restrict the coolant flow area.

5. Cage Dimensions. The cage is outer land guided, so its outer diameter is dictated by the outer race inner diameter (dependent on bearing pitch diameter, ball diameter, and shoulder, height) and adequate minimum clearance. Cage diametral clearance, 0.076 mm (0.003 inch) minimum at ambient temperature, is based on experience with larger cryogenic bearings and scaled to bearing size. The cage inner diameter was selected to maximize coolant flow area and to ensure that the ball equators would meet the cylindrical section of the ball pockets with a minimum of 0.254 mm (0.010 inch) margin. The ball is then prevented from "plowing under" the cage. The resulting diametral clearance between the cage inner diameter and the inner race outer diameter is 1.778 mm (0.070 inch) to 1.930 mm (0.076 inch), resulting in a minimum coolant flow area of 86.6 mm^2 (0.134 $in.^2$). The cage axial cross-sectional area is 170 mm^2 (263 $in.^2$). To provide adequate cage wear-life and strength, the cage web thickness between the ball pockets was held to 3.81 mm (0.150 inch)

minimum in selecting the number of balls (10). The resulting nominal cage web thickness at the pitch diameter is 3.96 mm (0.156 inch).

The cage ball pocket clearance was made large, 0.51 to 0.64 mm (0.025 inch) to permit ball position adjustments during operation without excessive cage forces. Adequate pocket clearance has been found to greatly reduce the amount of heat generated at the cage where radial loads or misalignments occur.

6. Diametral Clearance. The specified diametral clearance as measured on an unmounted bearing was based on the value required for dynamic operation with additional amounts to compensate for the expansion of the inner race due to press fit on the shaft and centrifugal expansion of the inner race at speed.

7. Analysis. The selected bearing design was analyzed using a digital computer program that calculates forces, deflections, and stresses for each ball, and overall forces, deflections, and fatigue life of the individual races and the entire bearing. The spring preloads required for satisfactory operation of the bearing were calculated using an emprically developed relationship of ball size, speed, contact angle, and pitch diameter. The preloads required are 245 N (55 pounds) for the LOX pump bearing.

In selecting the bearing design, a comparison was made of the effect on life of using the minimum bore diameter with the resulting bearing pitch diameter and required preload. Figure 27 presents the B_1 (99% survival) life for a 19 mm bore and 20 mm bore bearing. The 20 mm size was selected to obtain a standard bore size as well as provide some margin on the shaft size. As can be seen in Fig. 27, no substantial benefit in life would have been achieved by using a 19 mm bore bearing. The 10,472 rad/s (100,000 rpm) speed used in the Mark 48-F bearing analysis was later reduced to 9948 rad/s (95,000 rpm), but this change would not alter the results significantly. Figure 28 presents the selected design's fatigue life (shown here as B_{10} or 90% survival life) as a function of axial load at the Mark 48-F speed of 9948 rad/s (95,000 rpm). The preload criterion resulted in a required axial load of 431 N (97 pounds) at this condition. For the LOX pump, Fig. 29 indicates the calculated life at the required preload of 245 N (55 pounds).

Figure 30 presents the analytical values of radial stiffness (used in shaft dynamic analysis) as a function of axial load and speed. Radial stiffness affects shaft dynamic response and is affected by axial load; therefore, proper design and deflection control of the preload springs is important. Figure 31 presents the effect of speed on the relative axial deflections for given axial loads. This relationship was used in specifying the thickness of the inner race spacers so that both the following will be achieved:

1. Adequate preload at speed

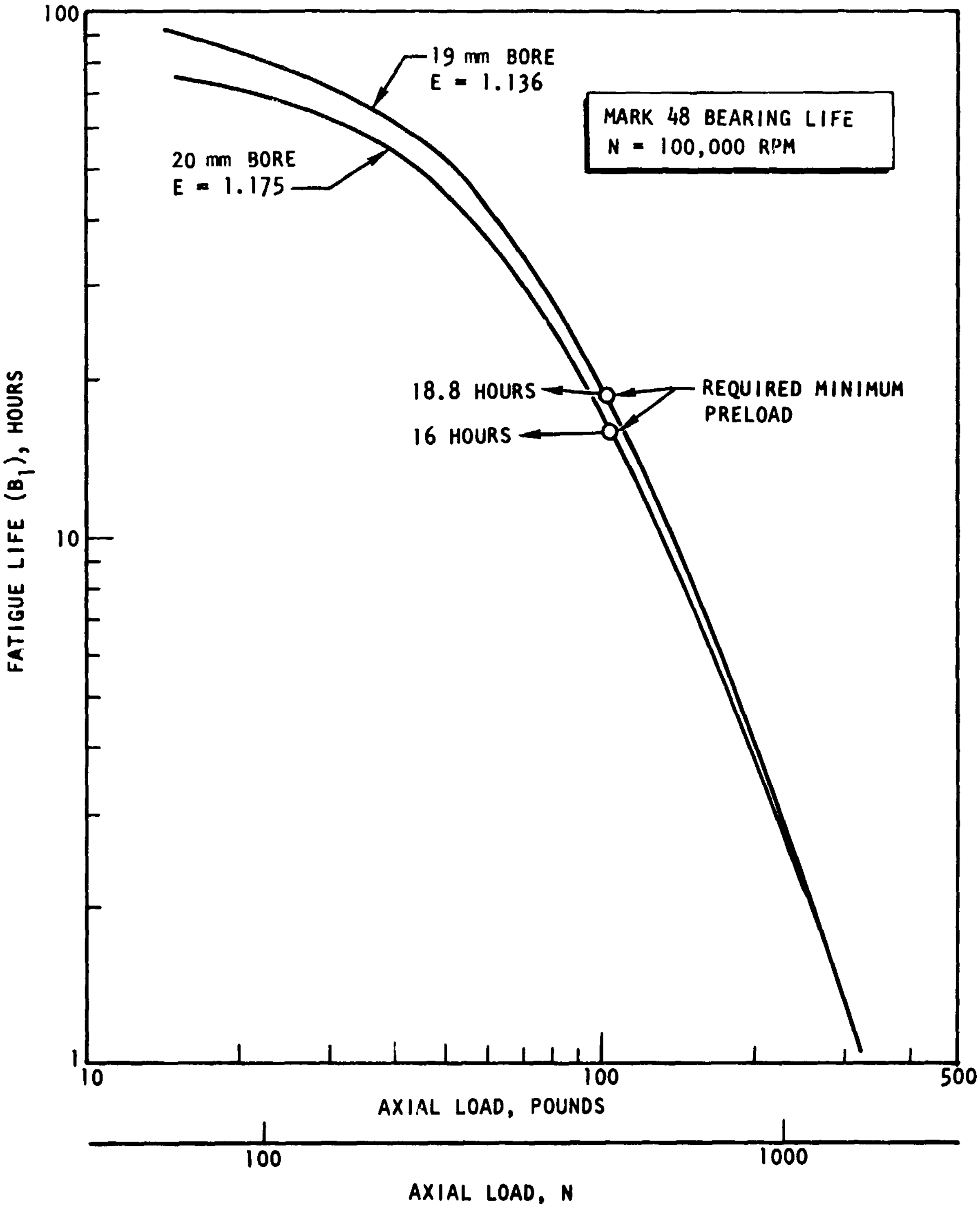

Figure 27. Mark 48-F Bearing B_1 Life

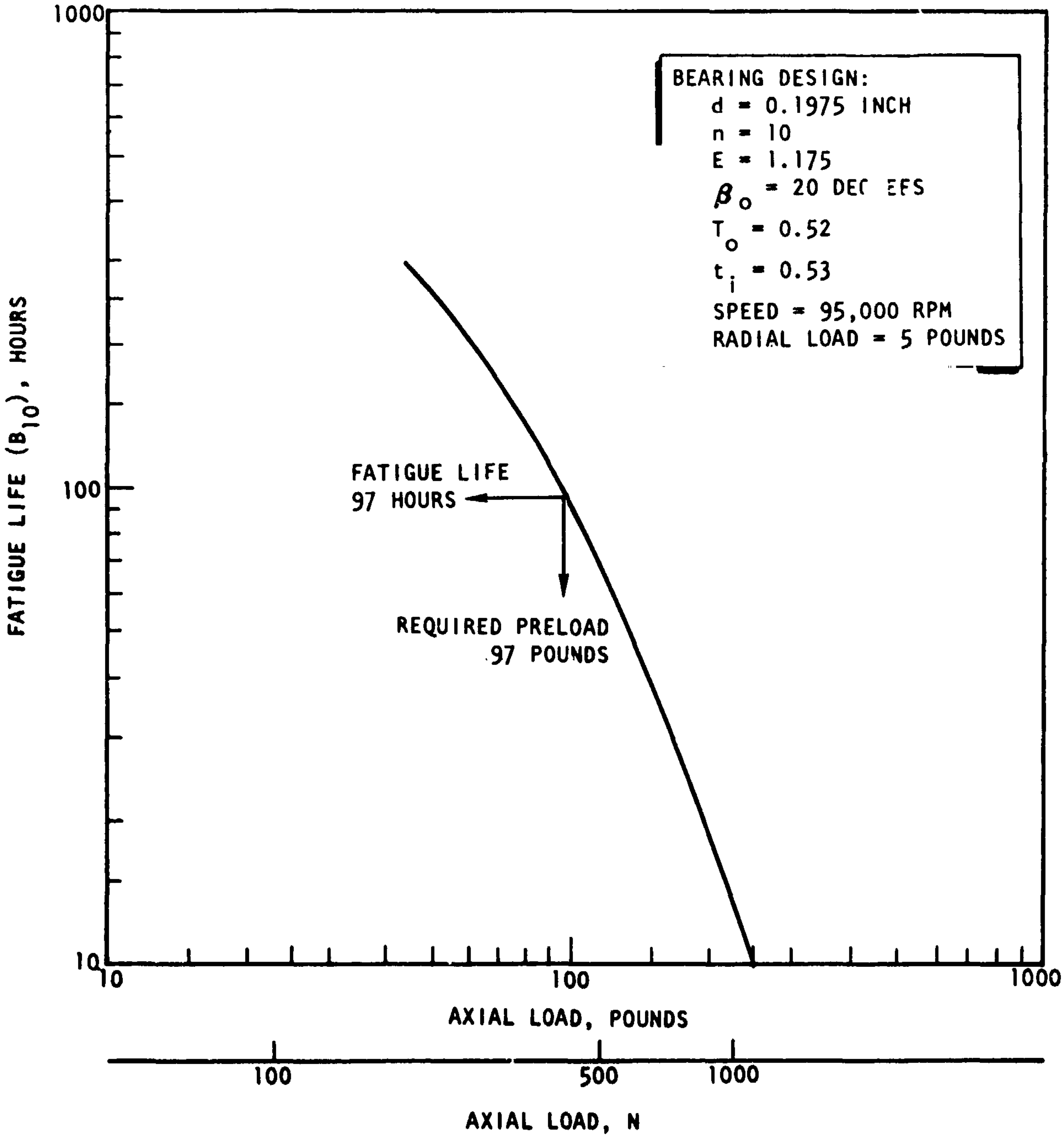

Figure 28. Mark 48-F Bearing B_{10} Life

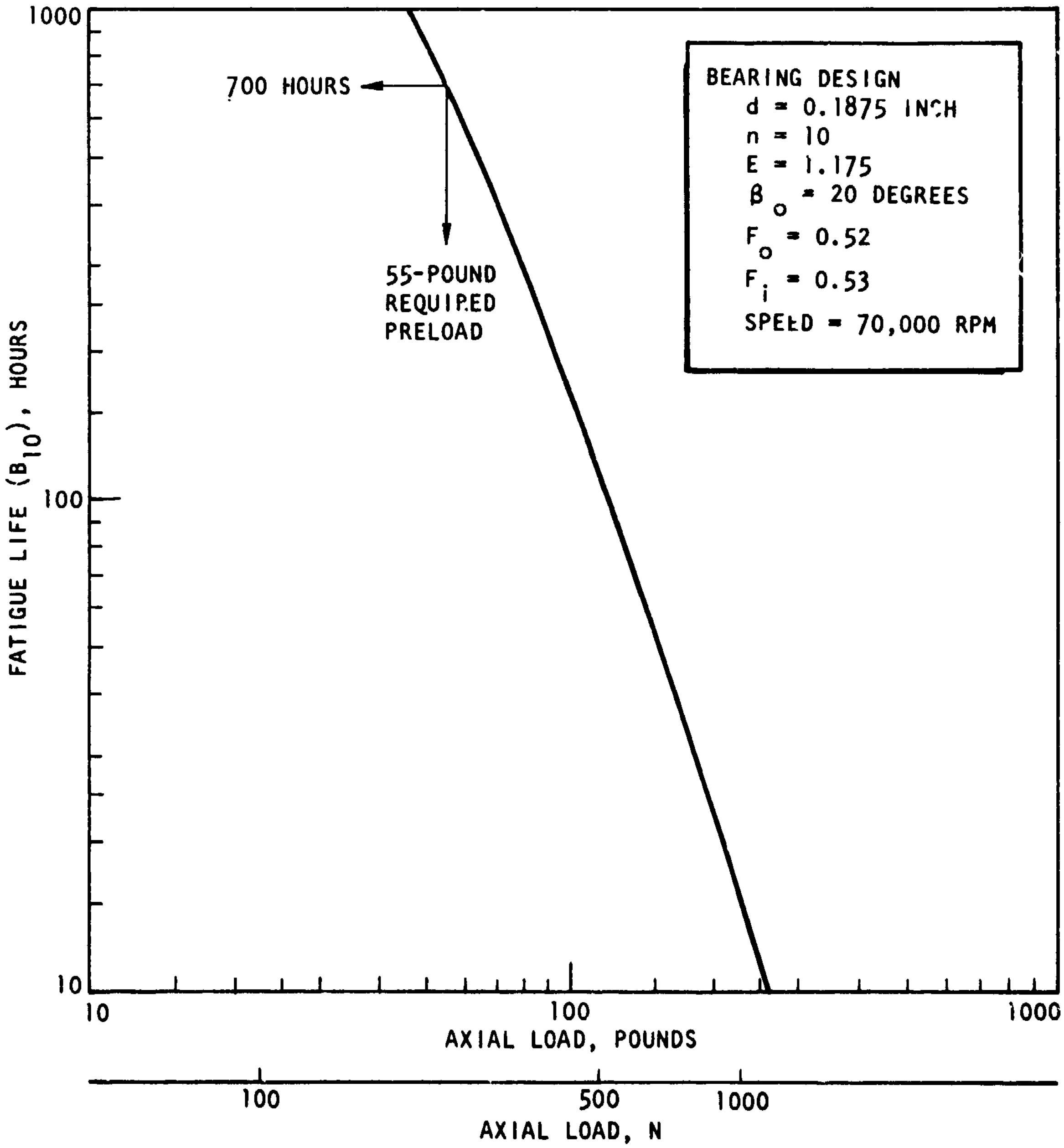

Figure 29. Mark 48-0 Bearing B_{10} Life

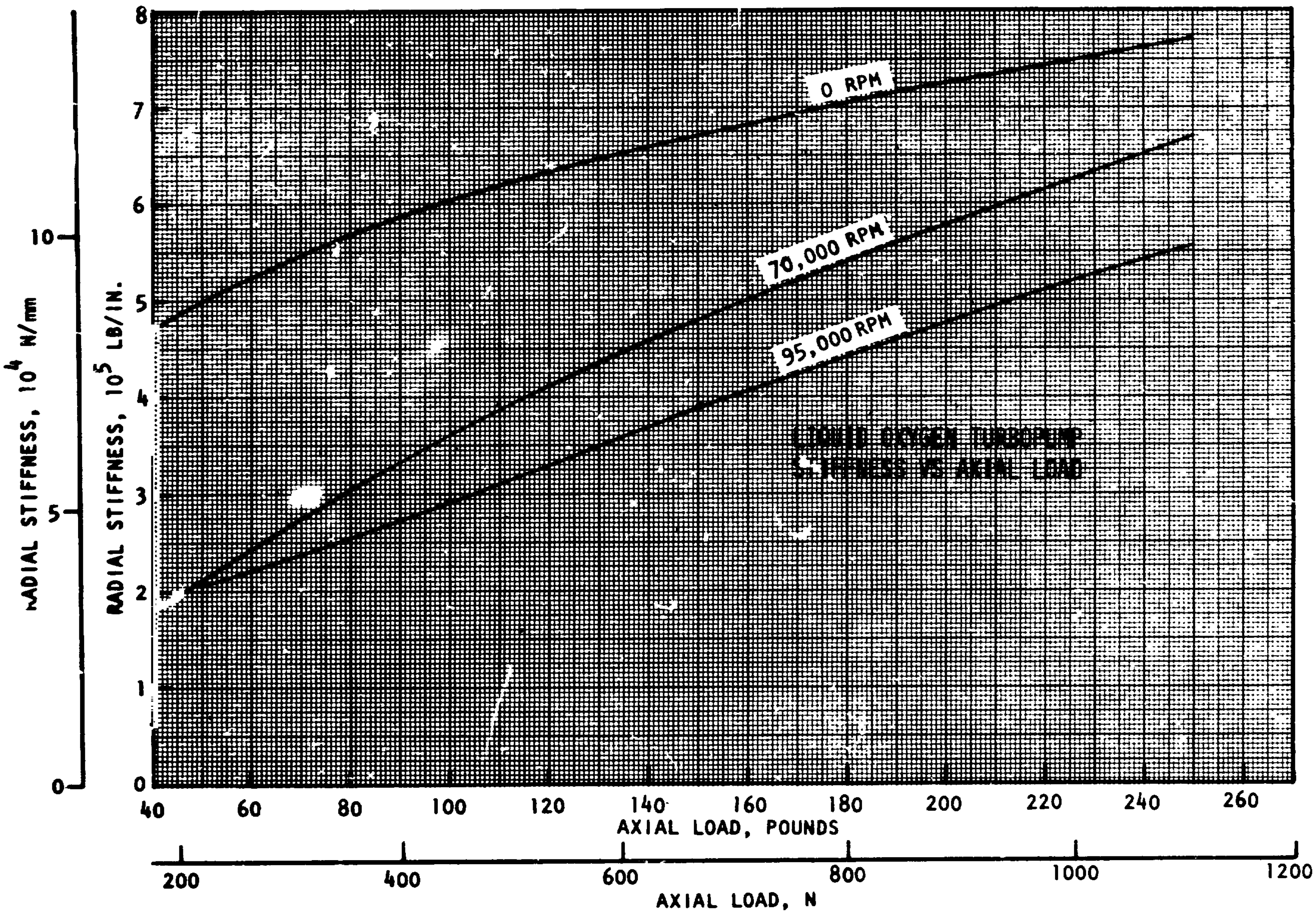

Figure 30. Mark 48 Bearing Stiffness versus Axial Load

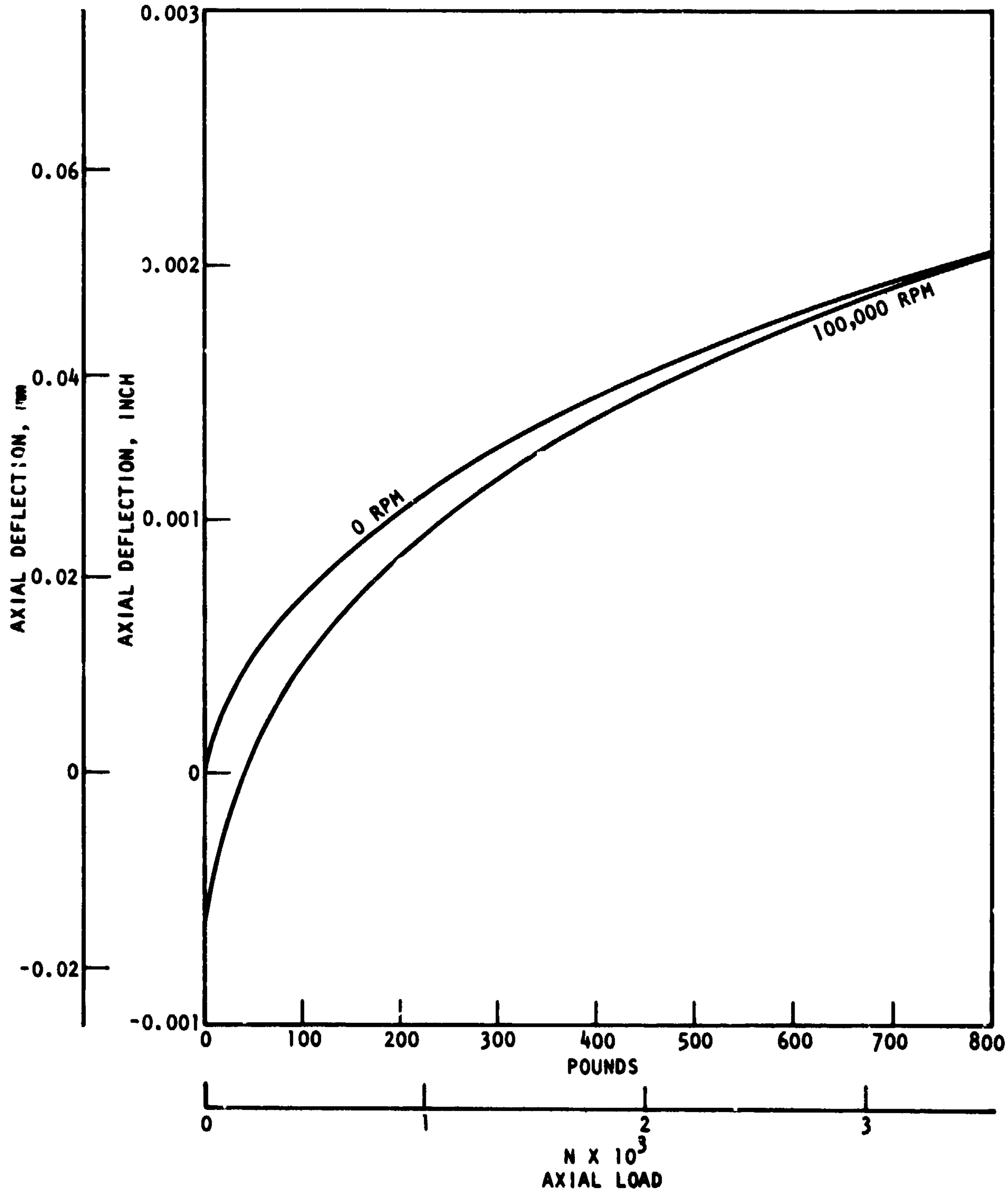

Figure 31. Mark 48-F Bearing Axial Deflection Versus Axial Load

2. Compensation for the increased loading by speed effects, therefore avoiding unnecessary increase in axial load with attendant reduction in life.

Seal Design

Main Shaft Seal System. The oxidizer seal system is designed to contain the high-pressure LOX and turbine hot gas and maintain safe separation of the oxidizer and fuel-rich, hot-gas drain cavities. The seal system (Fig. 32) consists of a rotating slinger containing pumping ribs upstream of the primary LOX seal to reduce the pressure from 1637 to 79 N/cm^2 (2375 to 115 psia). The LOX is vaporized in the slinger pumping region to reduce the seal leakage. The LOX seal leakage is drained overboard from the cavity formed by the primary and intermediate seals.

The intermediate seal is purged with gaseous helium at 35 N/cm^2 (50 psia) to maintain a pressure barrier between the oxidizer and hot-gas drain cavities for safe separation of the combustible fluids. Approximately one-half of the purge gas leaks out through each side of the intermediate seal and mixes with the seal leakage for overboard drainage.

The high-pressure 1631 N/cm^2 (2365 psia) turbine hot gas is contained with a double seal and a two-stage drain system. The primary turbine seal and overboard drain reduces the pressure to 41 N/cm^2 (60 psia). The secondary turbine seal further reduces the pressure to 11 N/cm^2 (16 psia) in the drain cavity formed by the intermediate and turbine seals.

The system allows failure of one seal at a time without the hot-gas pressure exceeding the intermediate seal purge pressure. The seal drains are sized to accommodate the additional leakage of a failed seal without exceeding safe pressure levels. Table 6 presents a summary of the seal leakages and pressures for nominal and failed conditions.

Turbine Bearing Seal System. A three-element seal with a high-pressure, 2410 $N/cm2$ (3497 psia) hydrogen purge is utilized to contain the turbine hot gas and provide coolant to the turbine bearings (Fig. 33). The hydrogen purge provides a pressure barrier to prevent turbine hot gas from leaking into the bearing area. A portion of the purge leaks into the turbine area where it mixes with the hot gas. Part of the purge is vented through the turbine wheel for cooling. The remainder of the purge leaks through the two seal elements into the bearing area to provide bearing coolant.

A bypass vent hole is provided in the seal housing to ensure sufficient bearing coolant flow in the event of low seal leakage.

The three-element seal and purge system provides fail-safe operation in the event of one seal failure at a time. A summary of the leakages and pressures for nominal and failed conditions is given in Table 7.

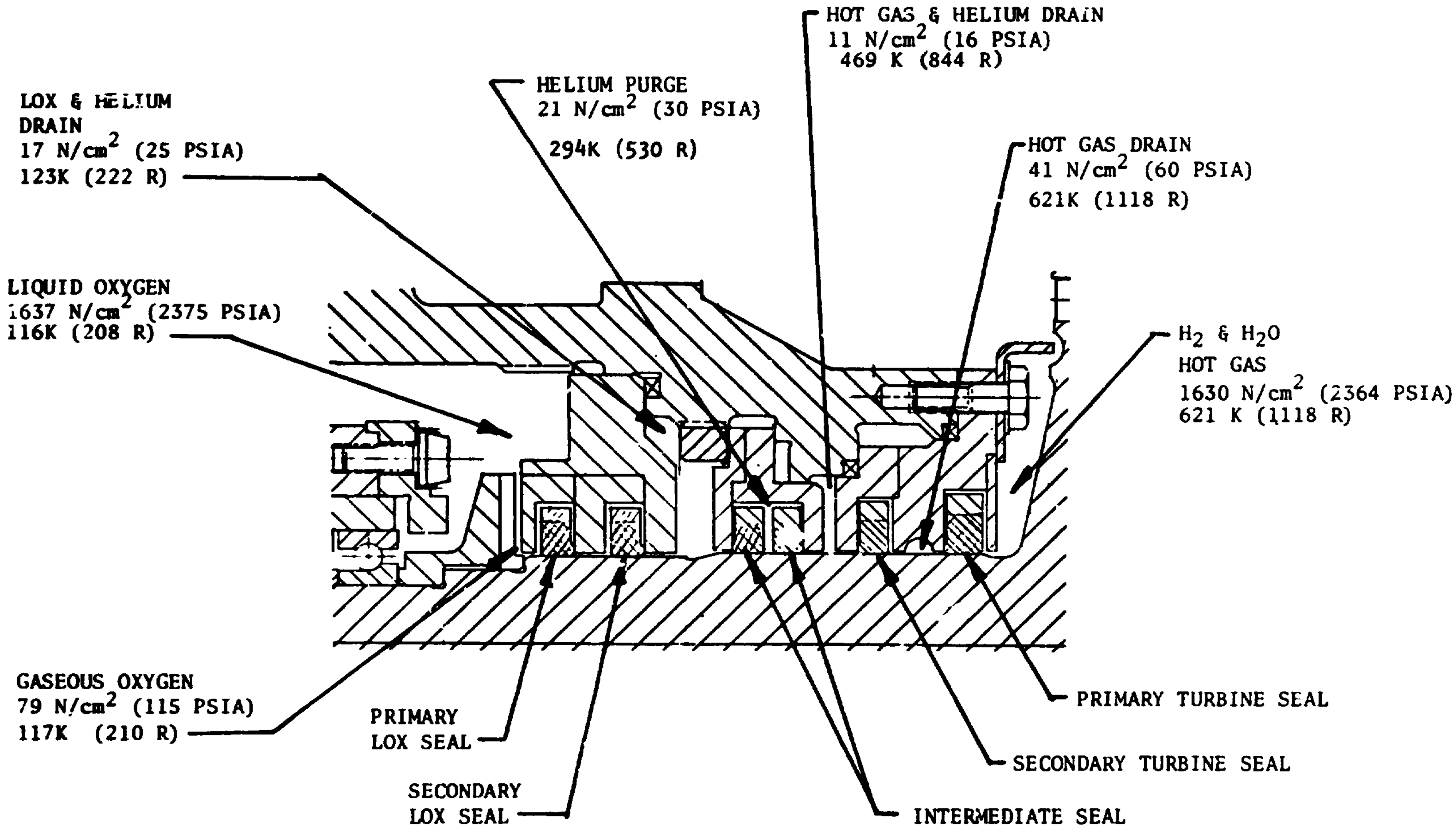

Figure 32. Main Shaft Seals

TABLE 6. MAIN SHAFT AND SEAL LEAKAGE AND PRESSURE SUMMARY

(METRIC UNITS)

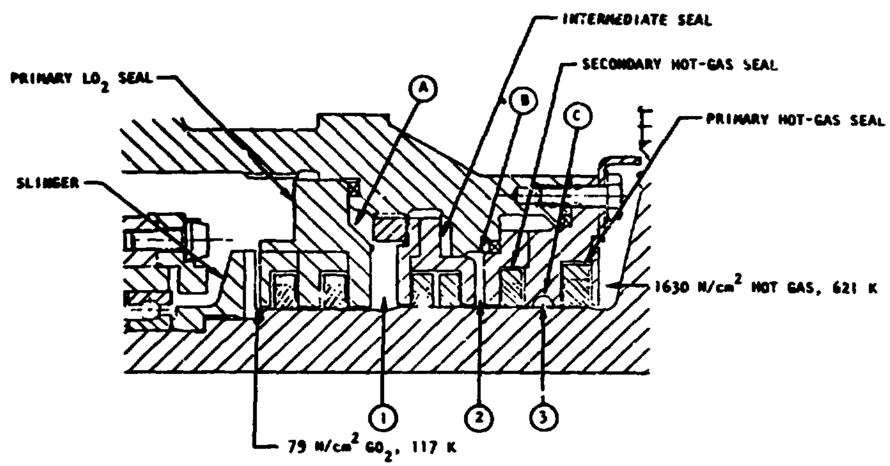

DRAIN \ CONFIGURATION	MINIMUM ALLOWABLE FLOW AREA, CM^2	MAXIMUM ALLOWABLE DRAIN RESISTANCE, L/D
PRIMARY LOX (A)	.70	44.4
SECONDARY HOT GAS (B)	.34	43.7
PRIMARY HOT GAS (C)	6.45	352

SEAL CONDITION \ CAVITY	(1)			(2)			(3)		
	Kg/s	N/cm^2	K	Kg/s	N/cm^2	K	Kg/s	N/cm^2	K
NOMINAL*	.044	17	123	.0009	11	469	.014	41	621
FAILED PRIMARY**	.044	17	123	.004	21	593	.13	414	978
FAILED SECONDARY	.044	17	123	.002	15	579	.013	37	621
FAILED PRIMARY LOX	.050	21	121	.0009	11	469	.014	41	621

*Nominal: Radial Clearance, .025 mm
**Failed: Radial Clearance, .25 mm

TABLE 6. (Concluded)

(ENGLISH UNITS)

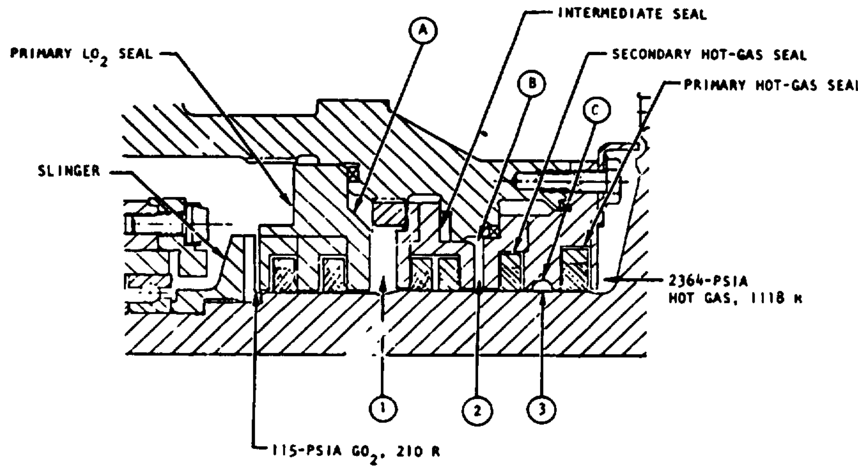

CONFIGURATION / DRAIN	MINIMUM ALLOWABLE FLOW AREA, in^2	MAXIMUM ALLOWABLE DRAIN RESISTANCE, L/D
PRIMARY LOX (A)	.0.109	44.42
SECONDARY HOT GAS (B)	0.052	43.67
PRIMARY HOT GAS (C)	0.225	352.30

CAVITY / SEAL CONDITION	1			2			3		
	lb/s	psia	R	lb/s	psia	R	lb/s	psia	R
NOMINAL *	.096	25	222	.002	16	844	.031	60	1118
FAILED PRIMARY **	.096	25	222	.008	30	1067	.279	601	1760
FAILED SECONDARY	.096	25	222	.005	22	1043	.028	54	1118
FAILED PRIMARY LOX	.110	30	217	.002	16	844	.031	60	1118

*Nominal: Radial Clearance, .001 inch
**Failed: Radial Clearance, .01 inch

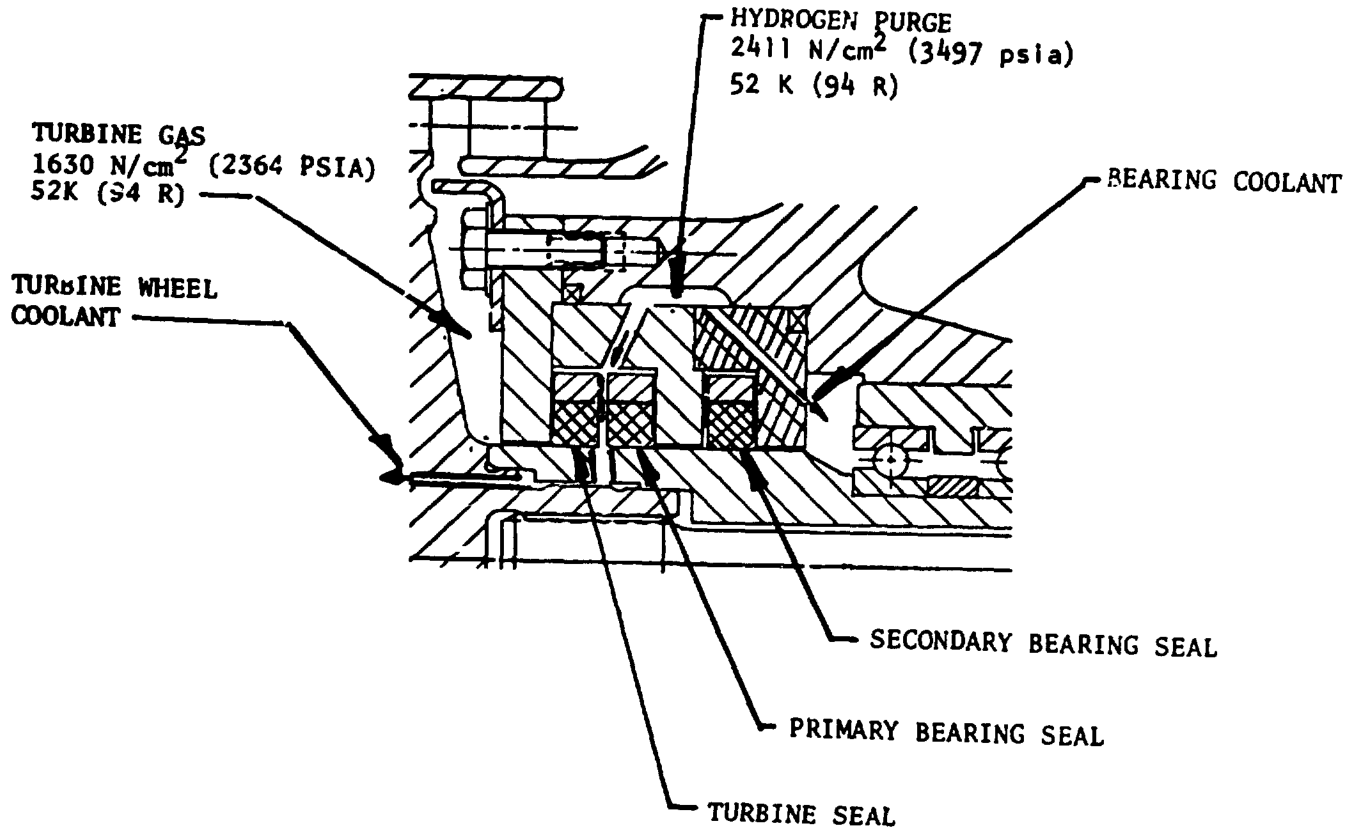

Figure 33. Turbine Bearing Seal (Outboard Seal)

TABLE 7. TURBINE BEARING SEAL LEAKAGE AND PRESSURE SUMMARY

(METRIC UNITS)

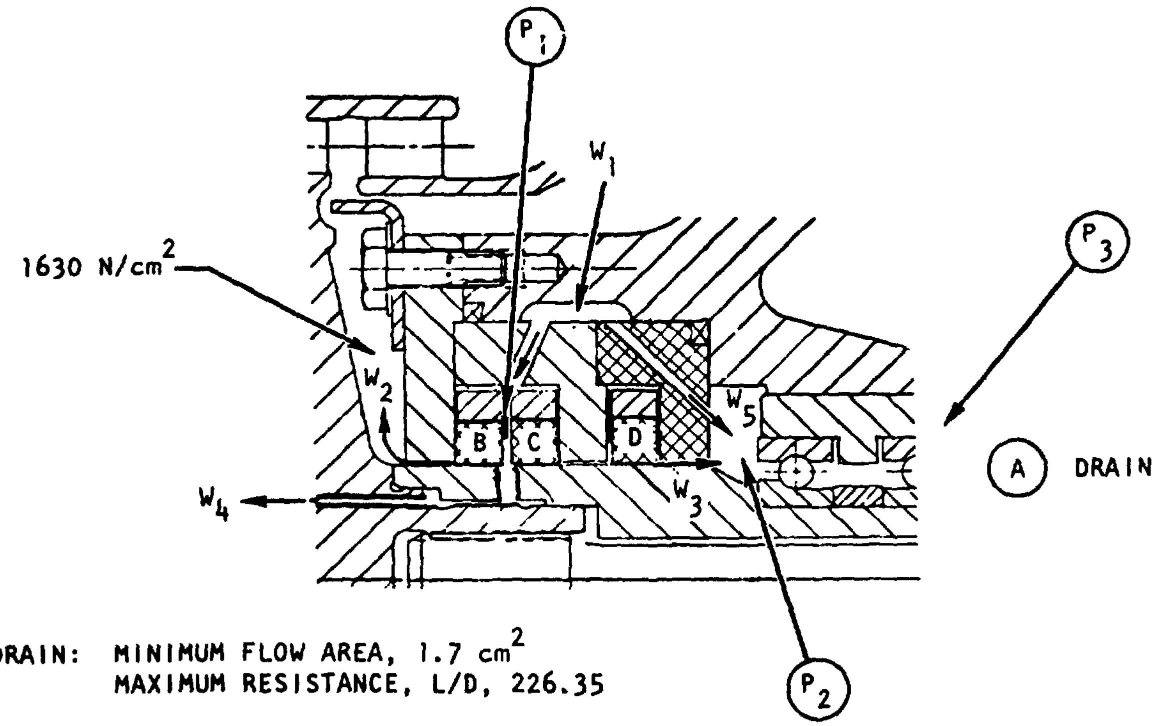

(A) DRAIN: MINIMUM FLOW AREA, 1.7 cm^2
MAXIMUM RESISTANCE, L/D, 226.35

Seal Condition	W_1, Kg/s	W_2, Kg/s	W_3, Kg/s	W_4, Kg/s	W_5, Kg/s	P_1, N/cm^2	P_2, N/cm^2	P_3, N/cm^2
Nominal*	0.18	0.048	0.059	0.005	0.064	2411	56	41
B Failed**	0.22	0.11	0.049	0.001	0.054	1671	42	32
C Failed	0.19	0.042	0.080	0.004	0.059	2233	92	66
D Failed	0.19	0.042	0.080	0.004	0.059	2233	92	66

*Nominal: Radial Clearance, (0.025 mm)
**Failed: Radial Clearance, (0.25 mm)

TABLE 7. (Concluded)
(ENGLISH UNITS)

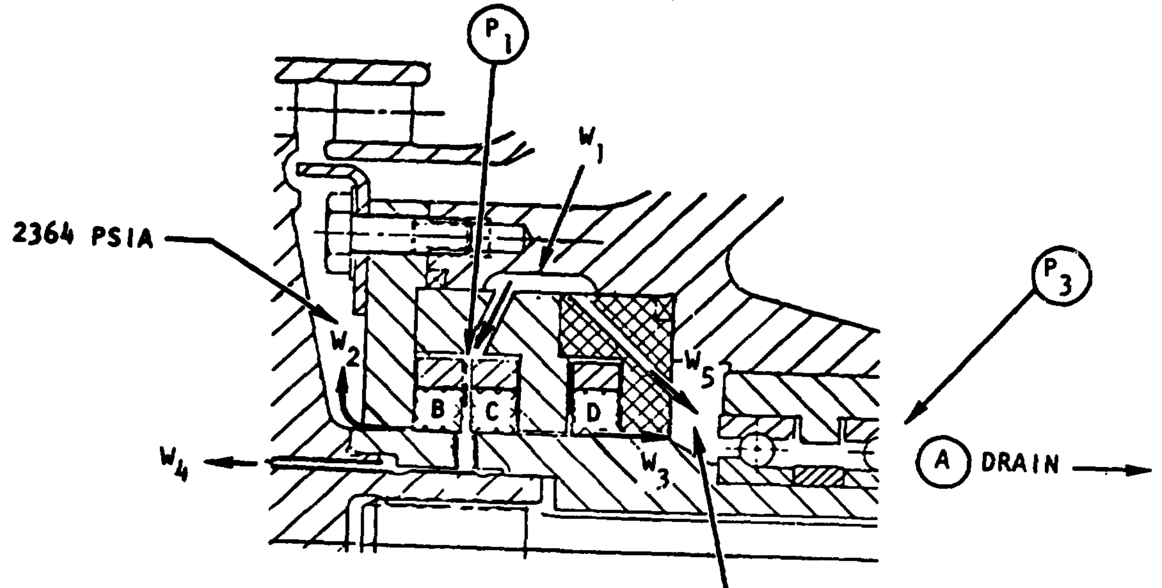

(A) DRAIN: MINIMUM FLOW AREA, 0.267 IN
MAXIMUM RESISTANCE, L/D, 226.35

Seal Condition	W_1, lb/s	W_2, lb/s	W_3, lb/s	W_4, lb/s	W_5, lb/s	P_1, psia	P_2, psi	P_3, psia
Nominal*	0.39	0.106	0.131	0.010	0.14	3497	82	60
B Failed**	0.48	0.244	0.109	0.002	0.12	2424	61	46
C Failed	0.41	[illegible]3	0.176	0.008	0.13	3239	134	95
D Failed	0.41	[illegible]93	0.176	0.008	0.13	3239	134	96

*Nominal: Radial Clearance, (0.001 inch)
**Failed: Radial Clearance, (0.010 inch)

Detail Design. All of the sealing elements utilize a floating-ring, controlled-gap seal ring. The floating-ring element consists of an inner carbon or AmCerMet ring for wear resistance, and an outer Inconel X-750 ring for strength and thermal expansion/contraction control. The outer ring material is selected to provide the same thermal expansion and contraction rate as the shaft material, so that a constant clearance gap is maintained as the temperature changes. The outer ring is sufficiently strong, relative to the inner ring, to control the diameter of the composite ring. The inner ring is maintained in compressive hoop stress with an interference fit.

The load induced by unbalanced radial pressure (Fig. 34) is supported by the composite ring in compressive hoop stress. The radial deflection caused by the compressive stress is proportional to ring rigidity. The radial section and modulus of elasticity are selected to minimize the deflection. The initial clearance is adjusted to allow for the deflection and provide the desired operating clearance.

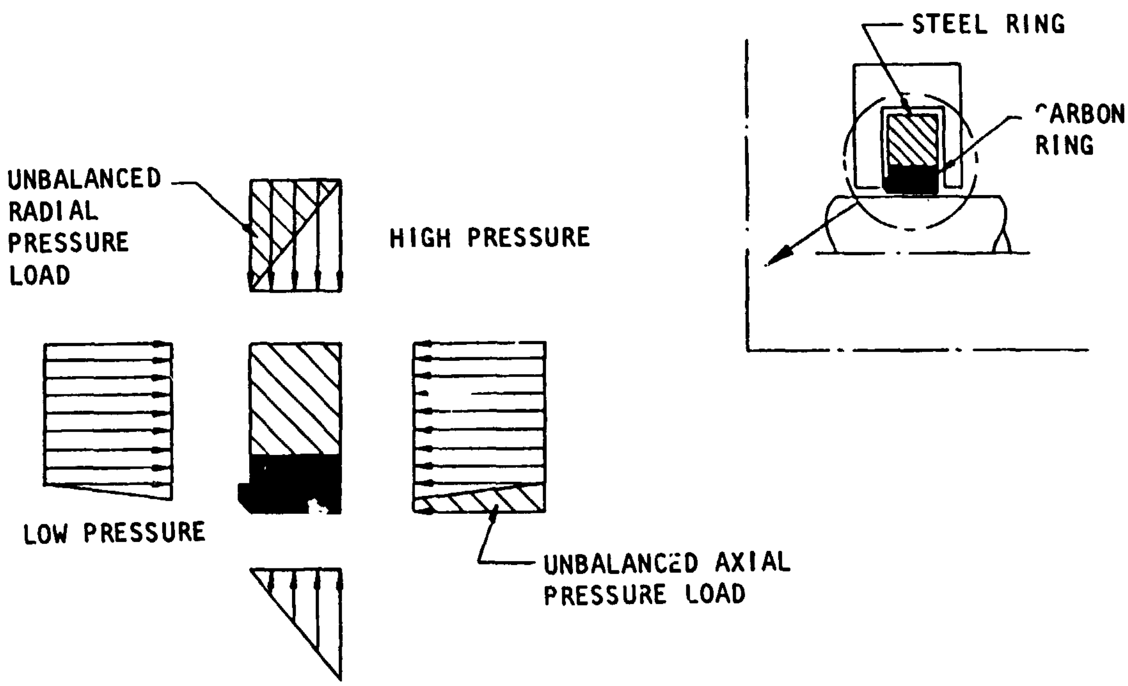

Figure 34. Pressure Forces on a Floating-Ring Seal

The axial force induced by differential pressure (Fig. 34) loads the floating ring against the stationary housing to provide a static seal. A wave spring is provided to ensure sufficient contact load to maintain a static seal. The seal ring is partially pressure balanced by relieving the axial contact surface and minimizing the housing-to-shaft clearance to reduce the unbalanced axial-pressure-induced load. The floating-ring element is restrained from rotation with two antirotation tangs that engage slots in the housing.

The seal ring clearance gap was established by first performing a thermal analysis to determine the temperature gradient in the turbopump shaft seal area. The shaft temperature distribution is shown on **Fig. 43 (page 78) for the main shaft seals and on Fig. 47 (page 83) for the turbine bearing seal.**

A nite-element stress analysis was performed using the temperature distribution and centrifugal loading to establish the shaft operating diameter. The seal ring design was established to maintain the required operating clearance gap. The Inconel X-750 retaining band material has approximately the same thermal contraction and expansion rate as the Waspaloy and Inconel 718 shaft materials to minimize the gap change due to temperature. The seal ring insert materials were selected for wear resistance and fluid compatibility. The shaft seal materials are given in Table 8.

The seal ring design was optimized by utilizing a computer program in which the temperature, pressure, materials, and overall dimensional data are input. The computer calculates the seal ring stresses and deflections for varying radial sections of the retaining band and insert. The seal ring dimensions were then selected, consistent with the proper stress levels, to provide the minimum change in clearance gap. The static ambient seal ring clearance gaps were established, consistent with the clearance differential, to provide the required operating clearance gaps. A summary of the seal ring stresses, deflections, and clearances is given in Table 9.

Static Flange Seals. All static flange seals are of the pressure-sensitive metal spring type (Fig. 35). The seals were designed and fabricated for each specific application by Hydrodyne Division of Donaldson Co., Inc. The base material was Inconel X-750 with a 0.0076 mm (0.0003 inch) thick silver plating applied to improve sealing effectiveness.

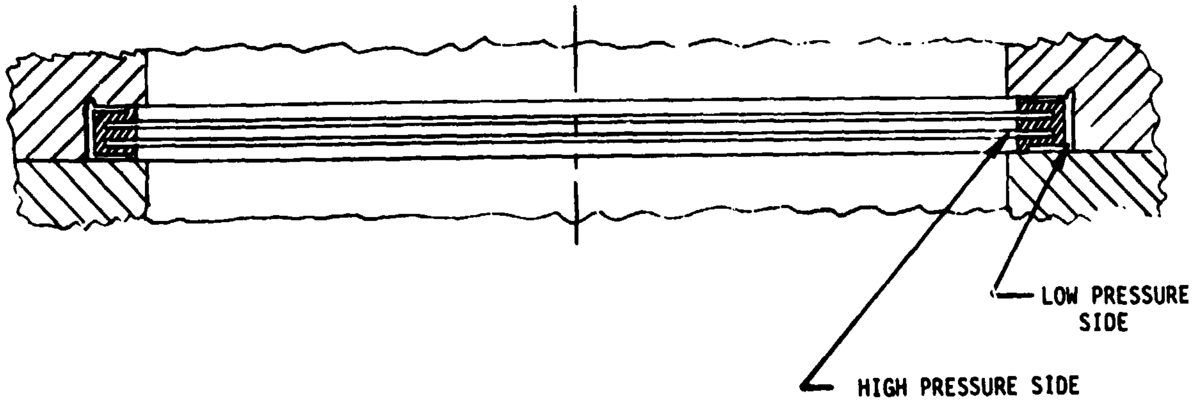

Figure 35. Typical Static Flange Seal Configuration

Impeller Wear Rings. Internal recirculation of LOX around the impeller front is controlled by step labyrinth wear rings (Fig. 36). The nominal diametral clearance between the rotating member and stationary platform is set at 0.15 mm (0.006 inch). With this clearance, some rubbing contact is expected because of eccentricities and deflection. To moderate the effect of rubbing, a 0.25 mm (0.010 inch) thick layer of silver plating is applied to the stationary platforms.

TABLE 8. SHAFT SEAL MATERIAL SUMMARY

Seal	Housing Material	Seal Ring Material	Retaining Ring Material	Shaft Material	Shaft Surface Treatment
Primary LOX	Inconel X-750	P 692 Carbon	Inconel X-750	Waspaloy	Chrome Plate
Intermediate	↓	G 84 Carbon	↓	↓	↓
Turbine Hot Gas	↓	701-65 AmCerMet	↓	↓	↓
Turbine Bearing	↓	P5N Carbon	↓	Inconel 718	↓

TABLE 9. SEAL RING STRESS, DEFLECTION AND CLEARANCE SUMMARY (METRIC UNITS)

Seal	Installed Inner Ring Stress, N/cm^2	Installed Outer Ring Stress, N/cm^2	Operating Inner Ring Stress, N/cm^2	Operating Outer Ring Stress, N/cm^2	Operating Deflection (diameter), mm	Ambient Static Clearance (diameter), mm		Operating Clearance (diameter), mm	
						Minimum	Maximum	Minimum	Maximum
Oxidizer									
Primary	-6,404	13,691	10,340	22,134	-0.074	0.071	0.086	0.041	0.056
Secondary	-6,413	13,710	10,340	22,242	-0.074	0.081	0.097	0.041	0.056
Intermediate									
Pump Side	-9,177	16,036	10,340	17,765	-0.020	0.064	0.079	0.041	0.056
Turbine Side	-9,177	16,036	10,340	17,765	-0.020	0.084	0.099	0.041	0.056
Turbine Hot Gas									
Primary	-28,681	40,771	27,576	29,482	0.127	0.051	0.066	0.086	0.102
Secondary	-28,971	41,410	27,576	36,786	0.058	0.074	0.089	0.051	0.066
Turbine Bearing									
Turbine	-8,551	18,053	13,788	17,871	-0.097	0.074	0.089	0.041	0.056
Primary Bearing	-8,305	17,534	13,788	15,948	-0.102	0.074	0.089	0.041	0.056
Secondary Bearing	-8,577	18,107	13,788	19,637	-0.102	0.074	0.089	0.041	0.056

TABLE 9. (CONCLUDED)

(ENGLISH UNITS)

Seal	Installed Inner Ring Stress, psi	Installed Outer Ring Stress, psi	Operating Inner Ring Stress, psi	Operating Outer Ring Stress, psi	Operating Deflection (diameter), inch	Ambient Static Clearance (diameter), inch		Operating Clearance (diameter), inch	
						Minimum	Maximum	Minimum	Maximum
Oxidizer									
Primary	-9,290	19,859	-15,000	32,106	-0.0029	0.0028	0.0034	0.0016	0.0022
Secondary	-9,302	19,887	-15,000	32,263	-0.0029	0.0032	0.0038	0.0016	0.0022
Intermediate									
Pump Side	-13,312	23,261	-15,000	25,769	-0.0008	0.0025	0.0031	0.0016	0.0022
Turbine Side	-13,312	23,261	-15,000	25,769	-0.0008	0.0033	0.0039	0.0016	0.0022
Turbine Hot Gas									
Primary	-41,603	59,140	-40,000	42,765	0.0050	0.0020	0.0026	0.0034	0.0040
Secondary	-42,024	60,066	-40,000	53,360	0.0023	0.0029	0.0035	0.0020	0.0026
Turbine Bearing									
Turbine	-12,404	26,187	-20,000	25,923	-0.0038	.029	0.0035	0.0016	0.0022
Primary Bearing	-12,047	25,434	-20,000	23,133	-0.0040	.029	0.0035	0.0016	0.0022
Secondary Bearing	-12,441	26,265	-20,000	28,484	-0.0040	0.0029	0.0035	0.0016	0.0022

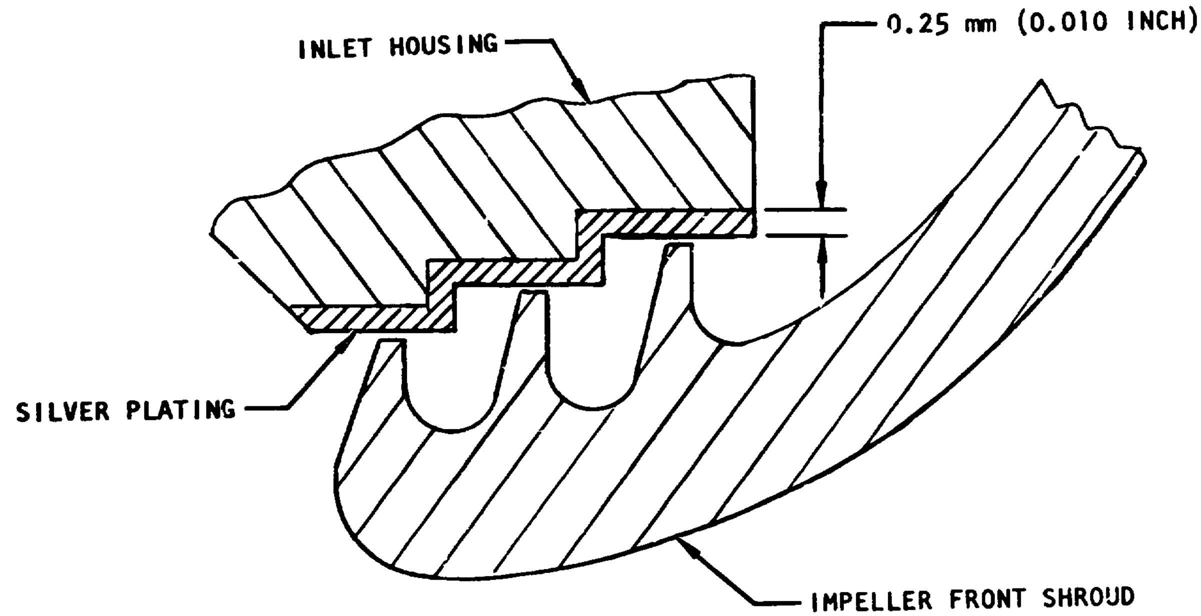

Figure 36. Mark 48-0 Impeller Wear Ring

Rotordynamics

The critical speeds of the rotating assembly were calculated by the lumped parameter method in which the rotor is simulated by a series of mass points whose spacing approximates the mass distribution of the actual hardware. The calculated mass properties of the rotating assembly are given in Table 10; a schematic of the rotordynamic model is shown in Fig. 37.

The initial approach was to have all four bearings share in carrying the radial load. The predicted critical speeds for this configuration are indicated in Fig. 38. It is evident that the second critical speed falls essentially on the operating speed of 7330 rad/s (70,000 rpm), which is not an acceptable condition. To resolve this problem, the radial constraint on the outboard pump bearing was removed. The critical speed prediction for this case is presented in Fig. 39. Since this configuration provides a satisfactory margin around the operating speed, it was accepted for the final design. The radial constraint is removed from the outboard pump bearing by making the bearing sleeve bore larger than the outer race diameter by 0.25 mm (0.010 inch).

The mode shapes for the first, second, and third critical speeds as a function location along the length of the rotor are given in Fig. 40.

Material Selection

The materials selected for the more significant components of the Mark 48-0 turbopump are indicated in Fig. 41. In Table 11 specifications and properties for these materials are summarized.

The principal criteria for choosing the materials in the pump were: strength and ductility at cryogenic temperature, LOX compatibility, resistance to corrosion, thermal contraction coefficient, and ease of fabrication.

The impeller, inlet housing, diffuser, and volute were all made of Inconel 718. Inconel 718 is a nickel-base, precipitation-hardenable alloy which has both excellent strength and ductility at cryogenic temperatures. The same material was used for these four parts because it was desirable to have a common thermal coefficient to maintain control over critical radial and axial clearances. Silver plating was applied to the inlet housing in the inducer tunnel and on the impeller front wear ring labyrinth lands to permit light contact with the rotating parts in these areas with a minimum of local heating. For the same reason, the stationary lands of the balance piston low- and high-pressure orifices were also plated with silver.

K-monel, an age-hardenable, nickel-copper alloy, was selected as the inducer material because it has satisfactory strength, excellent ductility at cryogenic temperatures, and it has roughly twice the thermal conductivity of Inconel 718. The latter is a desirable quality because it tends to minimize local heat buildup in the event of rubbing.

TABLE 10. LOX TURBOPUMP ROTATING ASSEMBLY MASS PROPERTIES (METRIC UNITS)

Joint Number (J)	Mass Group Number (G)	Distance Along Axis (X)	Wet Mass (W), gm	Diametral Mass Moment of Inertia, (I_D), gm cm^2	Point Mass Moment of Inertia, (I_P) gm cm^2
1	1	3.05	81.2	85.4	100
2	--	4.57			
3	--	5.33			
4	2	6.1	332.0	730	1165
5	--	7.16			
6	3	8.33	42.6	21.7	36.6
7	4	9.09	29.9	13.5	24.0
8	3	9.96	42.6	21.7	36.6
9	5	11.10	75.3	54.4	92.5
10	6	12.10	232.7	509	974
11	--	13.21			
12	7	14.12	161.5	190	246
13	--	12.95			
14	8	16.84	172.4	209	214
15	8	19.30	172.4	209	214
16	9	21.76	1026.9	6903	13420
17	--	22.86			
18	10	24.51	194.6	290	244
19	--	25.91			
20	11	26.92	38.6	22.2	37.8
21	12	27.69	24.0	26.9	22.5
22	11	28.58	38.[illegible]	22.2	37.8
23	14	29.72	43.1	25.2	37.2
24	15	32.39	132.4	201	101
Total		2840.7			

TABLE 10. (Concluded)
(ENGLISH UNITS)

Joint Number (J)	Mass Group Number (G)	Distance Along Axis (X), inches	Wet Mass (W), pounds	Diametral Mass Moment of Inertia (I_D), lb/in.^{2}	Polar Mass Moment of Inertia (I_P), lb/in.^{2}
1	1	1.20	0.179	0.0292	0.0342
2	--	1.80			
3	--	2.10			
4	2	2.40	0.732	0.260	0.398
5	--	2.82			
6	3	3.28	0.094	0.0074	0.0125
7	4	3.58	0.066	0.0046	0.0082
8	3	3.92	0.094	0.0074	0.0125
9	5	4.37	0.166	0.0186	0.0316
10	6	4.80	0.513	0.1739	0.3330
11	--	5.20			
12	7	5.56	0.356	0.0648	0.0841
13	--	5.10			
14	8	6.63	0.380	0.0715	0.0731
15	8	7.60	0.380	0.0715	0.0731
16	9	8.57	2.262	2.3588	4.5856
17	--	9.00			
18	10	9.65	0.429	0.0992	0.0834
19	--	10.20			
20	11	10.60	0.085	0.0076	0.0129
21	12	10.90	0.053	0.0092	0.0077
22	11	11.25	0.085	0.0076	0.0129
23	14	11.70	0.095	0.0086	0.0127
24	15	12.75	0.292	0.0686	0.0344
Total			6.25		

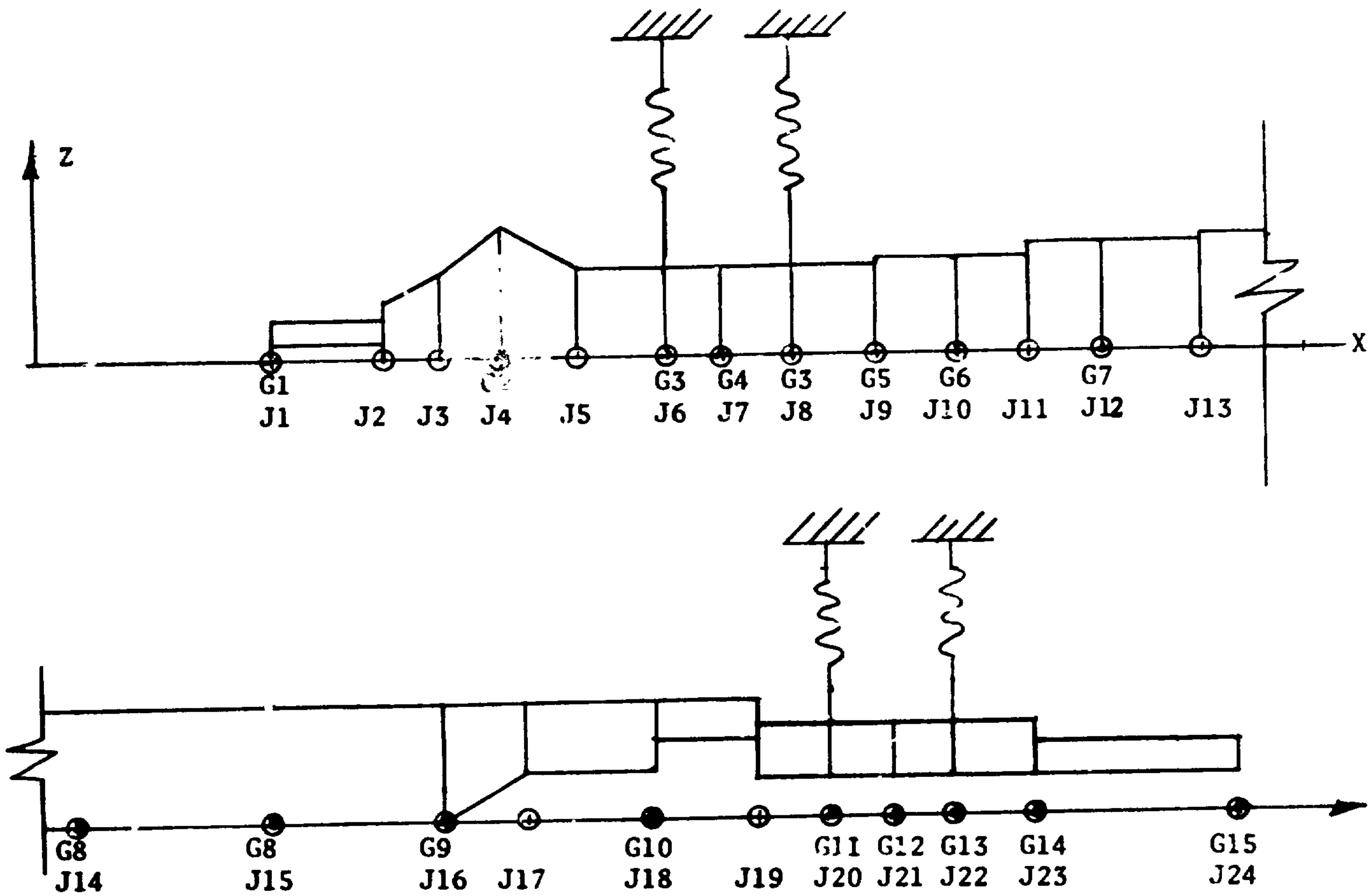

Figure 37. Rotor Stiffness and Mass Distribution Diagram

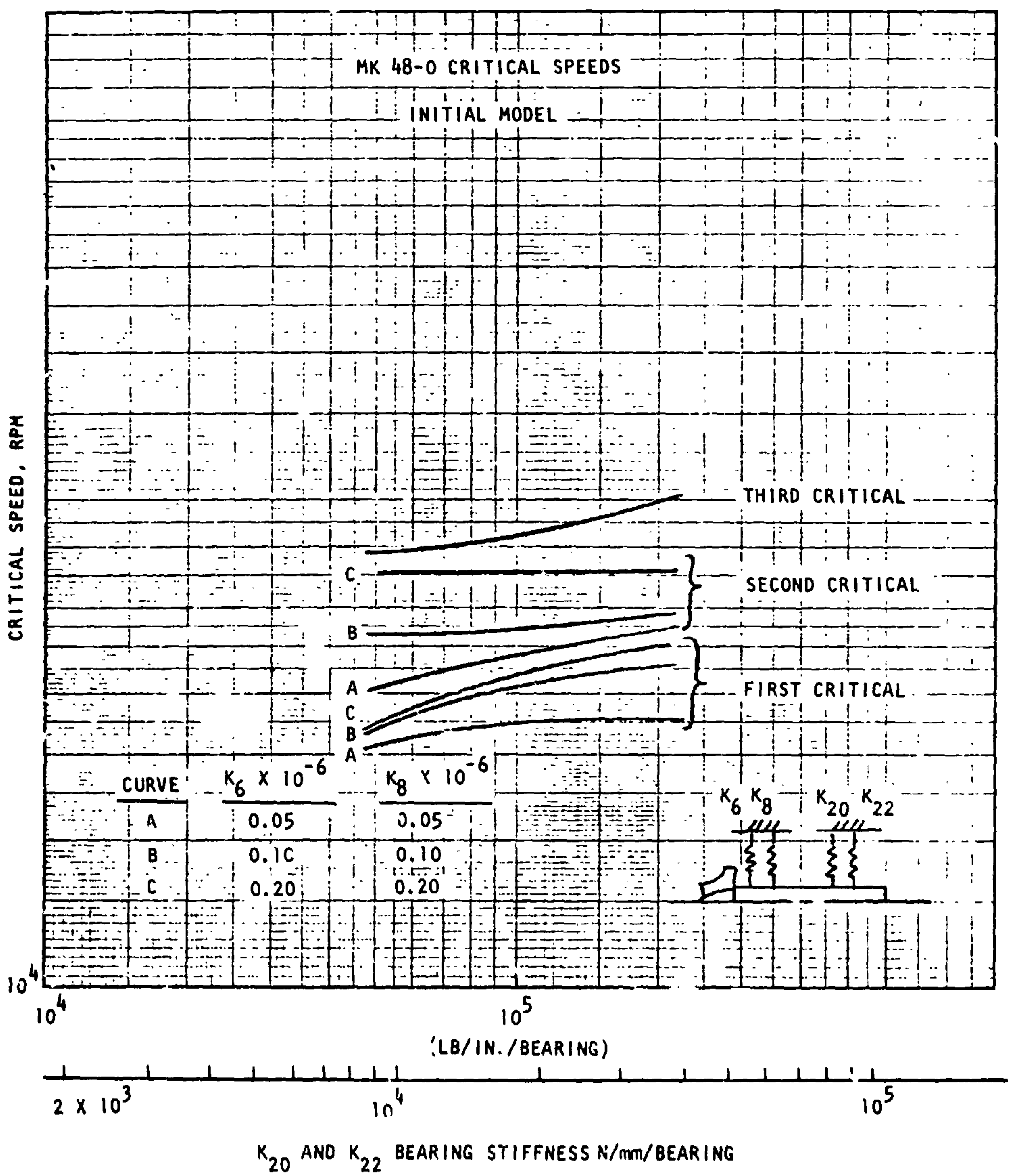

Figure 38. Mark 48-0 Rotor Critical Speeds, Initial Model

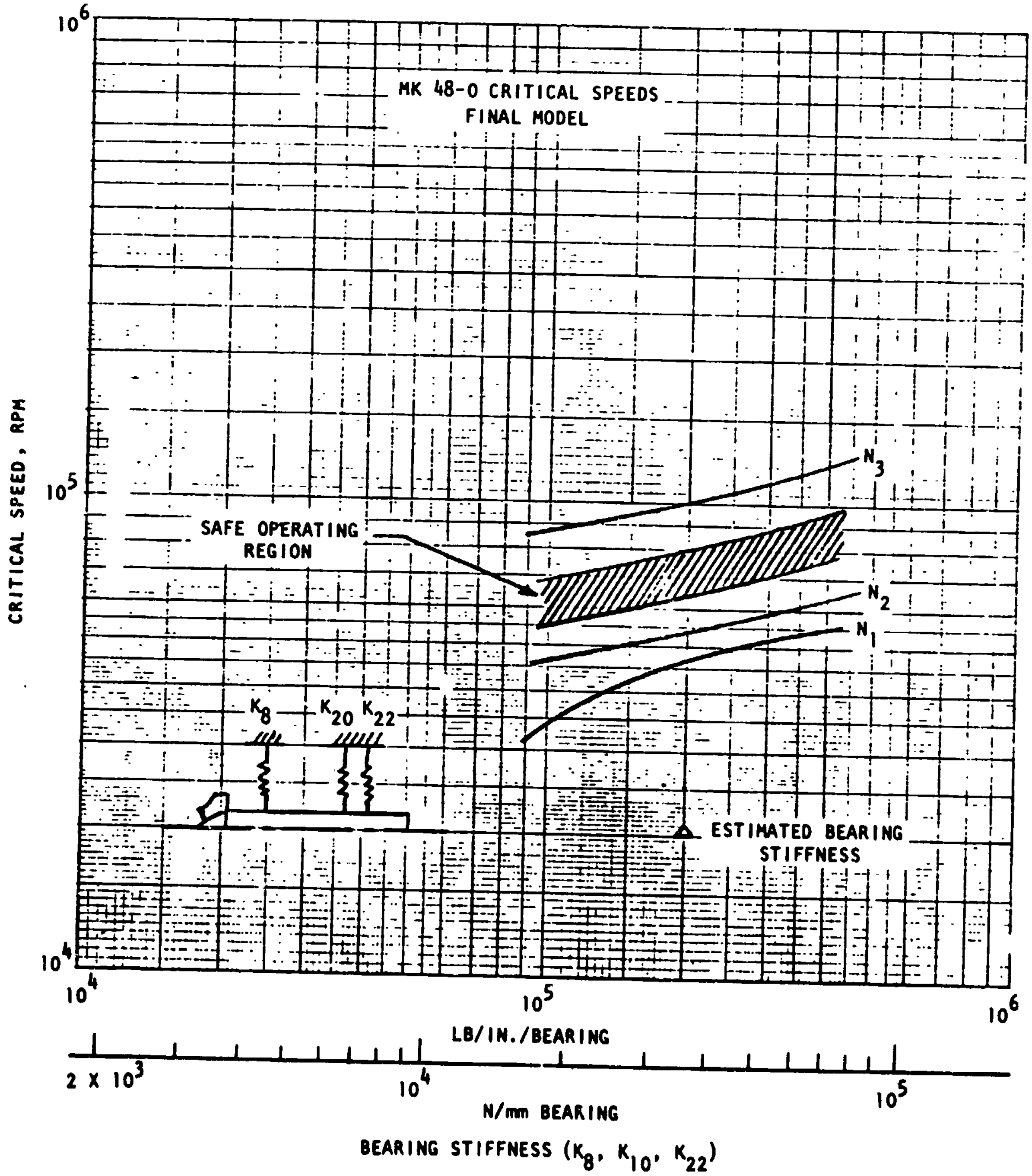

Figure 39. Mark 48-0 Rotor Critical Speeds, Final Model

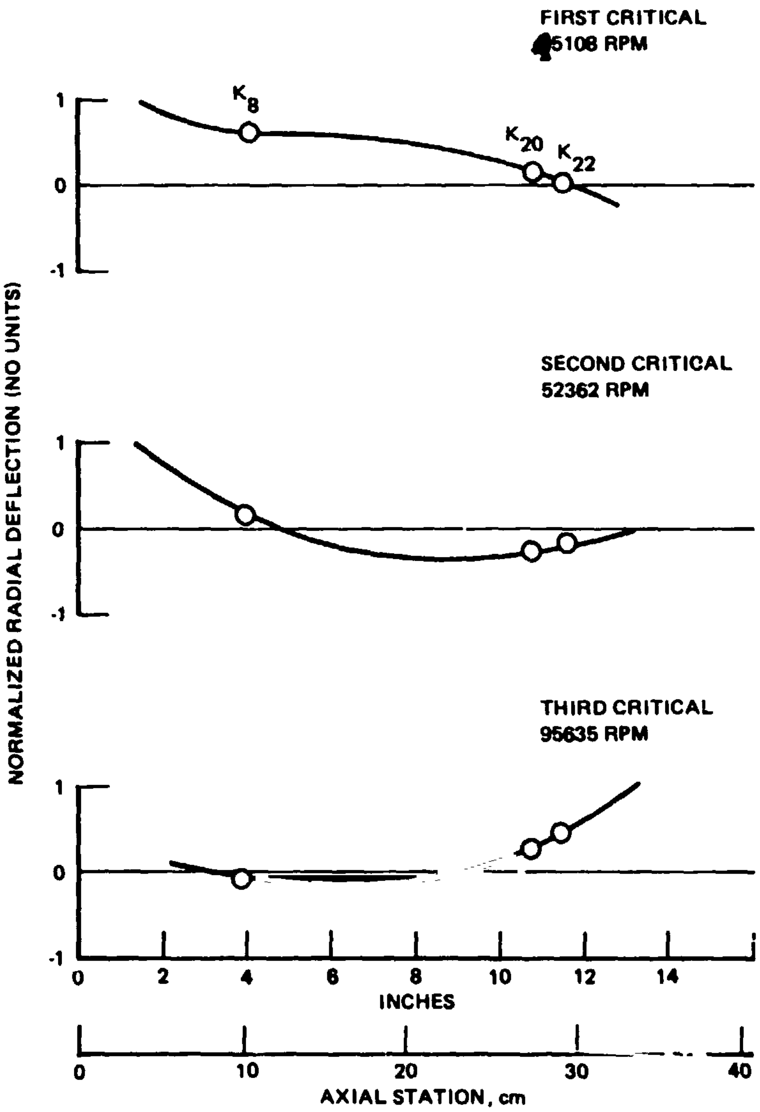

Figure 40. Mark 48-0 Mode Shapes

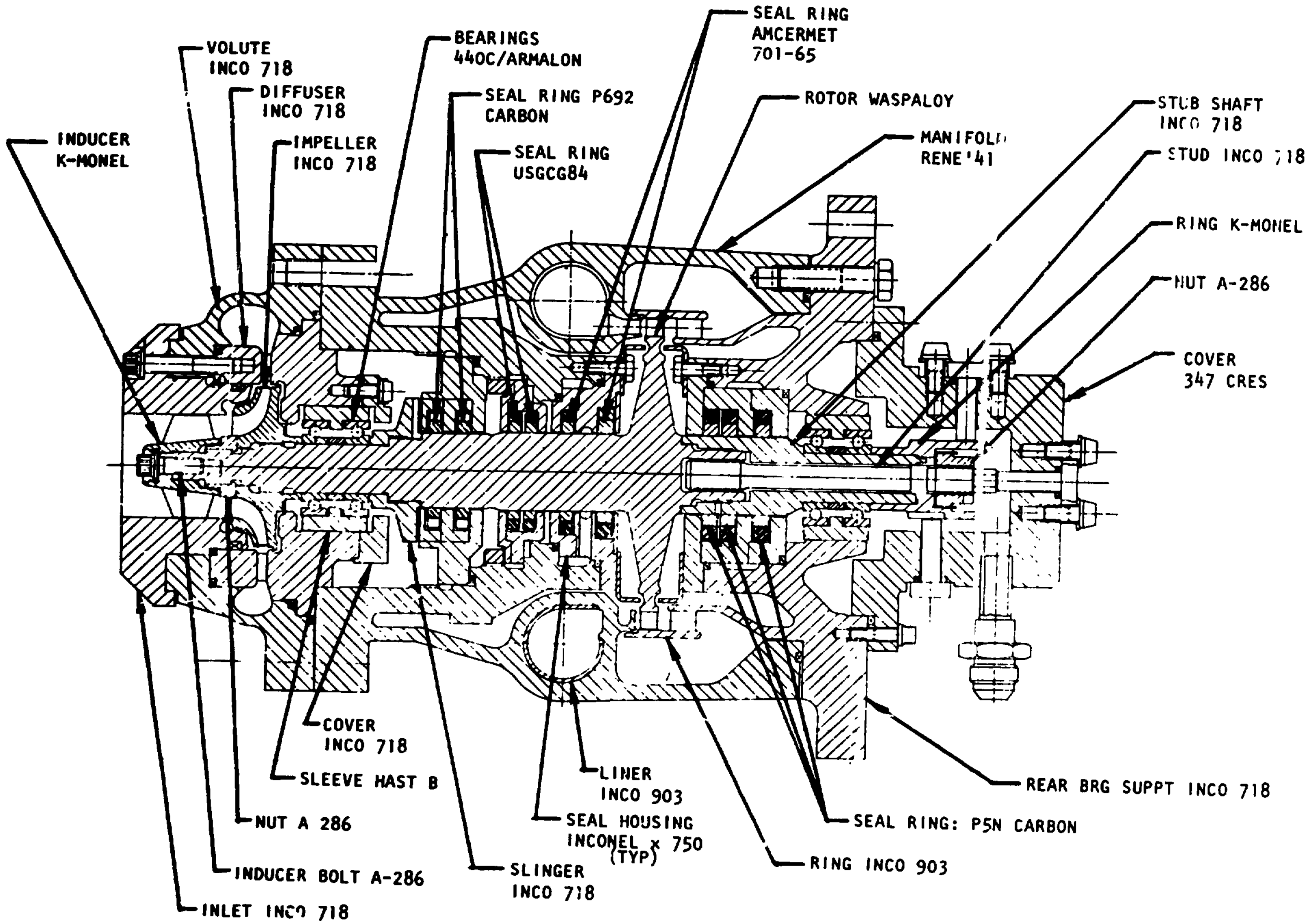

Figure 41. Mark 48-0 Materials

TABLE 11. MARK 48-0 TURBOPUMP MATERIAL PROPERTIES

(METRIC UNITS)

Part	Material	Specification	Room Temperature			Operating Temperature				
			F_{TY} N/CM^2	F_{TU} N/CM^2	e	T °K	F_{TY} N/CM^2	F_{TU} N/CM^2	e	10 Hour Stress Rupture, N/CM2
Impeller Pump Inlet Volute Diffuser Slinger	Inconel 718	RB0170-153	103,400	124,000	12	106	110,000	139,000	12	-
Rear Stub Shaft Rear Bearing Support	Inconel 718	RB0170-153	103,400	124,000	12	56	123,000	146,000	12	-
Inducer	K-Monel	RB0170-051	62,000	90,000	24		74,000	109,000	30	-
Housing, Seal Support	Haynes 188	AMS 5772	38,000	86,000	45		57,000	112,000	38	-
Nozzle	Haynes 188	AMS 5772	38,000	86,000	45		21,000	55,000	26	30,000
Housing, Turbine Manifold	Rene'41	AMS 5712	90,000	117,000	8		75,000	87,000	4	52,000
Impeller Nut Stud Nut, Stud	A 286	AMS 5737	65,000	97,000	12		83,000	124,000	15	-
Rotor	Waspalloy	RB0170-182	83,000	121,000	25		75,000	92,000	26	-
Rear Cover	347 CRES	QQ-S-763"A"	21,000		40				27	-
Bearing Sleeve	Hastalloy B	RB0170-002"A"								
Rear Bearing Spat	Inconel 903	RB0170-196	103,000	124,000	12		83,000	97,000	12	69,000

TABLE 11. (Concluded)
(ENGLISH UNITS)

Part	Material	Specification	Room Temperature			Operating Temperature				
			F_{TY}, ksi	F_{TU}, ksi	e,%	T ^oK	F_{TY}, ksi	F_{TU}, ksi	e	10 Hour Stress Rupture, ksi
Impeller Pump Inlet Volute Diffuser Slinger	Inconel 718	RB0170-153	150	180	12	-270	160	202	12	-
Rear Stub Shaft Rear Bearing Support	Inconel 718	RB0170-153	150	180	12	-370	178	212	12	-
Inducer	K-Monel	RB0170-051	90	130	24	-270	108	158	30	-
Housing, Seal Support	Haynes 188	AMS 5772	55	125	45	-270	82	162	38	-
Nozzle	Haynes 188	AMS 5772	55	125	45	1400	30	80	26	43
Housing, Turbine Manifold	Reñe'41	AMS 5712	130	170	8	1400	109	126	4	75
Impeller Nut Stud Nut, Stud	A 286	AMS 5737	95	140	12	-270	120	180	15	-
Rotor	Waspalloy	RB0170-182	120	175	25	1200	94	140	26	-
Rear Cover	347 CRES	QQ-S-763"A"	30	75	50	-400	43	173	27	-
Bearing Sleeve	Hastalloy B	RB0170-002"A"								
Rear Bearing Spat	Inconel 903	RB0170-196	150	180	12	1200	120	140	12	100

Two alloys were in primary contention for the rotor (Astroloy and Waspaloy); both would have satisfied the structural requirements. The decision to use Waspaloy was based on procurement time and cost considerations.

The high operating pressures and temperature dictated the use of Rene'41 for the main structural walls of the turbine manifold. Rene'41 is a double, vacuum-melted, precipitation-hardenable, nickel-base alloy. Although difficult to fabricate because of strain-age cracking in weld heat-affected zones, it has superior strength in the operating temperature zone of the Mark 48-0 turbine manifold.

The turbine nozzle and the seal support section of the housing were made of Haynes 188 which is easier to fabricate, has adequate strength, and is unaffected by the heat treatment cycle to which the Rene'41 details have to be subjected after assembly welding.

The main section of the rear bearing support, which is primarily in a cryogenic environment, was made of Inconel 718. However, the section which forms the tip seal over the rotor blades required a special consideration because of a need to minimize the blade tip clearance growth at the high operating temperatures. To accomplish this, Inconel 903, an iron-nickel-cobalt base alloy with excellent properties at the operating temperature and a very low thermal expansion coefficient was selected.

<u>Heat Transfer Analysis</u>

Heat transfer calculations were made to establish the thermal conditions on those components that would be subject to high temperatures or thermal stresses. These included primarily the turbine wheel and turbine manifold; but calculations were also made to determine the critical diameters of the shafts in the dynamic seal areas during operation.

The initial rotor configuration analyzed did not include coolant holes in the turbine disk. As a result, the downstream side of the disk was exposed to cold hydrogen coolant from the outboard seal purge; whereas, the upstream side of the disk was surrounded by hot gas. Analysis of this configuration indicated high axial thermal gradients, which led to unacceptable strains and deflections. To equalize the temperatures on either side of the disk, coolant bleed holes were added as shown in Fig. 42.

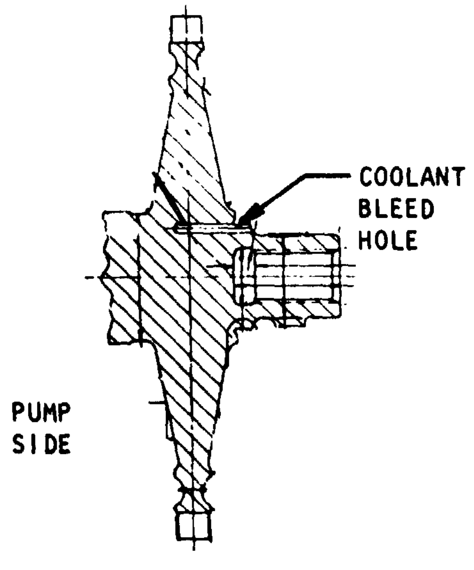

Figure 42. Mark 48-0 Turbine Wheel

The steady-state thermal profile of the rotor with the coolant passages and a turbine gas temperature of 1060 K (1909 R) is shown in Fig. 43. An enlarged view of the disk thermal map is included in Fig. 44. The bulk of the disk operates at

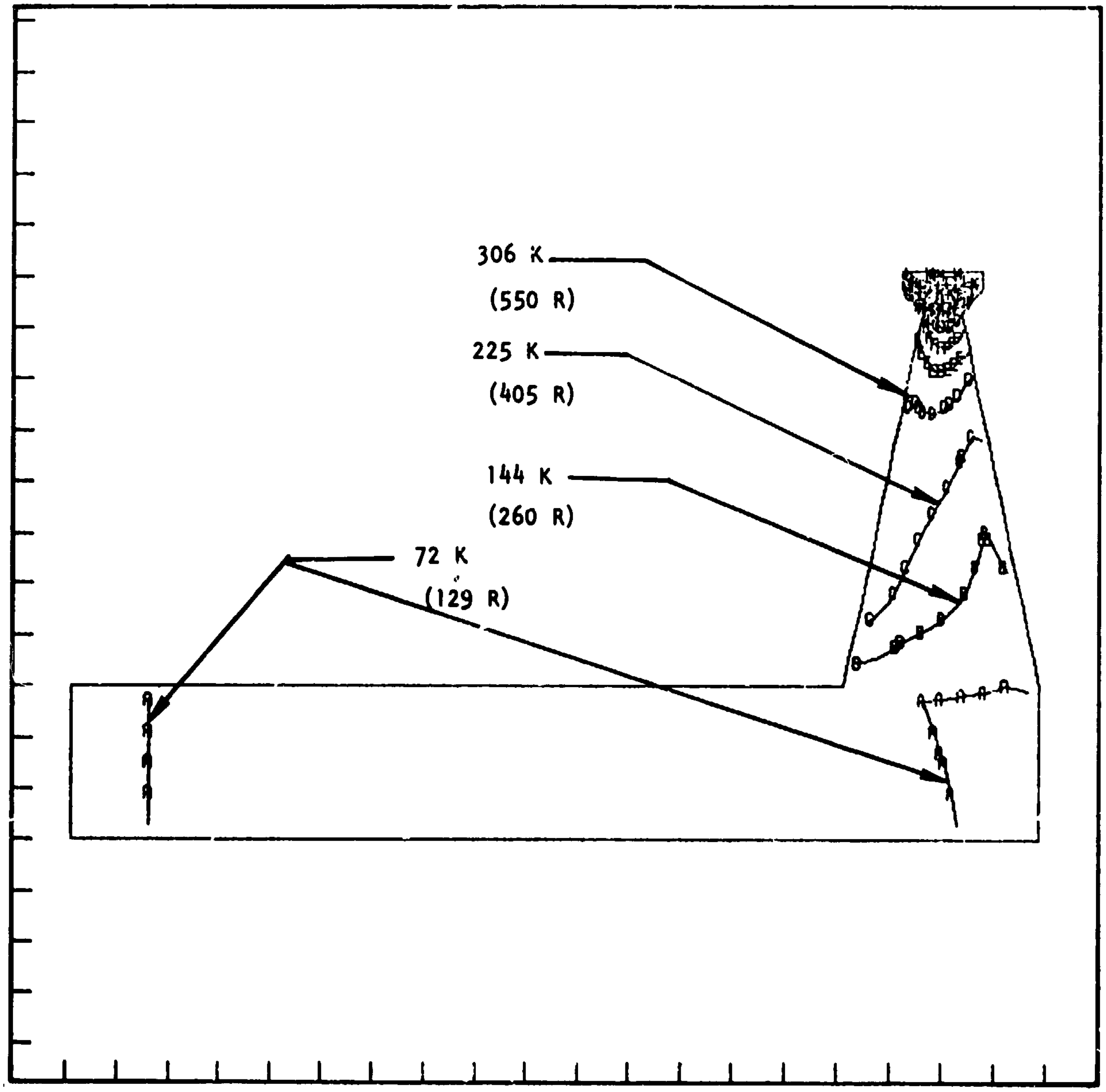

Figure 43. Finite Element Temperature Profile of Shaft and Disk at Maximum Gas Temperature (1061 K, 1909 R)

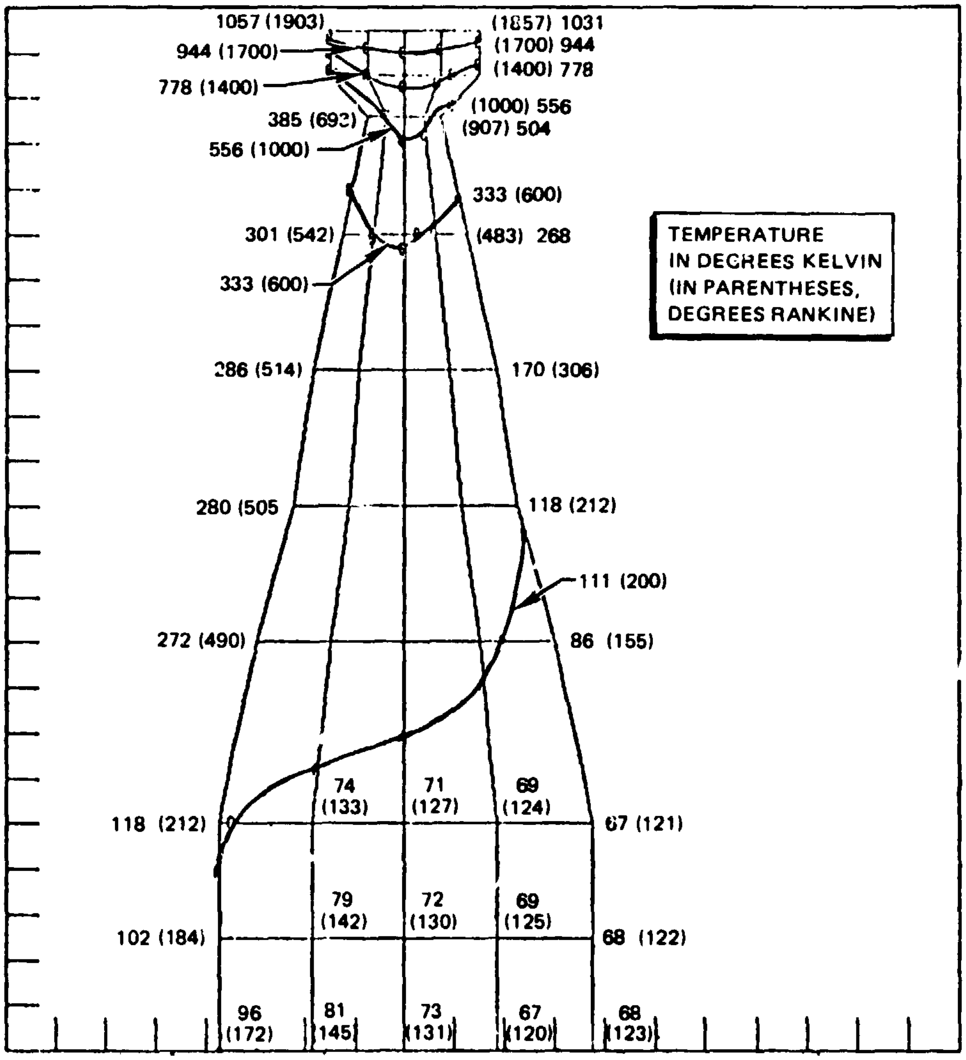

Figure 44. Temperature Profile of Turbine Disk at Maximum Temperature 1061 K, (1909 R)

very low temperature; only at the rim does the temperature level increase to approach the gas temperature. The temperature of the turbine blades during steady-state conditions is equal to the gas temperature.

Analysis of the turbine manifold included both transient and steady-state conditions. Because of idle-mode start planned for the Advanced Space Engine, the start transients did not impose any significant thermal gradients on the manifold. Steady-state thermal grandients and resulting strains were also acceptable. In contrast, the cold-gas shutdown purge introduced severe transient thermal gradients that would have precluded meeting the 300 life cycle requirement with a safety factor of four. The shutdown temperature characteristics are illustrated in Fig. 45. To improve the situation, a 1.57 mm (0.062 inch) thick Inconel 903 liner was included in the design, which acts as a thermal shield for the main structural walls during cutoff transients. The predicted temperatures (Fig. 46) are such that the 300 life cycles can be achieved with adequate safety margin.

Figure 47 presents the results of the analysis relative to the thermal profile of the aft-stud shaft in the area of the outboard seal.

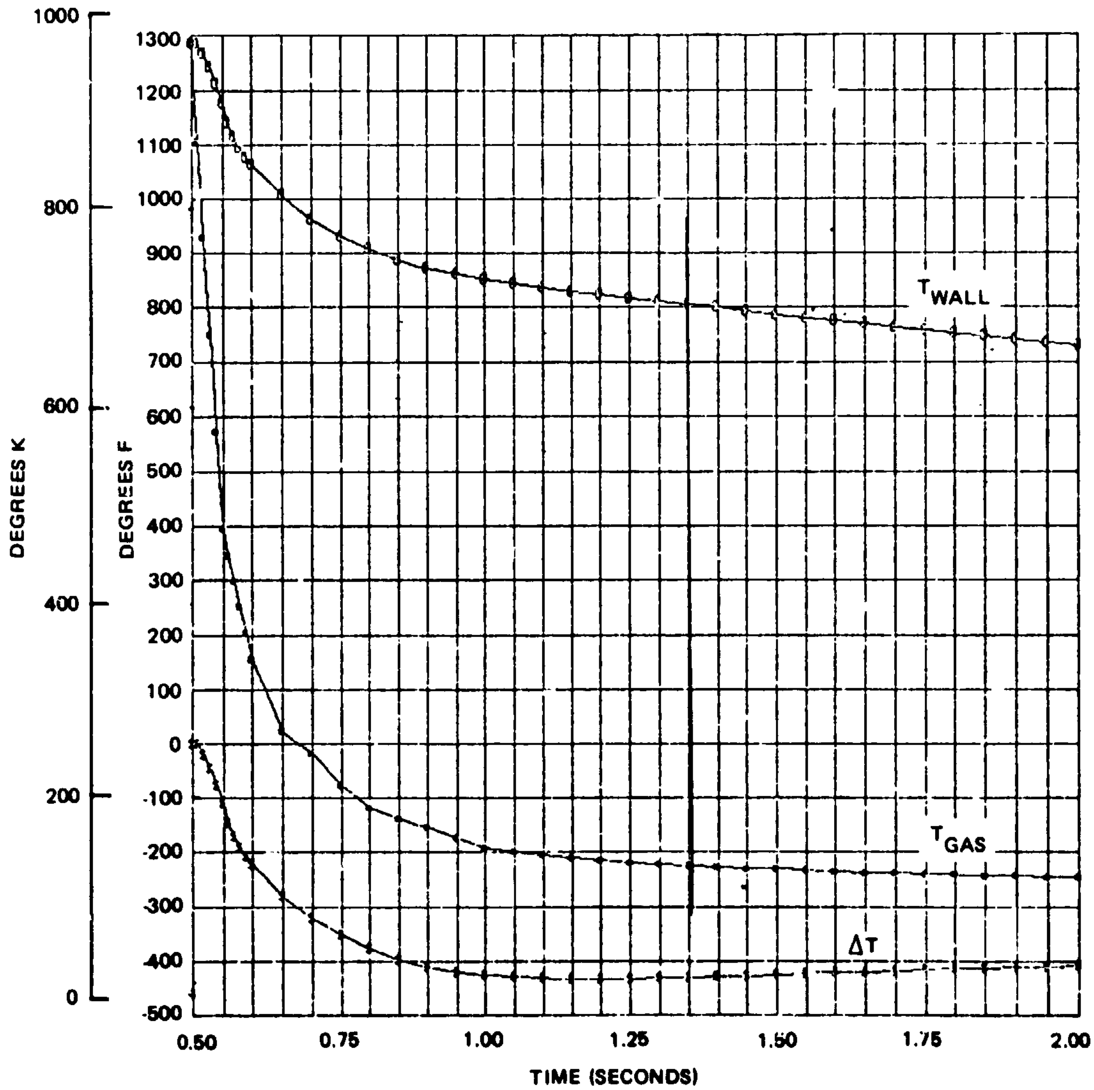

Figure 45. ASE LO_2 Turbine Manifold Shutdown Transient

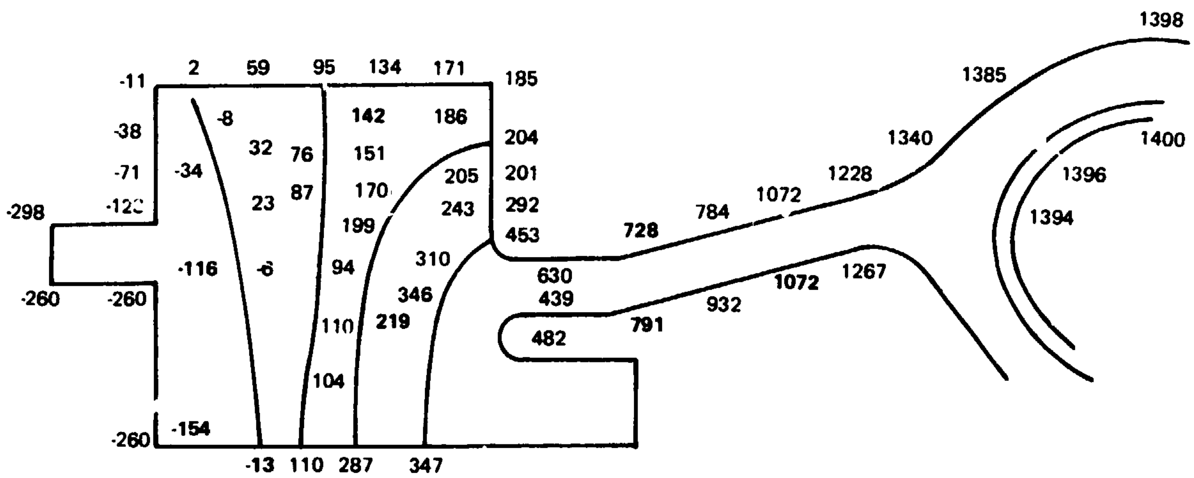

Kelvin Scale

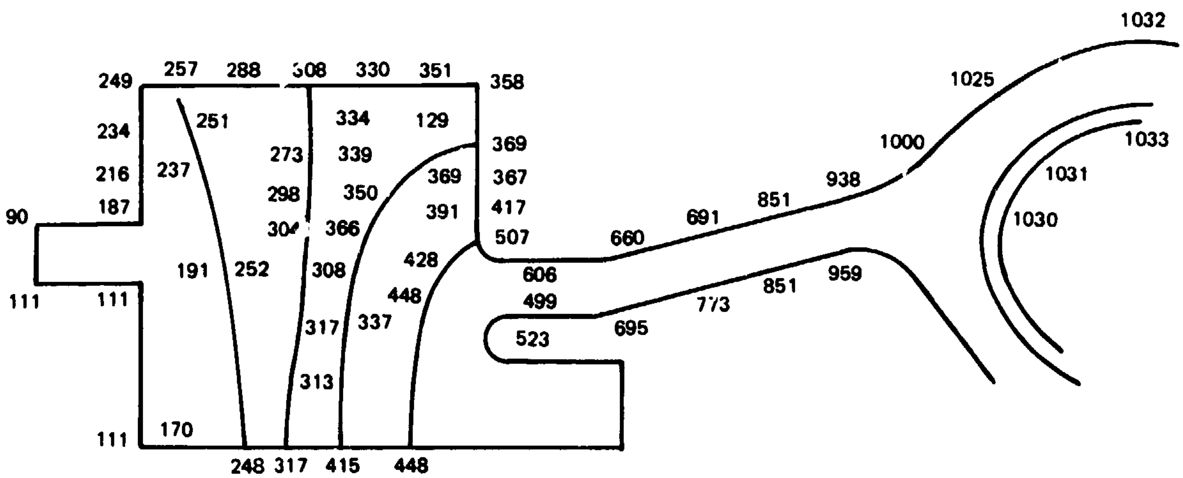

Fahrenheit Scale

Figure 46. ASE LO_2 Turbine Inlet Manifold Temperature Distribution (Steady State)

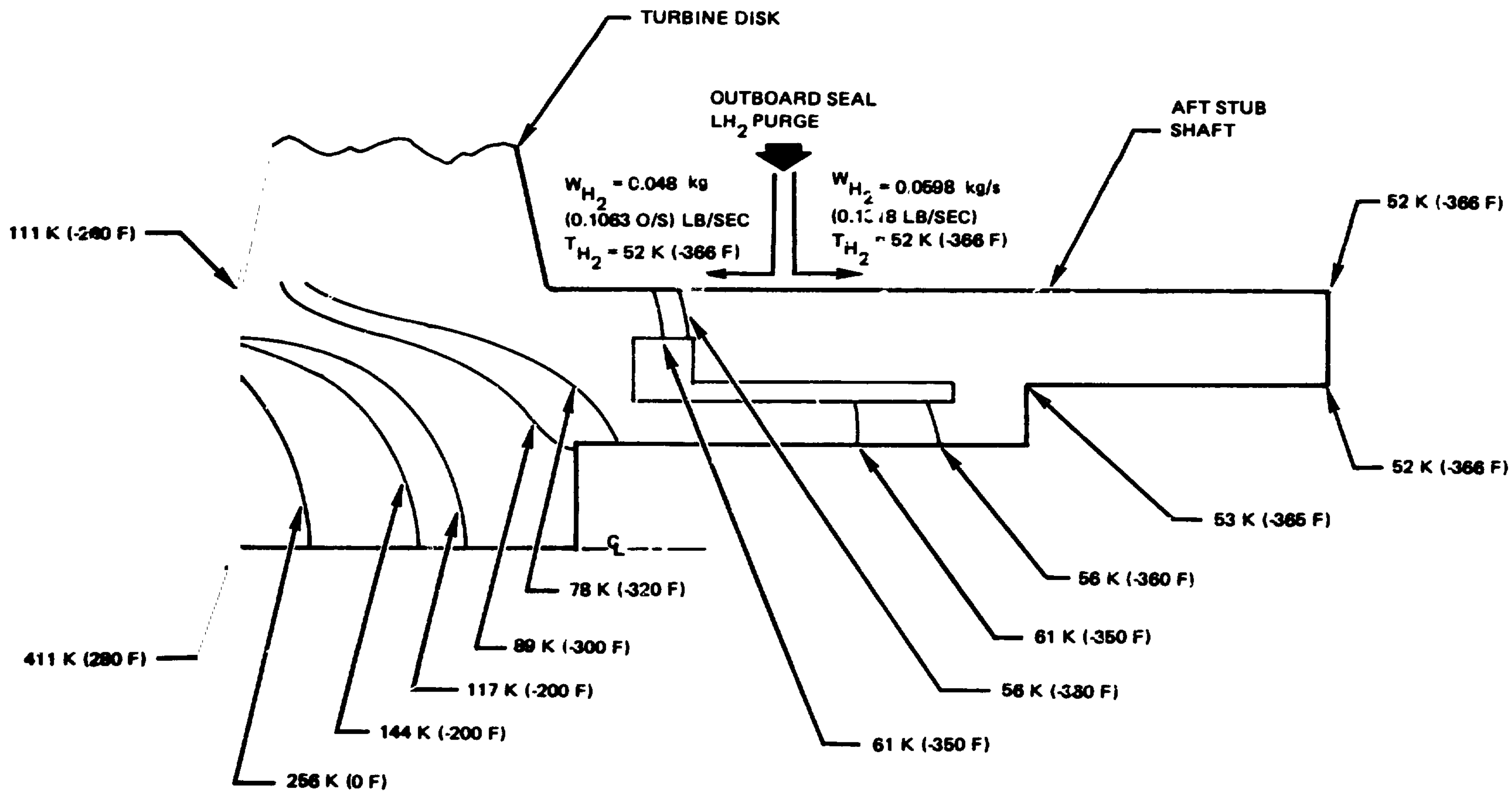

Figure 47. Oxidizer Turbopump Turbine Bearing Seal Area Shaft

Stress Analysis

A detailed structural analysis was conducted in accordance with established Rocketdyne procedures and the ground rules included in Appendix A. Detail information is presented below on the most critical components.

Impeller. A finite element model of impeller back plate was constructed and used to establish stress, strain, and deflection levels. The analysis was based on a maximum required operating speed of 8063 rad/s (77,000 rpm) and the pressure load schedule shown on Fig. 48. The basic sizing of the impeller was performed using the following cast Inconel 718 properties.

F_{ty}	69,000 N/cm^2 (100,000 psi)
F_{ru}	82,700 N/cm^2 (120,000 psi)
Elong	5.5%

This was to provide the flexibility of producing the impeller either by casting or machining from a wrought alloy. The first two impellers were fabricated by the latter method; consequently, they have higher safety factors by a ratio of 1.6:1.0.

Based on cast properties and a notch factor of 2.0, the burst speed was calculated at 10,000 rad/s (95,500 rpm), which establishes the allowable operating speed at 8335 rad/s (79,600 rpm) using a 20% margin. The factor of safety on the spline was 3.83 based on shear ultimate. The factor of safety on the vane stresses was calculated at 1.93. The radial and tangential stress profile resulting from centrifugal effects on the backplate is plotted in Fig. 49, as a function of radial location. Figures 50 and 51 present effective stress profile and maximum effective stresses resulting from combined centrifugal and pressure loads. The effective strain profile from the combined loading is shown in Fig. 52; Fig. 53 shows the deformed structure of the impeller with radial and axial deflections indicated at the critical location of the balance piston high-pressure orifice lip. The Goodman diagram for the vanes, taking into account centrifugal and pressure effects, is included in Fig. 54. It shows that the calculated alternating stress of 1944 N/cm^2 (2820 psi), 30 percent of pressure loading, is far below the allowable 6984 N/cm^2 (10,000 psi) for a mean stress of 43,300 N/cm^2 (62.000 psi).

Inducer. The inducer blade stresses were computed by dividing the blade into a series of pie-shaped sections, loading each section with pressure and centrifugal forces, and calculating the measurements and stresses at the blade root. The computed stresses and factors of safety were:

Net bending stress	9075 N/cm^2 (13,164 psi)
Centrifugal direct stress	5600 N/cm^2 (8,127 psi)
Mean stress	14,675 N/cm^2(21,291 psi)

Alternating stress (30% of Pressure Bending) = 11,424 N/cm^2 (16,571 psi)

Factor of safety on mean stress = 6.0

Factor of safety on alternating stress = 2.0

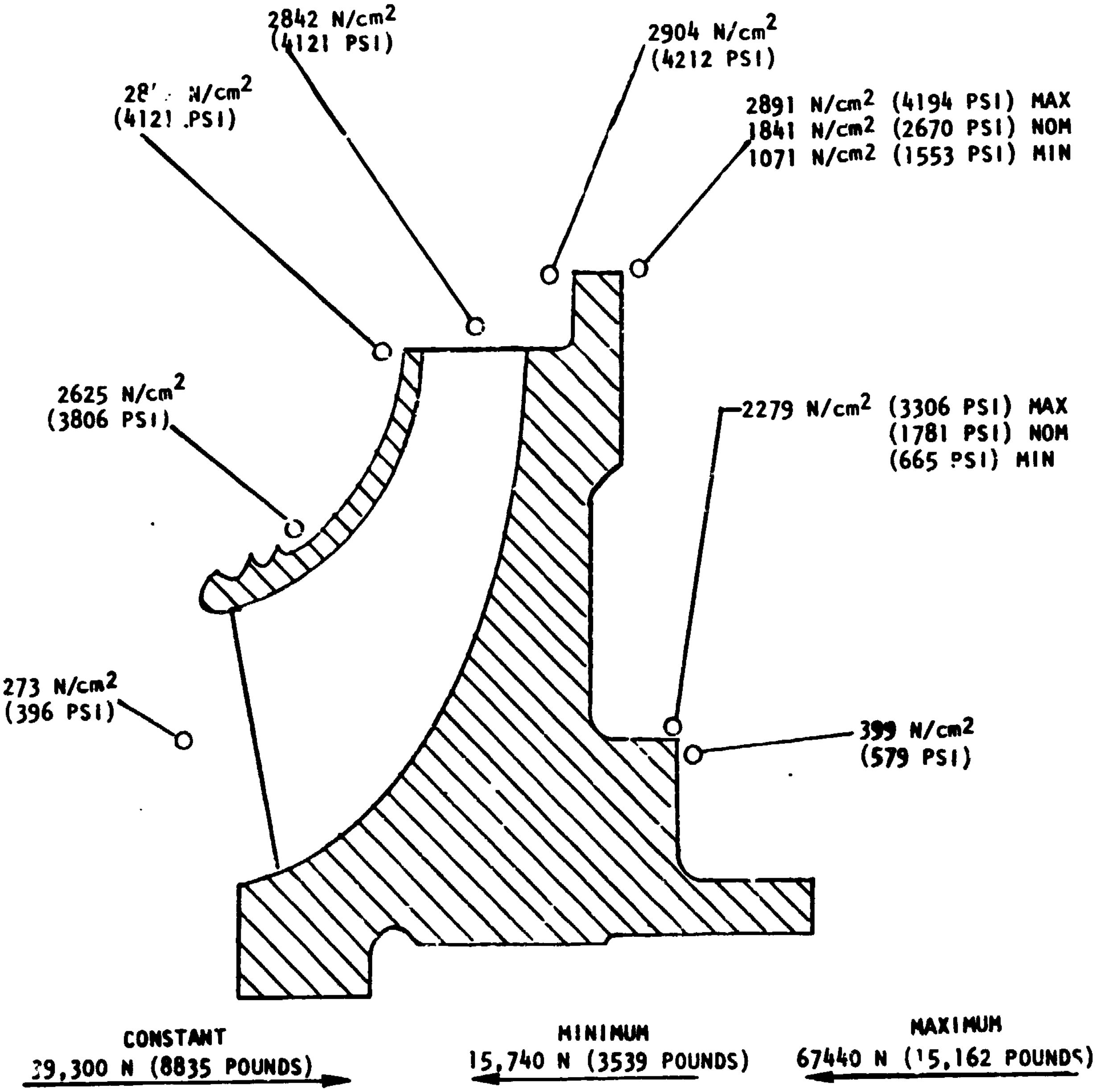

Figure 48. Pressure Loads on Oxidizer Pump Impeller

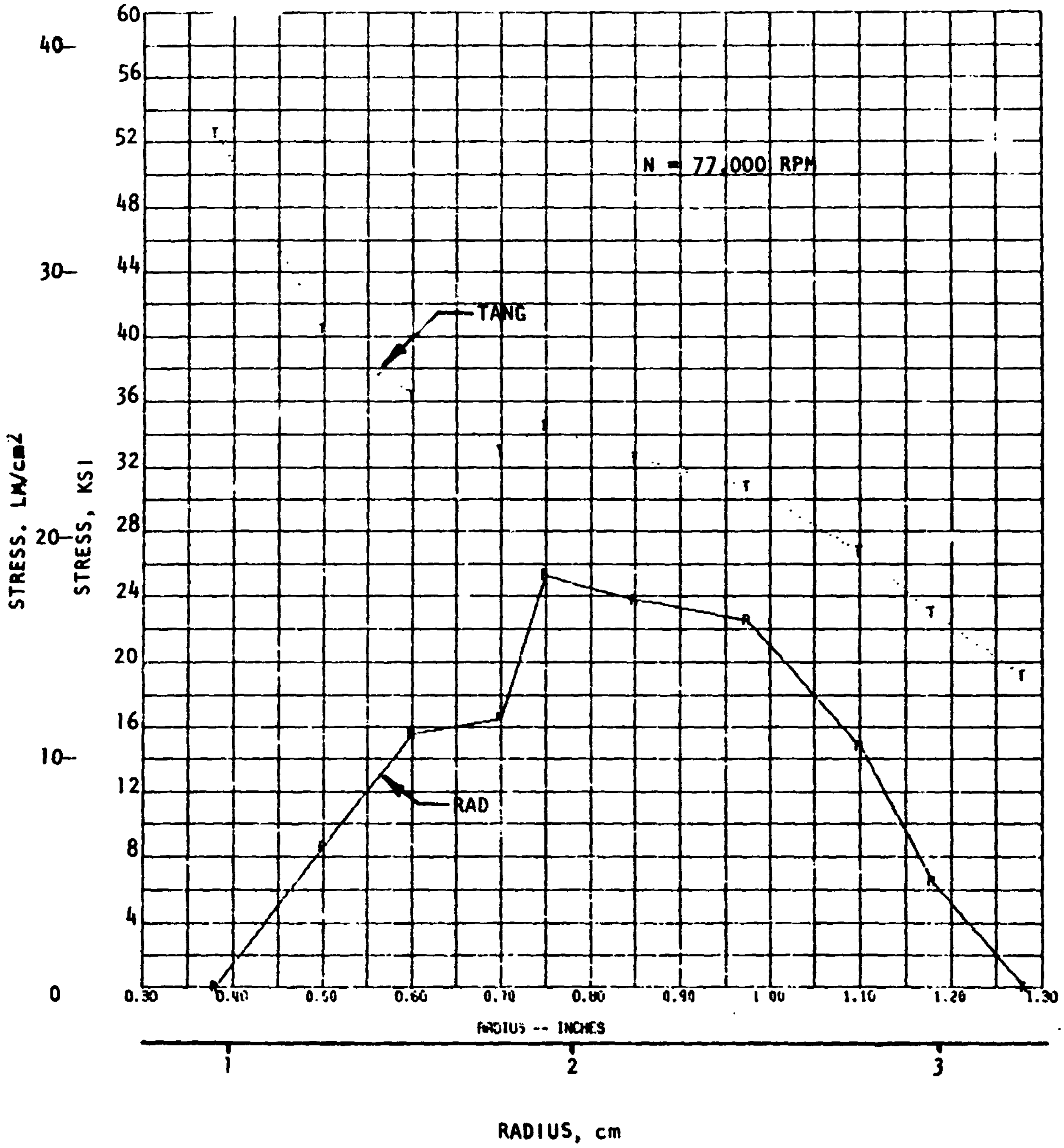

Figure 49. Mark 48-0 Impeller Tangential and Radial Stresses

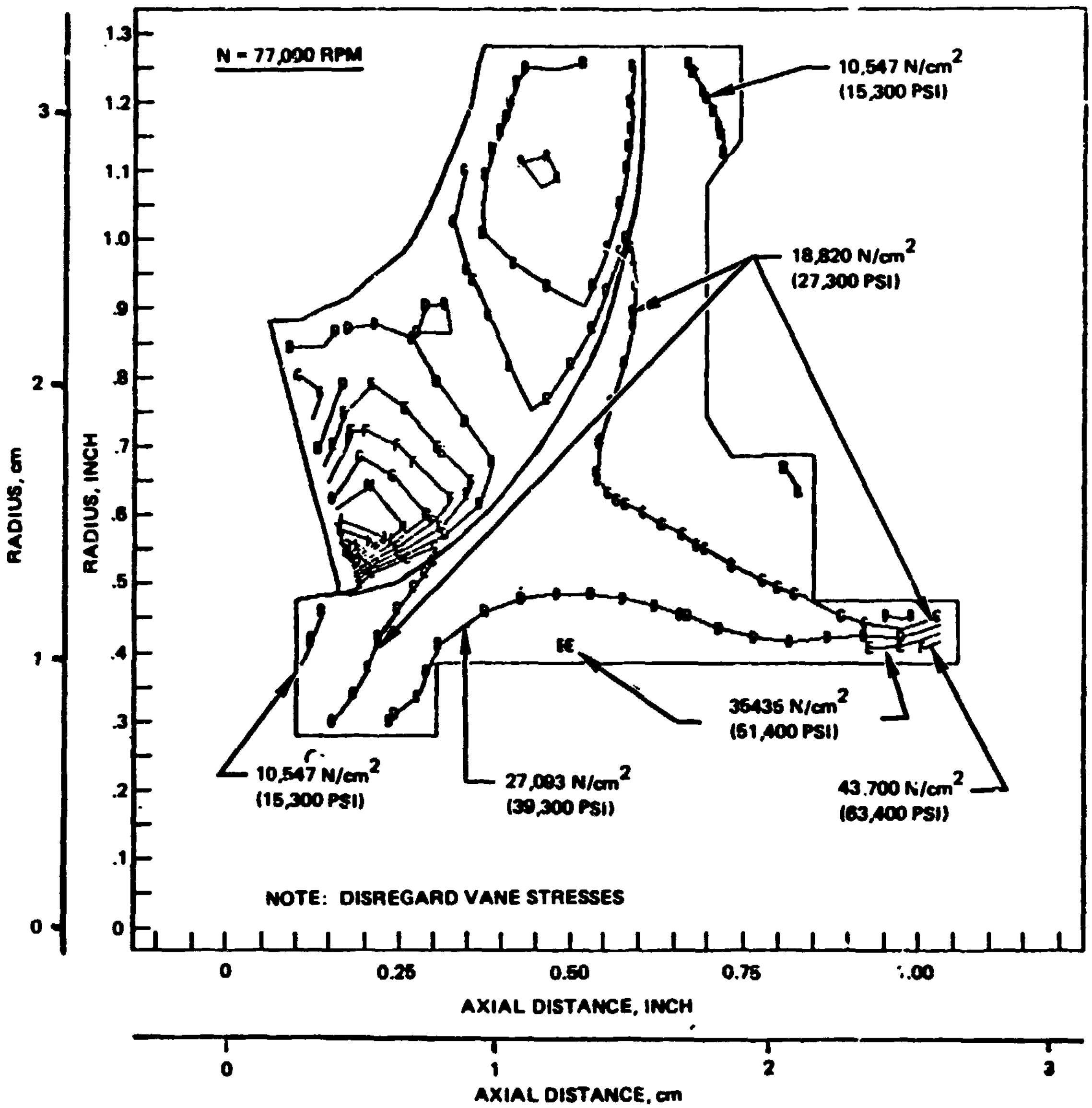

Figure 50. Profile Plot of Effective Stress in Impeller Back Plate for Maximum Centrifugal and Pressure Loads

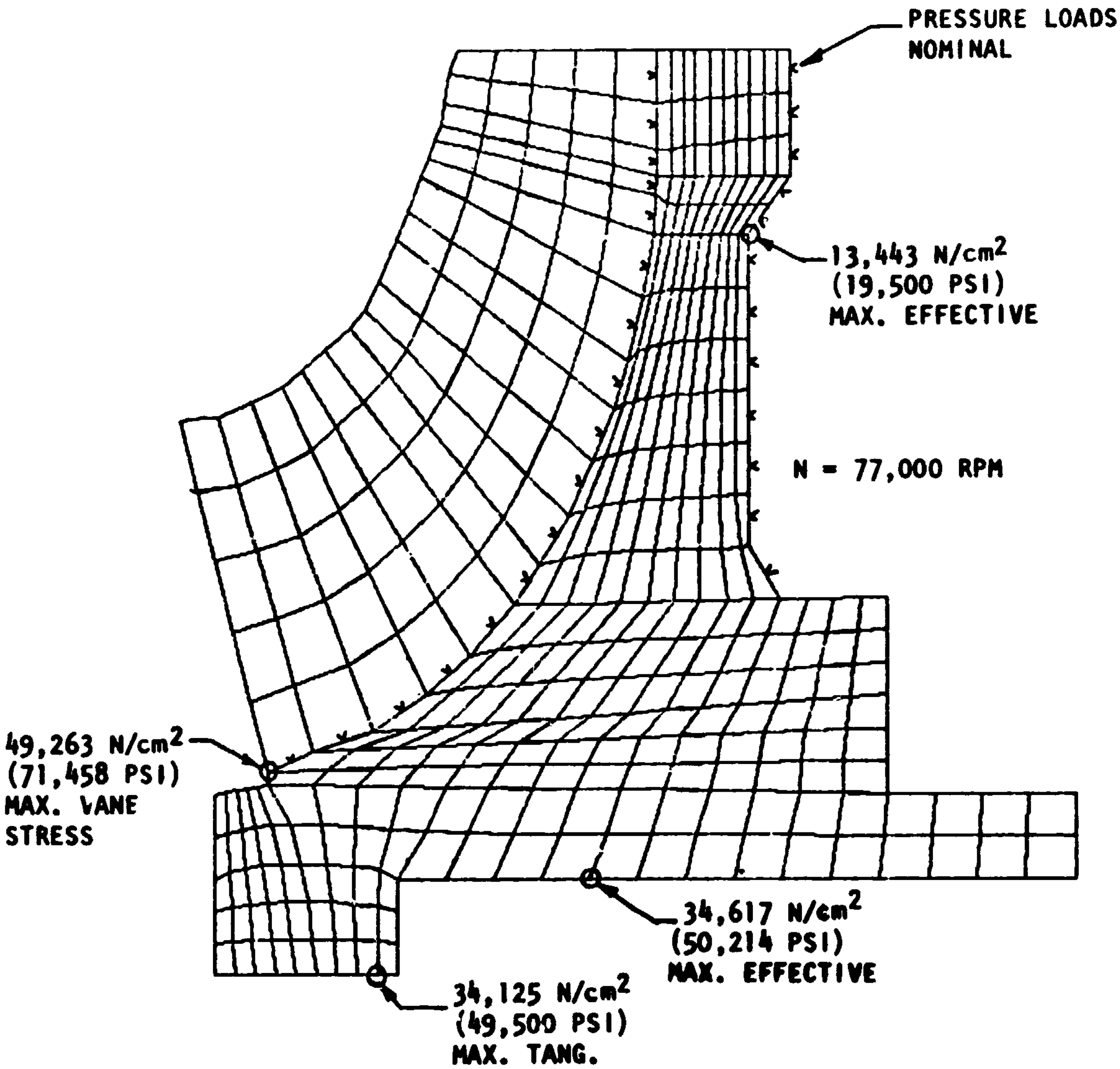

Figure 51. Maximum Effective Stress Under Centrifugal and Pressure Loads

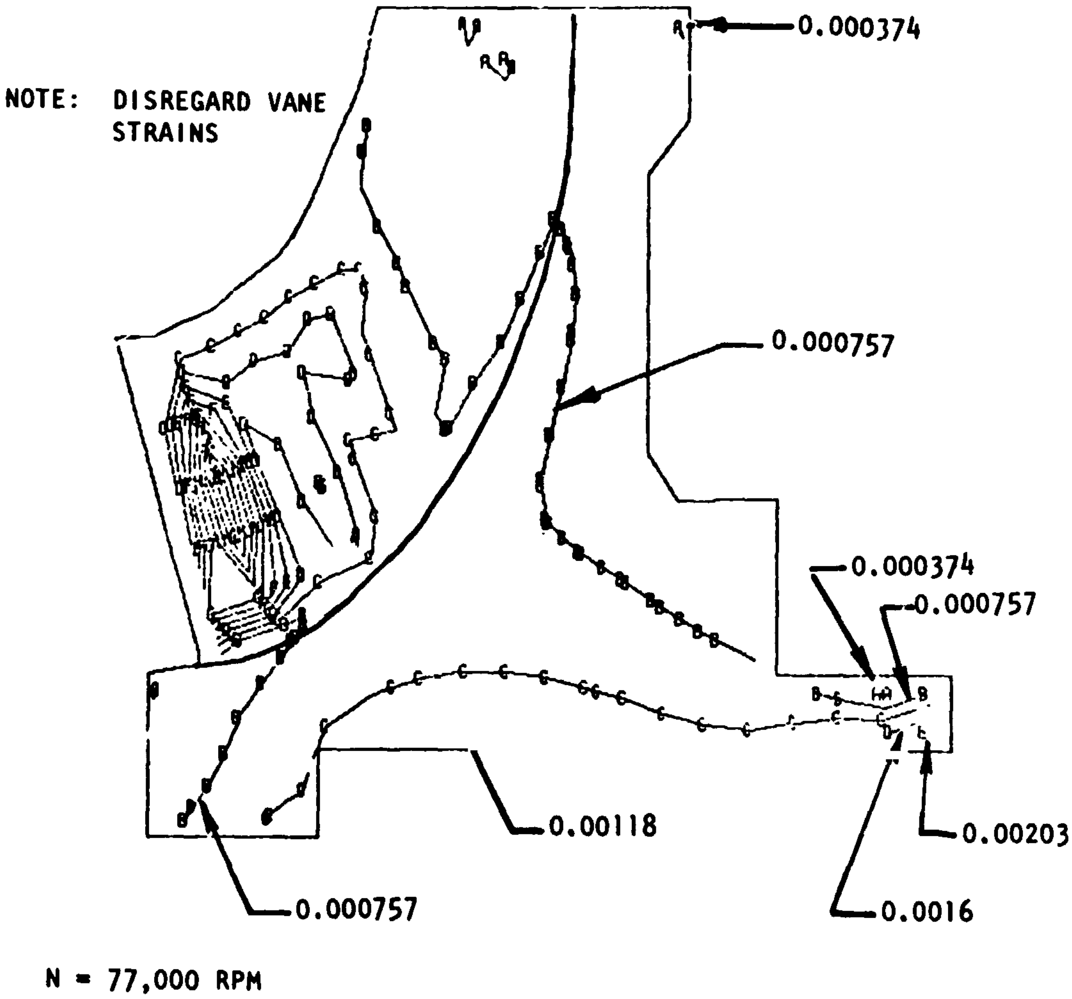

Figure 52. Profile Plot of Effective Strains Impeller Back Plate for Maximum Centrifugal and Nominal Pressure Loads

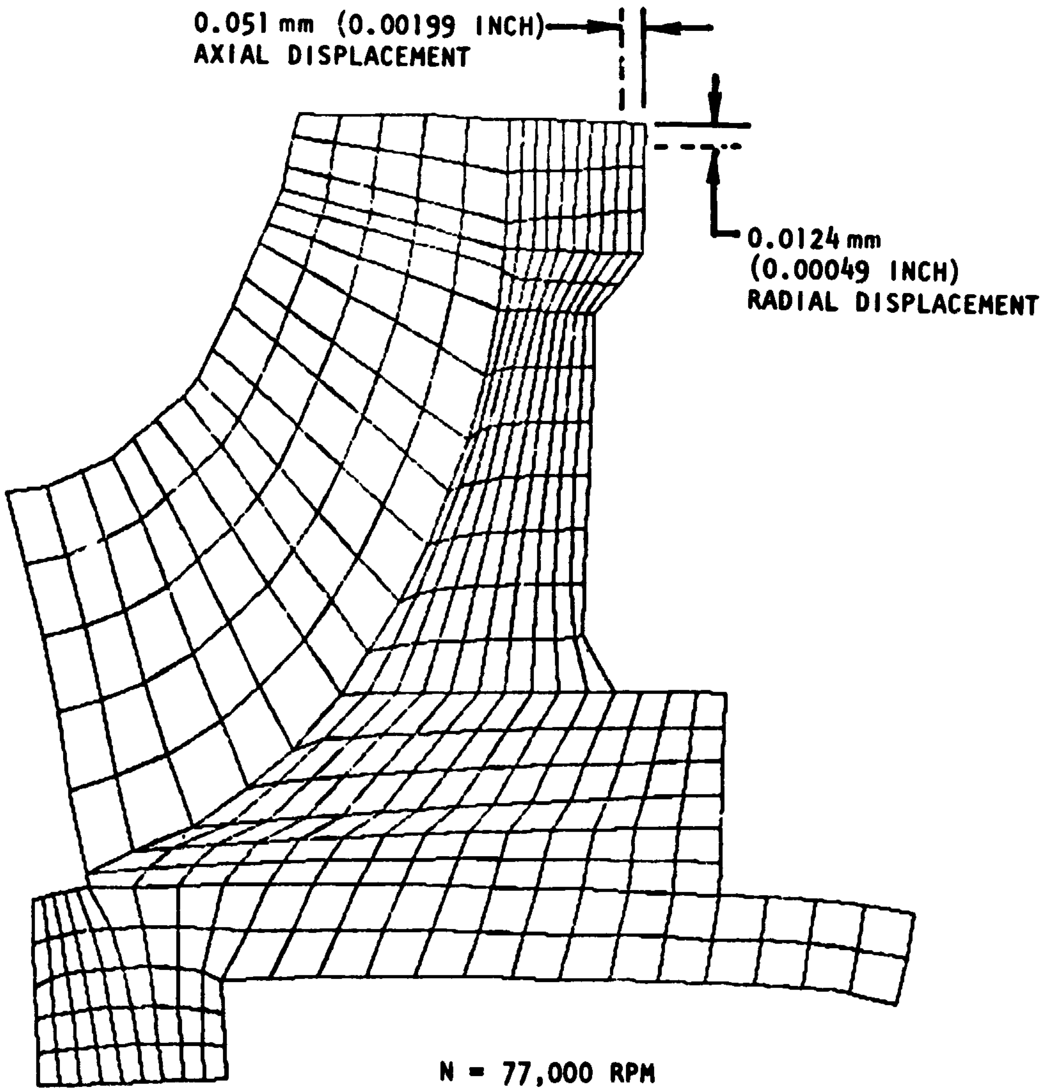

Figure 53. Radial and Axial Displacements of Impeller Under Nominal Pressure and Maximum Centrifugal Loads

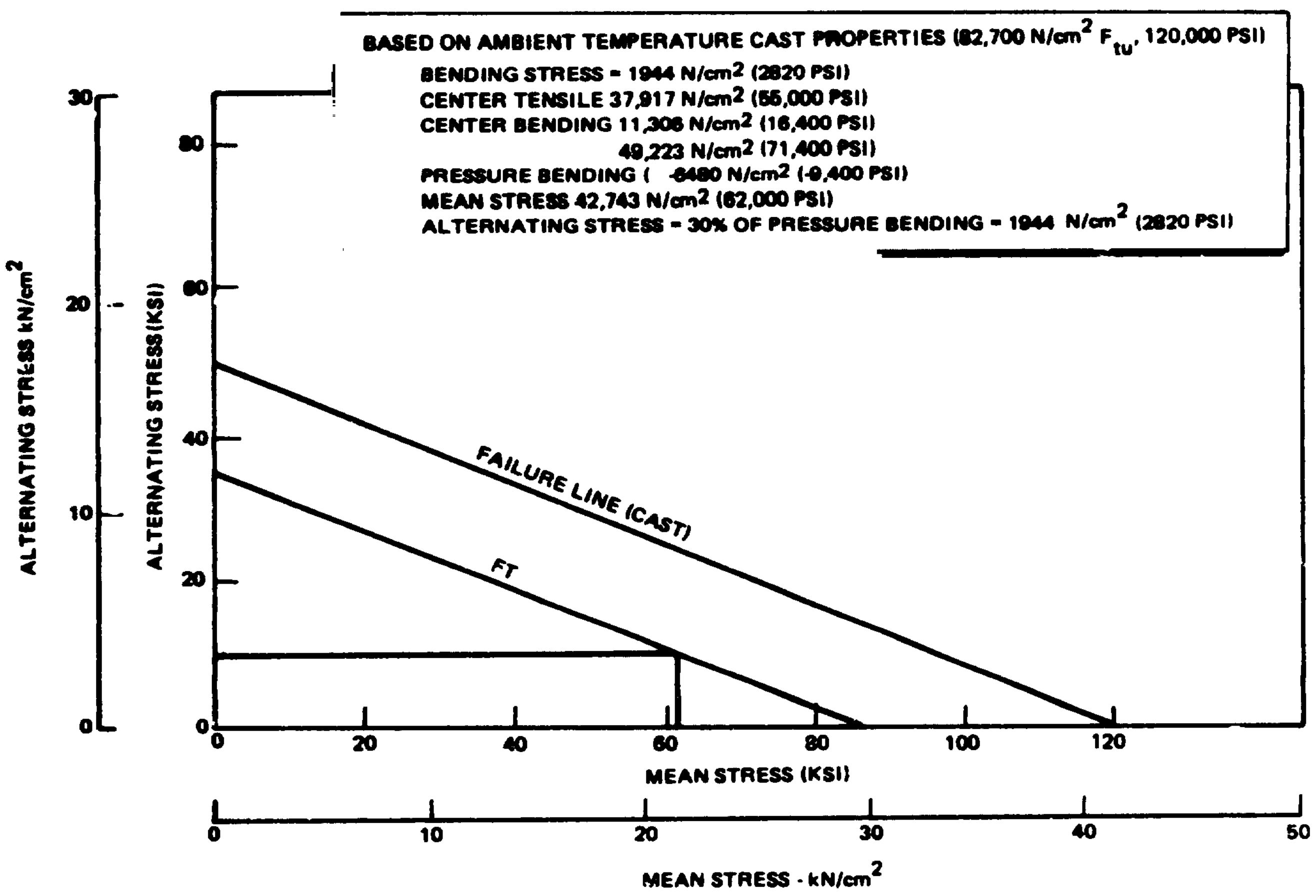

Figure 54. Goodman Diagram, Oxidizer Impeller Vanes

A Goodman diagram for the inducer blade (Fig. 55) shows that the calculated alternating stress of 11,424 N/cm^2 (16,571 psi) is well below the allowable alternating stress of 23,800 N/cm^2 (34,500 psi) at the mean stress of 14,675 N/cm^2 (21,291 psi).

Volute. To aid in establishing the structural characteristics of the volute a finite element model was made. The effective stress profile obtained from the computer run of the model is shown in Fig. 56. Strain levels in the structure are presented in Fig. 57. The deflections calculated at the critical locations (seal joints), assuming and unrestrained structure, are noted in Fig. 58. The factor of safety on ultimate strength using cast Inconel 718 properties was 2.81.

Turbine Wheel. The finite element model of the turbine disk used for heat transfer analysis was also utilized to calculate the stress and strain levels. Using a conservative assumption of 866 K (1100 F) for an average disk temperature and corresponding properties of 93,760 N/cm^2 (136 ksi) for ultimate strength, 73,100 N/cm^2 (106 ksi) for yield strength and 15% elongation, the burst speed was calculated at 10,158 rad/s (97,000 rpm). The maximum allowable operating speed, with a safety factor of 1.4 on the ultimate is 8587 rad/s (82,000 rpm).

The radial and tangential stress levels as a function of radius are presented in Fig. 59. The effective strain profile is shown in Fig. 60 and 61 for the maximum and nominal gas temperature condition. Radial and axial deflections were established at the rim to permit proper setting of assembly clearances. The rim deflections are indicated in Fig. 62. The stress rupture life of the disk , as a function of temperature, is shown in Fig. 63; included in the curve is a safety factor of 1.4. Figure 64 is a modified Goodman diagram of the stresses in the turbine blades at a gas temperature of 1055 K (1900 R). It shows that the calculated alternating stress of 2070 N/cm^2 (3000 psi) is well below the allowable alternating stress of 8270 N/cm^2 (12,000 psi) at a mean stress of 27,600 N/cm^2 (40,000 psi).

Turbine Manifold. The turbine manifold was analyzed for steady-state and transient conditions using a finite element model (Fig. 65). Because of the type of idle mode start planned for the ASE, the start transients did not present structural problems. The engine cutoff on the other hand is characterized by a cold hydrogen lag in the preburner, which introduces severe thermal gradients in the manifold walls. To reduce these thermal gradients, a 1.57 mm (0.062 inch) thick Inconel 903 liner was incorporated in the inlet torus. The strain profiles with the liner are included in Fig. 66 for steady-state conditions and Fig. 67 for cutoff. The maximum strain observed is 0.0037 for steady-state and 0.0058 for cutoff transient.

The maximum pressure-induced stress level in the manifold is 27,600 N/cm^2 (40 ksi) with the resulting safety factor of 3.5 on pressure stresses. The steady-state effective stress profile, including thermal effects is shown in Fig. 68; the maximum stress level is 64,000 N/cm^2 (93 ksi). Similarly, the stress distribution under cutoff transients is shown in Fig. 69; the maximum stress observed is 68,100 N/cm^2 (98.8 ksi), which results in a factor of safety of 1.4, based on a tensile ultimate of 96,500 N/cm^2 (140 ksi).

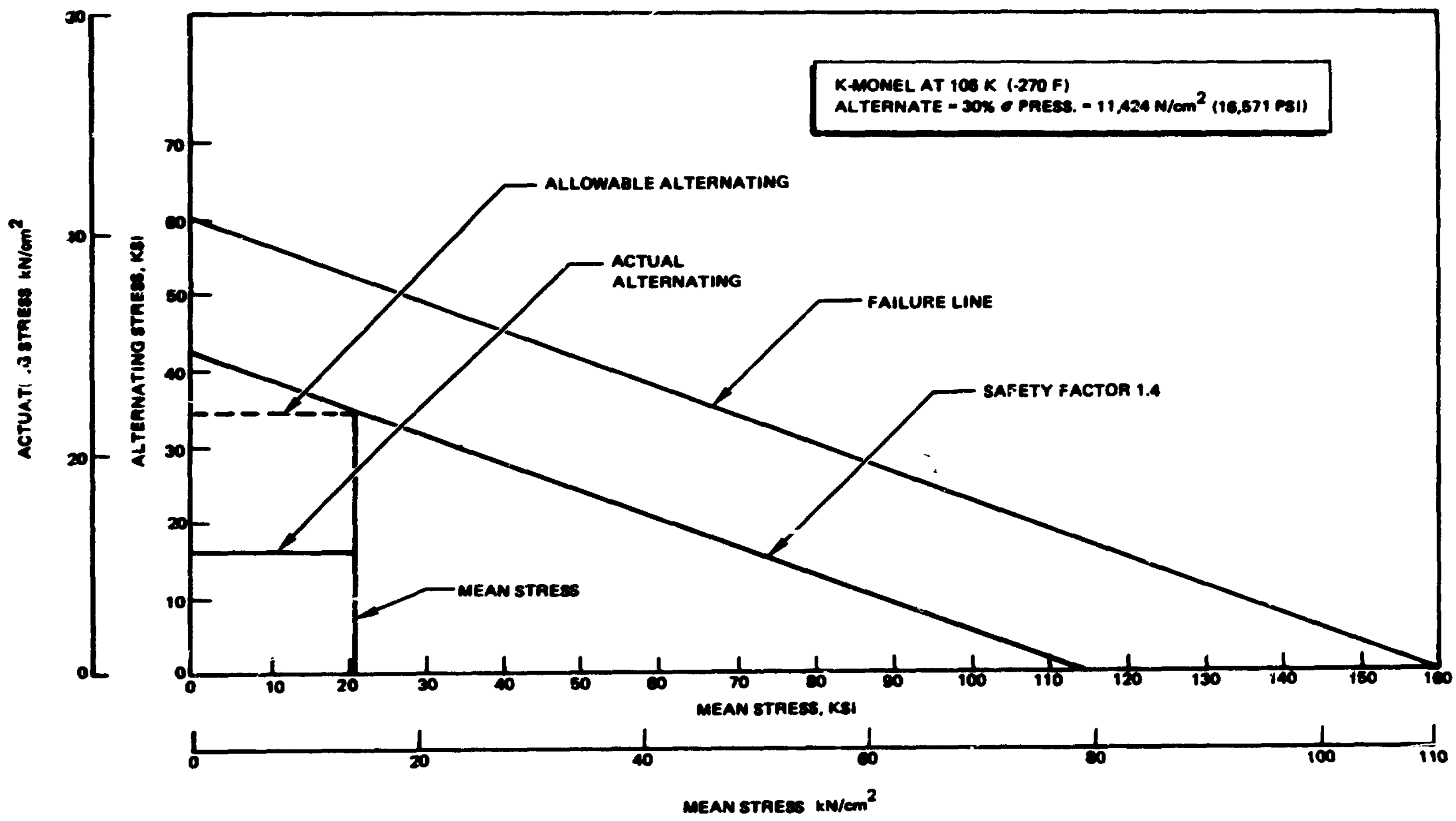

Figure 55. LO_2 Inducer Blade Goodman Diagram

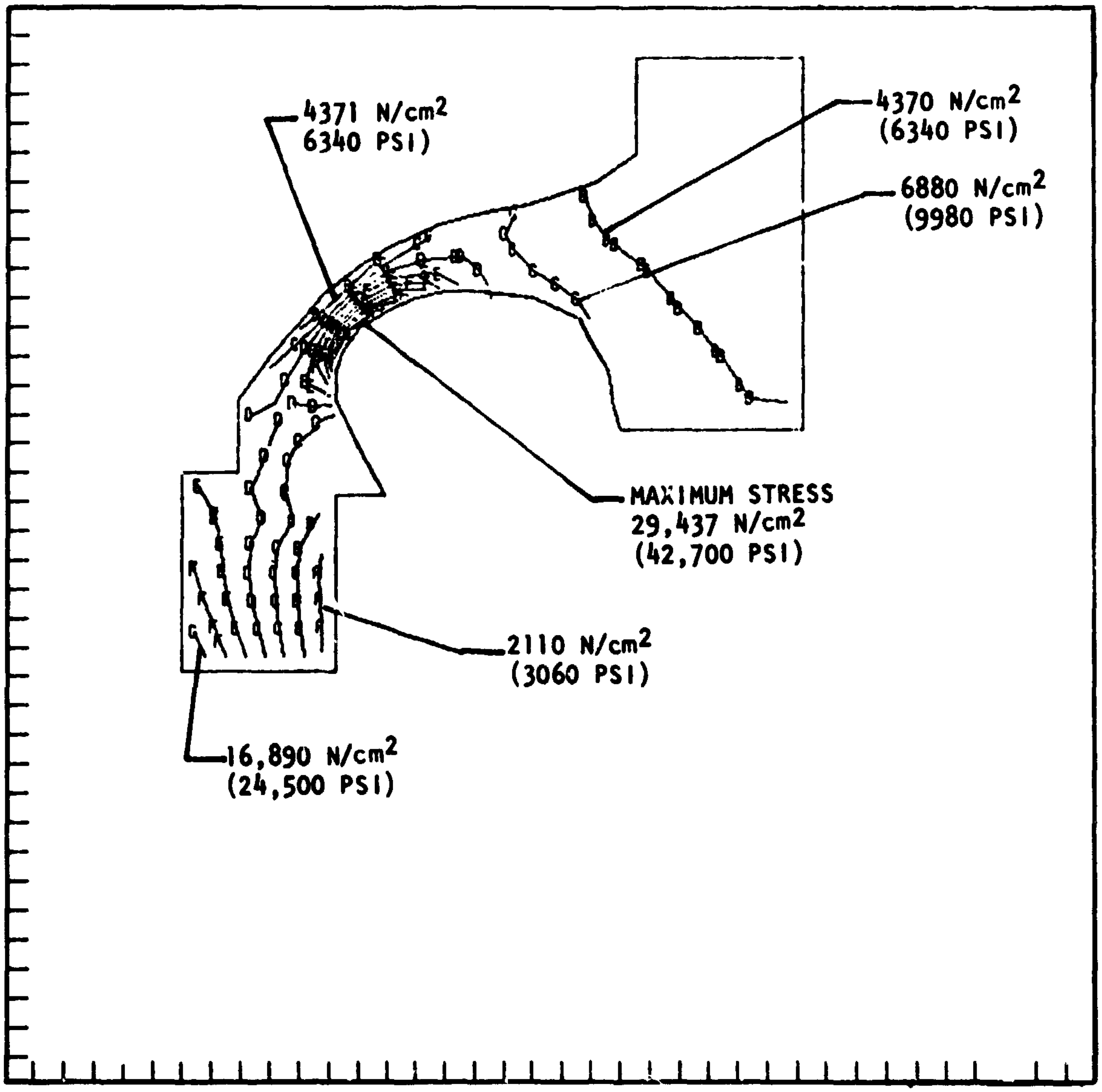

Figure 56. Finite Element Effective Stress Profile in Volute

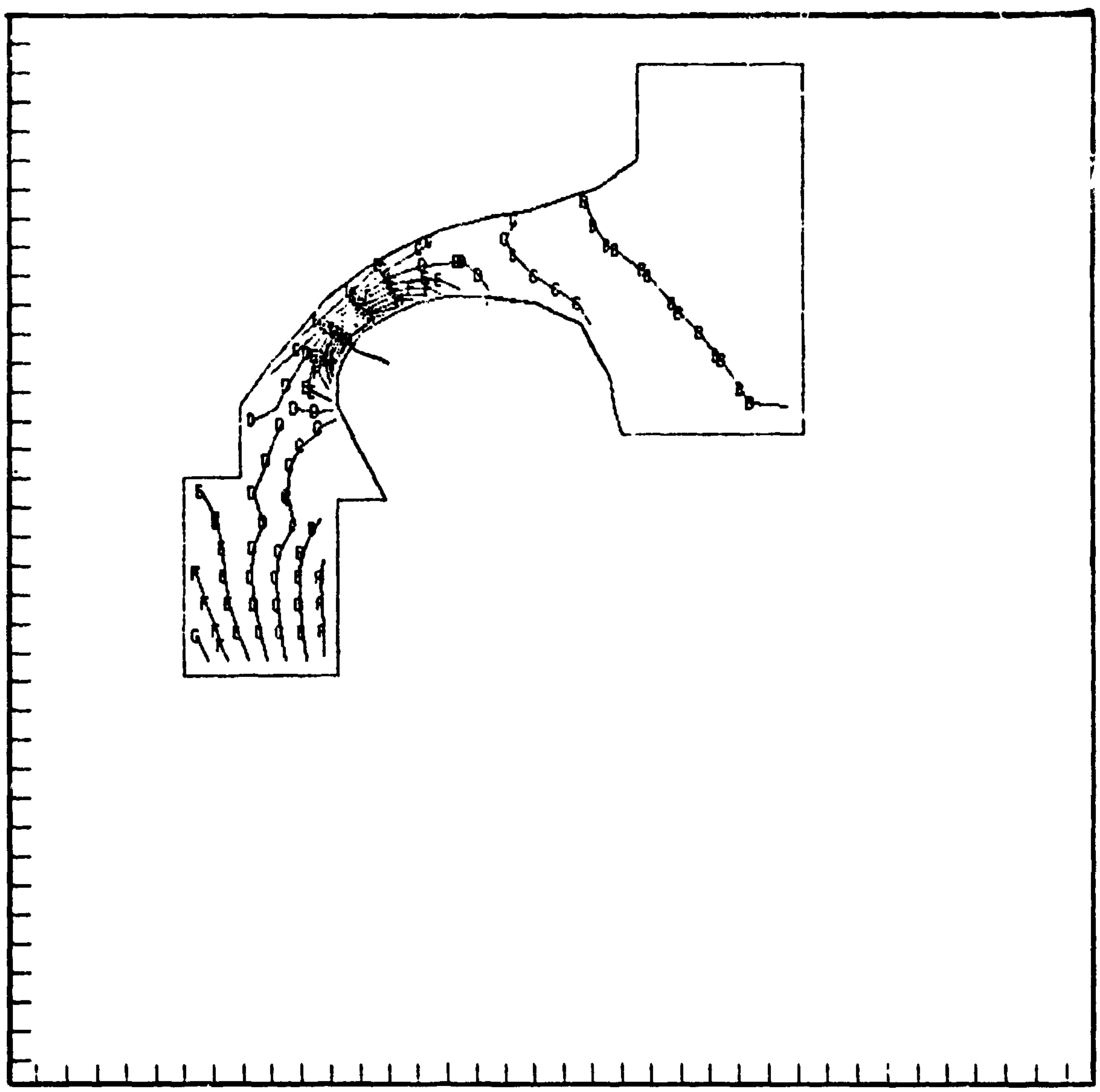

A 8.94×10^{-05}	B 1.85×10^{-04}	C 2.91×10^{-04}	D 3.97×10^{-04}
E 5.04×10^{-04}	F 6.10×10^{-04}	G 7.17×10^{-04}	H 8.23×10^{-04}
J 9.29×10^{-04}	K 1.08×10^{-03}	L 1.14×10^{-03}	M 1.23×10^{-03}

Z. AXIS

Figure 57. Finite Element Effective Strain in Pump Volute (Ambient, Worst Case)

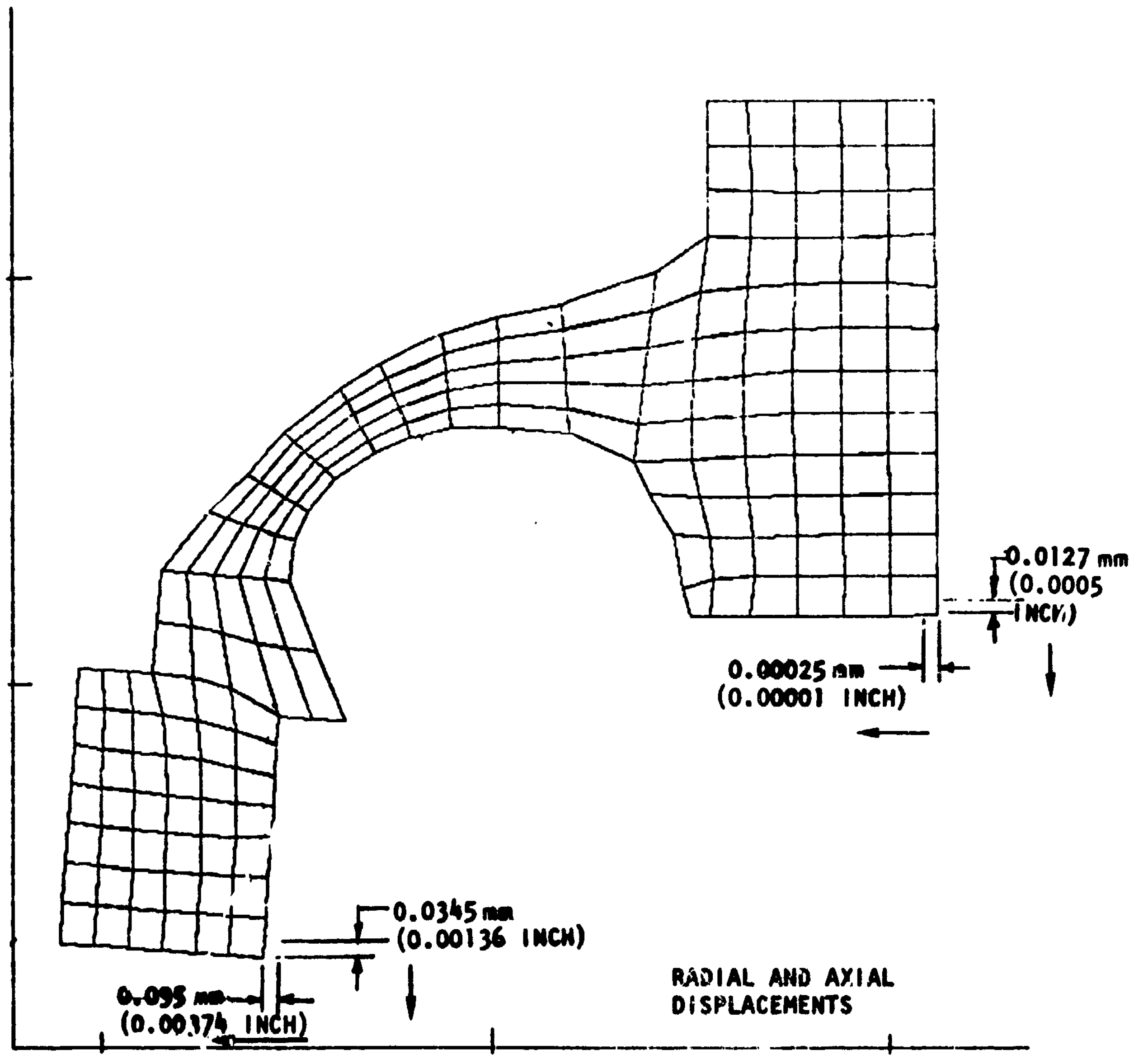

Figure 58. Displacements of Volute at Maximum Pressure

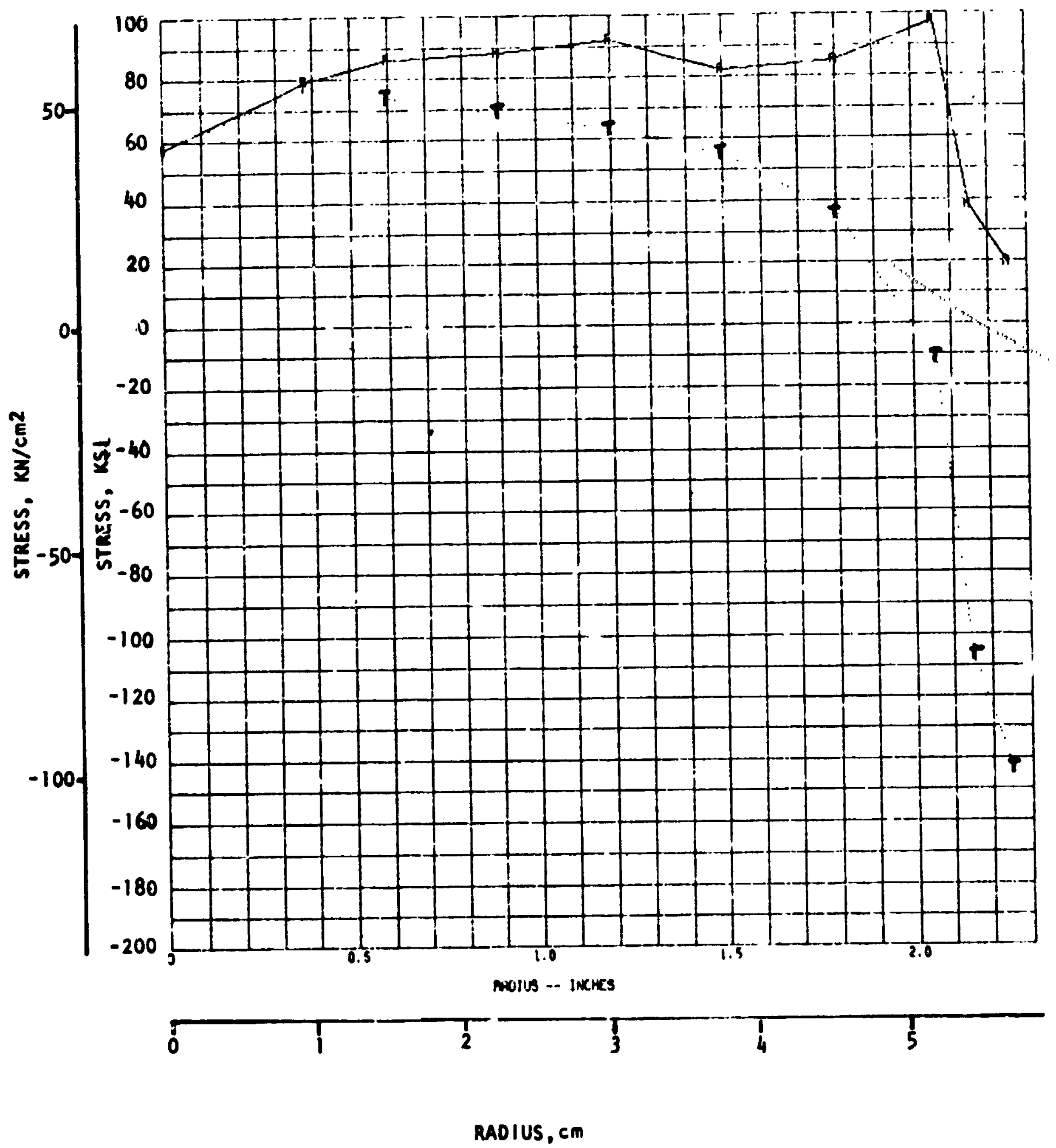

Figure 59. Turbine Disk Radial and Tangential Stresses at 1.1 x N Versus Radius

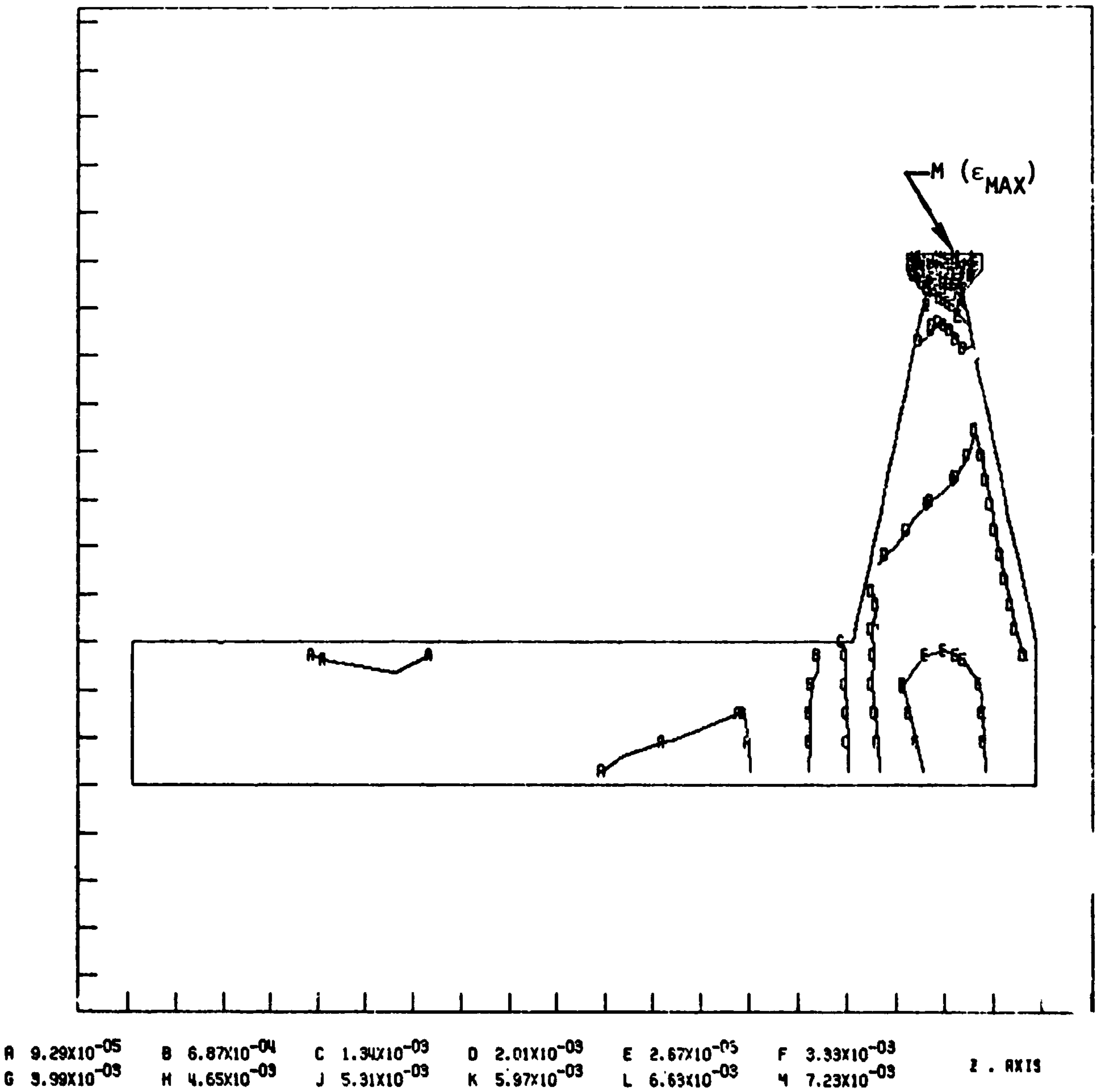

Figure 60. Finite Element Effective Strain Profile of Turbine Shaft S/Disk at Maximum Gas Temperature

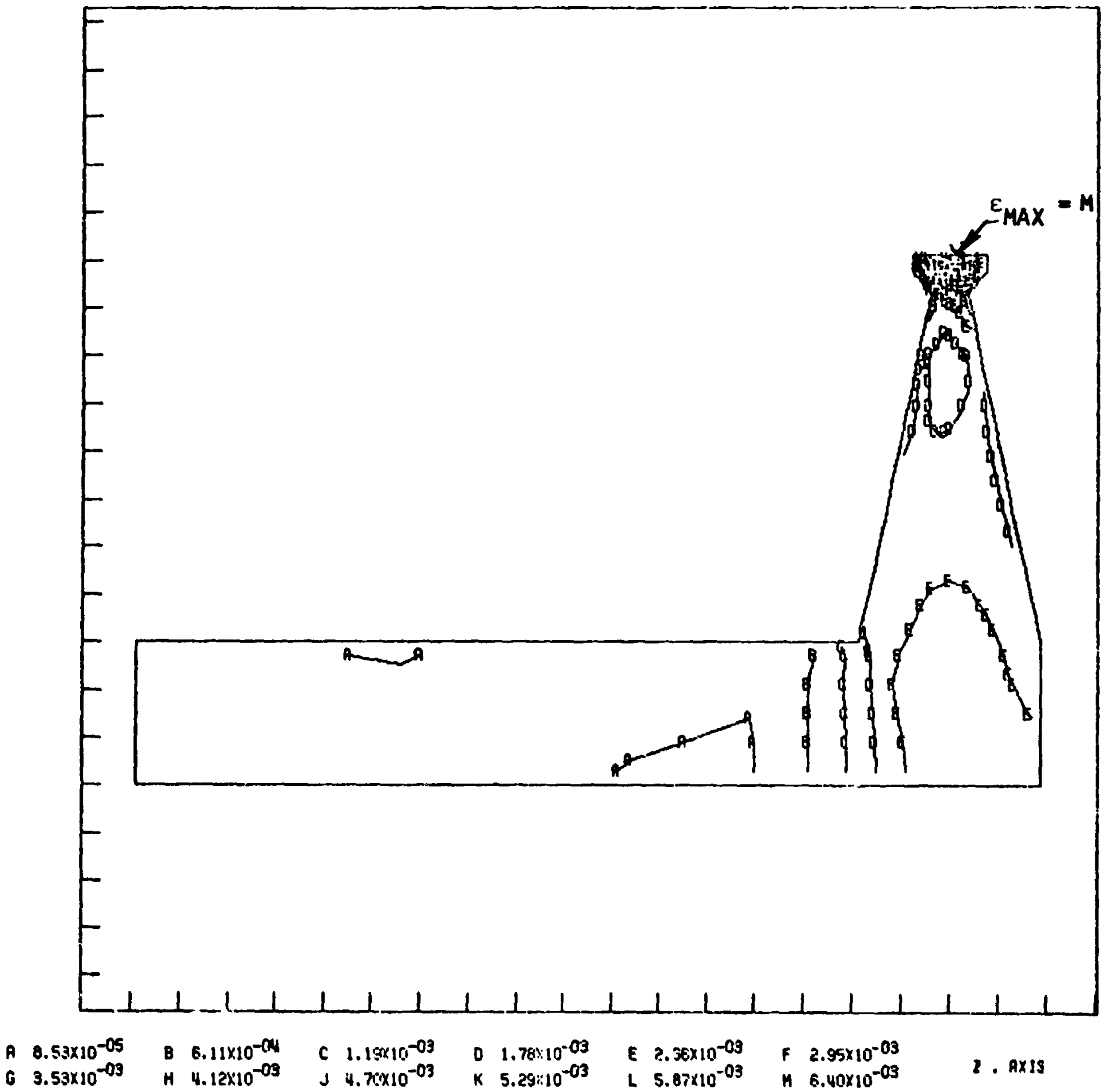

Figure 61. Finite Element Effective Strain Profile of Turbine Shaft and Disk at Nominal Gas Temperature

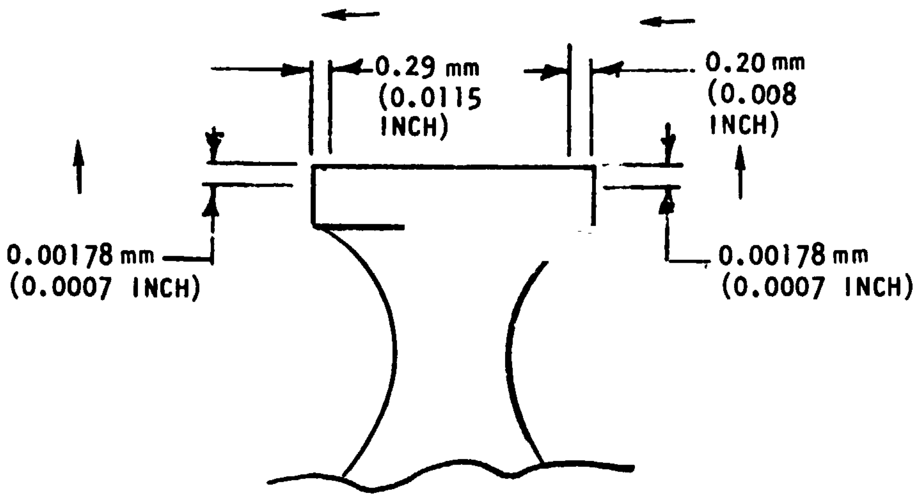

Figure 62. Oxidizer Turbine Nominal Temperature Rim Deflections

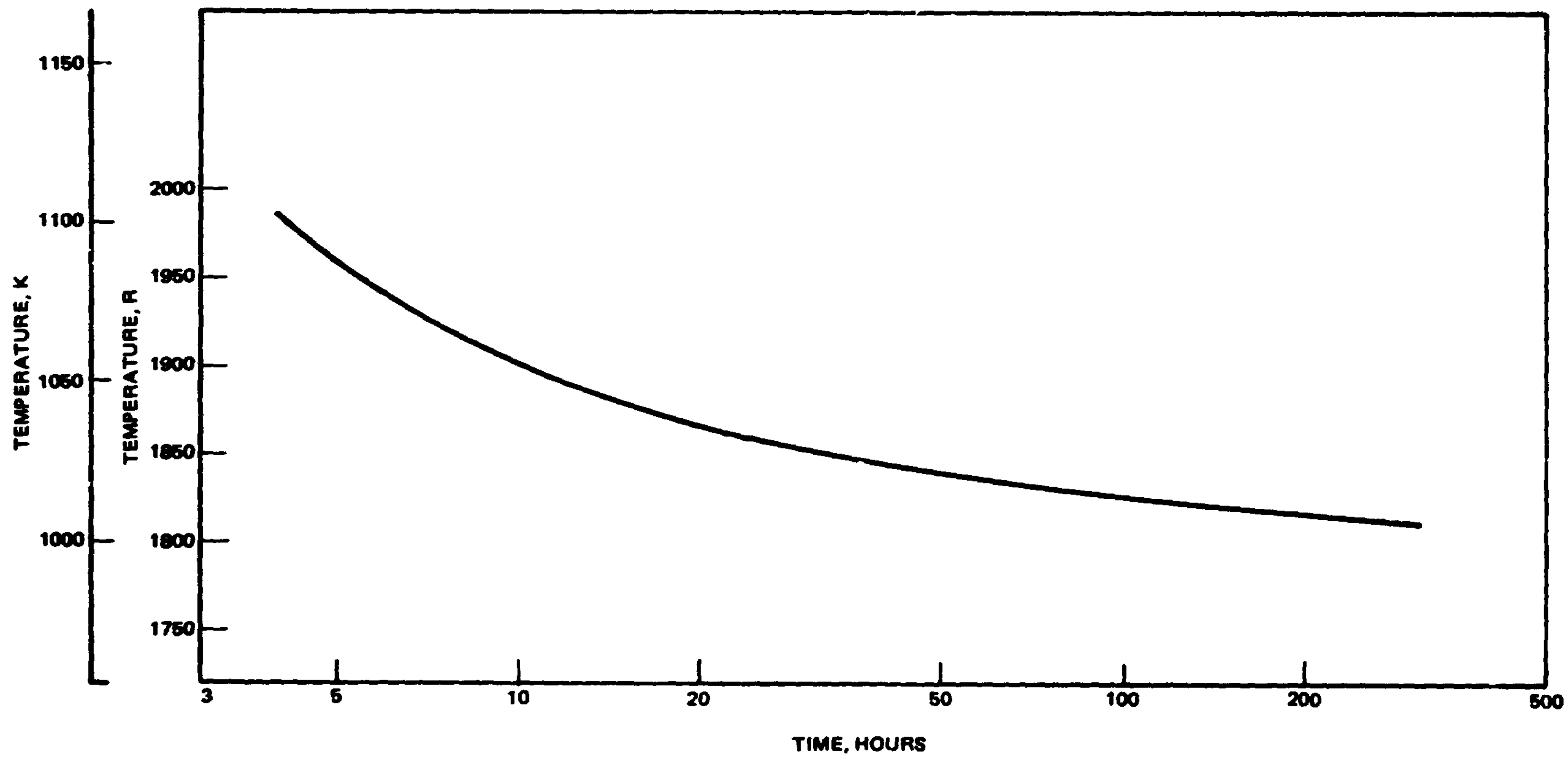

Figure 63. Oxidizer Turbine Disk Stress Rupture Life versus Temperature

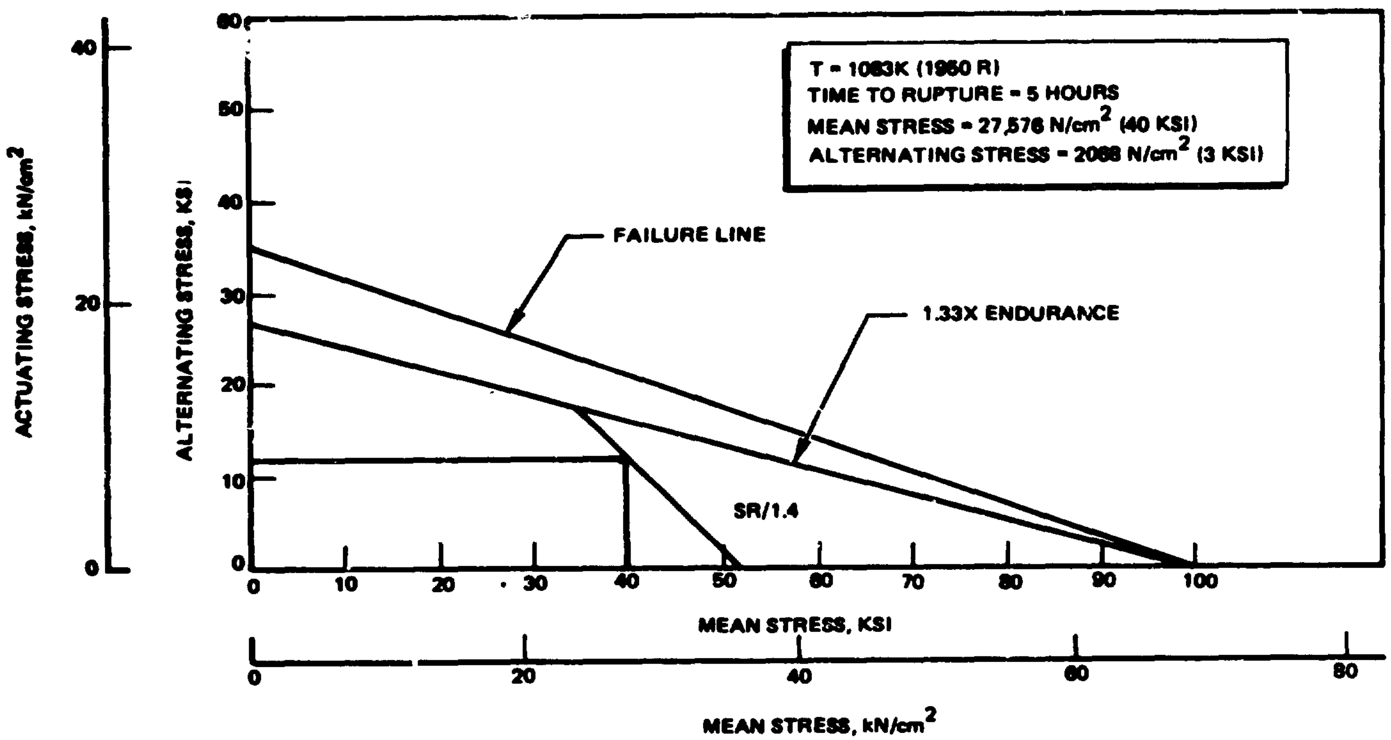

Figure 64. LOX Turbine Blade Modified Goodman Diagram

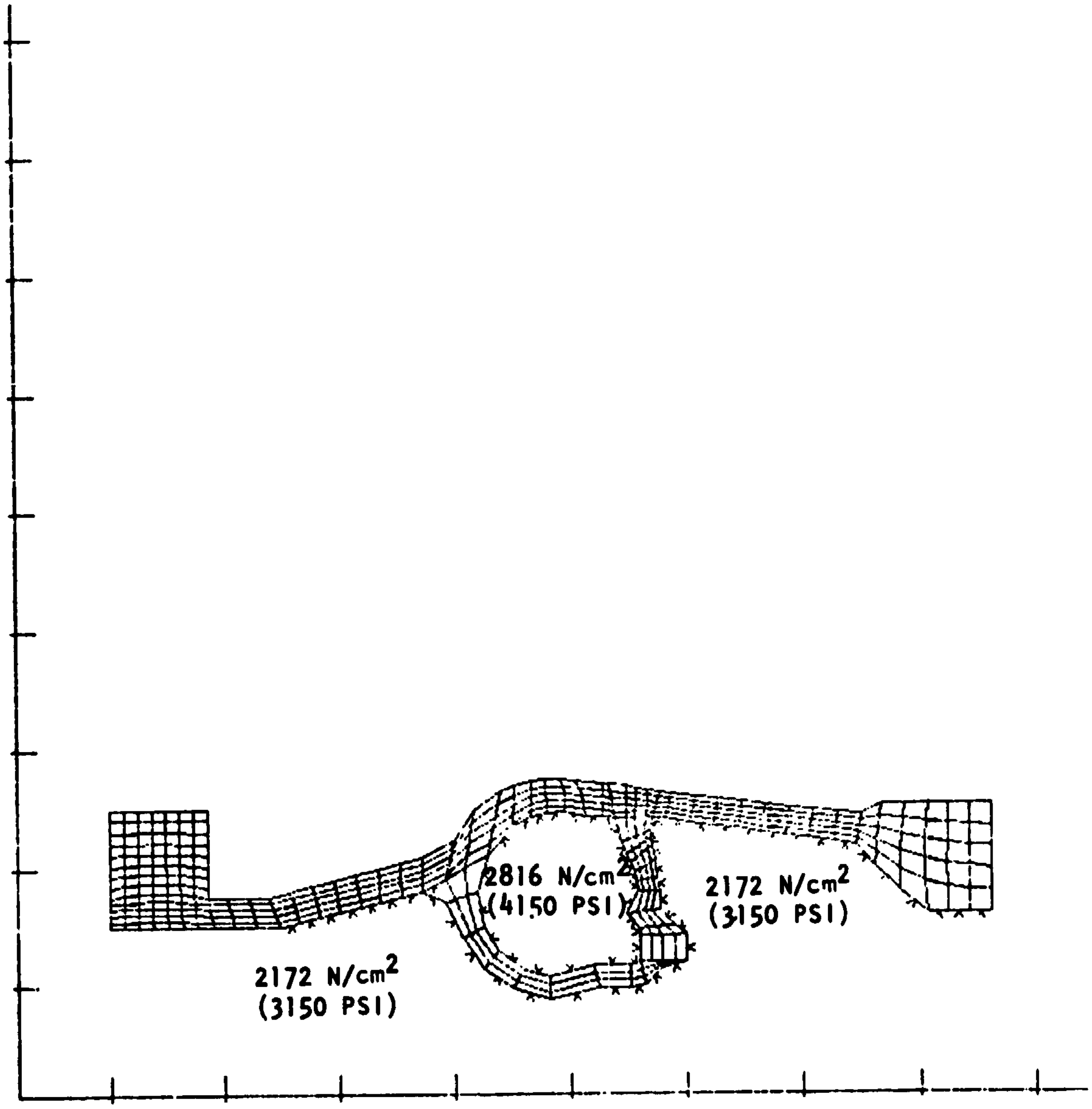

Figure 65. Finite Element Pressure Plus Temperature Steady-State Condition Model

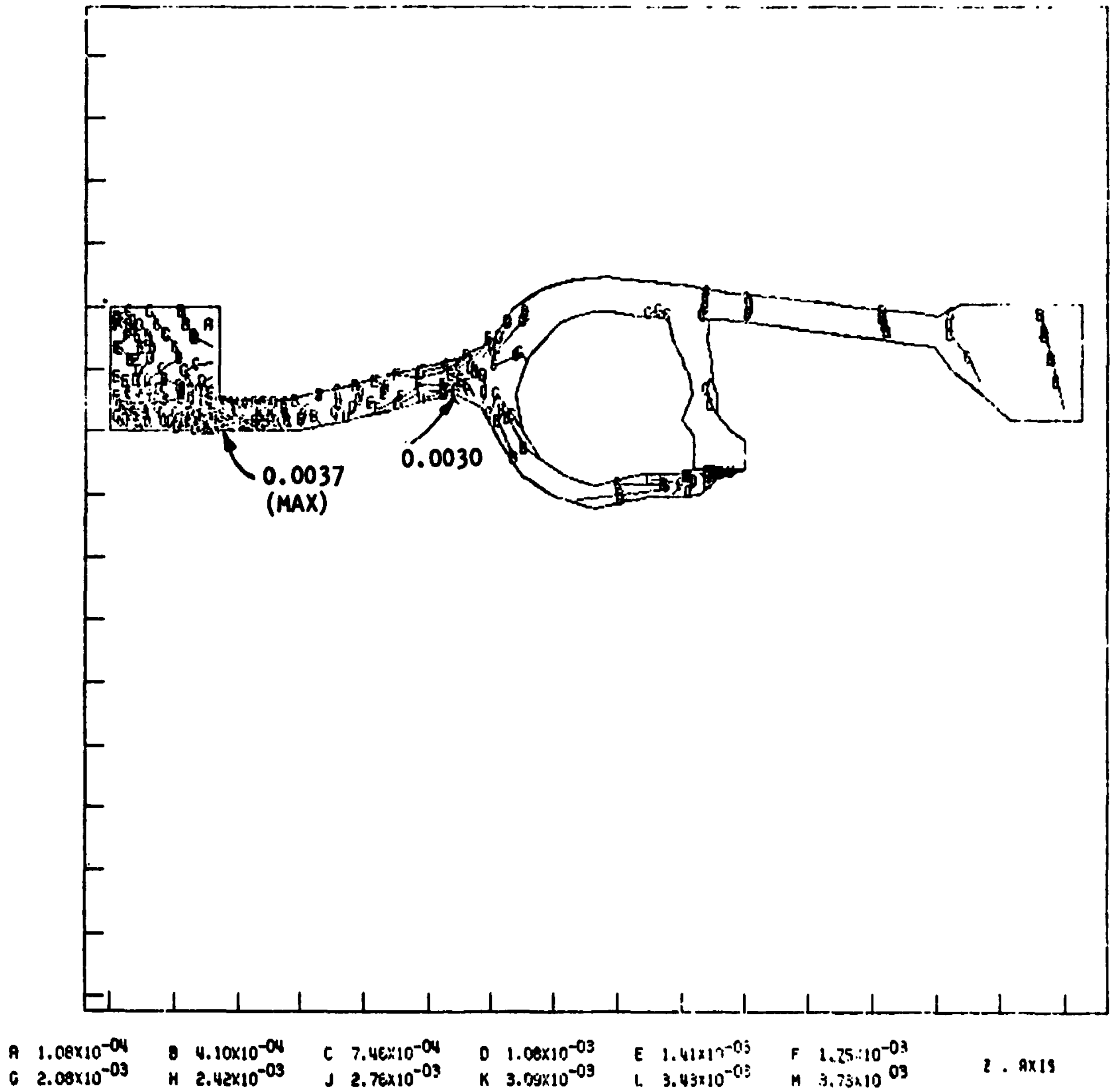

Figure 66. Finite-Element Effective Strain at Steady-State Conditions

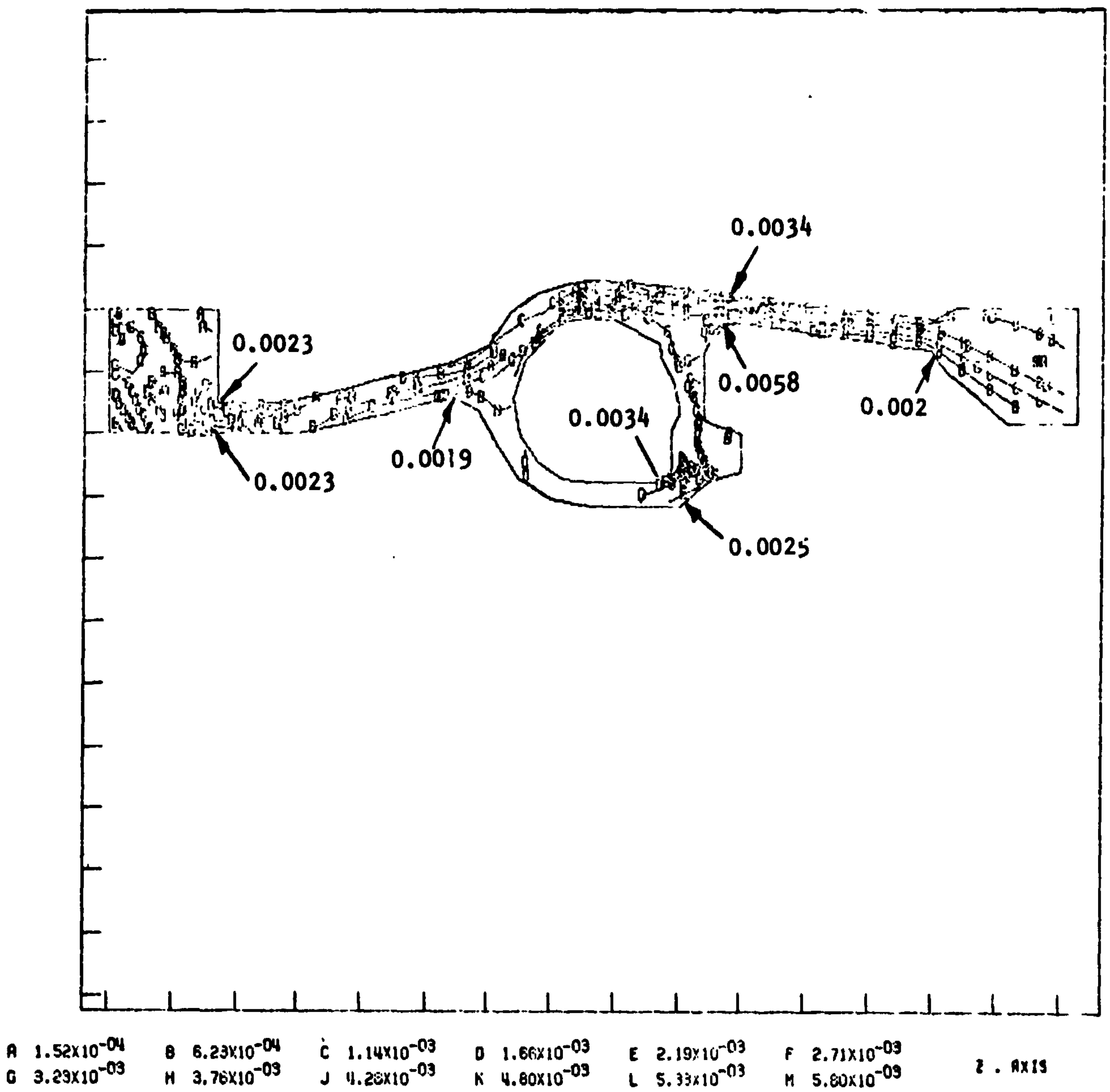

Figure 67. Finite-Element Effective Strain in Turbine Manifold Due to Shutdown Transient

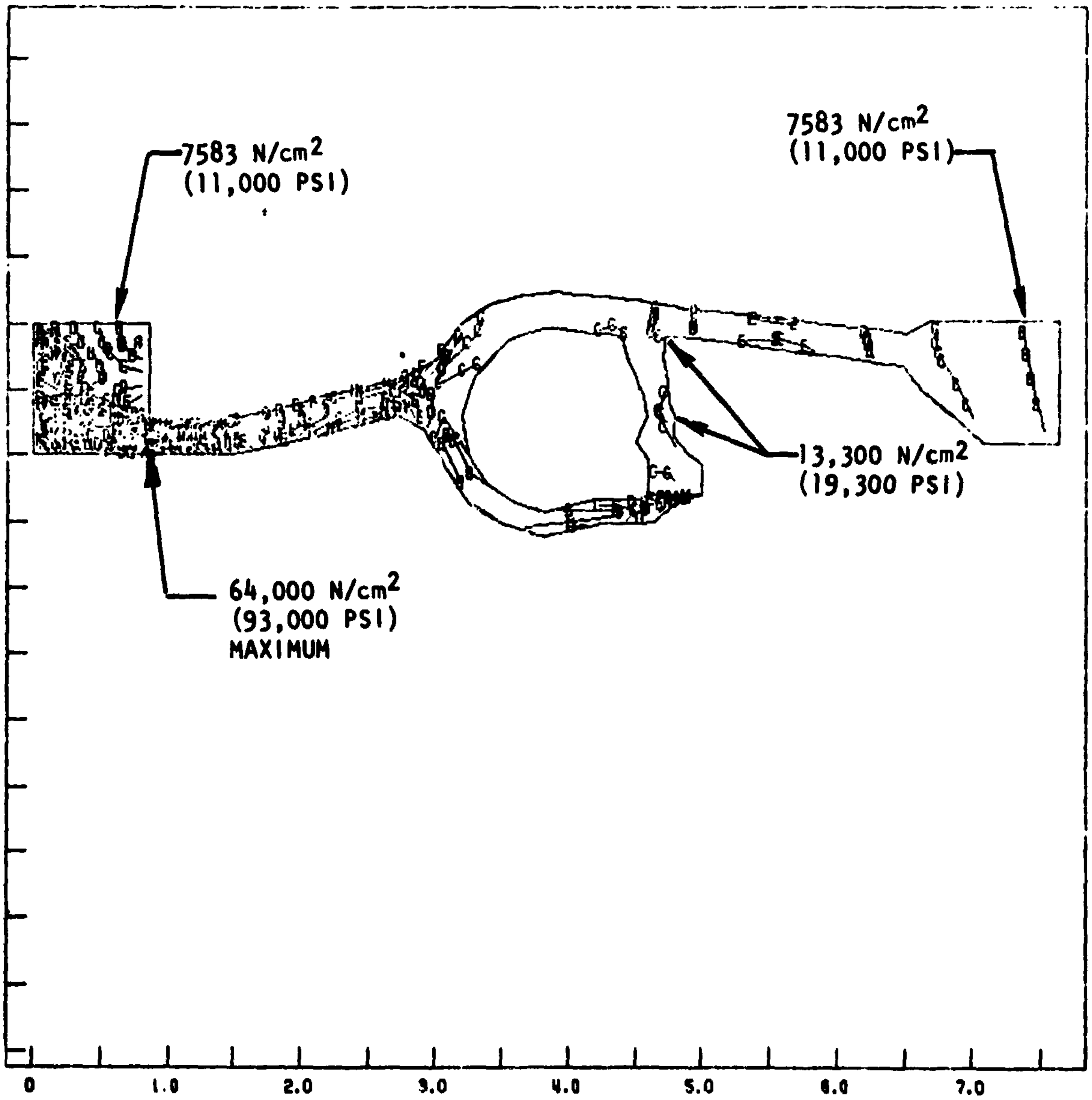

Figure 68. Finite-Element Effective Stress at Steady-State Conditions

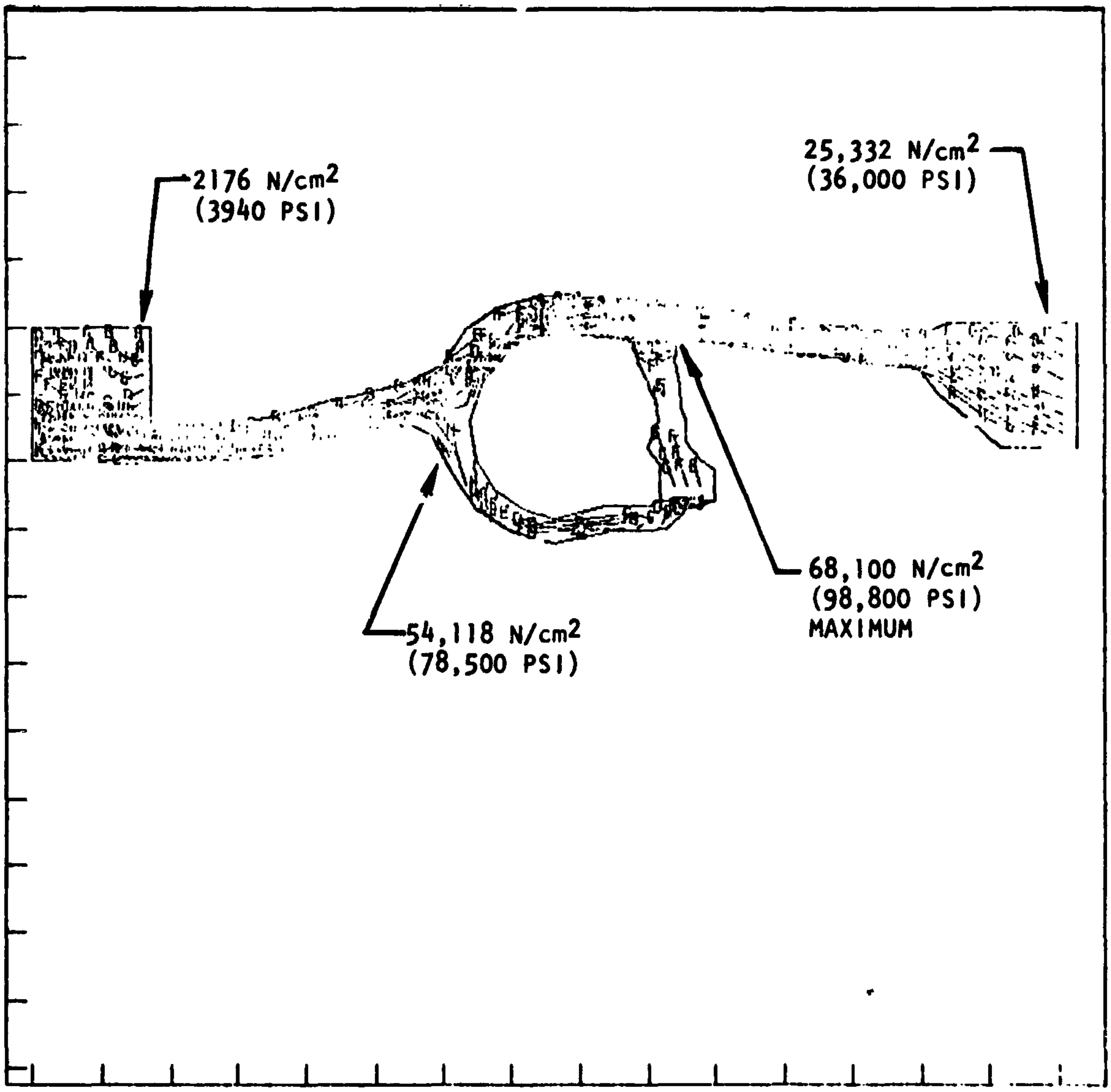

Figure 69. Finite-Element Effective Stress in Turbine Manifold Due to Shutdown Transient

Gas Generator

The gas generator was designed as a piece of special test equipment to provide the drive gas for turbopump testing. The requirements that are imposed to meet the basic intent of such a facility item were: (1) stable operation at all operating points, (2) repeatable high performance, (3) uniform exhaust gas temperature profile, (4) reliable ignition, and (5) durability and long life.

The gas generator design uses separate injector and combustor assemblies which are attached with a bolted flange (Fig. 70). The injector has five coaxial injection elements which are designed for stable operation, high-performance and complete mixing. The nominal operating parameters for the injection elements are given in Table 12. Analysis of the element design, using the Rocketdyne steady-state combustion model, indicated complete combustion within a distance of 3.5 inches from the injector face (Fig. 71). The output from this model was also used to conduct a Priem analysis to evaluate the sensitivity of the combustion process to transverse acoustic modes in the combustor. The results of this analysis indicated the gas generator will have stability superior to the J-2 and J-2S engines (higher A), which exhibited dynamic stability to all but intermediate size bombs (Fig. 72). The injector element was also designed with adequate injection pressure drop ($P/P_c = 0.13$) to isolate the gas generator from feed system coupled modes.

TABLE 12. LOX TURBOPUMP GAS GENERATOR INJECTOR NOMINAL OPERATING PARAMETERS

Nomenclature	SI Units	English Units
Number of Coaxial Elements	5	5
Number of Film Coolant Orifices	20	20
Flowrate/Element*	0.25 kg/s	0.55 lb/sec
Oxidizer Injection Velocity	22.6 m/s	74 ft/sec
Fuel Injection Velocity	218.7 m/s	718 ft/s
Minimum Fuel Sleeve Gas	3.68×10^{-4} m	0.0145 inch
Number of Centering Devices/ Element	4	4
*Film coolant flow≅5% total weight flow		

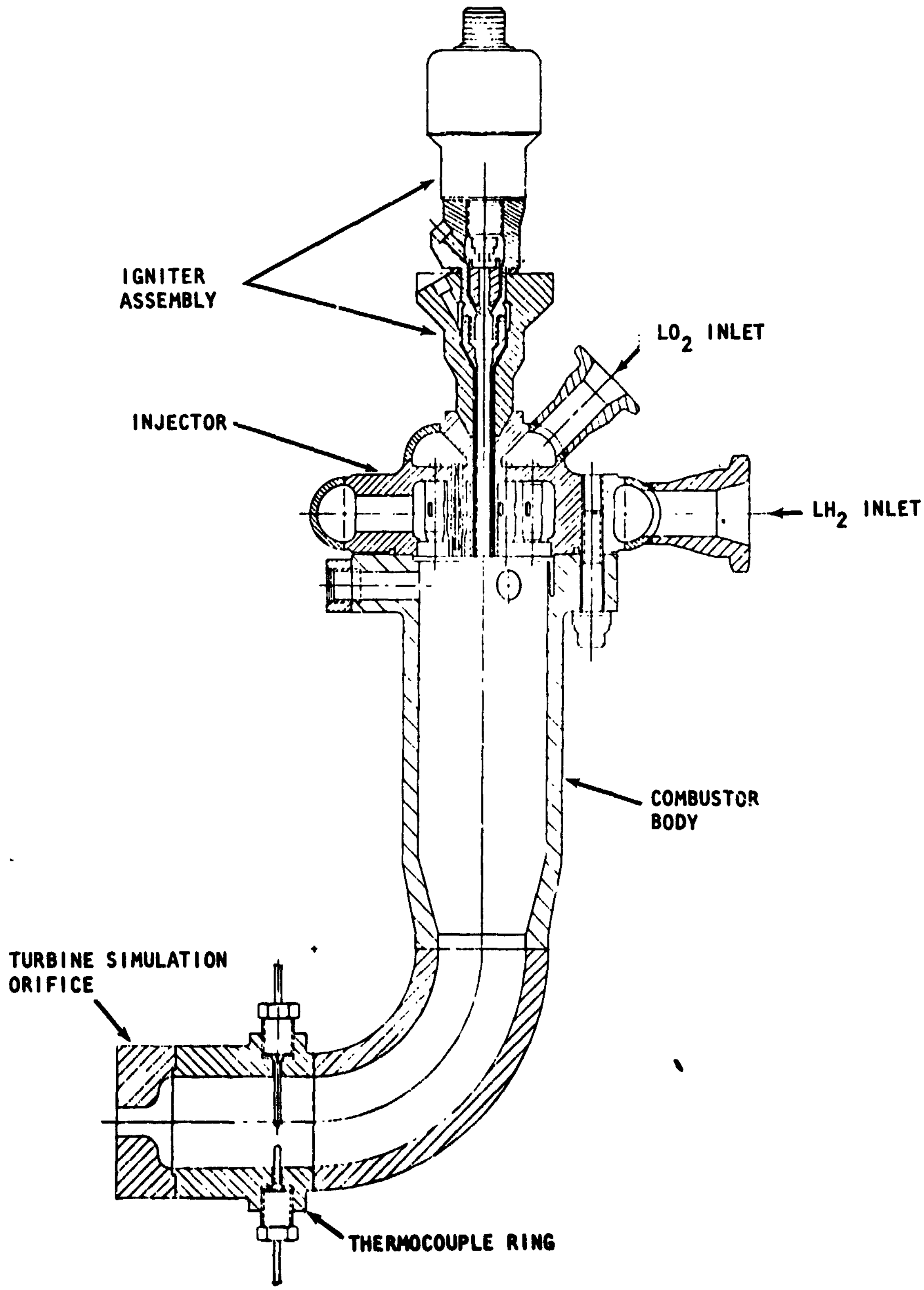

Figure 70. Gas Generator

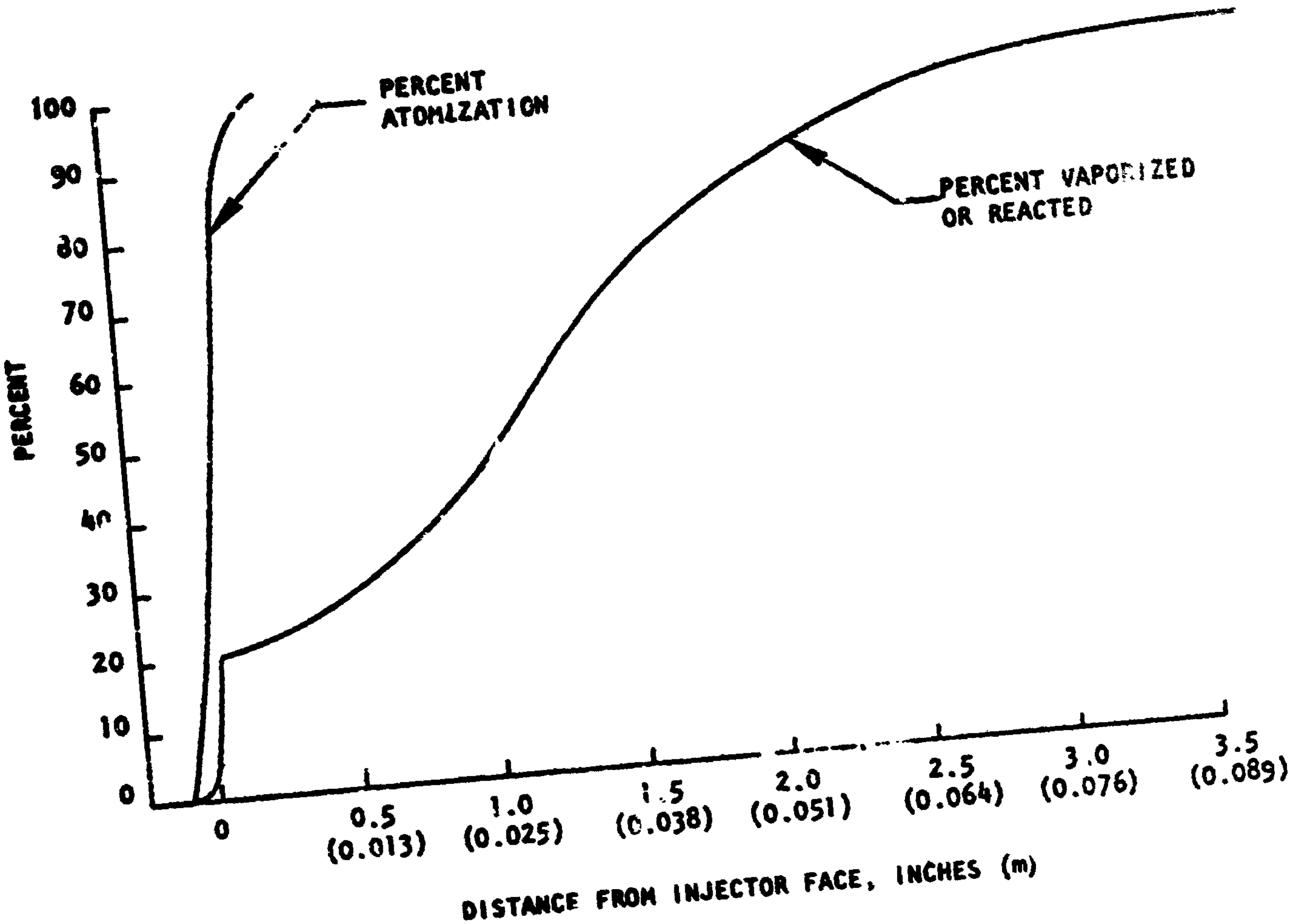

Figure 71. Gas Generator Coaxial Element

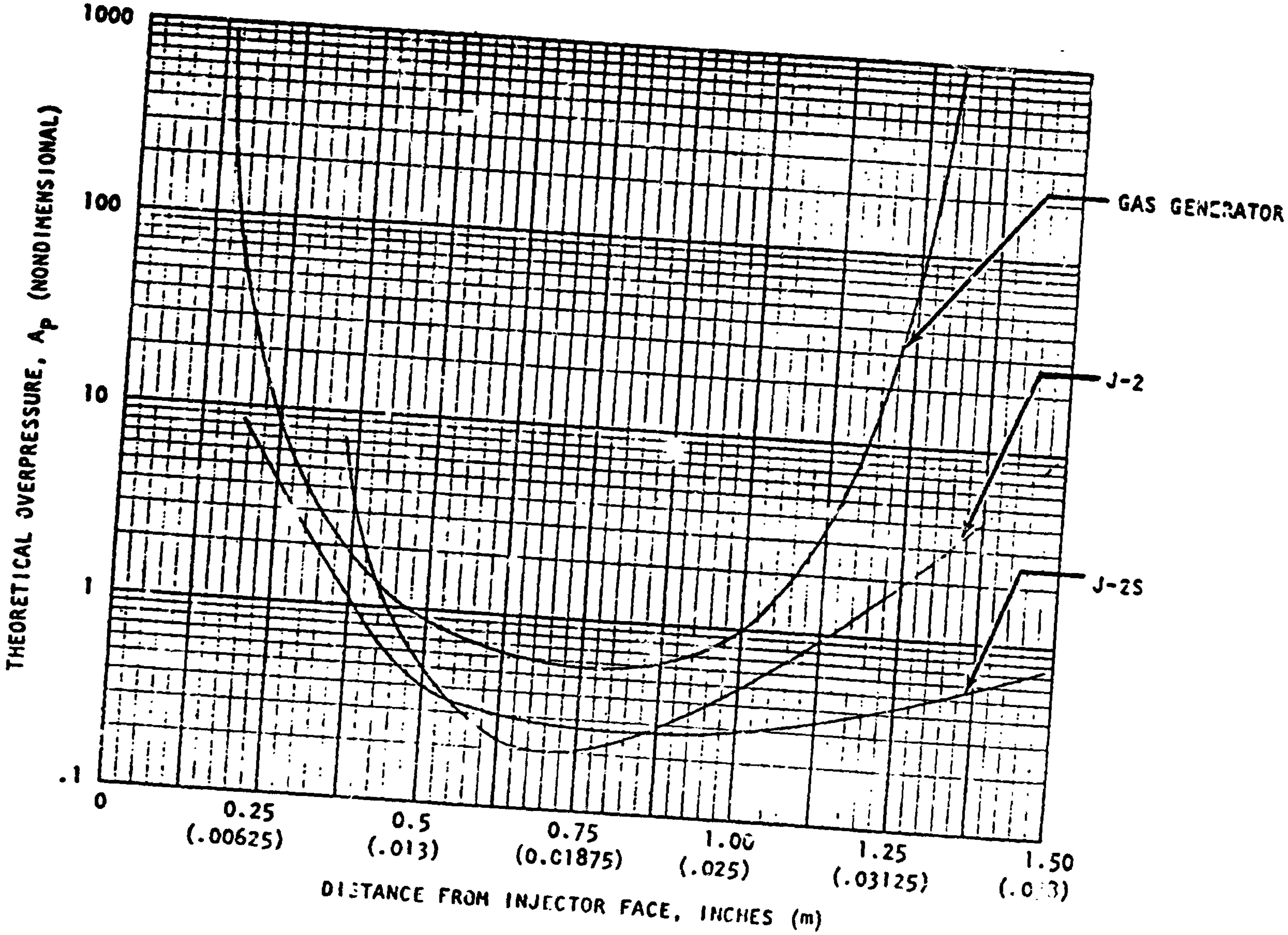

Figure 72. Gas Generator Prism Analysis

The injection elements are a self-contained design in which each element is built as a brazed assembly for individual calibration (Fig. 73). The elements have a recessed oxidizer post with four centering devices for positive alignment within the fuel sleeve. The element material is CRES 304L.

The injector body is an all-welded assembly fabricated from CRES 347. The injector elements and NARloy faceplate are brazed into the injector body. GRAYLOC fittings are used as propellant inlets to interface with the test facility. An envelope was retained in the center of the injector for use of the spark igniter.

The combustor is an all-welded assembly of the combustor body, elbow, and transition section. Added margin for complete mixing and a uniform exit temperature has been provided by using the elbow to induce circulation. The combustor is cooled by film coolant injected from orifices at the periphery of the injector. The film coolant temperature is shown in Fig. 74 as a function of the distance from the injector face.

Acoustic absorbers were placed in the combustor wall, directly below the injector face, to provide added stability margin by damping acoustic modes in the combustor. A summary of acoustic absorber experience (Fig. 75) shows that the design open area of the gas generator acoustic absorber lies in a favorable position.

A welded transition section was used between the gas generator and turbine manifold because analysis showed that the high temperature in this area would prohibit effecting a positive seal with a flanged joint. The joint is fabricated by welding the Inconel 625 transition piece to the Rene' 41 turbine manifold (Fig. 76). This weld is then heat treated. After the Inconel 625 gas generator transition piece is welded to the combustor elbow, the two transition pieces are joined with an electron beam weld. The gas generator transition piece has a liner section which extends over the transition piece welded to the turbine manifold. This forms a thermal barrier which ensures that the life of protected transition piece is consistent with that of the turbine manifold. The design of the transition section allows the gas generator to be removed and rewelded to the turbine manifold without harming the heat treat or weld between Rene' 41 and Inconel 625 since the rework can be made in the protected Inconel 625 transition pieces.

Ignition of the gas generator was to be accomplished using pyrotechnic igniters similar to the Rocketdyne part number 651876 igniter extensively used for J-2 gas generator and turbopump development testing. Two pyrotechnic igniter ports were originally provided in the combustor. The subsequent development of a spark torch igniter under company funding, based on prior work conducted under NASA-Lewis Research Center direction, obviated the necessity of utilizing the pyrotechnic igniters.

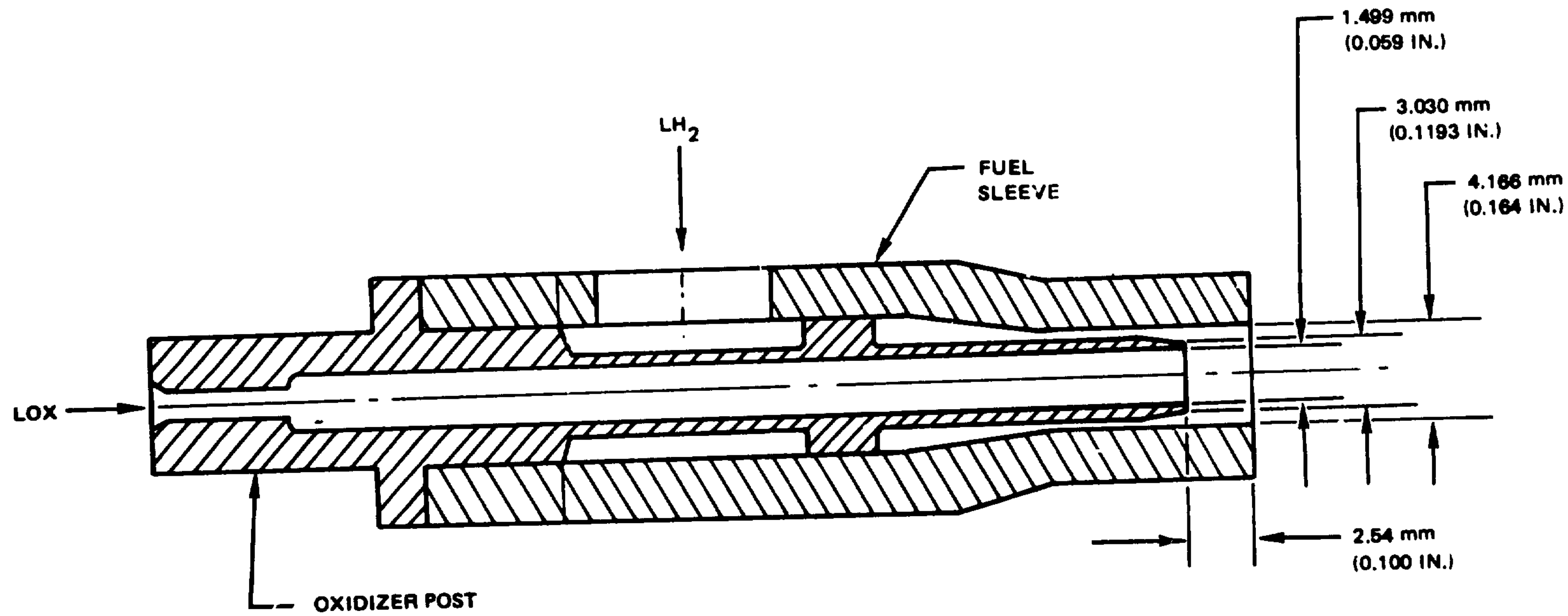

Figure 73. Injector Element

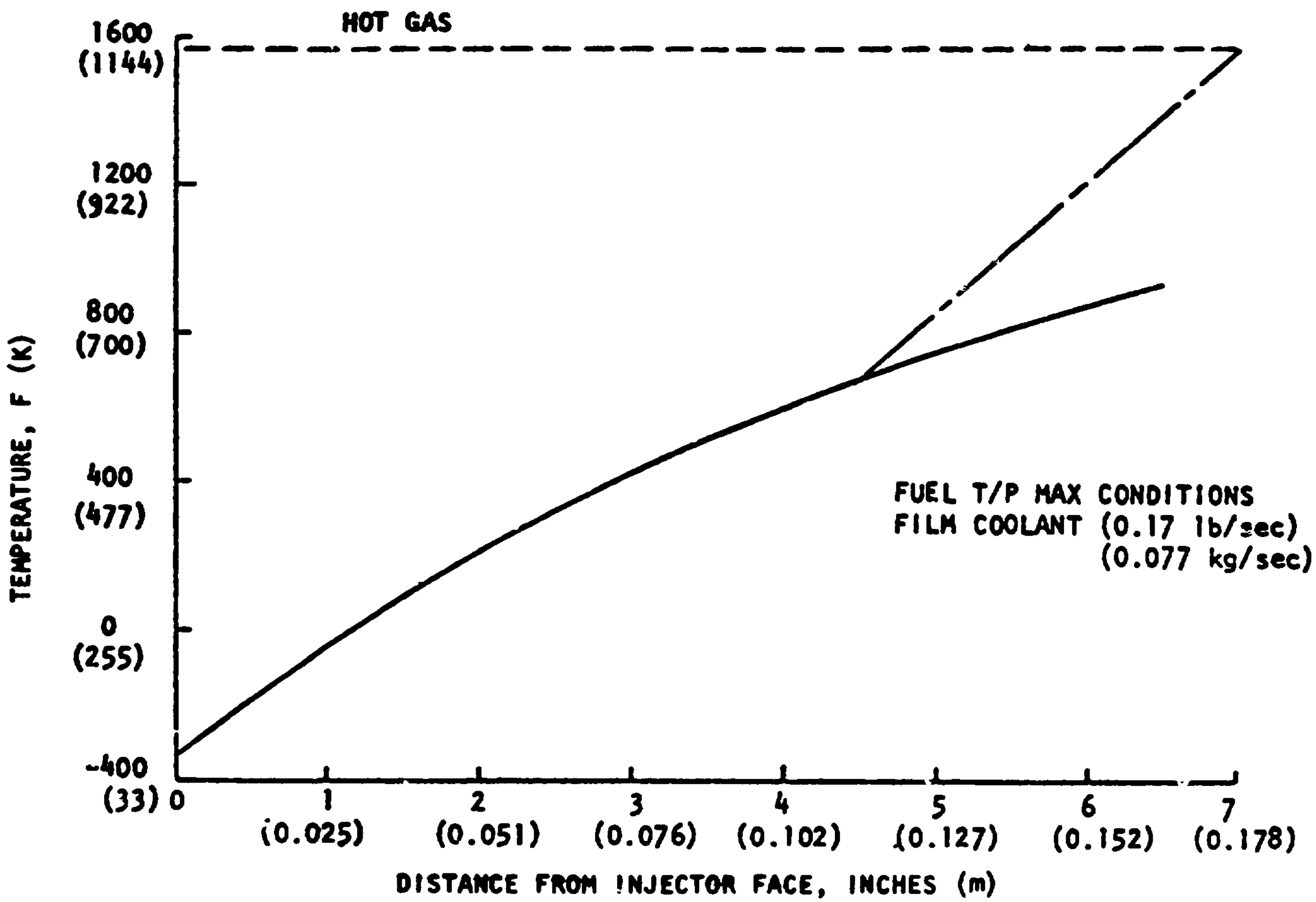

Figure 74. Gas Generator Film Coolant Temperature

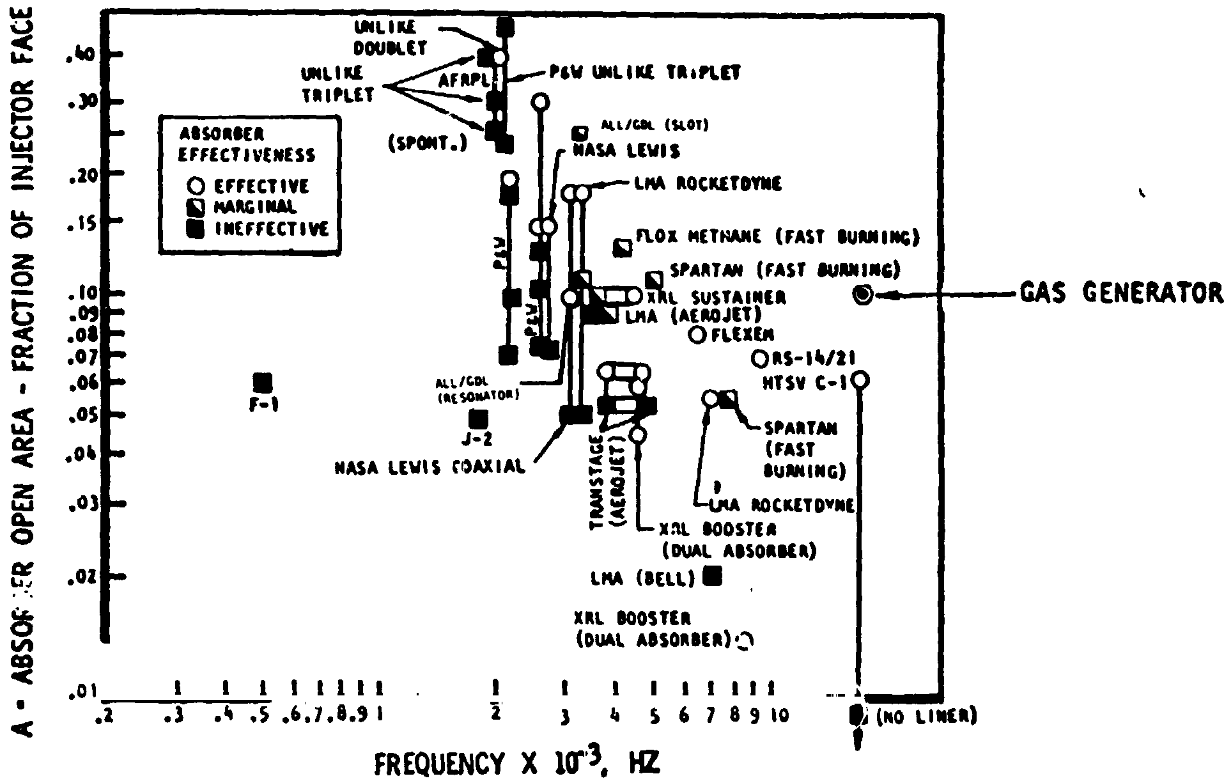

Figure 75. Absorber Experience

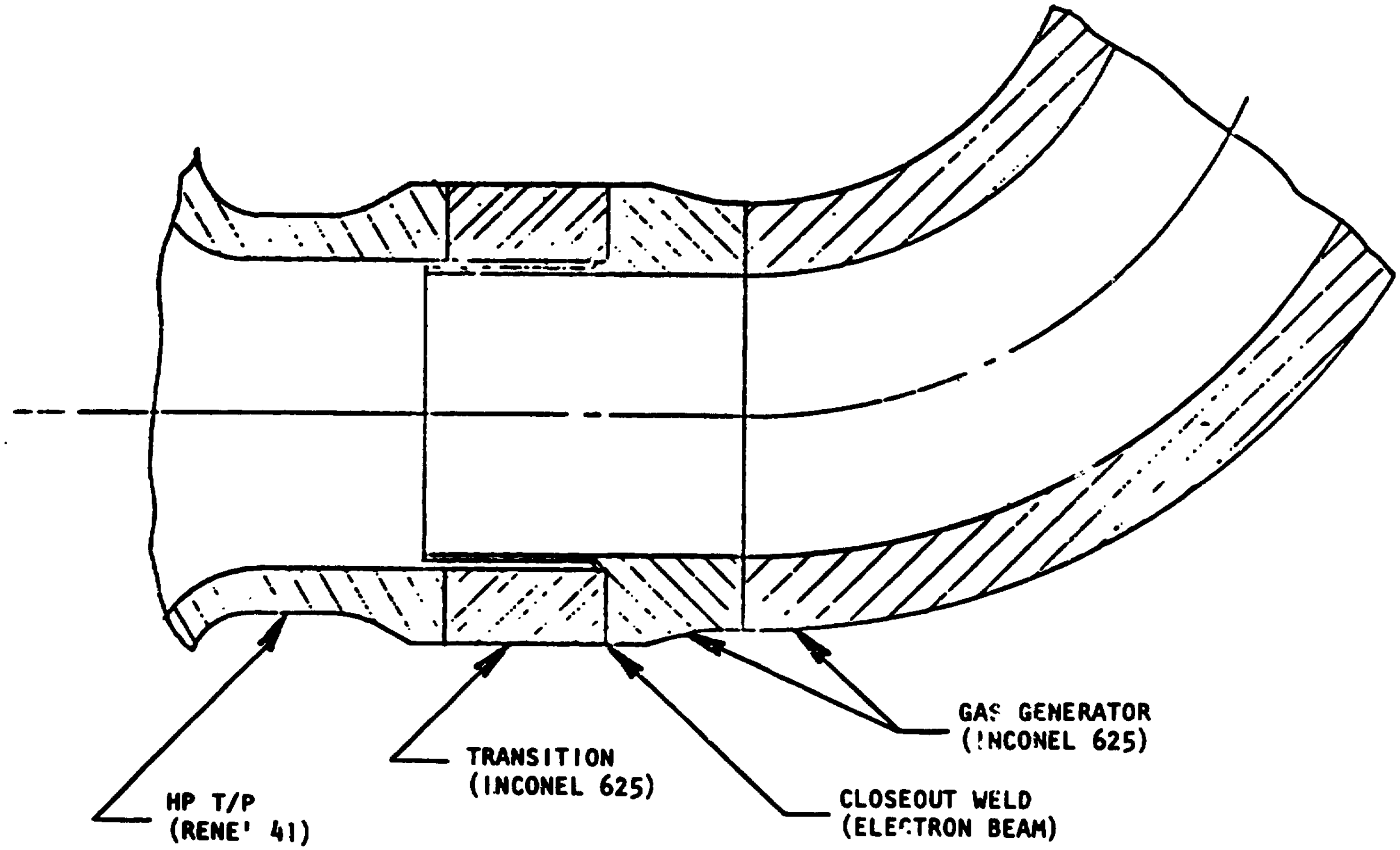

Figure 76. Turbopump to Gas Generator Transition Joint

FABRICATION

Component Fabrication

The methods employed in fabricating the major components of the LOX turbopump are discussed in the following paragraphs.

Inducer. The inducer blades were machined from K-monel bar by pantographing. No difficulties were encountered in its fabrication. Figure 77 shows the completed inducers.

Impeller. The impeller internal flow passages were generated by electrical discharge machining. Electrodes were introduced from the inlet as well as the discharge side to form the blade surfaces. Some difficulty was experienced in obtaining a smooth transition between the inlet and discharge, in the area where the leading edge of the partial blade is located. The difficulty was presented by a combination of small passage width (3.81 mm, 0.15 inch) and small blade angle at the discharge (0.49 rad, 28 degrees) and large blade wrap angle (2.65 rad, 152 degrees). One set of impellers were scrapped because of discontinuity in the passages as a result of a machine indexing error. The delivered impellers were accepted only after several hand rework operations were performed to obtain a smooth transition.

Diffuser. The diffuser was machined from an Inconel 718 forging by conventional methods with the exception of the vane surfaces which were generated by electrical discharge machining. No difficulties were encountered in fabricating this part.

Volute. Because of the contoured surfaces included in the volute, it was more economical to produce it by casting. The investment casting technique yielded an excellent quality part from the standpoint of conformance to drawing dimensions and surface finishes in the flow passage. The unmachined castings are shown in Fig. 78.

Turbine Manifold and Housing. The fabrication process of the housing is illustrated with a series of photographs in Fig. 79. It was the most costly of the LOX turbopump parts, and it required the longest time to complete.

The housing (Fig. 79A) was machined from a Haynes 188 forging. Intersecting holes were drilled or electrical discharge machined and capped by welded plates to provide drain ports for the primary hot-gas seal, secondary hot-gas seal, and primary LOX seal, as well as purge passage for the intermediate seal. In addition, six instrumentation ports and passages were incorporated.

The nozzle (Fig. 79B) was also fabricated from Haynes 188 forging, with the flow passages generated by electrical discharge machining. The throat area of one of the two nozzles fabricated was 5% over the nominal required per blueprint. It was estimated that this would degrade the efficiency of the turbine 2.7% but would reduce the engine chamber pressure only 0.165×10^6 N/m^2 (24 psi). The deviation was accepted.

ORIGINAL PAGE IS
OF POOR QUALITY

1XY52-11/21/74-C1B*

Figure 77. Mark 48-0 Inducers

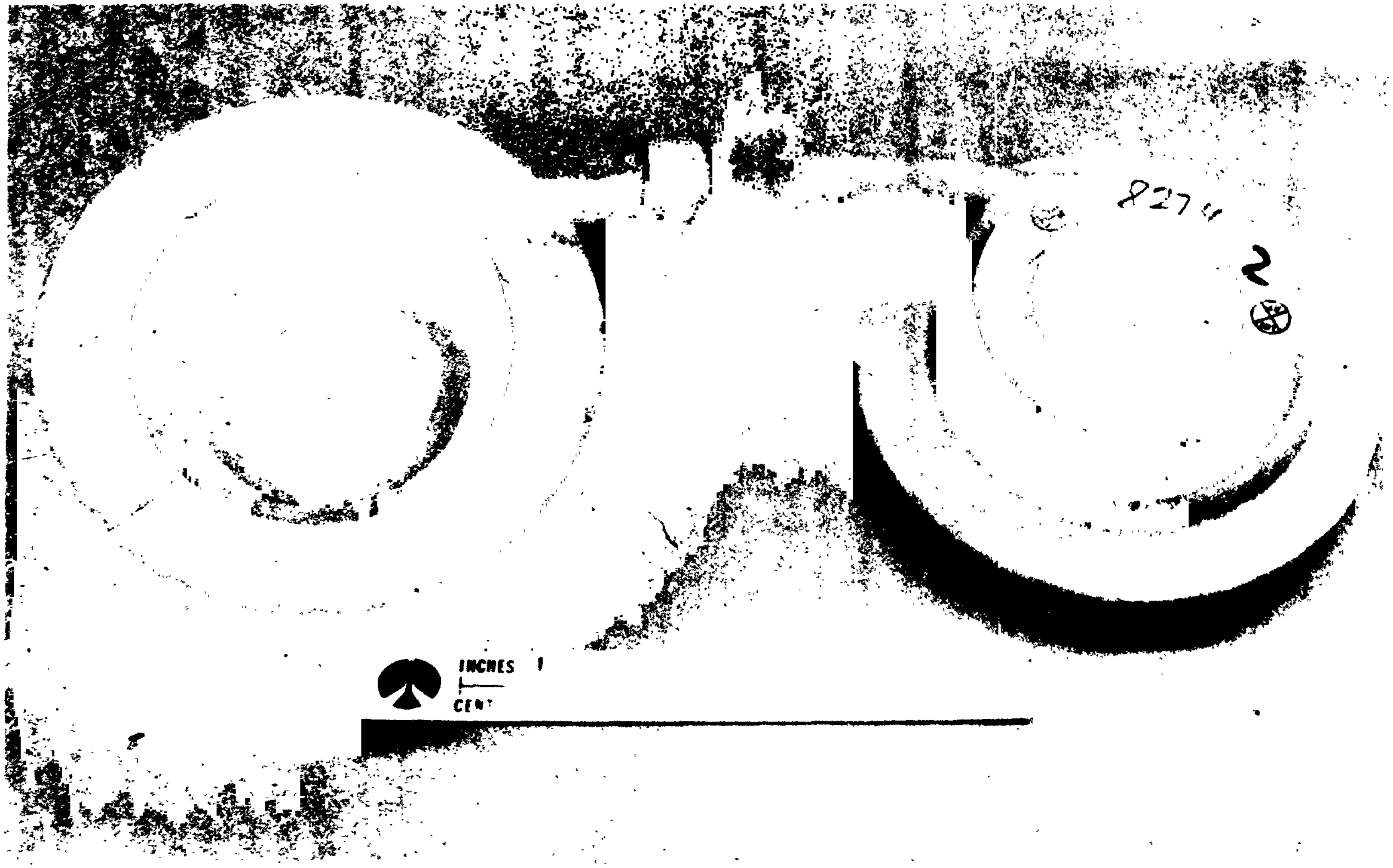

1XY52-3/17/75-C1B*

Figure 78. Mark 48-0 Volute Castings

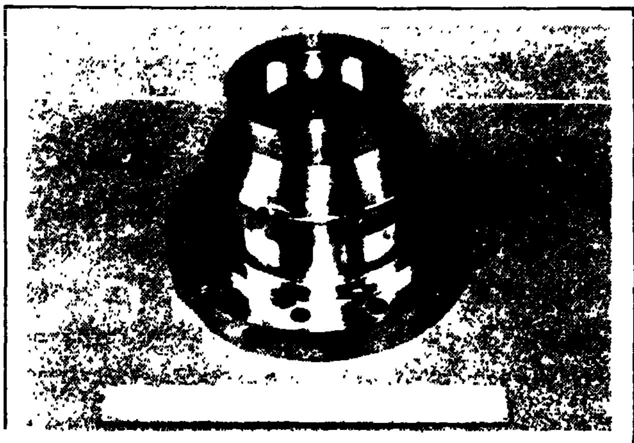

(A)

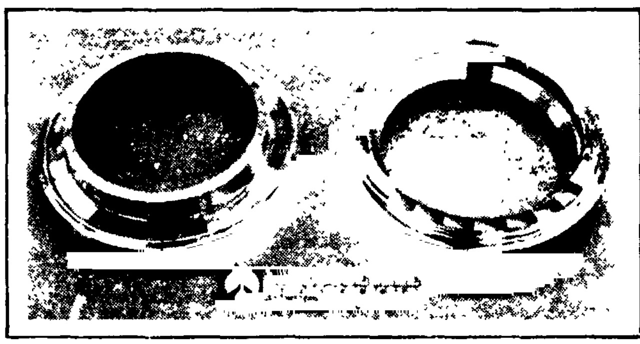

(B)

(C)

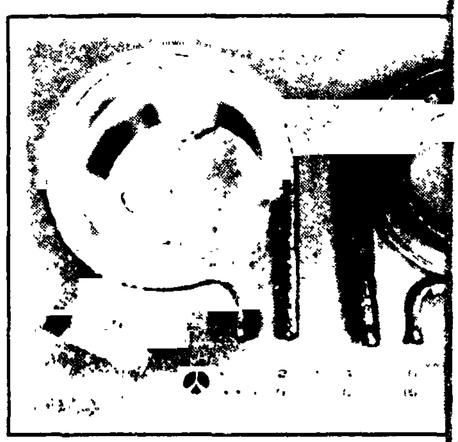

(E)

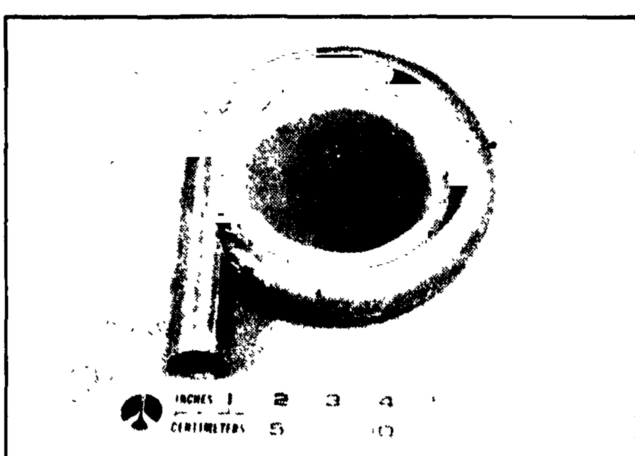

(D)

FOLDOUT FRAME 1

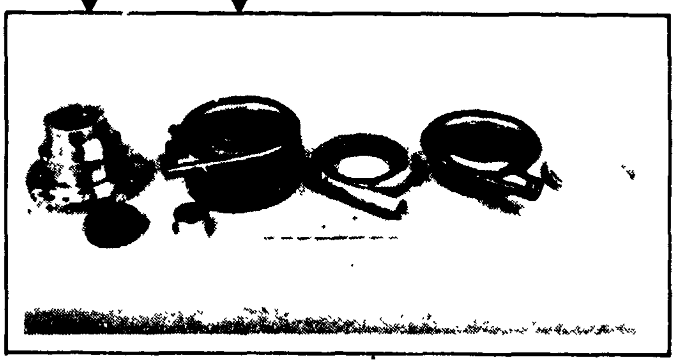

(F)

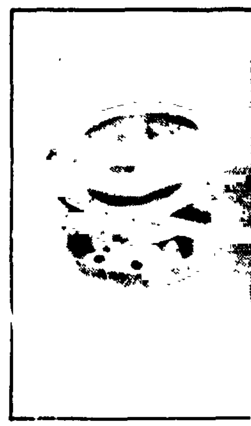

FOLDOUT FRAME 2

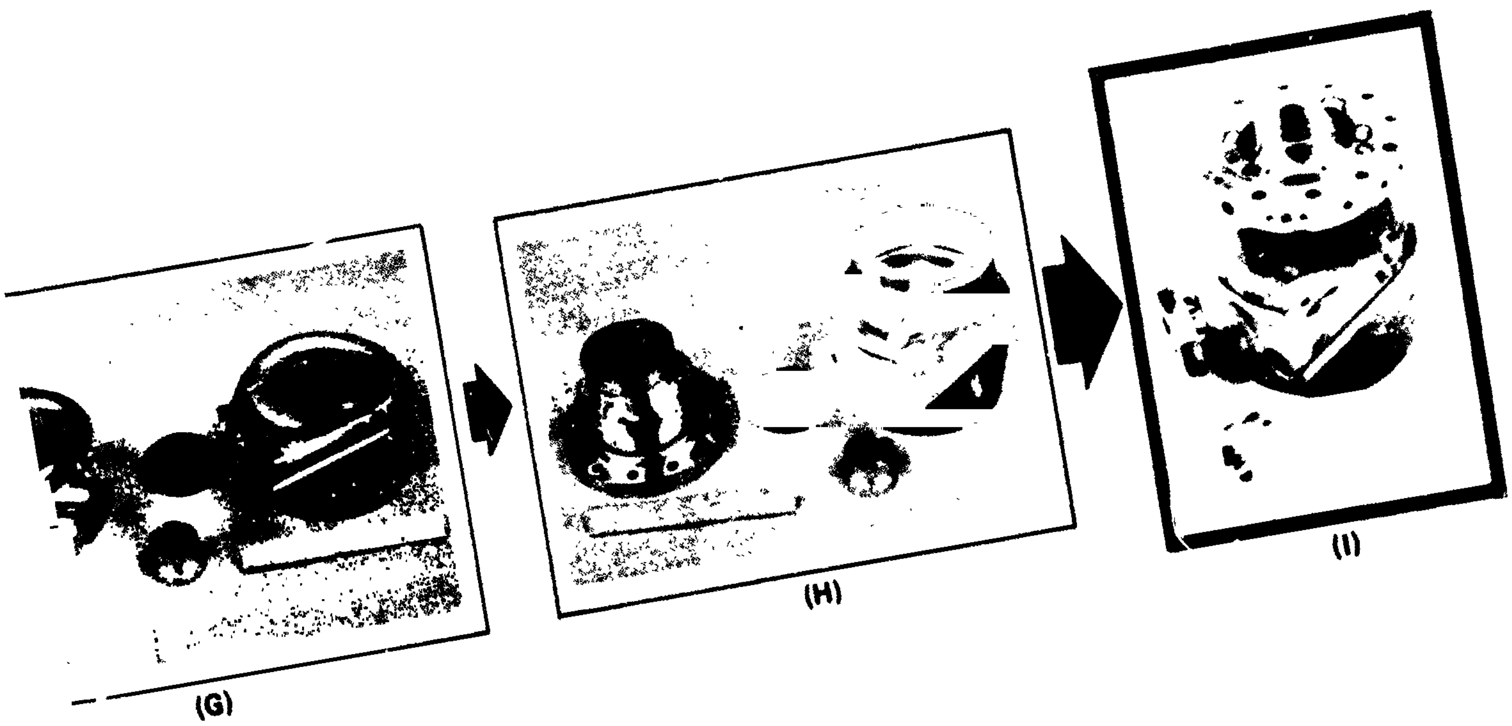

Figure 79. Mark 48-0 Turbopump Housing Fabrication Process

To maintain thermal gradients at cutoff at an acceptable level, the liner shown in Fig. 79D was formed from Incoloy 903, and the liner details were joined by welding. Metal-to-metal contact between the liner and the manifold was limited by chem milling 0.13 mm (0.005 inch) from part of the outer surface of the liner leaving only high spots to contact.

The main structural details of the manifold were machined from Rene' 41 and joined by welding. The two principal details are shown in Fig. 79C with the inlet transition welded to each cylindrical half. Hastelloy was used as the principal weld filler metal, but an Incoloy 88 weld overlay was applied on the inside surface of each Rene' 41 joint to minimize hydrogen environment embrittlement. An example of the weld overlay is shown in Fig. 79E for the closeout weld that joined the two manifold halves. Figure 79F through 79I show the housing and manifold in successive stages of assembly. Difficulties were encountered in obtaining sound welds where the inlet and discharge transitions were attached to the manifold halves, primarily because varying material thicknesses and difficult-to-fit conical welds were involved. Repeated grindouts and weld repairs were made before penetrant and radiographic inspection criteria could be satisfied. On future parts, it is recommended that these transitions be machined integral with the manifold halves.

Rotor. The rotor (Fig. 80) with the pump inlet, volute, diffuser, and inducer, was machined as an integral piece from Waspalloy forging. The unshrouded blades were generated by electrical discharge machining, plunging radically inward with an electrode plate which formed both sides of the blade concurrently. The electrical discharge machining setup is illustrated in Fig. 81.

Rear Bearing Support. The rear bearing support was a welded assembly, with the main support machined from Inconel 718 and the discharge gas straightening vanes from Inconel 903. Copper plating and Incoloy 88 weld overlay was applied to the transition ring that supports the straightening vanes, since this area is potentially subject to hydrogen environment embrittlement factors such as high strain and high-pressure hydrogen at close to ambient temperature.

Turbopump Assembly

Rotor Balance. The Mark 48-0 rotor operates at a maximum speed of 8063 rad/s (77,000 rpm); as a result, a high degree of precision in its balancing is imperative. A Gisholt dynamic balance machine with a capability for detecting 6 x 10^{-4} mm (25 μinch) radial motion was used. For the Mark 48-0 rotor mass of 2.84 kg (6.25 pounds) this translates into machine accuracy limit of 0.18 gm cm (0.07 gm inch), which would cause a radial load of 98 N (22 pounds) at the design speed of 7330 rad/s (70,000 rpm). The rotor was supported in the balance cradle by two pairs of turbopump bearings, each pair axially preloaded in the bearing cartridge exactly as in the turbopump assembly (Fig. 82). Balancing was initiated using the main rotor and the rear stub shaft assembly, and wax corrections were made in the plane of the turbine wheel and the stub shaft.

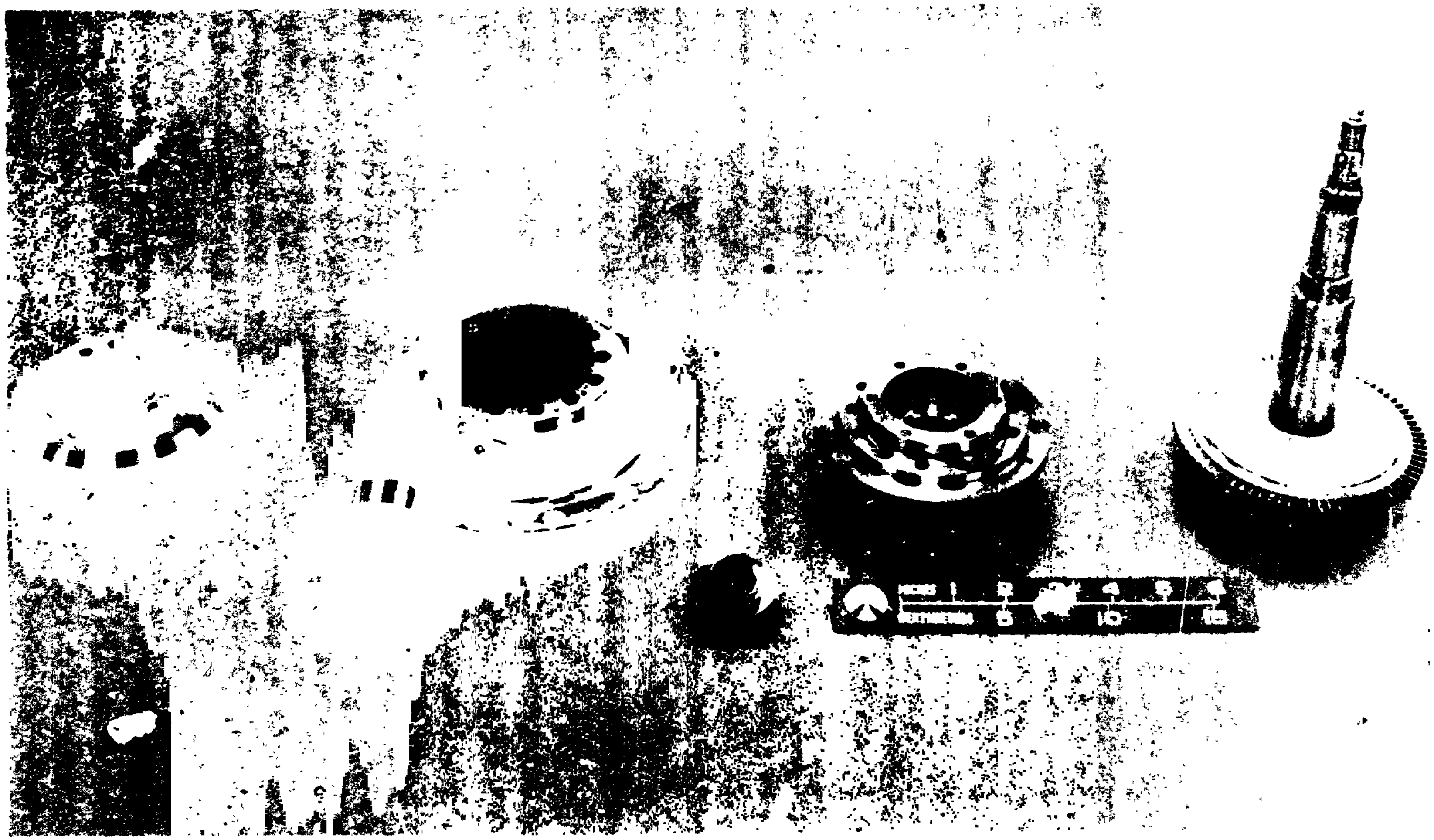

1XY52-6/12/75-C1H*

Figure 80. Mark 48-0 Inlet, Volute, Inducer, Diffuser and Rotor

1XY52-12/18/74-C1H*

Figure 81. Mark 48-0 Turbine Rotor Blade Electric Discharge Machining

Figure 82. Mark 48-0 Rotor on the Gisholt Balancing Machine

Subsequently, the slinger, impeller, inducer, and instrumentation sleeves were added, making wax correction in the plane of each component before the next part was added. After the wax corrections were completed, several repeatability checks were made in which the rotor was disassembled and reassembled, and the change in residual imbalance was established and the runouts at several stations were measured. Satisfactory repeatability was obtained in the amounts of imbalance as well as the runouts of the parts. The final runout values are shown in Fig. 83. Subsequently, the permanent balance of the rotor was effected by grinding material in designated areas of the component parts.

Turbopump Buildup. The buildup of the turbopump was accomplished in the following sequence:

1. All components were cleaned for LOX service.
2. Front and rear bearing inner race spacer thicknesses were established to provide the desired bearing preloads. The final preload characteristics obtained are shown in Fig. 84 and 85.
3. The slinger hub thickness was adjusted to obtain 3.175 mm (0.125 inch) turbine nozzle to rotor blade axial clearance.
4. Diametral clearances and fits of critical mating parts were established. The measured values are shown in Fig. 86 through 89.
5. Dimensions were taken to determine the impeller position when bottomed axially on the stationary parts. This was required to establish minimum operational clearances.
6. Measurements were taken to determine the slinger and turbine wheel bottomed positions.
7. Measurements were taken to establish the relative positions of the balance piston stationary and rotating orifice features to facilitate measuring bearing axial loads as a function of balance piston position.
8. Rotor push/pull tests were performed with a dummpy shaft to establish the bearing loads as a function of balance piston position. Shim thicknesses at the front bearing cartridge were adjusted until the satisfactory characteristics shown in Fig. 90 were obtained.
9. Final assembly was initiated by installing into the main housing the intermediate and primary LOX seals, slinger, and the rotor subassembly consisting of the rotor, stub shaft, and stud.
10. The rear bearing seal was installed in the rear bearing support, and the created subassembly was installed on the housing.
11. The rear bearing cartridge subassembly was added.
12. The diffuser subassembly including the front bearing package and the volute were added to the pump end of the housing.
13. The impeller and impeller nut were installed.
14. Measurements were taken to establish the impeller, slinger, and turbine wheel axial clearances.

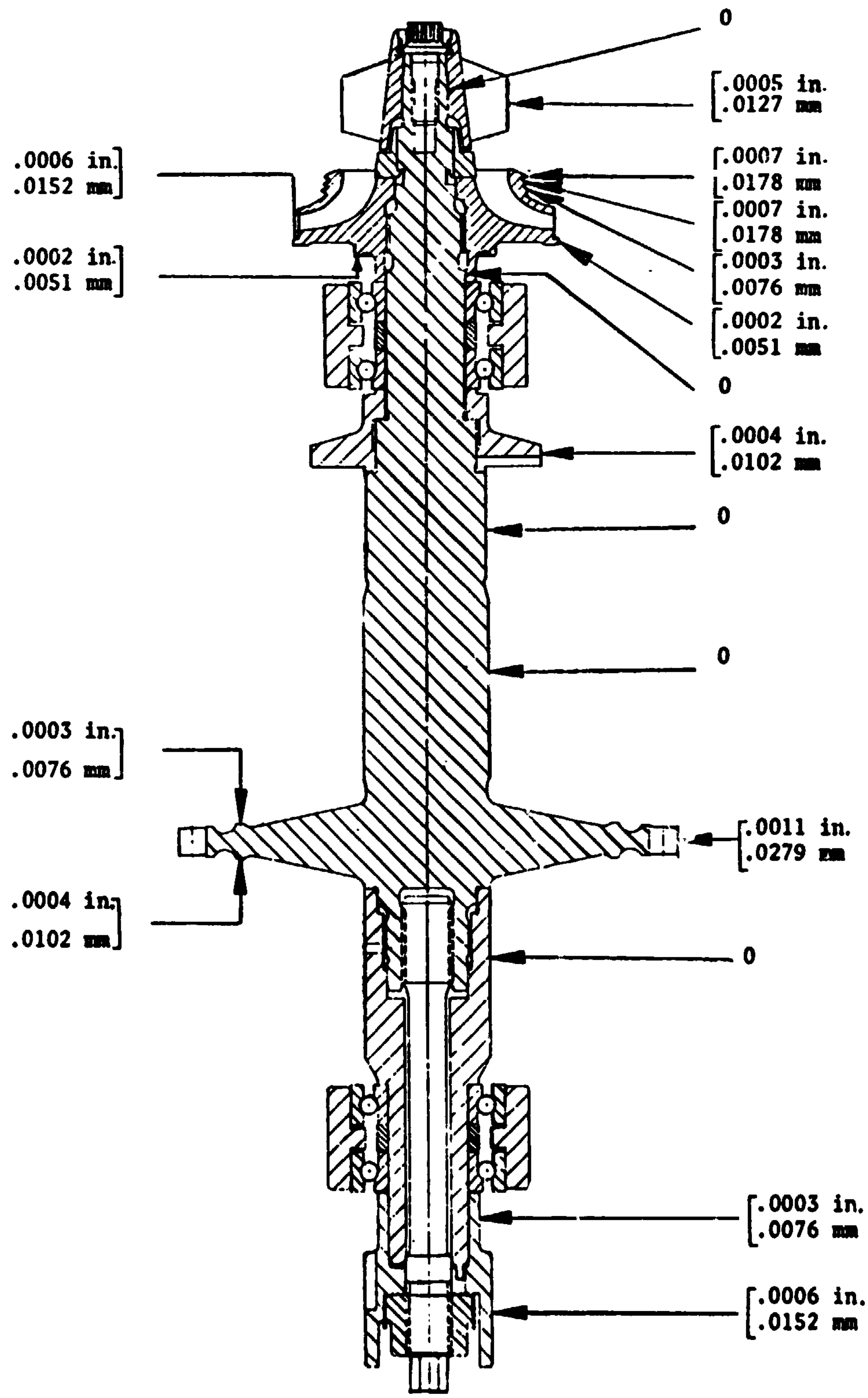

Figure 83. Mark 48-0 Turbopump S/N 01-0 Runouts

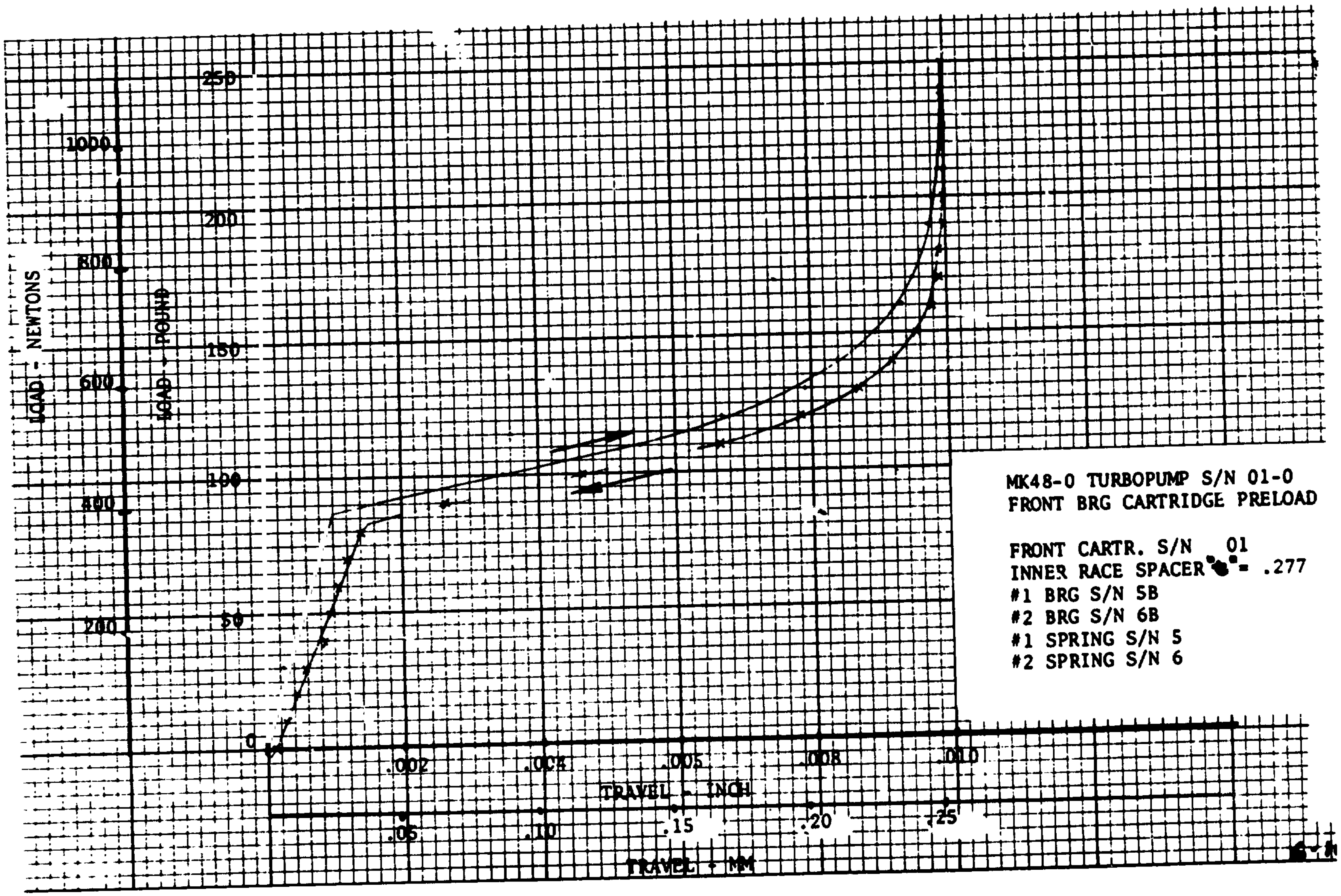

Figure 84. Mark 48-0 Turbopump Front Bearing Cartridge Preload

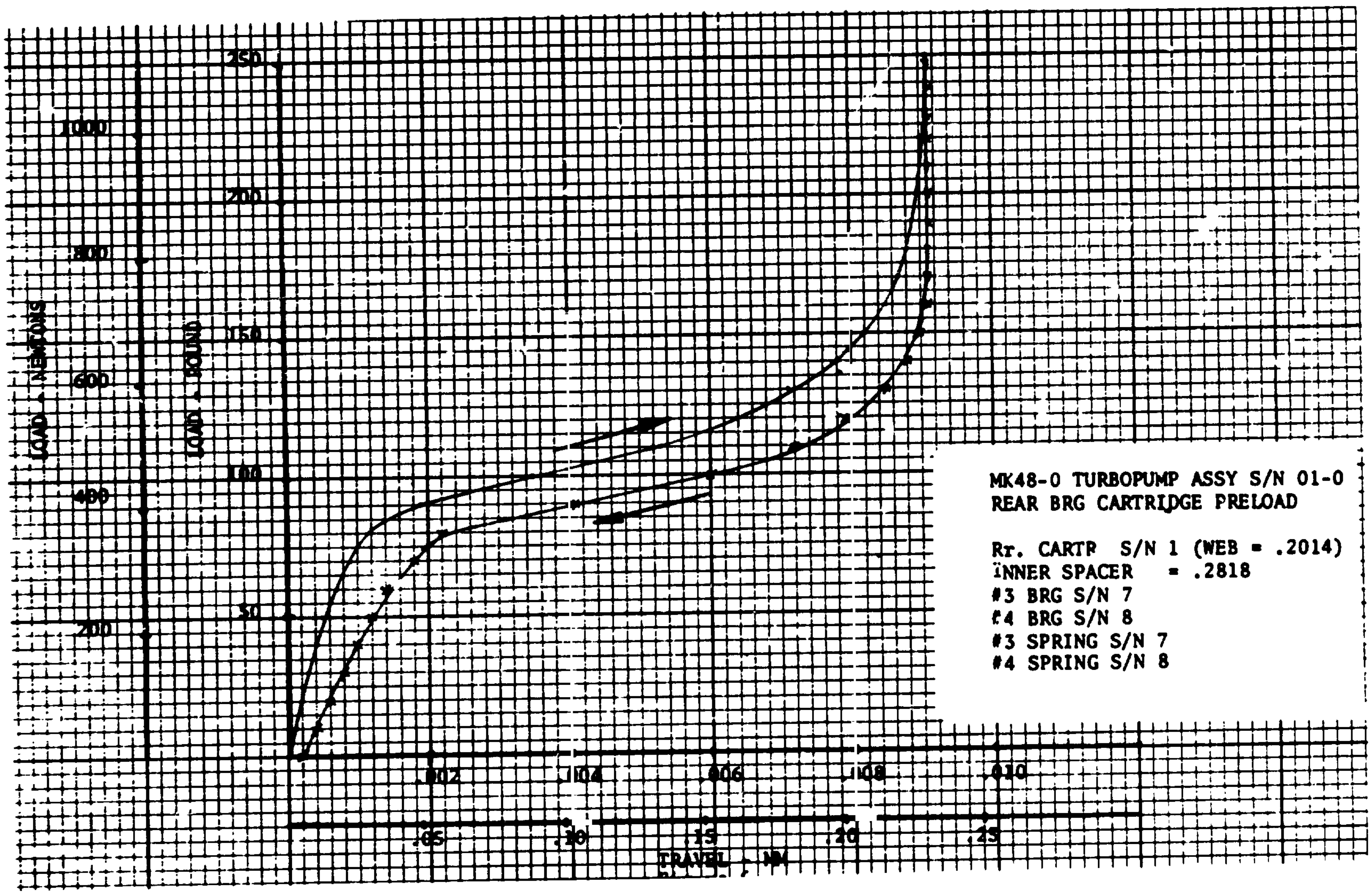

Figure 85. Mark 48-0 Turbopump Rear Bearing Cartridge Preload

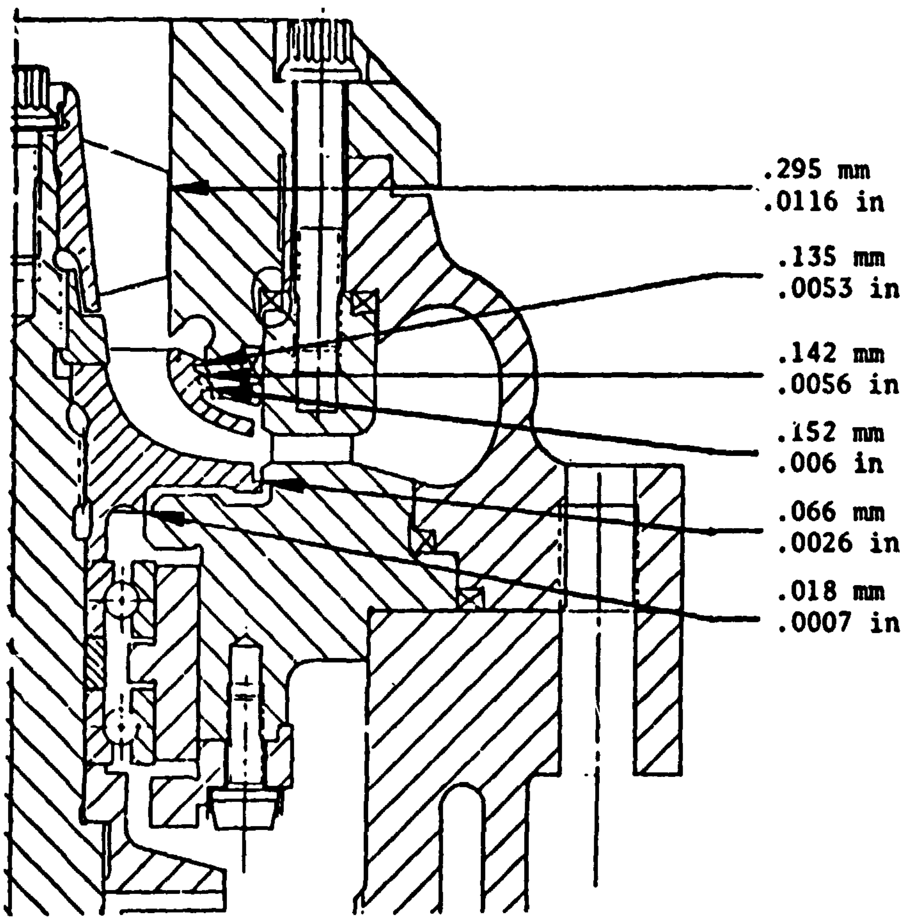

Figure 86. Mark 48-O Turbopump S/N 01-0 Pump Diametral Clearances

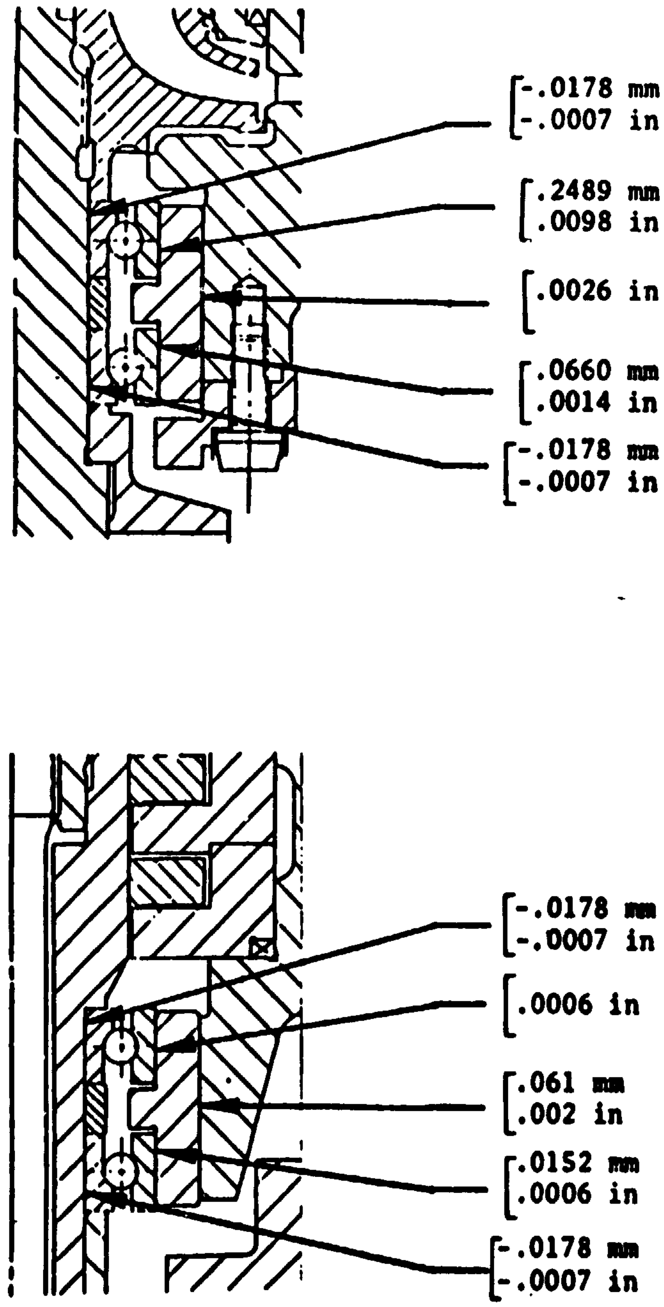

Figure 87. Mark 48-0 Turbopump S/N 01-0 Bearing Fits

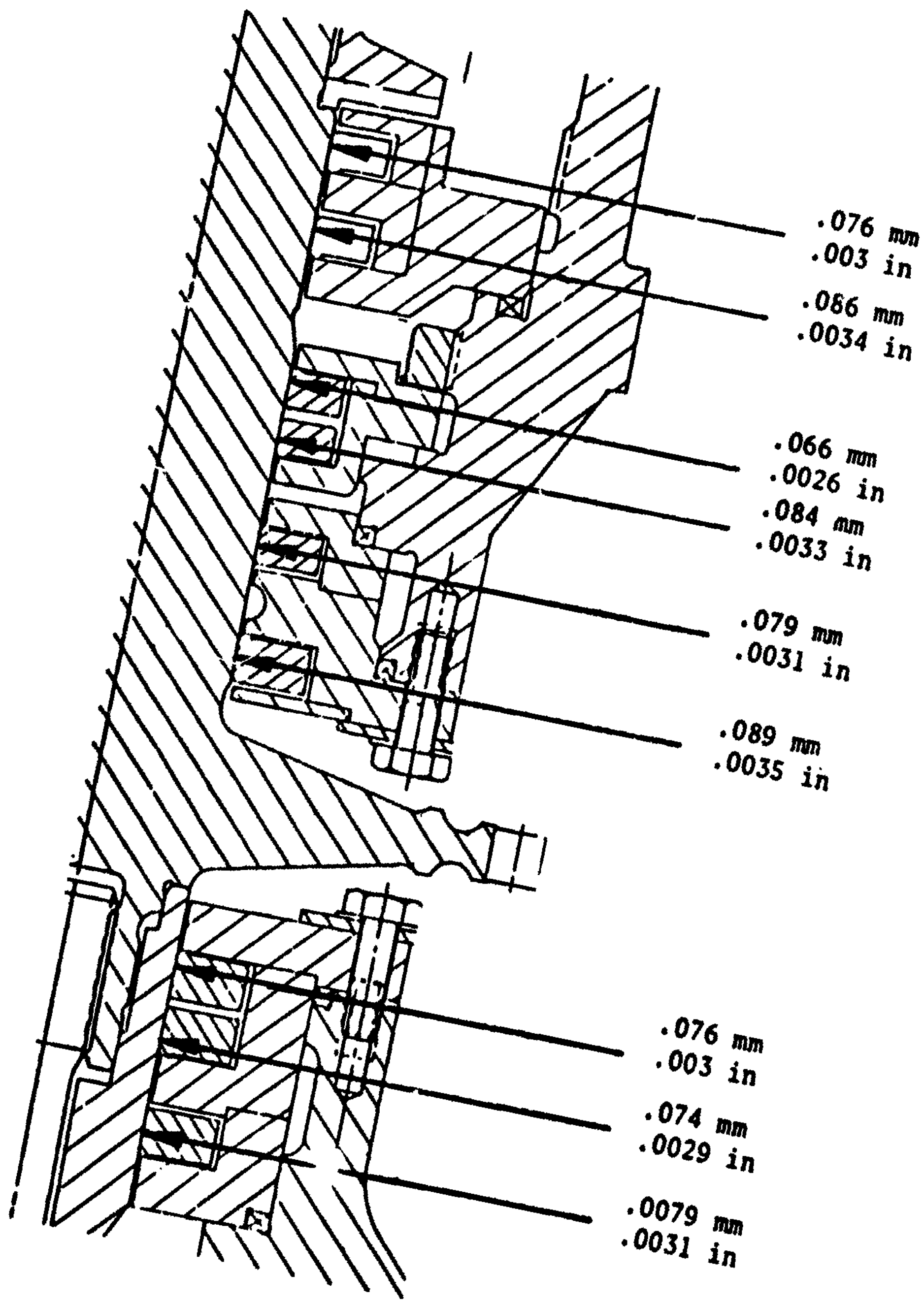

Figure 88. Mark 48-0 S/N 01-0 Seal Diametral Clearances

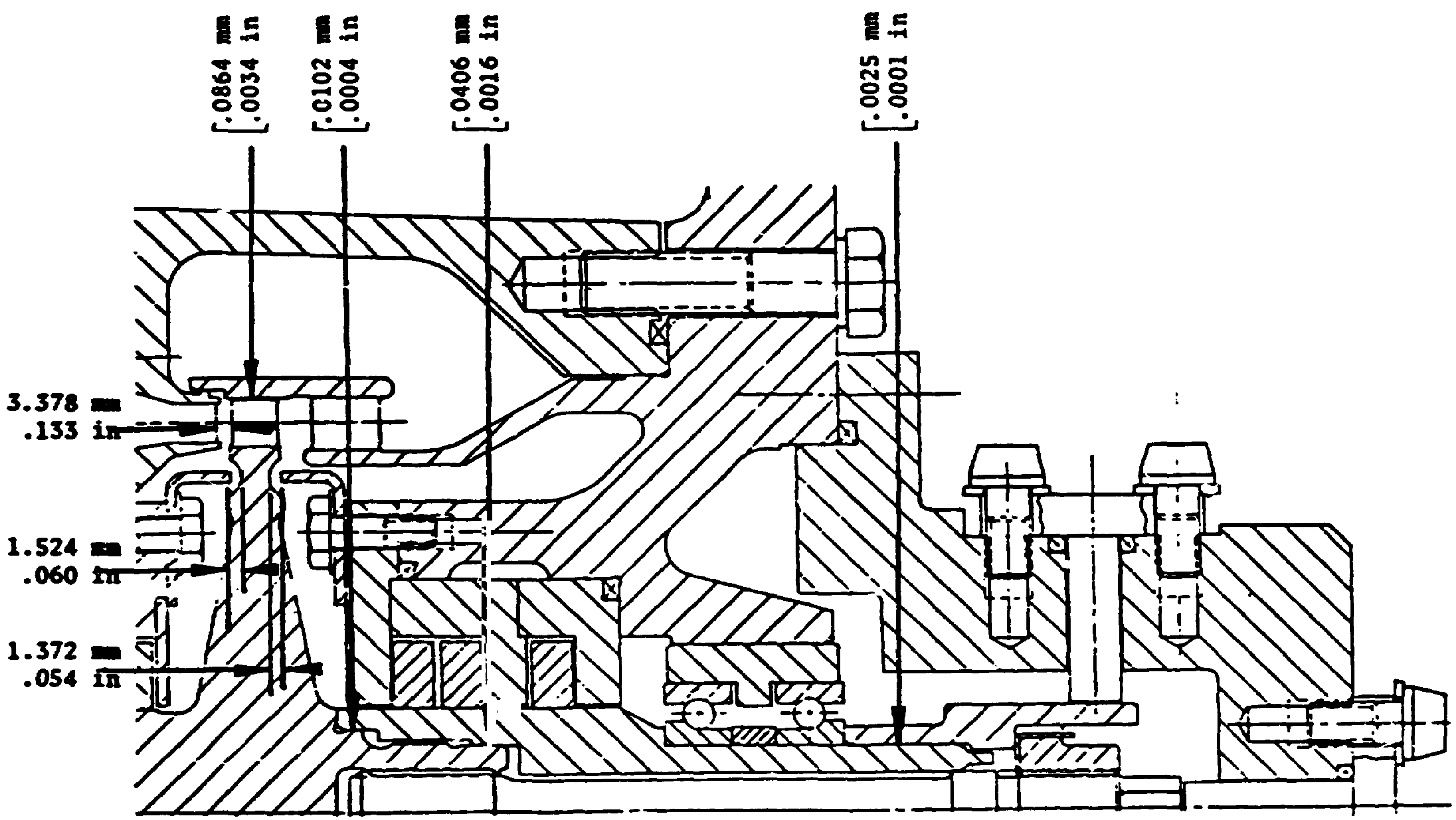

Figure 89. Mark 48-0 Turbopump S/N 01-0 Turbine End Clearances and Fits

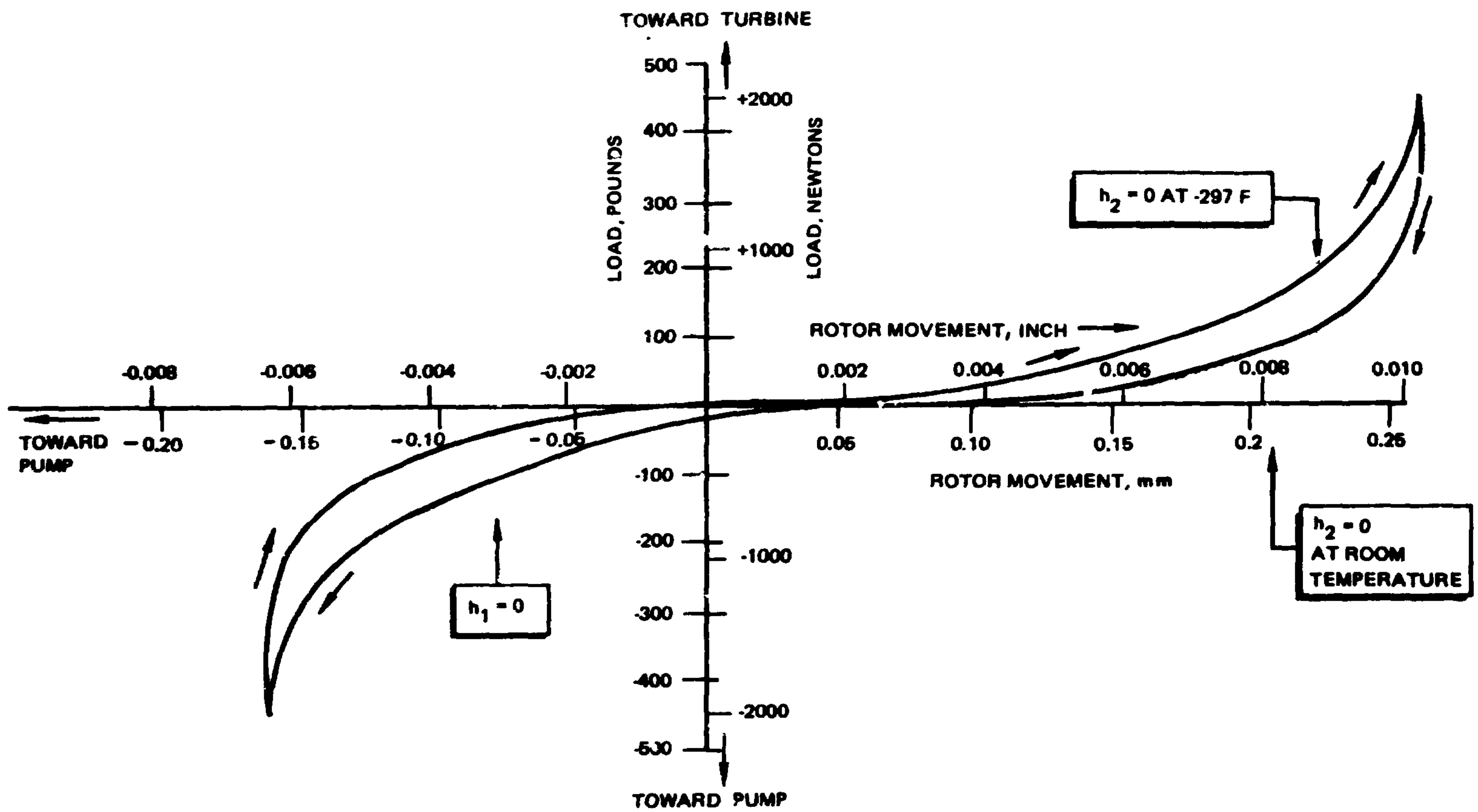

Figure 90. Mark 48-0 Rctor Push-Pull

15. Bearing preloads as a function of balance piston position were verified.
16. The inducer was installed.
17. The instrumentation sleeve rear cover, three Bently proximity indicators, speed and temperature probes were installed.
18. The shaft seals and external flanges were checked for leakage rates. The measured values are shown in Table 13.
19. The shaft torque was measured. It ranged between 3.5 and 10.6 N cm (5 and 15 in-oz).
20. The turbopump was weighed. The total weight was 54.5 kg (120 pounds), including gas generator body and auxiliary gear drive features.

TABLE 13. MARK 48-0 TURBOPUMP S/N 01-OA SHAFT SEAL LEAK CHECK RESULTS

Pressurizing Medium: Gaseous Helium

Pressure Level = 21 N/cm^2 (30 psig)

Seal	Flow	
	m^3/sec	scfm
Primary LOX	0.012	2.4
Intermediate		
Pump Side	0.015	3
Turbine Side	0.030	6
Primary Hot Gas		
Primary Drain Open Only	0.024	4.8
Secondary Drain Open Only	0.018	3.5
Outboard Seal		
Turbine Side	0.020	4.0
Outboard Side	0.019	3.8

The assembled turbopump was installed on a support fixture, as illustrated in Fig. 91 and 92. Mounting was accomplished by two brackets attached to the volute flange, each of which provided support in the axial, vertical, and lateral direction. Additional vertical stabilization was provided by a ball joint support attached to the rear bearing carrier flange.

ORIGINAL PAGE IS
OF POOR QUALITY

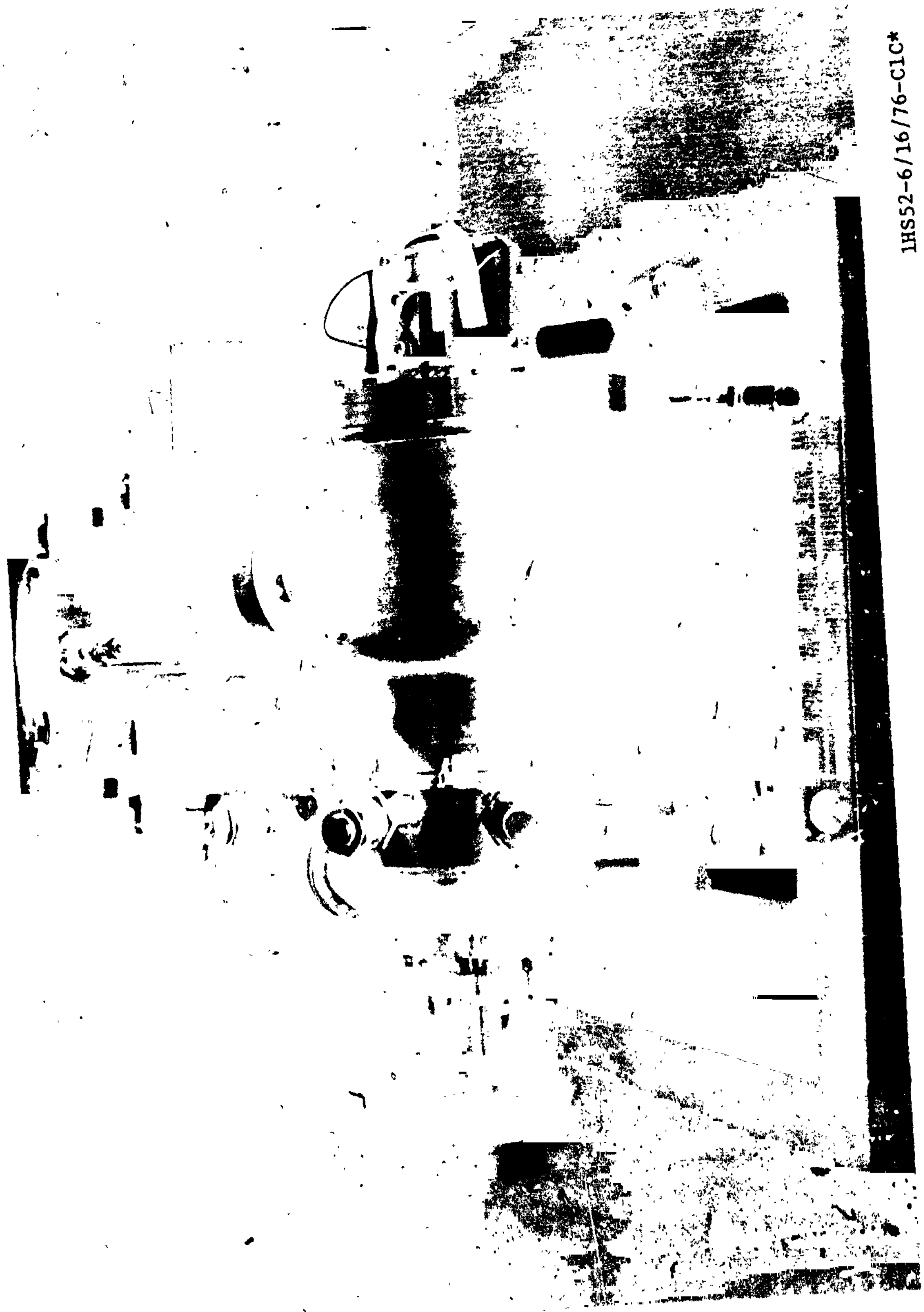

1HS52-6/16/76-C1C*

Figure 91. Mark 48-0 Turbopump Assembly

ORIGINAL PAGE IS
OF POOR QUALITY

1HS52-6/16/76-C1B*

Figure 92. Mark 48-0 Turbopump Assembly

TESTING

Gas Generator Testing

In conjunction with the hot-streak/erosion problem encountered with the LH_2 turbopump gas generator combustor, the two LO_2 turbopump gas generator injectors were dimensionally inspected and water-flowed to evaluate impingement patterns and coaxial-element, quantitative-flow distributions. During the hydrogen-side, water-flow tests on both injectors, leaks were observed between the fuel sleeves and the injector-face material. A microscopic inspection of the braze joints in the affected areas revealed voids in the braze material. Both injectors were rebrazed successfully at Rocketdyne. A vacuum leak check of the oxidizer manifold showed no evidence of interpropellant leak paths within the internal LO_2 posts/injector joints. Figure 93 shows the results of the initial water-flow tests showing the leakage areas. (Note: The outer 10 elements of the injector are plugged since the same injector pattern is used for the LH_2 turbopump gas generator injector.) Table 14 presents the dimensional inspection results on injector P/N RS005024E-161, Units 1 and 2, while Tables 15 and 16 presents the results of the water-flow tests after the rebraze cycle. Prior to the water-flow tests on each injector, the LO_2 posts were mechanically aligned with special fixtures. Subsequent to the water-flow tests, the posts were checked to ensure correct alignment.

Prior to the initial hot-fire test of the LO_2 turbopump gas generator, an LH_2 blowdown through the hardware was conducted to verify the analytical main fuel valve manual set-point position calculation during the hydrogen lead sequence of the test. The analytical calculations agreed closely to the cryogenic blowdown data. A manual set-point position of 16.5% open was selected for the main fuel valve (compared to 57% open for the LH_2 turbopump gas generator tests).

Table 17 presents an overall test summary of the LO_2 turbopump gas generator development testing, while a more detailed discussion of various aspects of the program is included below.

Propellant Servovalve Operation. The performance of the gas generator depends on a closed-loop pressure fuel back signal using propellant injection pressures as the control parameter. The hydrogen and oxygen servovalve injection set pressures are predetermined based on the required performance level and the hydraulic resistance of the individual injector system. The gas generator performance is balanced to achieve the desired flowrates through the injector by the use of a Rocketdyne-prepared GE-Timeshare computer program (RECAL 2). This information is translated into servovalve controller settings, which are manually set prior to the test.

Tests 016-030 and -031 failed to achieve main propellant ignition because of the system characteristics of both the gas generator injector and the facility LO_2 servovalve controller. The objective of these tests was to demonstrate the ignition transition characteristics of the LO_2 turbopump injector. The test sequence

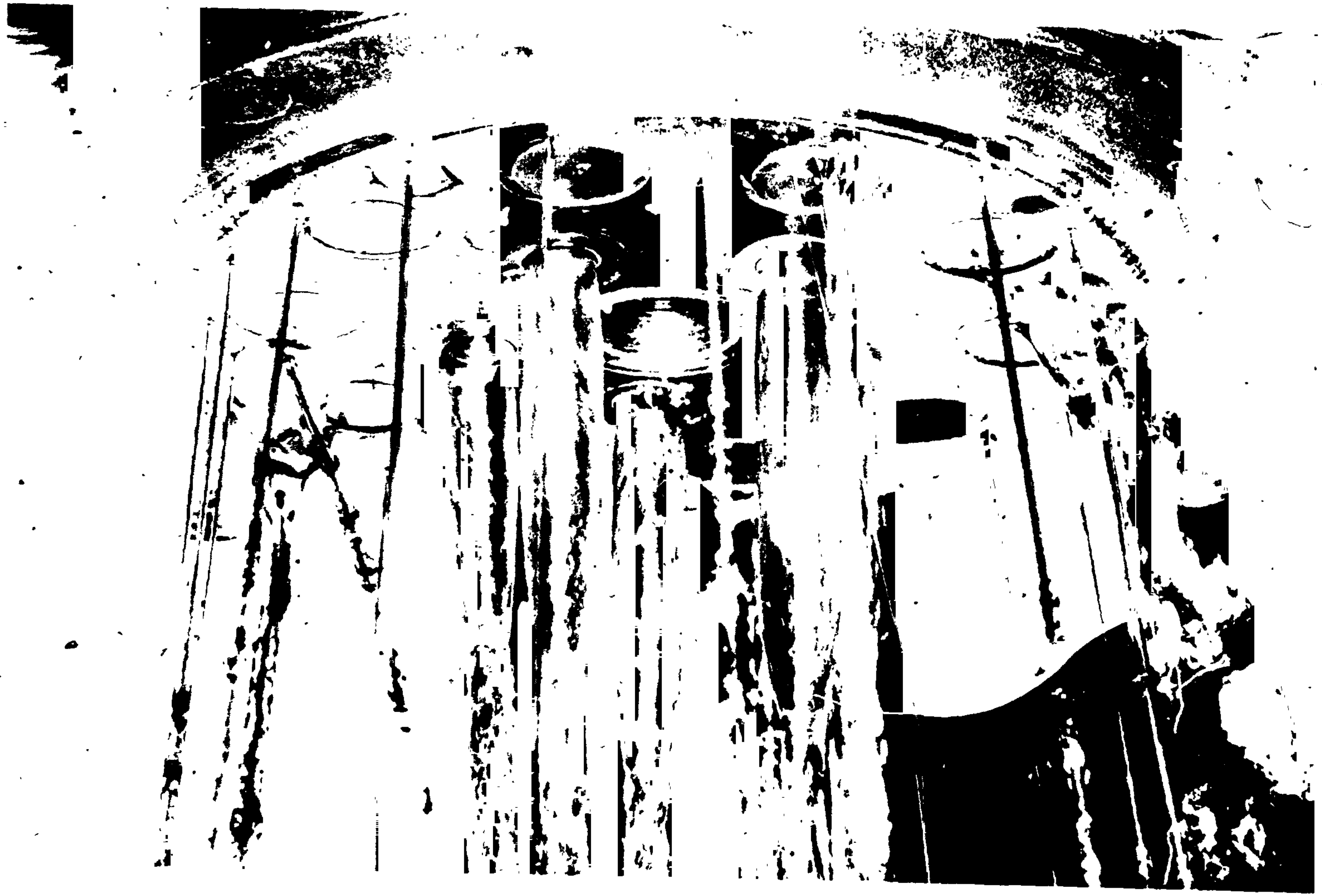

1HS49-9/18/75-C1

Figure 93. LO_2 Turbopump Injector Water-Flow Test, Leakage Noted Prior to Rebraze Cycle

ORIGINAL PAGE IS OF POOR QUALITY

TABLE 14. INJECTOR INSPECTION RESULTS
(METRIC UNITS)

Element No.	LO_2 Post ID, mm 2.51 +0.08 -0.00		LO_2 Post Orifice, mm 1.32 ±0.13		Fuel Sleeve ID, mm 4.166 +0.025 -0.000		Post Depth, mm 2.54 ±0.13	
	U/N 2	U/N 2	U/N 1	U/N 2	U/N 1	U/N 2	U/N 1	U/N 2
2-1	2.51	2.49	1.232	1.257	(1)	4.204	2.654	2.743
2-2	2.46	2.46	1.24	1.232	4.183	4.204	2.718	2.642
2-3	2.46	2.46	1.237	1.232	4.173	4.186	2.616	2.667
2-4	2.46	2.46	1.232	1.236	4.216	4.186	2.616	2.743
2-5	2.46	2.49	1.21	1.232	4.196	(2)	2.616	2.616

(1) Varied from 4.221 to 4.247
(2) Varied from 4.173 to 4.199
(3) No data

ID No.	Orifice Size, mm 0.508 ±0.05		Film Coolant Angle, rad 0.087 ±0.009	
	U/N 1	U/N 2	U/N 1	U/N 2
FC -1	0.483	(3)	0.085	(3)
-2	0.457	0.508	0.099	0.092
-3	0.483	0.483	0.105	0.083
-4	0.483	0.483	0.099	0.094
-5	0.483	0.483	0.099	0.094
-6	0.483	0.483	0.099	0.081
-7	0.508	0.483	0.099	0.077
-8	0.483	0.483	0.092	0.094
-9	0.483	0.483	0.099	0.086
-10	0.483	0.483	0.087	0.094
-11	0.483	0.483	0.180	0.100
-12	0.483	0.483	0.093	0.095
-13	0.508	0.483	0.087	0.099
-14	0.508	0.483	0.106	0.108
-15	0.483	0.483	0.093	0.103
-16	0.483	0.508	0.116	0.103
-17	0.508	0.508	0.093	0.103
-18	0.483	0.483	0.099	0.092
-19	0.508	0.483	0.093	0.095
-20	0.483	0.508	0.087	0.095

TABLE 14. (Concluded)

(ENGLISH UNITS)

Element No.	LO_2 Post ID, inch 0.099 +0.003 -0.000		LO_2 Post Orifice, inch 0.052 ±0.005		Fuel Sleeve ID, inch 0.164 +0.001 -0.000		Post Depth, inch 0.100 ±0.005	
	U/N 1	U/N 2	U/N 1	U/N 2	U/N 1	U/N 2	U/N 1	U/N 2
2-1	0.099	0.098	0.0485	0.0495	(1)	0.1655	0.1045	0.108
2-2	0.097	0.097	0.0490	0.0485	0.1647	0.1655	0.107	0.104
2-3	0.097	0.097	0.0487	0.0485	0.1543	0.1648	0.103	0.105
2-4	0.097	0.097	0.0485	0.0487	0.166	0.1650	0.105	0.108
2-5	0.097	0.098	0.0478	0.0485	0.1652	(2)	0.103	0.103

(1) Varied from 0.1662 to 0.1672
(2) Varied from 0.1643 to 0.1653
(3) No data

ID No.	Orifice Size, 0.020 ±0.002		Film Coolant Angle 5° ±0.5'	
	U/N 1	U/N 2	U/N 1	U/N 2
FC-1	0.019	(3)	4°55'	(3)
-2	0.018	0.020	5°42'	5°14'
-3	0.019	0.019	6°00'	4°45'
-4	0.019	0.019	5°43'	5°22'
-5	0.019	0.019	5°43'	5°20'
-6	0.019	0.019	5°40'	4°40'
-7	0.020	0.019	5°41'	4°25'
-8	0.019	0.019	5°16'	4°45'
-9	0.019	0.019	5°40'	4°55'
-10	0.019	0.019	5°05'	5°24'
-11	0.019	0.019	5°32'	5°47'
-12	0.019	0.019	5°18'	5°28'
-13	0.020	0.019	5°35'	5°40'
-14	0.020	0.019	6°05'	6°12'
-15	0.019	0.019	5°19'	5°55'
-16	0.019	0.020	6°40'	5°53'
-17	0.020	0.020	5°18'	5°57'
-18	0.019	0.019	5°41'	5°10'
-19	0.020	0.019	5°20'	5°25'
-20	0.019	0.020	5°32'	5°25'

TABLE 15. LO_2 TURBOPUMP INJECTOR, P/N RS005024, U/N 1

(METRIC UNITS)

Water-Flow Test Results				
Element Number	LO_2 Post Flowrate, 10^{-6} m^3/s	Fuel Sleeve Flowrate, 10^{-6} m^3/s	Film Coolant Orifice Number	Film Coolant Flowrate, 10^{-6} m^3/s
2-1	7.32	11.55	FC -1	0.568
2-2	7.30	11.55	-2	0.480
2-3	7.38	11.42	-3	0.473
2-4	7.43	11.23	-4	0.448
2-5	7.28	11.42	-5	0.563
			-6	0.517
			-7	0.448
			-8	0.485
			-9	0.505
			-10	0.435
			-11	0.473
			-12	0.631
			-13	0.543
			-14	0.511
			-15	0.517
			-16	0.524
			-17	0.498
			-18	0.492
			-19	0.480
			-20	0.511
	$Q_T = 36.70$ $\overline{Q} = 7.34$ $\sigma = \pm 0.0631$	$Q_T = 57.17$ $\overline{Q} = 11.43$ $\sigma = \pm 0.129$		$Q_T = 10.11$ $\overline{Q} = 0.505$ $\sigma = 0.046$

TABLE 15. (Concluded)

(ENGLISH UNITS)

Water-Flow Test Results				
Element Number	LO_2 POST Flowrate, gpm	Fuel Sleeve Flowrate, gpm	Film Coolant Orifice Number	Film Coolant Flowrate, gpm
2-1	0.1160	0.183	FC-1	0.0090
2-2	0.1157	0.183	-2	0.0076
2-3	0.1169	0.181	-3	0.0075
2-4	0.1178	0.178	-4	0.0071
2-5	0.1153	0.181	-5	0.0090
			-6	0.0082
			-7	0.0071
			-8	0.0077
			-9	0.0080
			-10	0.0069
			-11	0.0075
			-12	0.0100
			-13	0.0086
			-14	0.0081
			-15	0.0082
			-16	0.0083
			-17	C 0079
			-18	0.0078
			-19	0.0076
			-20	0.0081
	Q_T = 0.5817 $\bar{Q}$ = 0.1163 σ = ±0.0010	Q_T = 0.906 $\bar{Q}$ = 0.1812 σ = ±0.00204		Q_T = 0.1602 $\bar{Q}$ = 0.00801 σ = ±0.00073

TABLE 16. LO_2 TURBOPUMP INJECTOR, P/N RS005024, U/N 2

(METRIC UNITS)

Water-Flow Test Results				
Element Number	LO_2 Post Flowrate, 10^{-6} m^3/s	Fuel Sleeve Flowrate, 10^{-6} m^3/s	Film Coolant Orifice Number	Film Coolant Flowrate, 10^{-6} m^3/s
2-1	9.21	12.37	FC -1	0.581
2-2	9.40	12.30	-2	0.524
2-3	9.28	12.43	-3	0.492
2-4	9.33	12.37	-4	0.517
2-5	9.21	12.37	-5	0.541
			-6	0.555
			-7	0.555
			-8	0.524
			-9	0.524
			-10	0.555
			-11	0.517
			-12	0.511
			-13	0.530
			-14	0.530
			-15	0.562
			-16	0.511
			-17	0.549
			-18	0.511
			-19	0.492
			-20	0.543
	Q_T = 46.44 $\overline{Q}$ = 9.29 σ = 0.082	Q_T = 61.83 $\overline{Q}$ = 12.36 σ = 0.044		Q_T = 10.59 $\overline{Q}$ = 0.529 σ = 0.0233

TABLE 16. (Concluded)

(ENGLISH UNITS)

Water Flow Test Results				
Element Number	LO_2 Post Flowrate, gpm	Fuel Sleeve Flowrate, gpm	Film Coolant Orifice Number	Film Coolant Flowrate, gpm
2-1	0.146	0.196	FC-1	0.0092
2-2	0.149	0.195	FC-2	0.0083
2-3	0.147	0.197	FC-3	0.0078
2-4	0.148	0.196	FC-4	0.0082
2-5	0.146	0.196	FC-5	0.0081
			FC-6	0.0088
			FC-7	0.0088
			FC-8	0.0083
			FC-9	0.0083
			FC-10	0.0088
			FC-11	0.0082
			FC-12	0.0081
			FC-13	0.0084
			FC-14	0.0084
			FC-15	0.0089
			FC-16	0.0081
			FC-17	0.0087
			FC-18	0.0081
			FC-19	0.0078
			FC-20	0.0086
	$Q_T = 0.736$ $\overline{Q} = 0.1472$ $\sigma = \pm 0.0013$	$Q_T = 0.980$ $\overline{Q} = 0.196$ $\sigma = \pm 0.0007$		$Q_T = 0.1679$ $\overline{Q} = 0.00839$ $\sigma = \pm 0.00037$

TABLE 17. LO_2 TURBOPUMP GAS GENERATOR TEST HISTORY
INJECTOR, P/N RS005024E-161, U/N 2

Test Number	Test Date	Objective	Test Duration, seconds	Accumulated Tests	Accumulated Duration seconds	Remarks
016-030	10-7-75	Main Propellant Ignition (MPI)	0.0	1	0.0	Igniter stage OK. Mainstage (M/S) not achieved due to servovalve system response.
016-031	10-7-75	MPI	0.0	2	0.0	Mainstage not achieved. Cutoff initiated at time MLV started to open. Sequencing for next test modified.
016-032	10-9-75	MPI	0.32	3	0.32	Objective achieved.
016-033	10-9-75	Mainstage Transition	2.0	4	2.32	Objective achieved.
016-034	10-14-75	Mainstage-Injector Resistance Verification	2.0	5	4.32	Objective achieved.
016-035	11-6-75	Mainstage Performance	0.0	6	4.32	Fuel injector temperature continue gate cutoff - safety sequence problem.
016-036	11-7-75	Mainstage Performance	2.0	7	6.32	Objective achieved.
016-037	11-7-75	Mainstage Performance	5.0	8	11.32	Objective achieved.
016-038	11-7-75	Mainstage Performance	0.0	9	11.32	Ignition detect cutoff - spark problem
016-039	11-9-75	Mainstage Performance	5.0	10	16.32	Objective achieved.
016-040	11-11-75	Mainstage Duration	0.0	11	16.32	Ignition detect cutoff - spark problem.
016-041	11-11-75	Mainstage Duration	0.0	12	16.32	Ignition detect cutoff - spark problem.
016-042	11-11-75	Mainstage Duration	15.0	13	31.32	Objective achieved.
016-043	11-11-75	Mainstage Duration	0.0	14	31.32	Ignition detect cutoff - spark problem.
016-044	11-12-75	Mainstage Duration	0.0	15	31.32	Ignition detect cutoff - spark problem.
016-048	12-4-75	Mainstage Duration	33.0	16	64.32	Premature cutoff at 33 seconds mainstage due to an erroneously high chamber pressure auto-cut-off. An intermittant short in an instrumentation power supply cable caused spike in chamber pressure transducer output signal. Gas generator performance satisfactory.

times were based on the successful test sequencing demonstrated during the testing of the LH_2 turbopump gas generator. In the case of the LO_2 turbopump gas generator, two phenomena occurred:

1. The hydrogen lead flow was about one-half that of the LH_2 gas generator and required a significantly longer period during the fuel lead sequence for the fuel injection temperature to decay below 88.89 K (-300 F), which is a control gate to permit the main LO_2 valve to open, and

2. Since the hydraulic resistance of the LO_2 side of the injector was higher than the LH_2 turbopump gas generator LO_2 injector, the same injection purge lockup pressure of 1268 N/cm^2 (1850 psig) resulted in a LO_2 injection pressure (during fuel lead) of about 762 N/cm^2 (1113 psig). As a result, the actual opening of the main LO_2 servovalve was delayed, and the tests were terminated when the mainstage duration timer expired. Basically, the problem can be attributed to a lack of sequence characterization experience with the LO_2 turbopump gas generator system as well as the required short mainstage duration. Figure 94 depicts the LO_2 servovalve system operation for the LH_2 turbopump gas generator, while Fig. 95 shows the empirically observed results of tests 016-030 and -031. Note the difference in the control delay time between Fig. 94 and 95. An open-control enable signal is given to the LO_2 valve system, but the actual start of servosystem operation is delayed until the fuel injection temperature drops below 88.89 K (-300 F). The LO_2 turbopump gas generator hydrogen injection priming takes about 0.2 second longer due to the reduced flowrate. The LO_2 servovalve controller system was designed with a control pressure ramp time of about 2.0 seconds to reach the desired set pressure; therefore, the pressure ramp rates vary depending on the level of the injection set pressure. That is, P_c buildup may be expected to increase with higher LO_2 injection set pressures (higher required chamber pressures, or increased hydraulic resistance of the injector). Since the controller feedback control was based on monitoring LO_2 injection pressure, no opening command of the main LO_2 valve is signalled by the controller system because of the existing LO_2 injection pressure, which is the result of injector purging during the hydrogen-lead phase. Once the controller system internal set ramp rate pressure exceeds the actual monitored LO_2 injection pressure, the main LO_2 valve starts to open to maintain the required LO_2 injection pressure. Main propellant ignition is normally experienced about 0.35 second after opening of the main LO_2 valve. Pretest calculations had shown that the 1267 N/cm^2 (1850 psig) LO_2 system purge lockup pressure was necessary to maintain an acceptable gas generator mixture ratio during LO_2 feed line LO_2 expulsion at cutoff. Actual LO_2 feed line LO_2 expulsion time was 3 seconds as compared with 1 second for the LH_2 turbopump gas generator.

Although tests 016-030 and -031 did not achieve main propellant ignition, significant data were obtained to characterize the LO_2 turbopump gas generator sequencing control. Adjustment of the starting sequences from tests 016-030 and -031 was successful in achieving the first main propellant ignition test of the LO_2 turbopump gas generator. A main chamber pressure of about 2068 N/cm^2 (3000 psig) was obtained for a mainstage duration of 0.32 second. A posttest inspection of the injector and combustor revealed no damage.

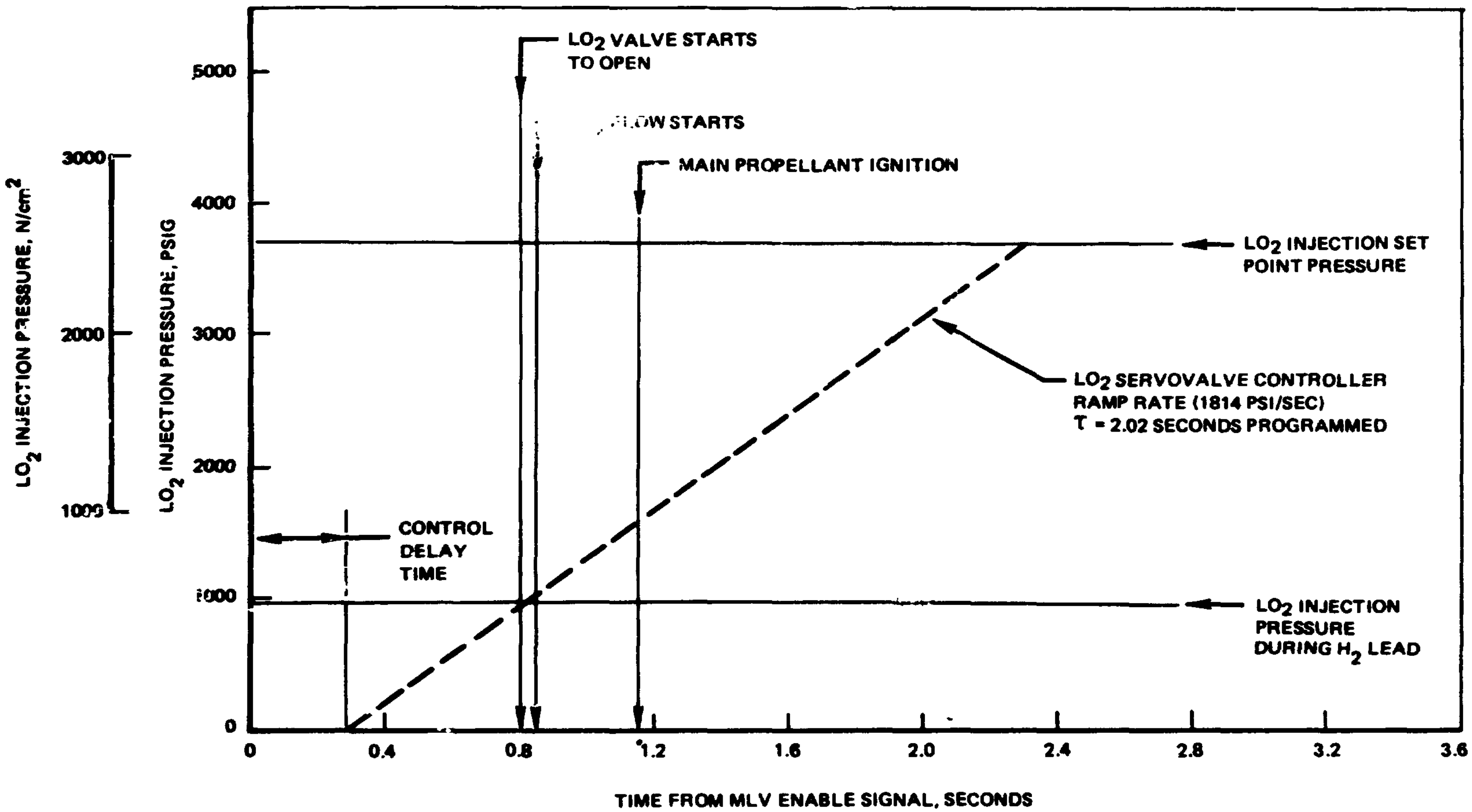

Figure 94. LH_2 Turbopump Gas Generator Injector, P/N RS005024E, U/N 3M, Test 016-029

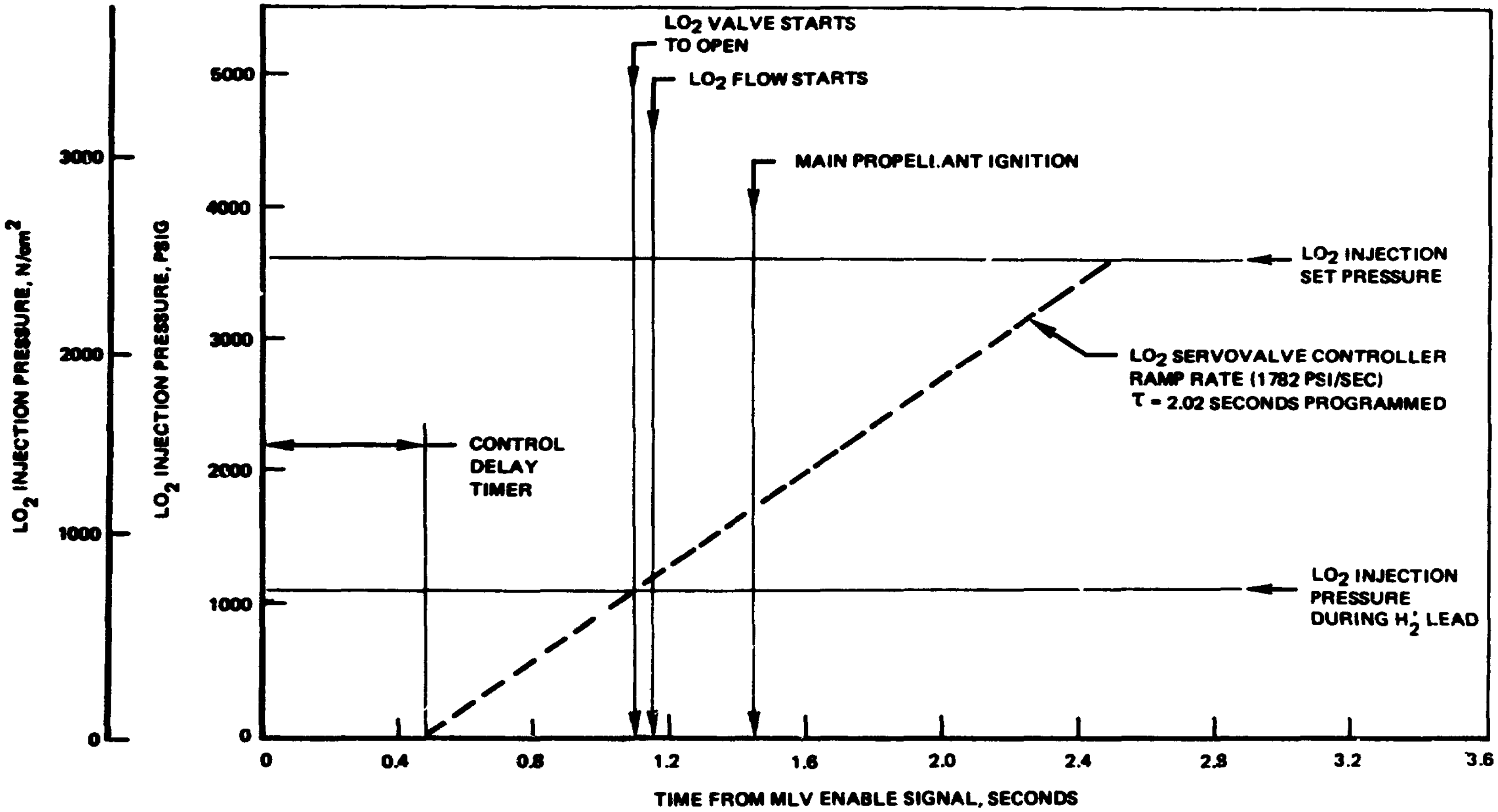

Figure 95. LO_2 Turbopump Gas Generator Injector, RS005024E-161, U/N 2, Test 016-031

Combustor Exit Plane Temperature Profile. During testing of the LH_2 turbopump gas generator, a large thermal gradient, wall to gas core, existed at the combustor exit plane. Eight thermocouples were used during that period and recorded temperature gradients of about 278 K (500 R). A modification to the combustor (90-degree meter bend) solved the problem by enhancing the mixing of the gas products prior to exiting the combustor. The LO_2 turbopump gas generator combustor was fabricated very close to the geometry of the initially designed LH_2 turbopump combustor. The major difference existed in the chamber characteristic length, L*, which increased as a function of the exit nozzle area change, or about 2.2 times the LH_2 turbopump gas generator combustor L*. It was concluded that the LO_2 turbopump gas generator combustor would be tested in the as-fabricated condition to observe the actual thermal gradient during hot fire before any modification, similar to the LH_2 turbopump gas generator combustor, could be considered. Four exit plane thermocouples (chromel-alumel) were inserted in the thermocouple exit ring at various insertion depths: 0.175, 0.196, 0.425, and 0.575 inch. In addition, prior to the last test (016-048), eight external-skin thermocouples were attached to the combustor exit to obtain heat transfer information on the long test as well as providing additional redlines as a safety precaution during the long test. Figure 96 presents a schematic of the gas generator combustor locating the external and internal thermocouples. Table 18 presents the results of the exit plane temperature study for all mainstage tests conducted during this phase of testing. Only one data slice is shown, but the data are representative of the entire applicable test.

Prior to test 016-048, eight thermocouples were attached to the combustor outer wall as previously discussed (Fig. 96). Five of the upper combustion zone skin thermocouples were monitored as redlines 1033 K (1860 R maximum) to ensure adequate safety precautions for the projected long-duration test. Previous calculations had indicated that the gas wall temperature and outside wall temperature would reach thermal equilibrium in about 100 seconds of mainstage duration. Figure 97 shows skin temperature No. 3, the maximum observed temperature for the eight locations versus the test time base. Figures 98 and 99 present graphs of the combustion gas temperature and chamber pressure versus the test time base for test 016-048. Figure 100 shows the gas generator installation prior to test 016-048, indicating the locations of the skin thermocouples. Figure 101 shows the condition of the combustor with the injector removed. No erosion or other damage to either the combustor or injector was noted.

Throughout the test program, a uniform gas temperature (minimum thermal gradient) had been recorded across the gas generator exit plane. The average temperature variation of the four-thermocouple measurement was about 20 K (36 R), or about 2% of the operating temperature. Since the gas generator combustor unit will provide the required hot-gas temperature with a minimum thermal gradient and a sufficient thermal margin in the hardware, it is concluded that the existing LO_2 turbopump gas generator injector and combustor design is acceptable for use with the LO_2 turbopump testing.

Performance Results. A total of 16 tests were conducted on the LO_2 turbopump gas generator using a five-element coaxial design injector, P/N RS005024, Unit No. 2. Seven of those tests achieved mainstage of sufficient duration to obtain performance characteristics of the system. Table 19 presents a summary of the

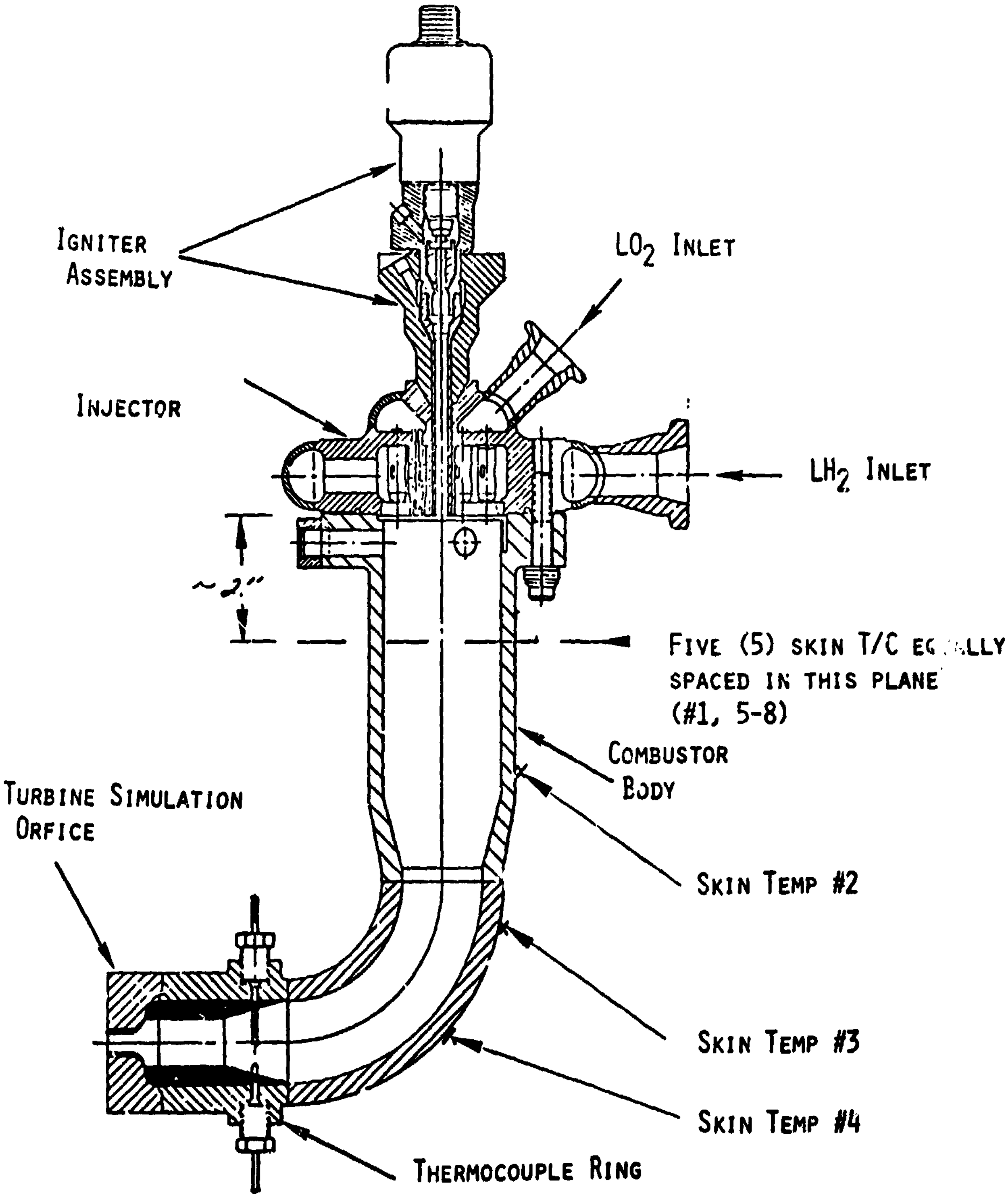

Figure 96. LO_2 Turbopump Gas Generator

TABLE 18. LO_2 TURBOPUMP GAS GENERATOR COMBUSTOR TEMPERATURE STUDY

(Metric Units)

Test No.	Test Duration, seconds	Pc, N/cm^2	Total GG Flowrate, kg/sec	Overall GG Mixture Ratio	Average Mainstage Combustor Exit Temperature, K	Exit Temperature Variation (4 Measurements), K
016-032	0.32	← TOO SHORT FOR PERFORMANCE →				
016-033	2.0	2097	1.456	0.713	744	19
016-034	2.0	2234	1.247	1.19	1030	52
016-036	2.0	2275	1.418	0.757	800	17
016-037	5.0	2279	1.431	0.759	795	24
016-039	5.0	2316	1.466	0.777	808	13
016-042	15.0	2309	1.383	0.888	924	8
016-048	33.0	2306	1.370	1.023	1077	7

(English Units)

Test No.	Test Duration, seconds	Pc, psia	Total GG Flowrate, lb/sec	Overall GG Mixture Ratio	Average Mainstage Combustor Exit Temperature, R	Exit Temperature Variation (4 Measurements), R
016-032	0.32	← TOO SHORT FOR PERFORMANCE →				
016-033	2.0	3042	3.209	0.713	1340	34
016-034	2.0	3240	2.749	1.19	1854	94
016-036	2.0	3300	3.127	0.757	1441	31
016-037	5.0	3309	3.154	0.759	1431	44
016-039	5.0	3359	3.231	0.777	1455	23
016-042	15.0	3349	3.050	0.888	1663	15
016-048	33.0	3345	3.021	1.023	1938	13

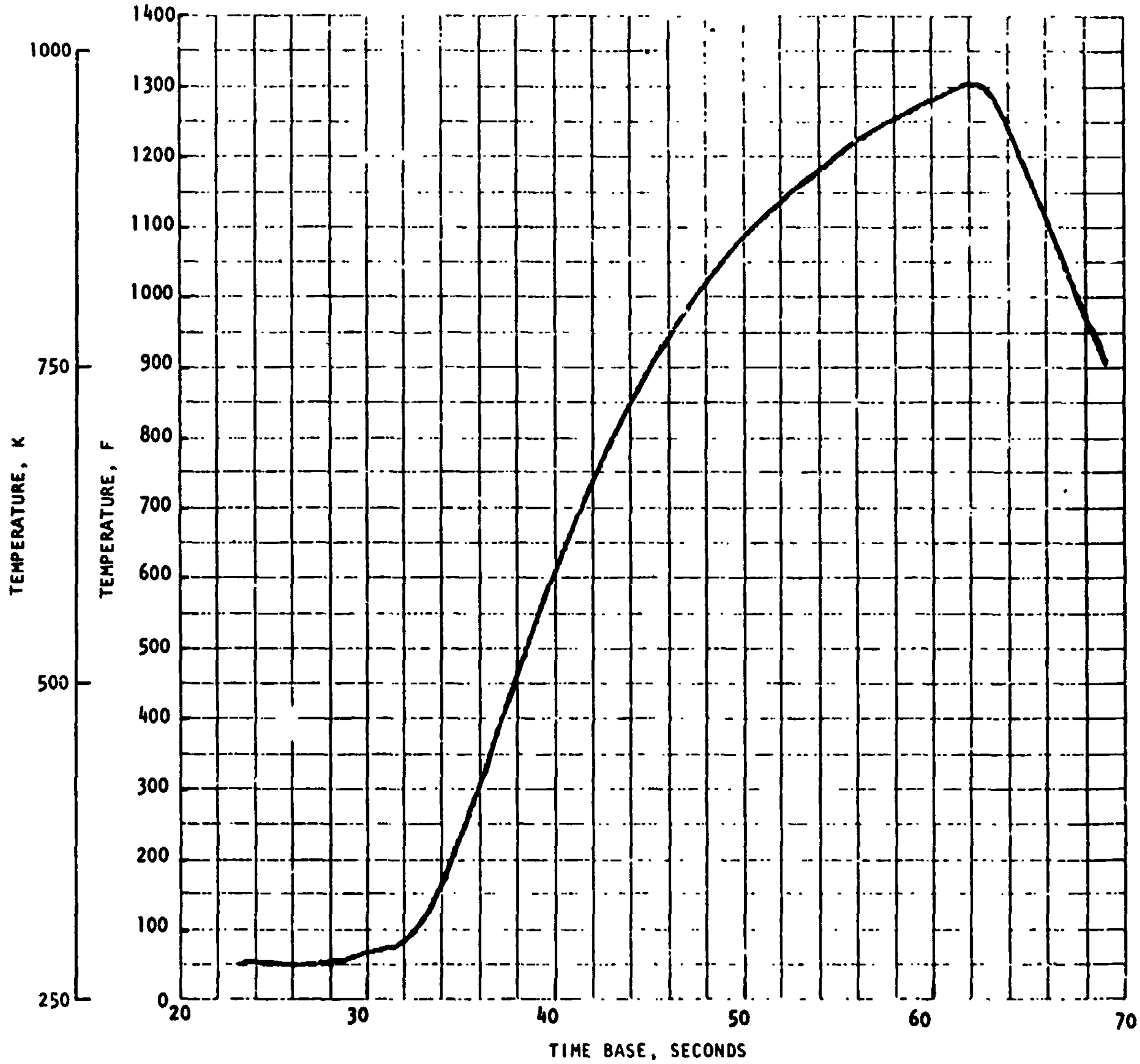

Figure 97. Combustion Skin Temperature No. 3 (Test 016-048)

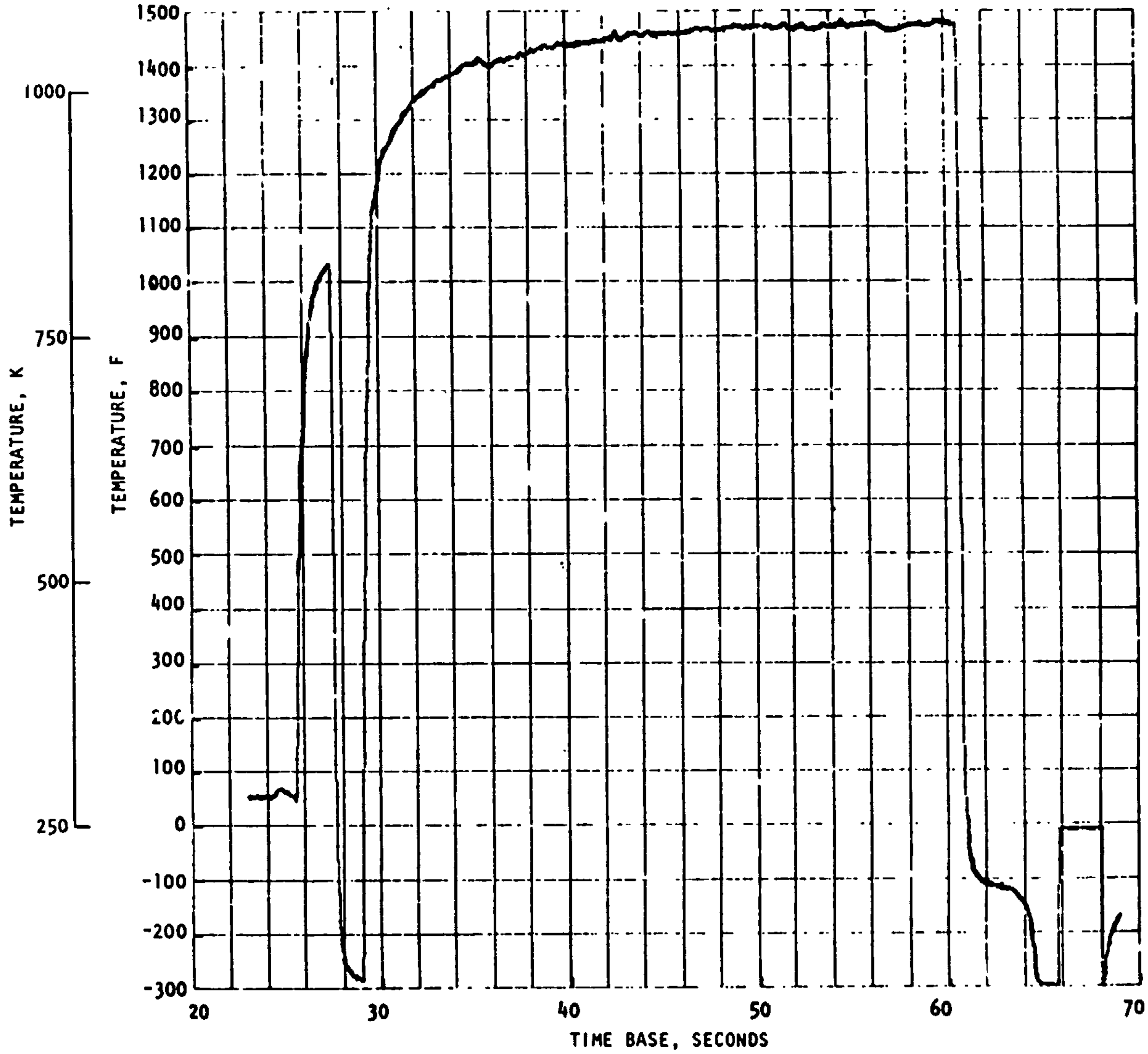

Figure 98. Combustion Gas Temperature (Test 016-048)

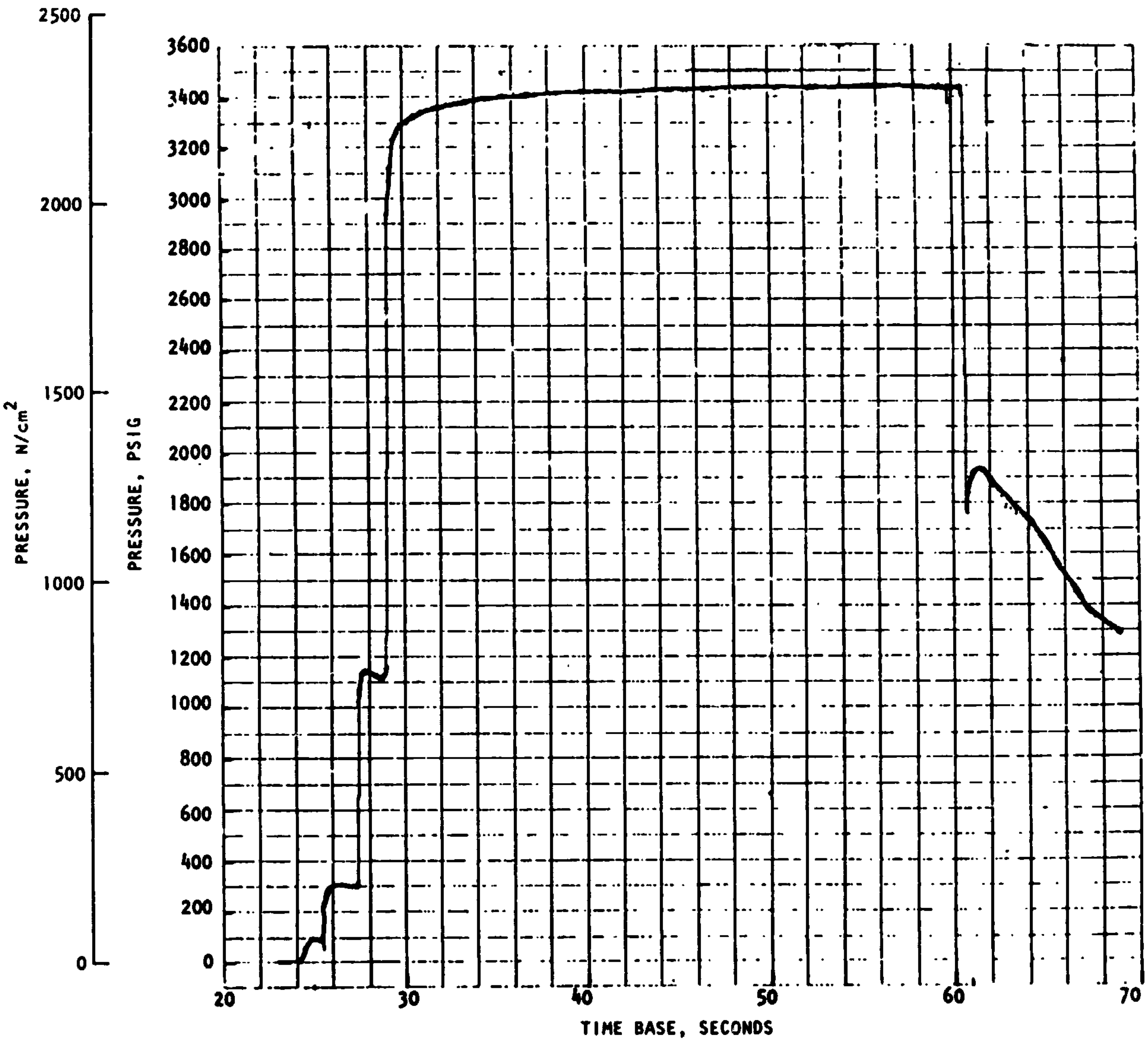

Figure 99. Chamber Pressure (Test 016-048)

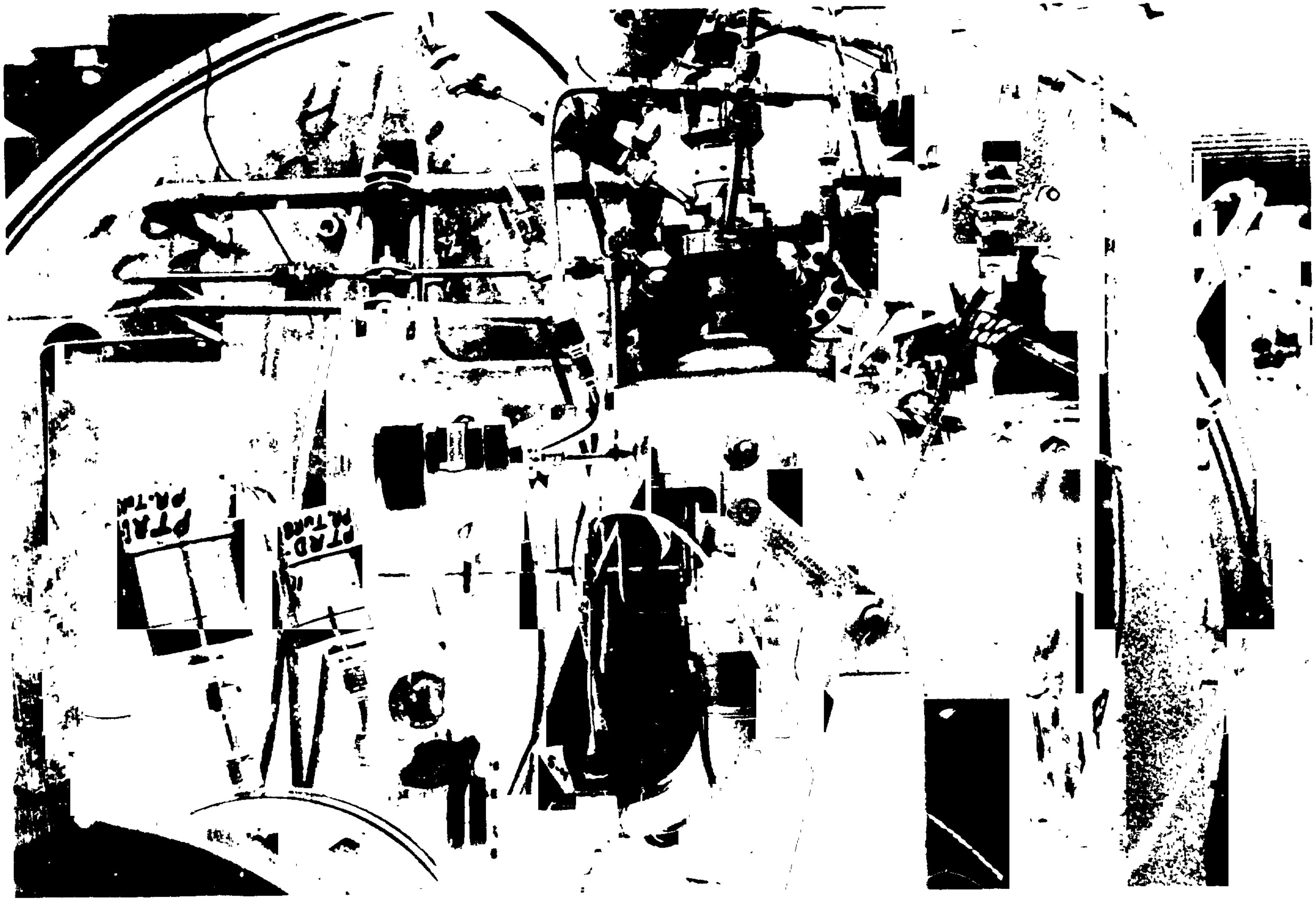

5AJ31-12/4/75-S1

Figure 100. LO_2 Turbopump Gas Generator Installation, Test 016-048

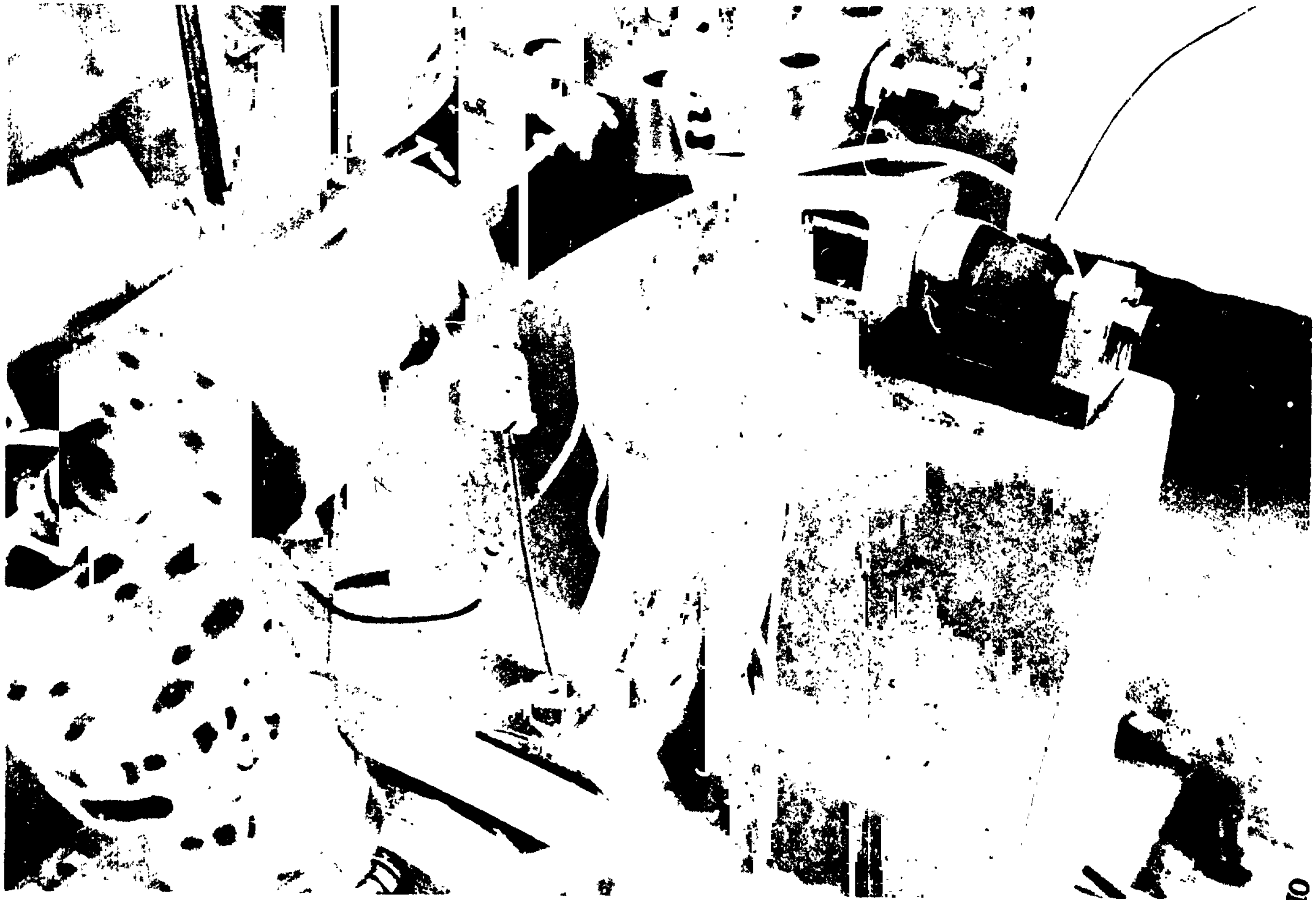

5AJ36-12/4/75-S1*

Figure 101. Condition of Combustor, Posttest 016-048

TABLE 19. GAS GENERATOR MAINSTAGE PERFORMANCE DATA: INJECTOR P/N RS005024, UNIT 2

(METRIC UNITS)

Test Number -016	Test Date	Duration, seconds	GG or T/P Test	P_c, N/cm^2	Combustion Temperature, K	Oxidizer Injector Flowrate, kg/s	Fuel Injector Flowrate, kg/s	Total Injector Flowrate, kg/s	Injector Mixture Ratio	Igniter Oxidizer Flowrate, kg/s	Igniter Fuel Flowrate, kg/s	Igniter Total Flowrate, kg/s	Igniter Mixture Ratio	Total Oxidizer Flowrate, kg/s	Total GG Fuel Flowrate, kg/s	Total GG Flowrate, kg/s	Overall GG Mixture Ratio
032	10-9-75	0.32	GG	TRANSIENT DATA													
033	10-9-75	2.0		2097	744	0.584	0.827	1.411	0.707	0.0218	0.0223	0.0441	0.978	0.606	0.849	1.455	0.714
034	10-14-75	2.0		2234	1030	0.657	0.547	1.204	1.200	0.0205	0.0219	0.0424	0.940	0.677	0.569	1.247	1.190
036	11-7-75	2.0		2275	801	0.592	0.786	1.378	0.753	0.0192	0.0219	0.0411	0.878	0.611	0.808	1.419	0.757
037	11-7-75	5.0		2281	795	0.530	0.792	1.390	0.755	0.0190	0.0211	0.0401	0.897	0.617	0.813	1.430	0.759
039	11-9-75	5.0		2316	808	0.623	0.802	1.425	0.777	0.0186	0.0210	0.0396	0.88[illegible]	0.642	0.823	1.465	0.780
042	11-11-75	15.0		2309	924	0.631	0.712	1.344	0.887	0.0193	0.0205	0.0398	0.94[illegible]	0.651	0.63[illegible]	1.383	0.880
048	12-4-75	33.0	GG	2375	1077	0.675	0.656	1.332	1.029	0.0176	0.0209	0.0386	0.844	0.693	0.677	1.370	1.023
019	8-3-76	2.81	T/P	1266	978	0.406	0.416	0.822	0.975	0.0252	0.0276	0.0528	0.914	0.431	0.444	0.874	0.971
020	8-3-76	0.58		1249	1043	0.431	0.376	0.806	1.145	0.0251	0.0280	0.0531	0.896	0.456	0.404	0.860	1.130
021	8-3-76	16.58		1313	958	0.411	0.432	0.843	0.951	0.0257	0.0281	0.0538	0.913	0.436	0.460	0.896	0.949
023	8-9-76	0.62		1688	812	0.571	0.619	1.190	0.922	0.0236	0.0279	0.0515	0.849	0.595	0.647	1.242	0.919
024	8-9-76	1.2		1697	1013	0.570	0.542	1.111	1.052	0.0236	0.0282	0.0518	0.836	0.593	0.570	1.163	1.041
025	8-9-76	2.39		1704	1087	0.577	0.520	1.097	1.110	0.0236	0.0279	0.0515	0.849	0.601	0.548	1.149	1.097
026	8-11-76	[illegible].82		1845	1038	0.600	0.593	1.192	1.011	0.0241	0.0275	0.0516	0.876	0.624	0.620	1.244	1.005
027	8-11-76	3.01		1446	1137	0.492	0.443	0.935	1.112	0.0248	0.0283	0.0531	0.875	0.517	0.471	0.988	1.097
28	8-11-76	40.79	T/P	1497	983	0.469	0.490	0.959	0.957	0.0251	0.0265	0.0517	0.947	0.494	0.516	1.011	0.957

TABLE 19. (Concluded)
(ENGLISH UNITS)

Test Number 016-	Test Date	Duration, seconds	GG or T/P Test	P_c*, psia	Combustion Temperature,	Oxidizer Injector Flowrate, lb/sec	Fuel Injector Flowrate, lb/sec	Total Injector Flowrate, lb/sec	Injector Mixture Ratio	Igniter Oxidizer Flowrate, lb/sec	Igniter Fuel Flowrate, lb/sec	Igniter Total Flowrate, lb/sec	Igniter Mixture Ratio	Total GG Oxidizer Flowrate, lb/sec	Total GG Fuel Flowrate, lb/sec	Total GG Flowrate, lb/sec	Overall GG Mixture Ratio
032	10-9-75	0.32	GG							TRANSIENT DATA							
033	10-9-75	2.0		3042	1340	1.288	1.823	3.111	0.707	0.0481	0.0492	0.0973	0.976	1.3361	1.8722	3.208	0.714
034	10-14-75	2.0		3240	1854	1.448	1.207	2.655	1.200	0.0453	0.0482	0.0935	0.940	1.4933	1.2552	2.749	1.190
036	11-7-75	2.0		3300	1442	1.305	1.732	3.037	0.753	0.0424	0.0483	0.0907	0.878	1.3474	1.7803	3.128	0.757
037	11-7-75	5.0		3309	1431	1.319	1.746	3.065	0.755	0.0418	0.0466	0.0884	0.897	1.3608	1.7926	3.153	0.759
039	11-9-75	5.0		3359	1455	1.374	1.769	3.143	0.777	0.0411	0.0463	0.0874	0.888	1.4151	1.8153	3.230	0.780
042	11-11-75	15.0		3349	1663	1.392	1.570	2.962	0.887	0.0426	0.0452	0.0878	0.942	1.4346	1.6152	3.050	0.888
048	12-4-75	33.0	GG	3445	1938	1.489	1.447	2.936	1.029	0.0389	0.0461	0.085	0.844	1.5279	1.4931	3.02[illegible]	1.023
019	8-3-76	2.81	T/P	1837	1760	0.894	0.9173	1.8113	0.975	0.0556	0.0608	0.1164	0.914	0.9496	0.9781	1.928	0.971
020	8-3-76	0.58		1812	1877	0.9498	0.8281	1.7778	1.145	0.0553	0.0617	0.1170	0.896	1.0051	0.8898	1.89[illegible]	1.130
021	8-3-76	16.58		1905	1725	0.9055	0.9521	1.8576	0.951	0.0566	0.0620	0.1186	0.913	0.9621	1.0141	1.976	0.949
023	8-9-76	0.62		2449	1461	1.259	1.3655	2.6245	0.922	0.0521	0.0614	0.1135	0.849	1.3111	1.4269	2.733	0.919
024	8-9-76	1.2		2462	1823	1.256	1.194	2.450	1.052	0.0520	0.0622	0.1142	0.836	1.308	1.2552	2.564	1.041
025	8-9-76	2.39		2472	1957	1.273	1.146	2.419	1.110	0.0521	0.0614	0.1135	0.849	1.3251	1.2074	2.533	1.097
026	8-11-76	5.82		2676	1868	1.322	1.307	2.629	1.311	0.0532	0.0607	0.1133	0.876	1.3752	1.3677	2.743	1.005
027	8-11-76	3.01		2098	2047	1.085	0.976	2.061	1.112	0.0546	0.0624	0.117	0.875	1.1396	1.0384	2.179	1.097
028	8-11-76	40.79	T/P	2172	1769	1.034	1.080	2.114	0.357	0.0554	0.0585	0.1139	0.947	1.0894	1.1385	2.228	0.957

*Probable P_c measurement error

Dimensional change of discharge system due to thermal influences not considered mainstage performance obtained during the gas generator testing phase (1975). Also included in Table 20 is the gas generator performance during the hot-fire testing of the Mark 48 oxidizer turbopump (1976).

As discussed earlier, the performan e level ot the gas generator is balanced using a GE-computer program (RECAL 2), which uses as input parameters, the LO_2 and hydrogen injector hydraulic resistances, required chamber pressure, flowrate, and mixture ratio. The control function used to obtain the required performance is the applicable system injection pressure, which is obtained by the use of servocontrol valves in a closed-loop mode. Figure 102 is an injector performance map for LO_2 turbopump injector, P/N RS005024, Unit No. 2, in the region near the design level. While testing the turbopump, a variation from the design level was necessary due to the off-nominal turbine pressure ratio; however, the off-nominal conditions proved to be no problem in the recalibration procedure.

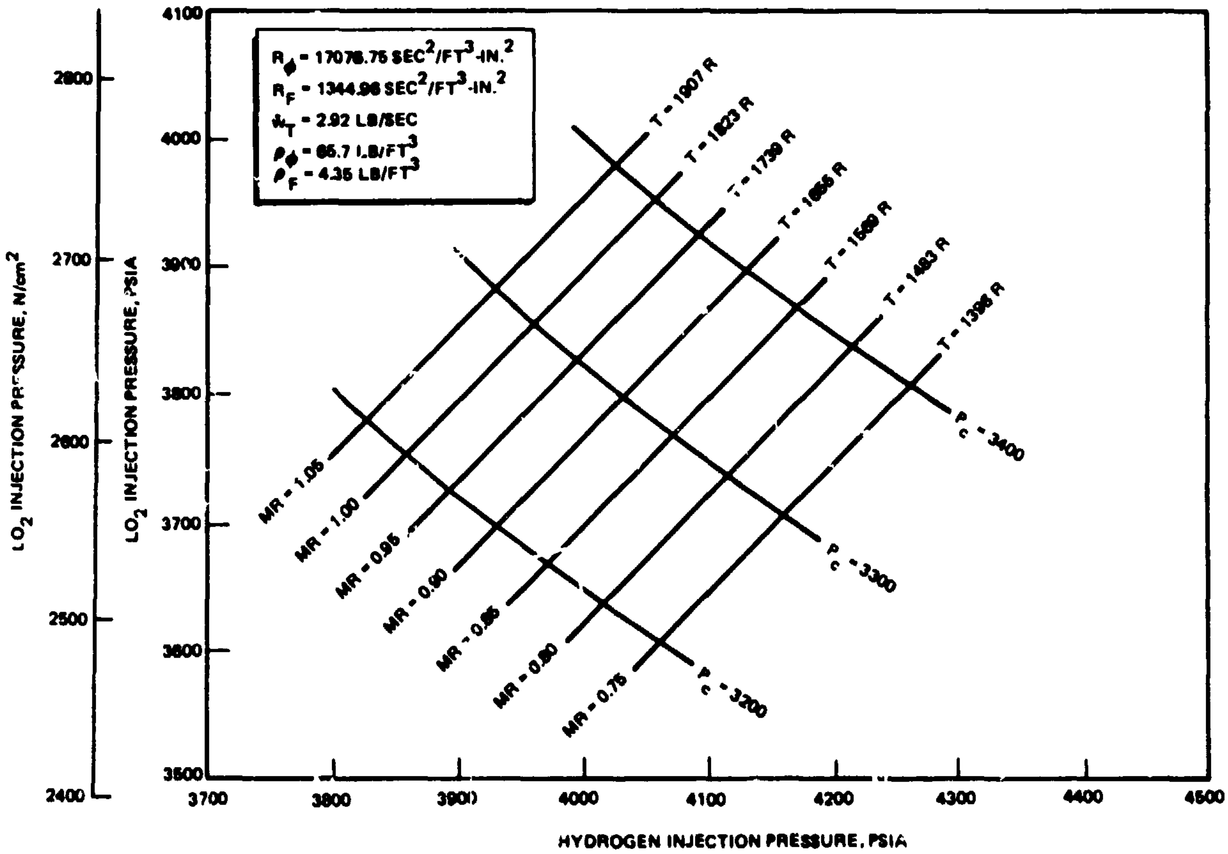

Figure 102. LO_2 Injector Unit 2 Performance Map

Turbine Calibration

Calibration of the Mark 48-F turbine to establish its aerothermodynamic performance was accomplished with ambient-temperature GN_2 as the propellant. The rotor speeds were maintained in the range of 523 to 1885 rad/s (5000 to 18,000 rpm) to simulate the operational wheel tip speed/gas spouting velocity ratios (U/C_o).

The basic test setup is illustrated in Fig. 103. Power developed by the turbine was absorbed by a Mark 4 pump which recirculated water from a reservoir. A Lebow in-line torquemeter was installed between the turbine and the power-absorbing pump to indicate the torque developed by the turbine.

Prior to assembly, the turbopump rotor was balanced dynamically. The radial run-outs on the significant rotor diameters were measured, and are noted in Fig. 104. Similarly, measurements were taken to establish the critical internal radial and axial clearances, and are presented in Fig. 105. Figure 106 shows the assembled turbine calibration unit.

The testing was performed at Wyle Laboratory, El Segundo, California, during the period 4 through 9 February 1976. The installation of the test unit in the facility is illustrated in Fig. 107 and 108.

A total of 11 tests were made, with GN_2 working fluid, at velocity ratio (μ/C_o, total to static) ranging from 0.115 to 0.606, and turbine speeds from 523 to 1885 rad/s (5000 to 18,000 rpm). A tabulation of turbine test data appears in Table 20, and a plot of turbine test efficiency is shown in Fig. 109. Turbine efficiency was calculated with Lebow torquemeter torque and isentropic available energy (total to-static) across the turbine. At a design velocity ratio of 0.343, the turbine total-to-static measured efficiency was 51% compared with a predicted value of 59.8%. Calculations show that with the measured performance the pressure ratio of the turbine would have to be increased from the design value of 1.424 to 1.54 to generate the required power level.

The combination of low-pressure ratio (1.42) and low arc of admission (28.5% of circumference) places this turbine in an operating region in which turbine technology has not been developed. Potential improvement in the performance may be realized by increasing the number of active nozzle passages and reducing the throat width to obtain the required total throat area. Depending on the engine installation, improvements in the exhaust manifolding may be possible to minimize the pressure losses charged to the turbine.

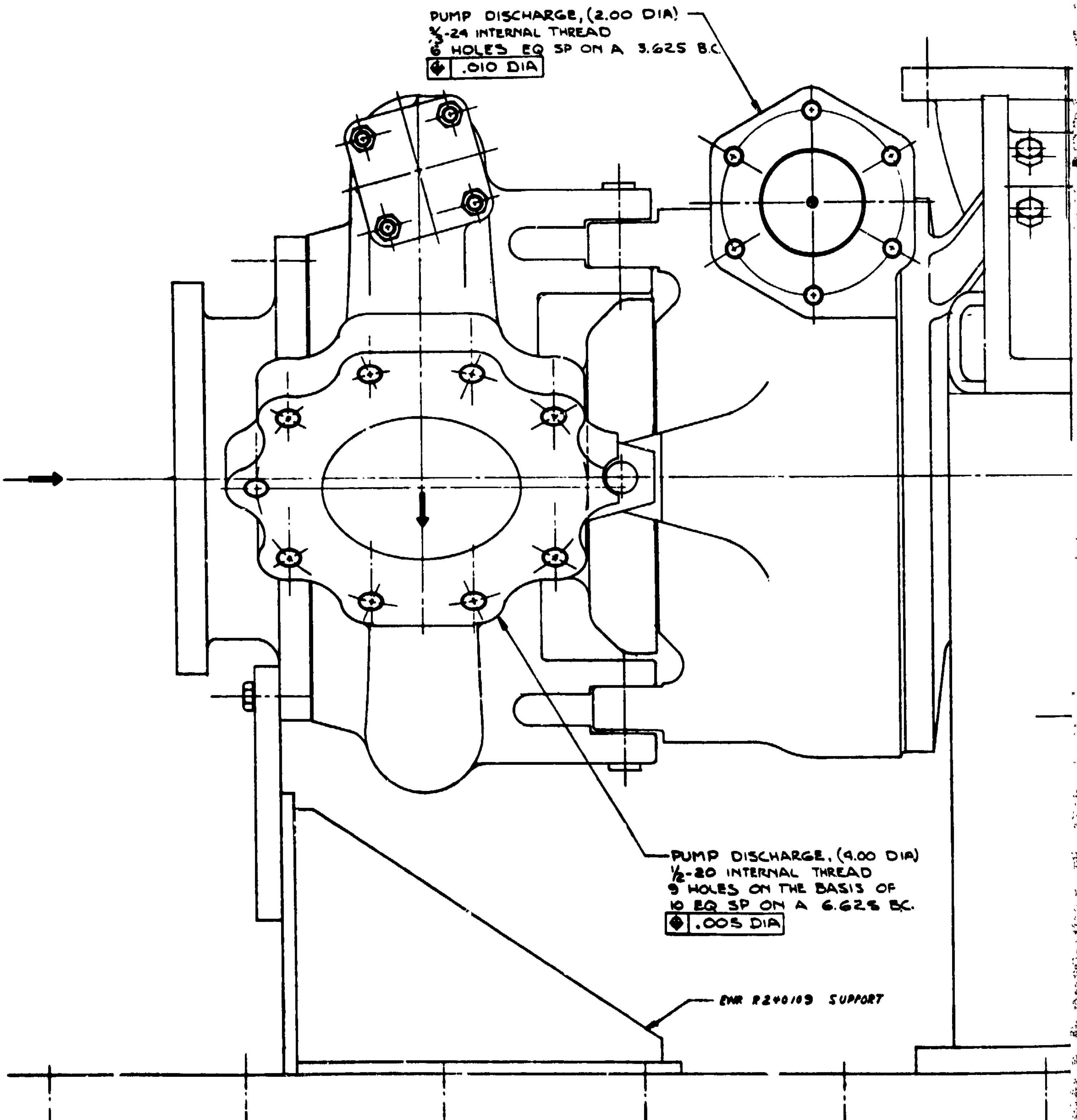

FOLDOUT FRAME 1

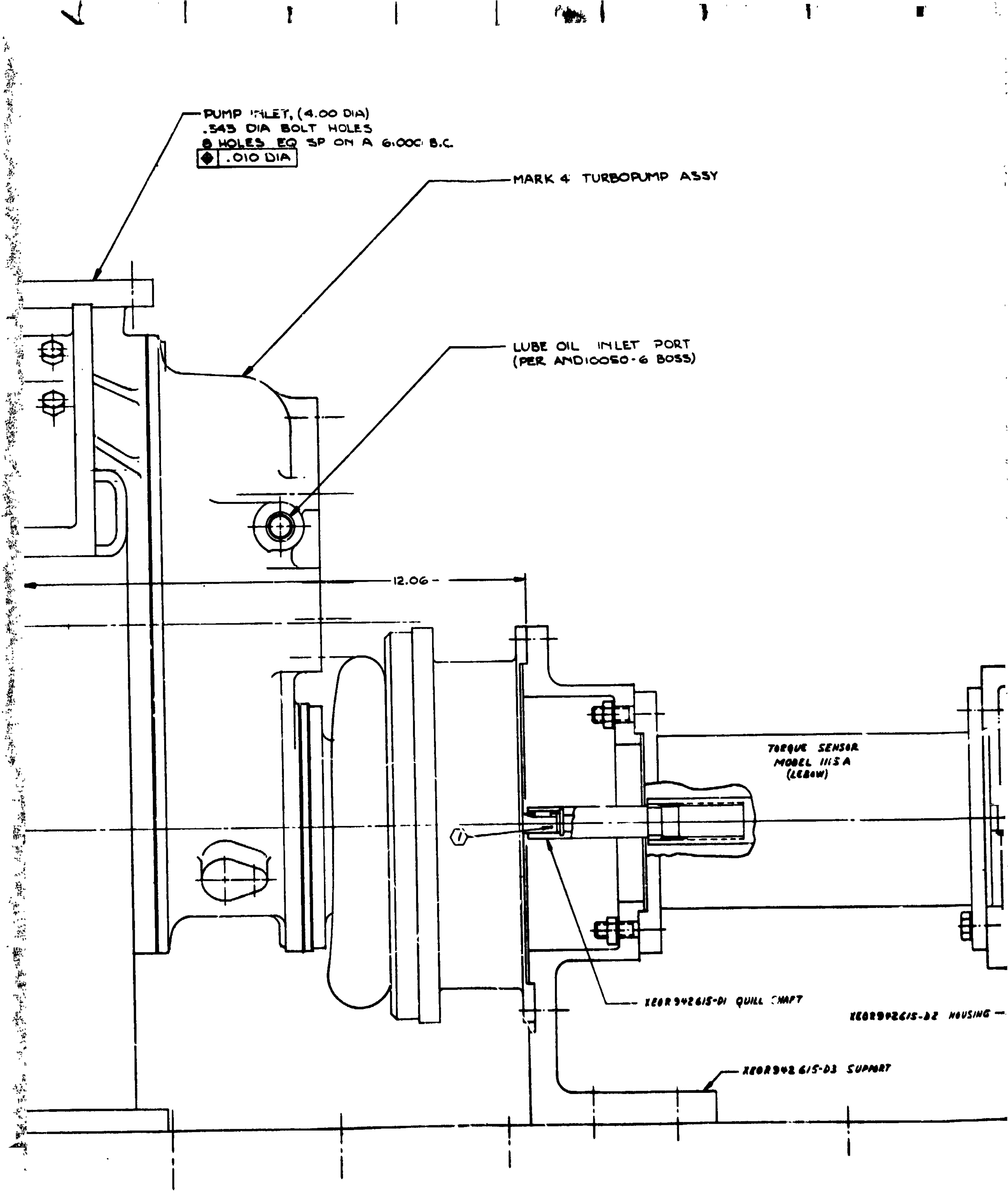

FOLDOUT FRAME 2

FOLD

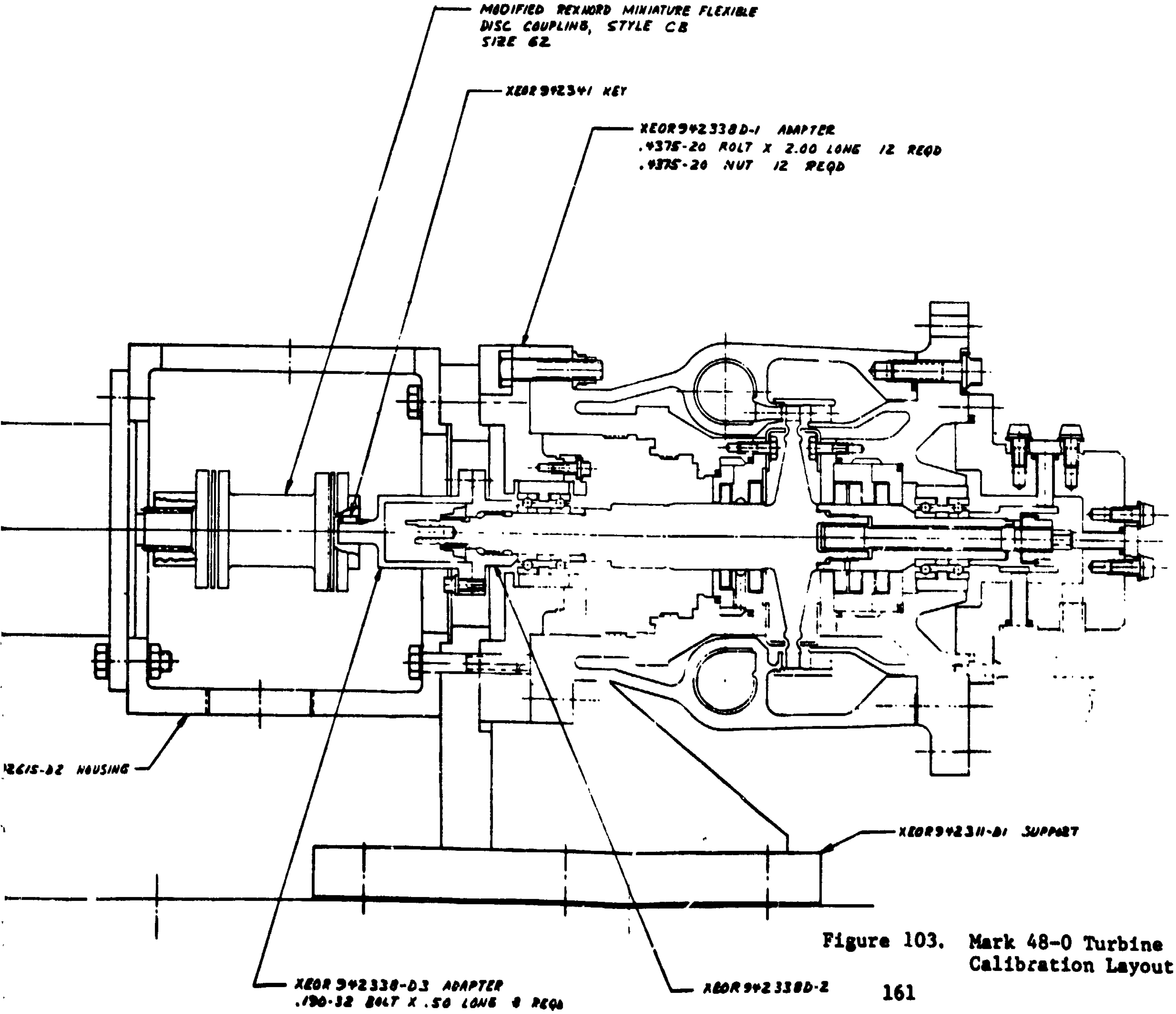

Figure 103. Mark 48-0 Turbine Calibration Layout

FOLDOUT FRAME 3

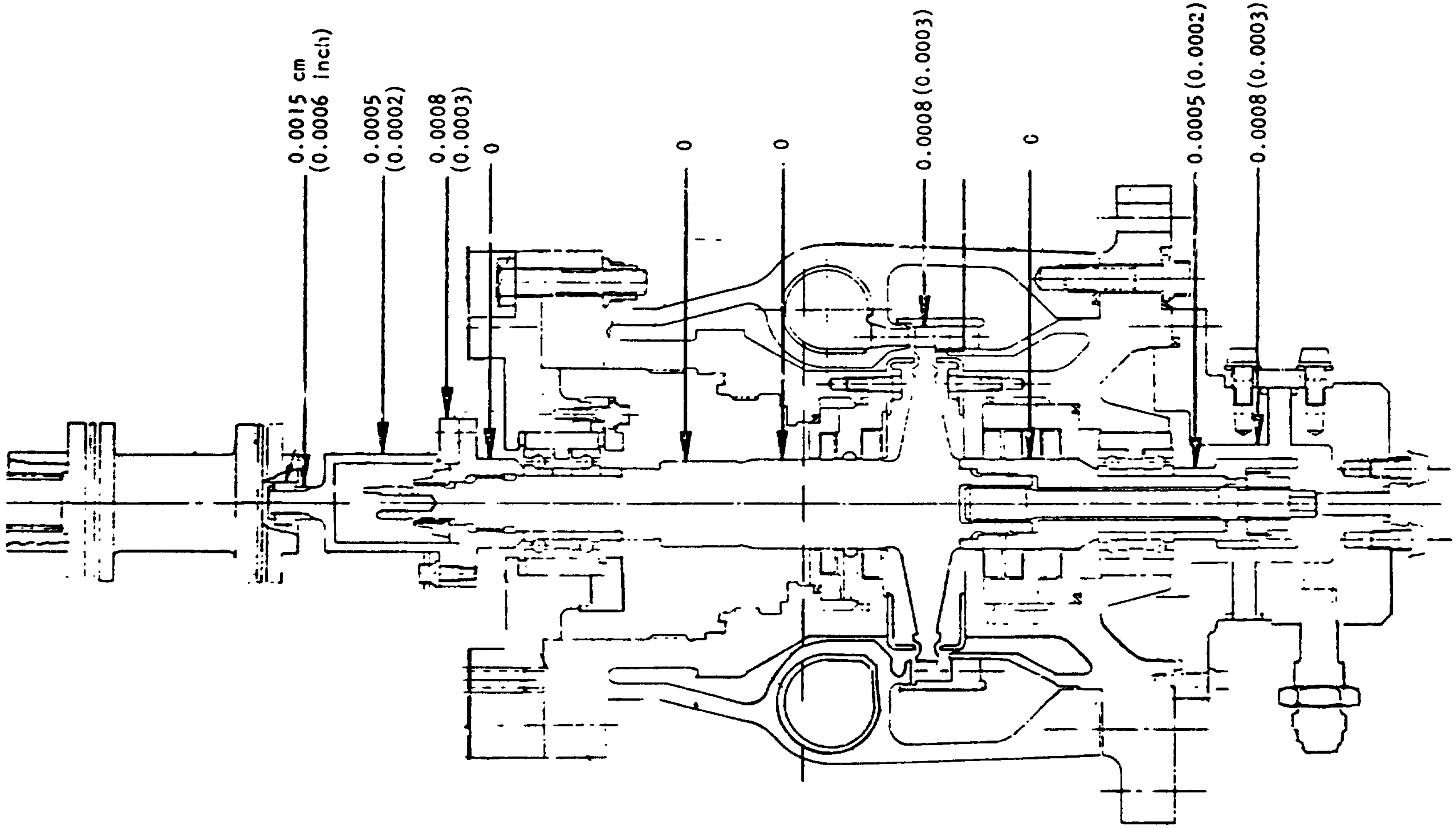

Figure 104. Mark 48-0 Turbine Calibration Assembly Runouts

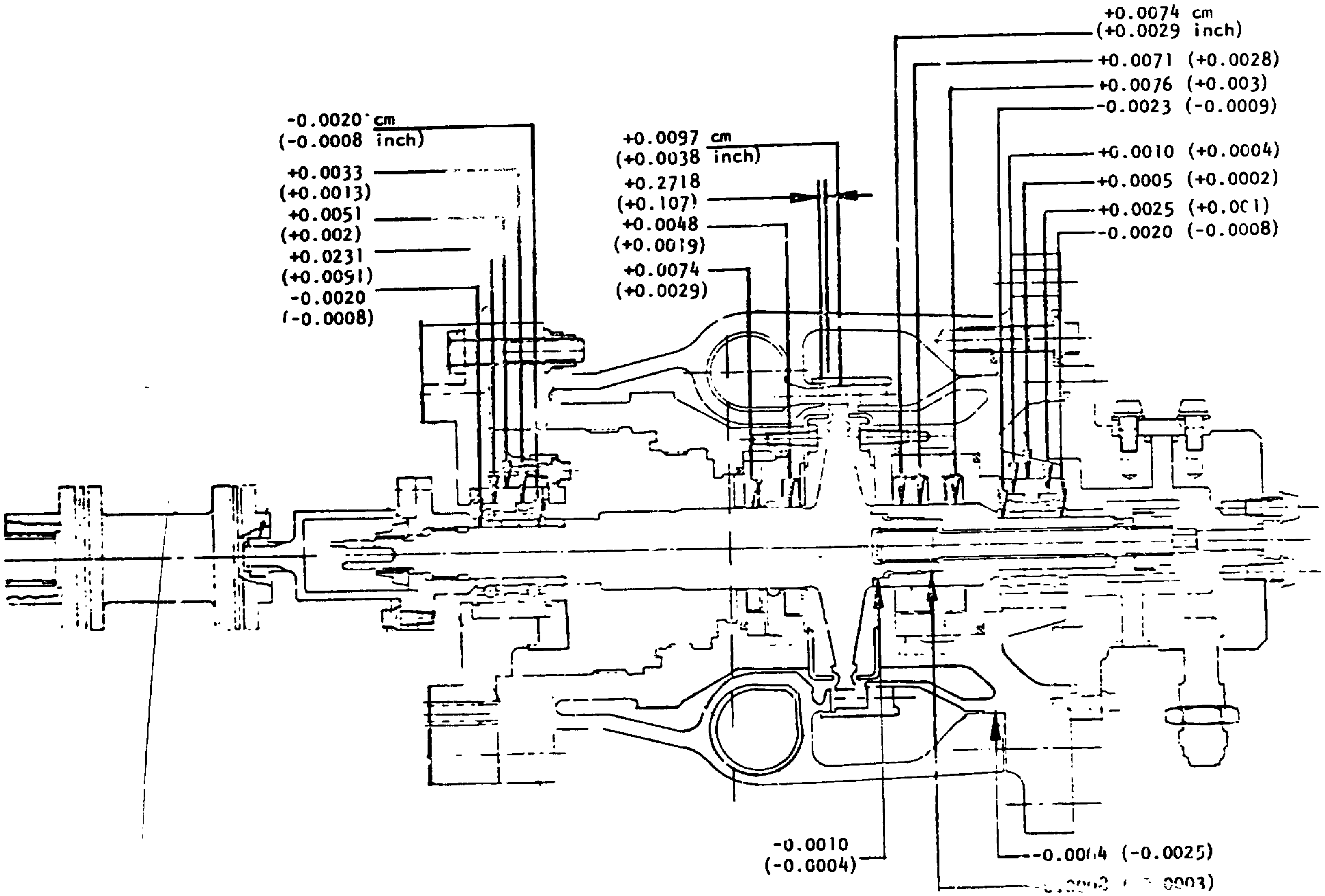

Figure 105. Mark 48-0 Turbine Calibration Build Fits

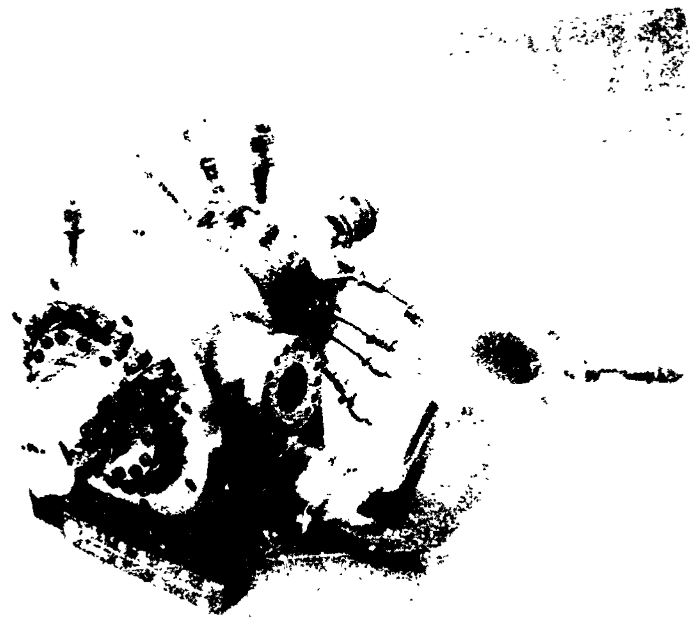

Figure 106. Mark 48-0 Turbine Calibration Assembly

Figure 107. Mark 48-0 Turbine Calibration Installation

ORIGINAL PAGE IS
OF POOR QUALITY

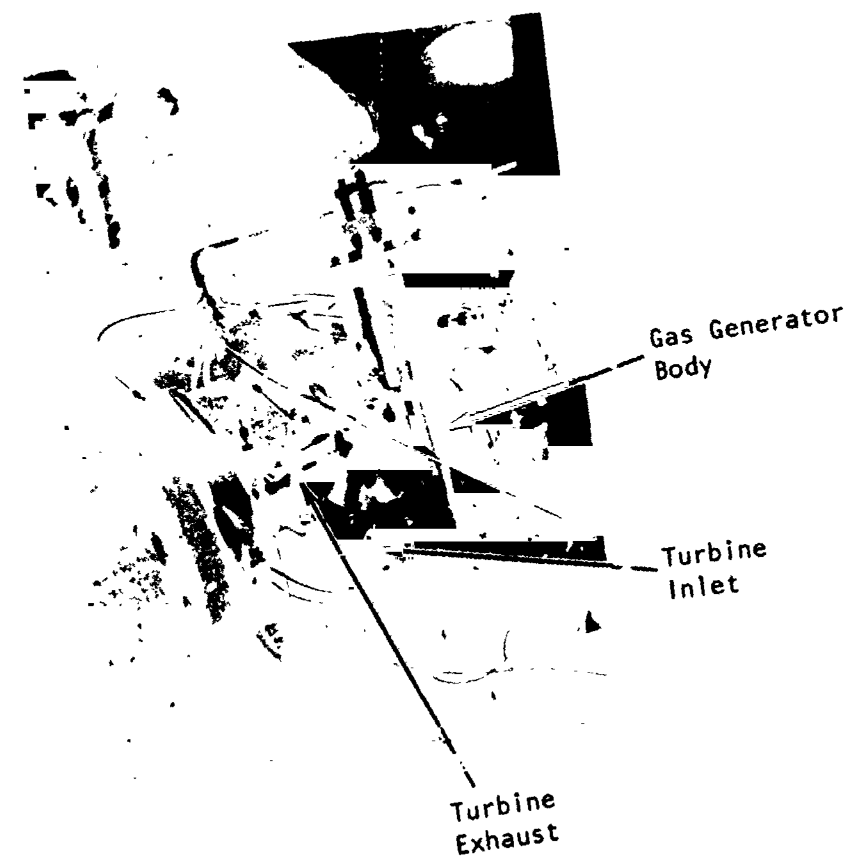

Figure 108. Mark 48-0 Turbine Calibration Installation

TABLE 20. MARK 48-0 TURBINE TEST DATA

	1 TEST NO.	2 TEST SLICE	3 TEST DATE	4 BAROMETER PRESSURE	5 SONIC FLOW NOZZLE INLET TOTAL TEMP	6 SONIC FLOW NOZZLE INLET STATIC PRESSURE	7 TURBINE INLET TOTAL TEMP	8 TURBINE EXIT STATIC PRESSURE	9 TURBINE TORQUE ELBOW TORQUE-METER	10 TURBINE SPEED N_t	11 TURBINE •	12 TURBINE INLET TOTAL PRESSURE	13 TURBINE MASS FLOW WT.	14 TURBINE PRESSURE RATIO	15 TURBINE VELOCITY RATIO U/C_0	16 TURBINE EFFICIENCY	17	18	19	20
1				IN HG	F	PSIG	F	PSIG	IN-LB	RPM	BTU/LB	PSIA	LB/SEC	T-S	T-S	T-S, %				
2	001		4 FEB '76														TEST ABORTED: NO SPEED DATA			
3	002	1	4 FEB '76	29.76	0	90	17	400	113	5599	7.98	532	2.324	1.283	0.182	0.323				
4		2		29.76	-1	93	18	410	118	5703	8.64	557	2.393	1.311	0.178	0.365				
5		3		29.76	0	93	20	415	113	5562	8.32	557	2.391	1.296	0.177	0.354				
6		4		29.76	-2	83	21	330	115	5608	10.49	479	2.173	1.389	0.159	0.317				
7	003	1	5 FEB '76	28.82	-21	120	9	320	183	9641	15.55	577	3.051	1.678	0.224	0.417				
8		2		28.82	-21	150	15	450	198	9938	13.30	716	3.738	1.542	0.250	0.444				
9		3		28.82	-14	125	18	560	123	7577	7.60	729	3.142	1.269	0.252	0.438				
10	004	1	5 FEB '76	29.81	-20	160	10	415	225	10709	15.15	712	3.975	1.657	0.252	0.449				
11	005	1	5 FEB '76	29.81	-25	135	15	340	165	14362	16.37	608	3.420	1.715	0.325	0.475				
12		2		29.81	-16	120	18	445	115	11460	9.808	627	3.046	1.363	0.335	0.495				
13		3		29.81	-18	125	20	380	145	13034	13.475	608	3.167	1.540	0.325	0.497				
14		4		29.81	-18	154	24	460	170	14435	13.367	726	3.829	1.530	0.362	0.538				
15	006		6 FEB '76														TEST ABORTED; TEMP PROBE LEAK			
16	007	1	6 FEB '76	29.88	-1	240	32	1035	60	16572	6.265	1271	5.446	1.211	0.606	0.376				
17		2		29.88	-6	250	32	870	145	16918	9.792	1200	5.950	1.356	0.495	0.472				
18		3		29.88	-7	238	30	840	140	17962	9.779	1160	5.685	1.357	0.526	0.507				
19	008	1	6 FEB '76	[illegible].97	-6	192	26	720	140	12846	8.661	962	4.639	1.310	0.400	0.502				
20		2		29.97	-6	192	24	720	80	17175	8.463	957	4.639	1.303	0.541	0.323				
21		3		29.97	-7	189	24	720	79	1[illegible]862	8.457	957	4.576	1.303	0.531	0.366				
22		4		29.97	-[illegible]	160	23.5	630	71	15698	7.710	619	3.912	1.270	0.518	0.415				
23	009	3	9 FEB '76	29.75	-10	150	14.5	600	112	10288	7.491	779	3.705	1.267	0.344	0.466				
24		5		29.75	-16	115	15.0	310	160	11221	15.843	545	2.932	1.681	0.258	0.434				
25	010	1	9 FEB '76	29.76	16.5	50	23.5	245	60	5427	8.312	335	1.408	1.290	0.172	0.312				
26		2		29.76	16.0	50	22.0	240	60	5436	8.435	330	1.410	1.296	0.171	0.308				
27	011	1	9 FEB '76	29.76	10.5	93	27.0	495	94	5042	5.546	602	2.363	1.182	0.196	0.406				
28		2		29.76	7.0	80	23.5	330	106	5345	9.239	458	2.085	1.330	0.161	0.330				
29		3		29.76	6.0	71	23.0	270	105	5344	11.261	404	1.888	1.421	0.146	0.296				
30		4		29.76	5.0	60	24.0	210	105	5331	13.266	340	1.647	1.516	0.134	0.287				
31		5		29.76	7.0	55	25.0	190	98	5036	14.303	321	1.533	1.567	0.122	0.253				
32		6		29.76	9.0	50	28.5	165	98	5015	15.927	296	1.420	1.648	0.115	0.244				
33		7		29.76	9.5	45	28.5	160	100	5105	1[illegible].239	281	1.309	1.610	0.120	0.287				
34																				
35																				

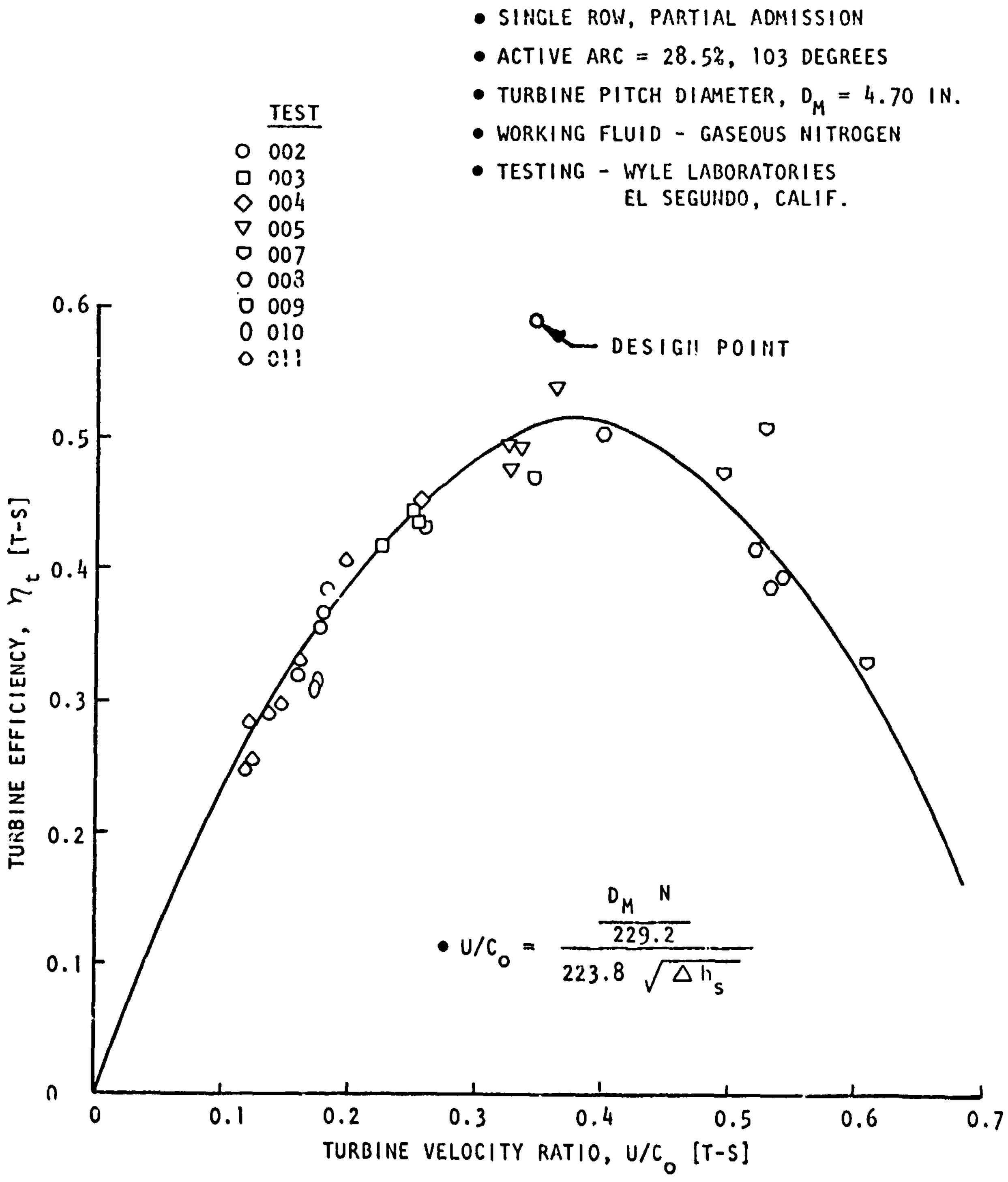

Figure 109. Mark 48-0 Turbine Performance

Turbopump Testing

Test Discussion: Testing of Mark 48-0 turbopump P/N RS009820E, S/N 01-0, began in the Lima test stand of the Rocketdyne Propulsion Research Area (PRA) on 9 July 1976 and was concluded on 11 August 1976. A total of 18 turbopump tests for an accumulated duration of 266.8 seconds was accomplished on the turbopump assembly. The test effort was divided into two main categories: Performance mapping, using GH_2 as turbine drive media, with LN_2 and LO_2 as the pumped fluid; and integrity testing, using a LO_2/LH_2 gas generator as the turbine drive gas media, with LO_2 as the pumped fluid. Gas generator injector P/N RS005024-131, S/N 2, a coaxial five-element design, was used during the hot-fire testing.

Facility propellant supply and discharge systems are shown schematically in Fig. 110 (GH_2 turbine drive system) and Fig. 111 (gas generator turbine drive system).

Figures 112 through 115 show the turbopump assembly in various views installed in the test stand during the initial LN_2 testing phase. After the third test (016-013), blast protection screens were added because of the amount and proximity of the two propellant combinations (LO_2/LH_2). Figures 116 and 117 show the protective blast screen installed as a precautionary measure in case of hardware failure during the LO_2 pumping test phase. Figure 118 shows the pretest chill conditioning during the hot-gas testing phase, with gas generator injector (LO_2 unit 2) installed.

Table 21 presents a summary of the turbopump test program accomplished while a more detailed discussion of the individual tests is presented below.

Test No. 1:	(016-011)
Test Date:	7-9-76
Duration:	30 seconds
Objective:	Checkout and integrity test of turbopump at 3141 rad/s (30,000 rpm) using LN_2 as the pumped fluid and GH_2 as turbine drive media.
Results:	Satisfactory. The turbopump speed and discharge pressure were manually adjusted simultaneously during the test by the controller operator. The performance of the turbopump was monitored on an X-Y plotter which displayed turbopump discharge pressure and turbopump discharge venturi differential pressure (a measure of the turbopump discharge flowrate). Maximum rpm achieved was 3204 rad/s (30603 rpm).
Analysis:	Prior to the test, a turbopump H-Q map chart was prepared for the X-Y plotter system which enabled the controller operator (GH_2 spin valve and turbopump discharge throttle valve controller) to evaluate the turbopump real-time performance. The system responded closely to the H-Q analytical predictions. A posttest review of the data revealed a turbine pressure ratio of 2.12 rather than a desired 1.4 to 1.6 value. The higher-than-desired pressure ratio was caused by too large a turbine discharge orifice (D = 1.7668 cm, 0.6956 inch). Prior to the next test, a turbine discharge orifice of 0.5765 inch was installed. A turbopump shaft torque check through the LO_2 inlet showed the torque to vary from 10.6 to 49.4 mN (15 to 70 in-oz). A visual examination of the rear bearing was accomplished by removing the rear bearing housing. No visual discrepancies were noted.

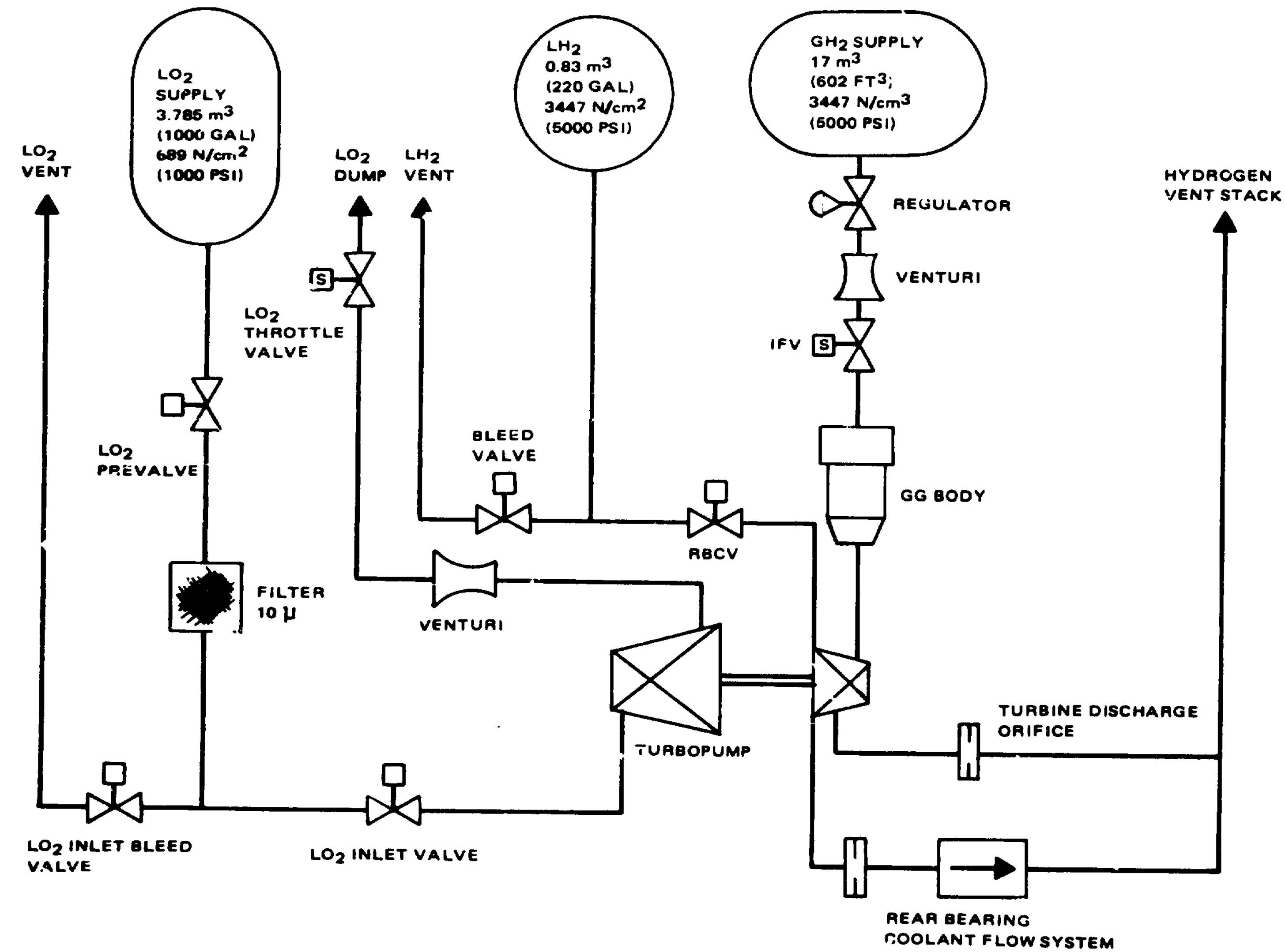

Figure 110. System I, Gaseous Hydrogen Turbine Drive

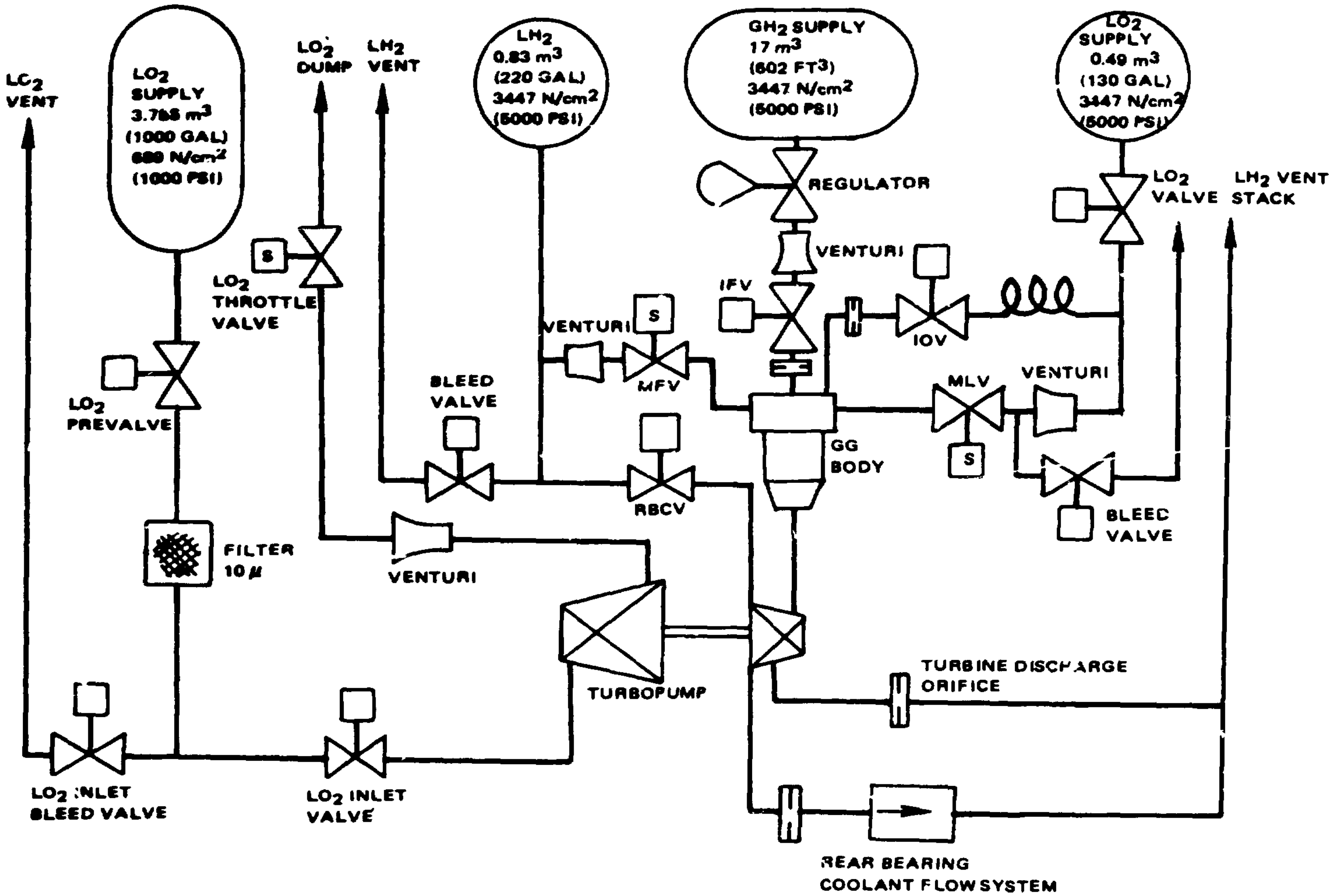

Figure 111. System II, Gas Generator Turbine Drive

ORIGINAL PAGE IS
OF POOR QUALITY

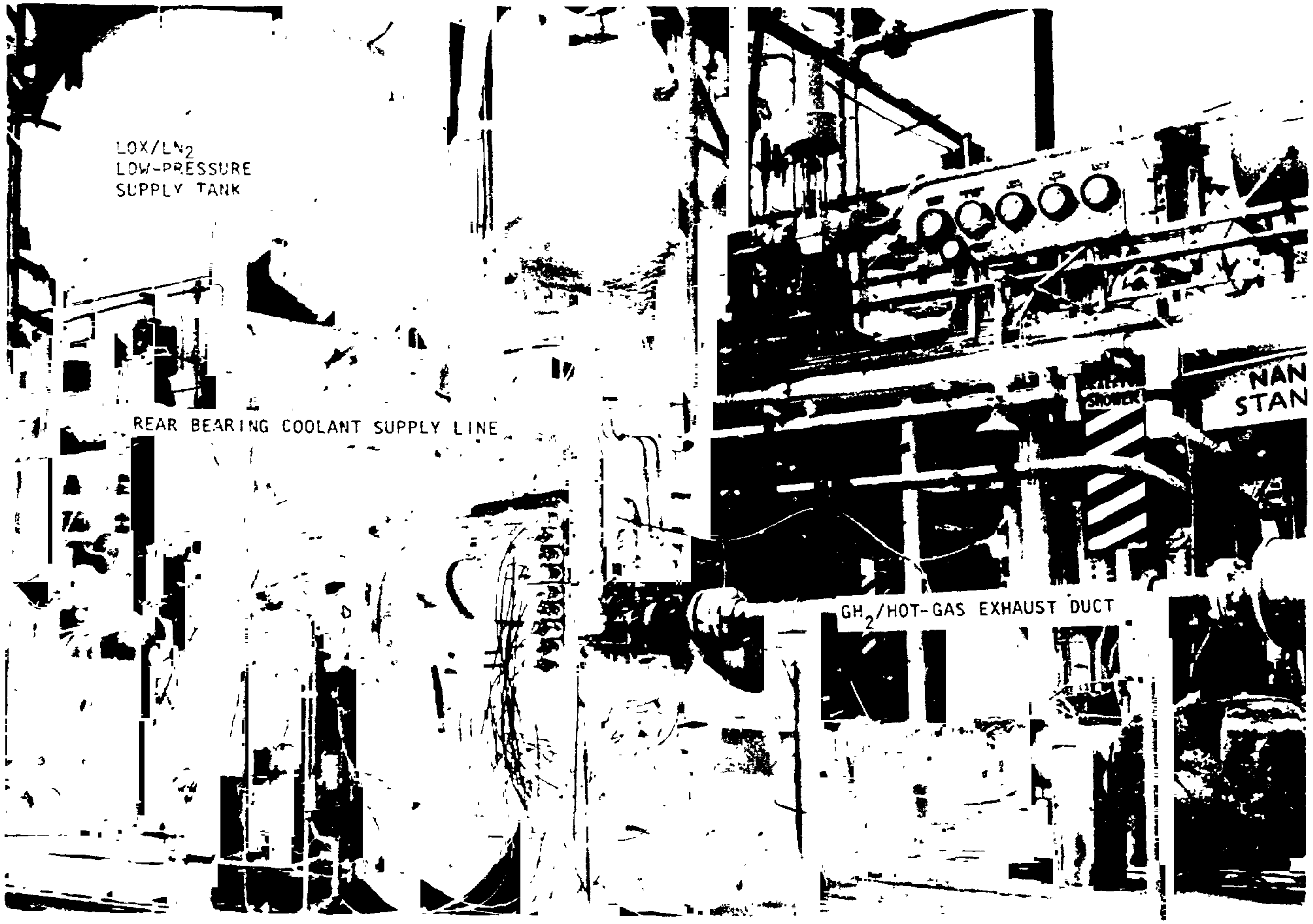

1HS53-7/9/76-S1A*

Figure 112. Series I Mark 48-0 Turbopump Testing

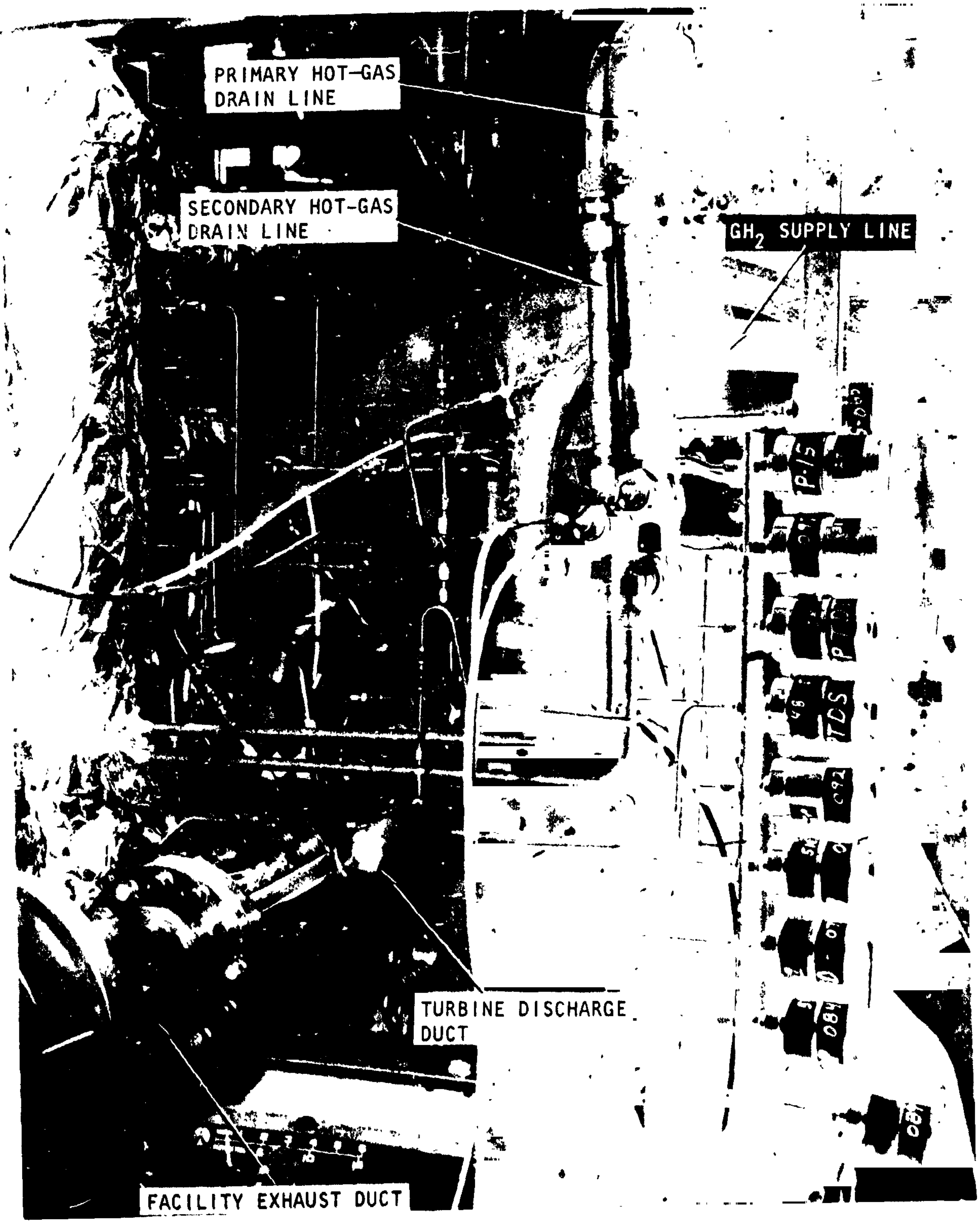

1HS53-7/9/76-S1E*

Figure 113. Mark 48-0 Turbopump Test Installation

ORIGINAL PAGE IS OF POOR QUALITY

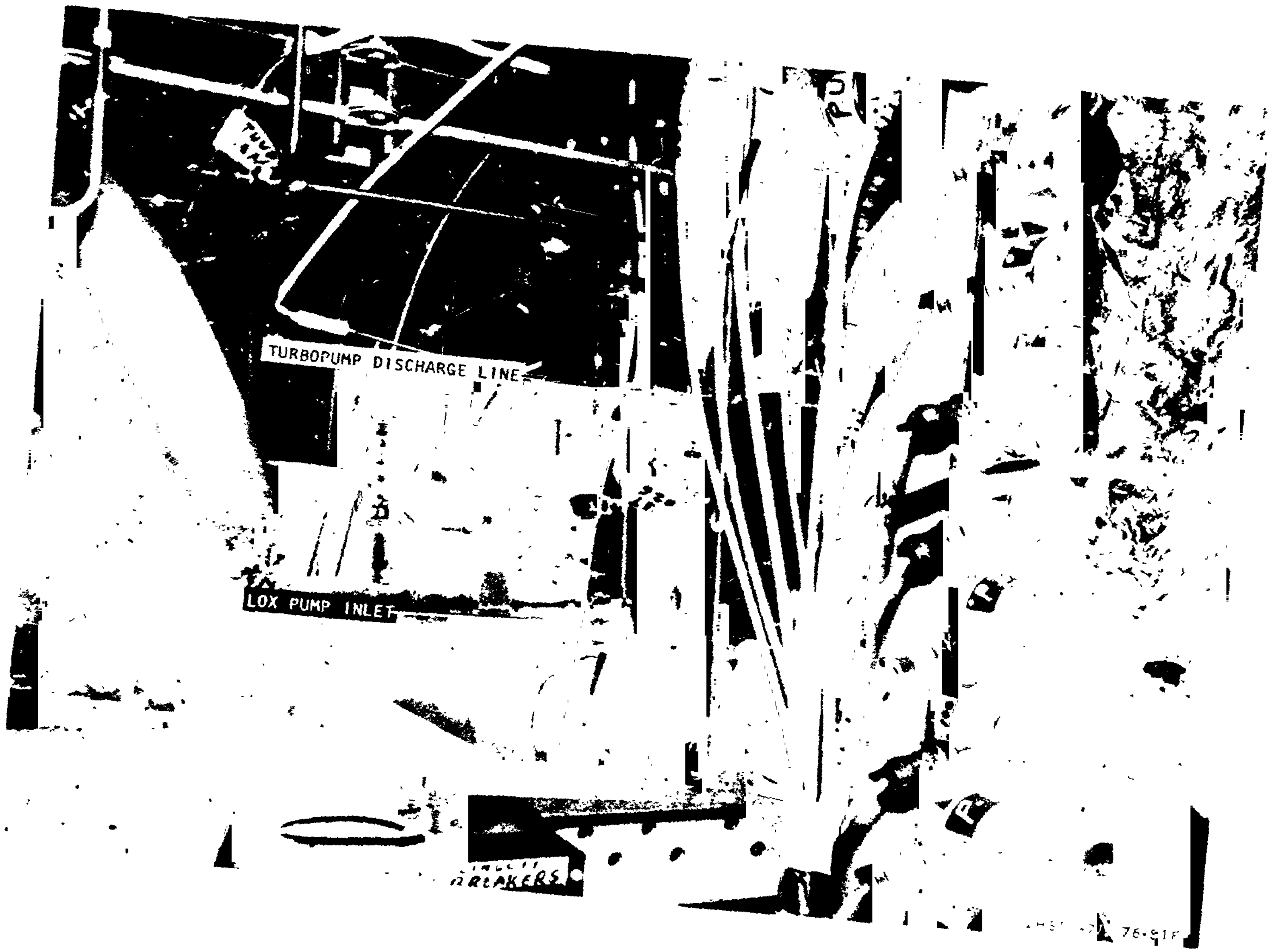

1HS53-7/9/76-S1F*

Figure 114. Mark 48-0 Turbopump Test Installation

1HS53-7/9/76-S1G*

Figure 115. Mark 48-0 Turbopump Test Installation

1HS93-7/19/76-S1B*

Figure 116. Lima Stand Turbopump Installa on

ORIGINAL PAGE IS
OF POOR QUALITY

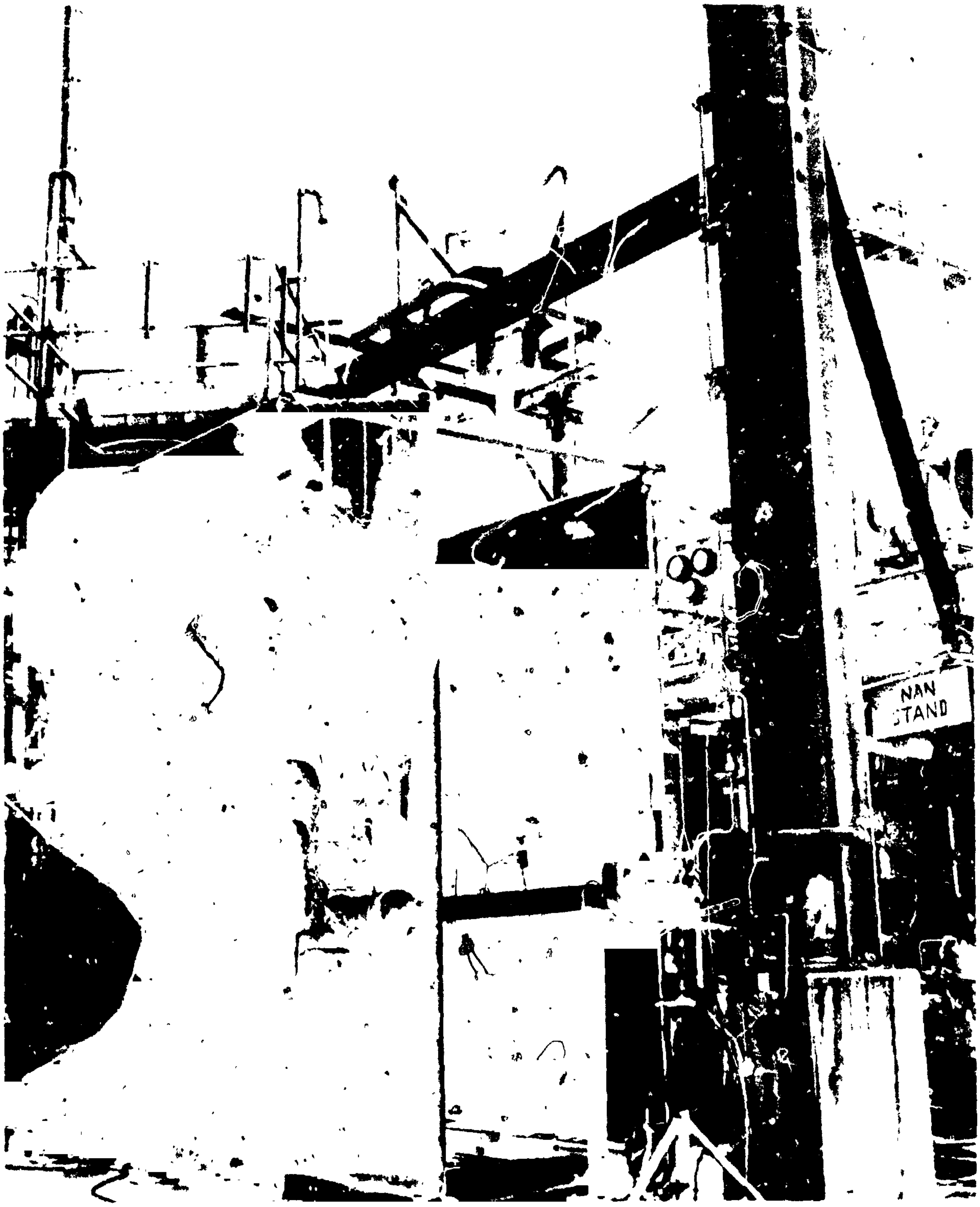

1HS93-7/19/76-S1A*

Figure 117. Lima Stand Turbopump Installation

ORIGINAL PAGE IS
OF POOR QUALITY

C-3

1HS53-8/4/76-S1A*

Figure 118. 48-0 Turbopump Installation

TABLE 21. MARK 48-0 TURBOPUMP TESTING
(P/N RS009820, S/N 01-0)

Test No.	Test Date	Test Duration, Seconds	Accumulated		Remarks
			Starts	Duration, Seconds	
016-011	7-9-76	30	1	30	Initial test using LN_2 as pumped fluid. Turbine drive media--GH_2. 30,800 rpm achieved satisfactorily.
016-012	7-13-76	9	2	39	Pumped fluid: LN_2, turbine drive media: GH_2 targeted rpm: 60,000. Premature cutoff by turbine radial accelerometer vibration safety cutoff system (VSC) exceeded 10 g rms. RPM attained: 45,979.
016-013	7-13-76	5	3	44	Pumped fluid: LN_2, turbine drive media: GH_2 satisfactory rotordynamic test. Maximum turbopump rpm: 61,965.
016-014	7-16-76	70	4	114	Pumped fluid: LO_2, turbine drive media: GH_2 planned H-Q at 30,000 and 60,000 rpm. H-Q obtained at 30,000 rpm. Turbine radial accelerometer VSC cutoff at 15 g rms at 52,500 rpm.
016-015	7-16-76	30	5	144	Pumped fluid: LO_2, turbine drive media: GH_2 planned objective: H-Q mapping at 60,000 rpm. Some H-Q data obtained at 60,850 rpm, but test prematurely cut off by observer due to a fire in a facility system.
016-016	7-16-76	12	6	156	Pumped fluid: LO_2, turbine drive media: GH_2 planned objective: H-Q at 60,000 rpm. Premature cutoff by turbine radial accelerometer VSC system at 52,000 rpm.
016-017	7-16-76	37	7	193	Pumped fluid: LO_2. turbine drive media: GH_2 planned objective: H-Q at 60,000 and 70,000 rpm. Achieved satisfactory H-Q data at 60,000 rpm. Attempted to increase turbopump speed to 70,000 rpm, but was prematurely cut off by turbine radial accelerometer VSC system at a speed of 64,000 rpm. This test concluded series I testing. The turbopump and facility system were modified for hot-fire testing with the gas generator system.

TABLE 21. (Continued)

Test No.	Test Date	Test Duration, Seconds	Accumulated Starts	Accumulated Duration, Seconds	Remarks
016-018	8-3-76	0	8	193	Gas generator ignition not achieved. Cutoff by ignition detect system. Posttest analysis showed problem to be associated with exciter system. Exciter changed prior to next test. Scheduled 60,000 rpm.
016-019	8-3-76	2.81	9	195.81	Objective: 60,000 rpm. Satisfactory test. A turbopump rpm of 57,629 was achieved with a turbine inlet total pressure of 1837 psia at 1761 R (Note: turbine discharge orificing resulted in a turbine pressure ratio of 1.85.) Gas generator c* efficiency: 98.9%
016-020	8-3-76	0.58	10	196.39	Objective: 60,000 rpm. Test prematurely terminated by turbine inlet overtemp. Maximum rpm achieved 58,378. Analysis revealed the fuel injection pressure lower than actual controller set pressure. Result: Higher GG mixture ratio with cutoff at 1960 R. Turbine inlet temperature controller readjusted using site data.
016-021	8-3-76	16.58	11	212.97	Objective: 60,000 rpm for test stand duration. Objective partially achieved. Maximum rpm achieved was 62,800, but the test was terminated prematurely by turbine inlet overtemp. Review of data shows main fuel valve position operating in high-flow gain region, only 2-1/2% open. For next test, the LH_2 tank pressure will be reduced to force MFV further open. Gas generator c* efficiency; 99.3%
016-022	8-9-76	0	12	212.97	Objective: 70,000 rpm for test stand duration (~50 seconds) Test prematurely terminated by turbine radial accelerometer VSC system. Test terminated during fuel-lead stage at 56,000 rpm and 15 g rms.
016-023	8-9-76	0.62	13	213.59	Objective: 70,000 rpm for test stand duration (~50 seconds) Test prematurely terminated by turbine radial VSC system at 20 g rms. Maximum rpm achieved was 68,725.

TABLE 21. (Concluded)

Test No.	Test Date	Test Duration, Seconds	Accumulated Starts	Accumulated Duration, Seconds	Remarks
016-024	8-9-76	1.2	14	214.79	Objective: 70,000 rpm for test stand duration (~50 seconds) Test prematurely terminated by turbine radial accelerometer at 20 g rms. Maximum turbopump rpm: 69,157.
016-025	8-9-76	2.39	15	217.18	Objective: 70,000 rpm for test stand duration (~50 seconds) Test prematurely terminated by turbine inlet overtemp. Fuel injection pressure again below controller set pressure resulting in high GG mixture ratio and overtemp. Maximum rpm: 68,199.
016-026	8-11-76	5.82	16	223.0	Objective: 70,000 rpm for test stand duration (~50 seconds) Test prematurely terminated by observer due to a fire in a facility system. Maximum rpm achieved: 74,191.
016-027	8-11-76	3.01	17	226.01	Objective: 70,000 rpm for test stand duration (~50 seconds) Test prematurely terminated by turbine inlet overtemp. Data analysis showed the fuel injection pressure controller to be lower than required by 69 N/cm^2 (100 psi). A site data correction was made for the next test. Maximum rpm achieved: 62,867.
016-028	8-11-76	40.79	18	266.8	Objective: H-Q excursion at 70,000 rpm, and test stand duration (~50 seconds) All objectives except duration were achieved. Manual control of turbopump discharge throttle valve achieved H-Q excursions. Maximum rpm achieved was 68,685. The test was automatically terminated when the intermediate seal purge supply level decreased below 150 psig (redline). The gas generator c* efficiency during the test averaged 99.7%.

Test No. 2: (016-012)

Test Date: 7-13-76

Duration: 9 seconds

Objective: Locate the first and second turbopump critical speeds using LN_2 as the pumped fluid and GH_2 as the turbine drive media.

Results: The test was terminated prematurely by the turbine radial accelerometer vibration safety cutoff (VSC) system at 10 g rms and 4814 rad/s (45,979 rpm).

Analysis: The speed of the turbopump was brought up to about 2094 rad/s (20,000 rpm) where adjustment of the throttle discharge valve was made to correct the pump performance to the design Q/N position. At that time, the spin valve was opened manually by the controller operator. Evidently the rate of speed increase was insufficient in the region of the critical speed range. Cutoff was initiated by the VSC system after accumulating 10 g rms count over 200-msec duration. A review of the data revealed the first critical speed to be about 4115 rad/s (39,300 rpm). The second critical speed was not well defined due to the abbreviated test duration. Another test was necessary to define the second critical speed and to verify the value of the first critical speed. The turbine pressure ratio for this test was about 1.4, with a 1.464 cm (0.5765 inch) turbine discharge orifice.

Test No. 3: (016-013)

Test Data: 7-13-76

Duration: 5 seconds

Objective: Locate the first and second turbopump critical speeds using LN_2 as the pumped fluid and GH_2 as the turbine drive media.

Results: Satisfactory test. All objectives attained. Maximum turbopump rpm achieved was 6488 rad/s (61,965 rpm).

Analysis: Experience gained in the previous two tests defined the overall response of the controller-GH_2 turbopump systems. As a result of the second test (016-012), a throttle valve setting of 39% open was required to maintain the design Q/N curve. For this test, just prior to opening the GH_2 spin valve, the throttle valve was adjusted to 39%. Since it was desired to limit the total turbopump accumulated time in LN_2 service, the test required a rapid increase in the turbopump speed to the targeted 6282 rad/s (60,000 rpm). The normal pause at about 2094 rad/s (20,000 rpm) was eliminated. From the time the GH_2 spin valve was opened to the time the maximum rpm (6488 rad/s, 61,965 rpm) was achieved took about 3 seconds. A 2-second dwell at 6488 rad/s (61,965 rpm) was followed by a planned controller operator cutoff. All objectives were attained with verification of the 4115 rad/s (39,300 rpm) first critical speed and a determination of the second critical speed to be about 5228 rad/s (52,800 rpm). Following this test, a visual inspection of the turbopump revealed no damage or discrepancies. The facility system was prepared for the next series of tests using LO_2 as the pumped fluid.

Test No. 4: (016-014)

Test Date: 7-16-76

Duration: 70 seconds

Objective: Obtain head-flow data at 3141 rad/s (30,000 rpm and 6282 rad/s (60,000 rpm) using LO_2 as the pumped fluid.

Results: Objectives partially attained. H-Q data was obtained at 2513 to 3036 rad/s (24,000 to 29,000 rpm) but, during the transition in speeds, the rate of increase within the critical speed region was slow enough to accumulate 200 msec of 15 g rms level, which triggered the VSC cutoff system at 5497 rad/s (52,500 rpm).

Analysis: The test progressed smoothly from tank pressurization, throttle valve adjustment and H-Q excursion in the 2513 to 3036 rad/s (24,000 to 29,000 rpm) region. Upon increasing turbopump speed by manually adjusting the GH_2 spin valve, the turbine radial accelerometer triggered the VSC cutoff system. No damage was noted to the hardware. For the next test, the turbine discharge orifice was changed to 1.628 cm (0.6411 inch) to target a 1.6 turbine pressure ratio.

Test No. 5: (016-015)

Test Date: 7-16-76

Duration: 30 seconds

Objective: Obtain H-Q mapping at turbopump speed of 6282 rad/s (60,000 rpm).

Results: Objective partially attained. Some H-Q mapping was achieved at 637 rad/s (60,850 rpm), but the test was terminated prematurely by the window observer due to a fire in the test area.

Analysis: A posttest analysis revealed the location of the fire to be behind the stand bulkhead and in a facility line connection. Real time television coverage of the test area, with replay capabilities, was a definite asset to the testing effort. At the start of the test, the pump discharge throttle valve was adjusted to 39% (390 dial setting), and the turbopump speed rapidly increased until an indicated 6282 rad/s (60,000 rpm) was reached. After a period of stabilization, an H-Q excursion from nominal to high head/low flow was achieved. During the excursion back through nominal H-Q toward low-head/high-flow region, cutoff was initiated. No damage to the turbopump system was evident. A turbine pressure ratio of 1.68 was achieved with the 1.628 cm (0.6411 inch) turbine discharge orifice.

Test No. 6:	(016-016)
Test Date:	7-16-76
Duration:	12 seconds
Objective:	Obtain H-Q performance at a turbopump speed of 6282 rad/s (60,000 rpm).
Results:	The test was terminated prematurely by the turbine radial accelerometer VSC system at a turbopump speed of 5444 rad/s (52,000 rpm).
Analysis:	At the start of the test, the GH_2 spin valve was opened to obtain a stabilized turbopump speed of 3141 rad/s (30,000 rpm). After stabilization, it was planned to rapidly increase the turbopump speed through the first and second critical speeds to the targeted 6282 rad/s (60,000 rpm). Again, since the speed control was manual, the rate of speed increase through the second critical was insufficient, and the test was terminated by the VSC cutoff system. No hardware damage was sustained.

Test No. 7:	(016-017)
Test Date:	7-16-76
Duration:	37 seconds
Objective:	Obtain H-Q performance at 6282 to 7329 rad/s (60,000 and 70,000 rpm).
Results:	Achieved satisfactory H-Q data at 6282 rad/s (60,000 rpm), but the test was terminated prematurely at 6700 rad/s (64,000 rpm) by the turbine radial accelerometer VSC system before any H-Q mapping could be obtained at 7329 rad/s (70,000 rpm).
Analysis:	The test proceeded smoothly through the first targeted H-Q mapping phase at 6282 rad/s (60,000 rpm). While adjusting the GH_2 spin valve to achieve 7329 rad/s (70,000 rpm), the VSC cutoff system initiated cutoff at 6700 rad/s (64,000 rpm). This speed level does not correspond to any projected critical speed region and, in fact, no operational parameters indicated any reason for the premature VSC cutoff. Checkout of the VSC system failed to show any abnormality within the facility data acquisition system. This test concluded the Series I GH_2 turbine drive test effort. The turbopump system and facility were modified for hot-fire testing using the gas generator.

Test No. 8:	(016-018)
Test Date:	8-3-76
Duration:	0. second
Objective:	Turbopump Performance at 6282 rad/s (60,000 rpm) and characterization of system start/cutoff transients
Results:	The test was terminated prematurely by the ignition detect system of the gas generator.
Analysis:	At "ignition OK" (combustion temperature greater than 700 K (800 F), the automatic comparator circuit initiated cutoff due to an indication that the igniter failed to ignite. A posttest failure analysis revealed the most probable cause to be in the spark exciter electrical network. A replacement spark exciter system was installed and a successful visual spark test was accomplished prior to the next test.

Test No. 9:	(016-019)
Test Date:	8-3-76
Duration:	2.81 seconds
Objective:	Turbopump Performance at 6282 rad/s (60,000 rpm) and characterization of system start/cutoff transients.
Results:	Satisfactory test with a maximum speed of 6034 rad/s (57,629 rpm) achieved.
Analysis:	Prior to test 016-018, the turbine discharge orifice was changed from 1.628 cm (0.6411 inch) to a 1.766 cm (0.6952) inch) diameter, with a well-rounded entrance condition, to obtain a 1.72 turbine pressure ratio with the hot-gas turbine drive. Actual measured turbine pressure ratio for this test was 1.85. Performance of the gas generator system was near nominal with a chamber pressure (turbine inlet pressure) within 41 N/cm^2 (59 psi) of the target condition (P_c target = 1307 N/cm^2 (1896 psia); actual = 1266 N/cm^2 (1837 psia) with a turbine inlet temperature of 978 K (1761 R). Start and cutoff transients of the gas generator system were normal. The characteristic velocity (c*) efficiency of the gas generator injector was 98.9%.

Test No. 10:	(016-020)
Test Date:	8-3-76
Duration:	0.58
Objective:	Turbopump performance at 6282 rad/s (60,000 rpm).
Results:	Test prematurely terminated by turbine inlet overtemperature redline (1088 K, 1969 R).

Analysis: The maximum rpm achieved was 6122 rad/s (58,378 rpm). Start and cutoff sequences were normal, with no damage sustained by either the turbopump or gas generator systems. This test was scheduled for a test stand propellant duration (~50 seconds mainstage) at the same performance conditions as the previous test. A posttest review of records showed the fuel injection pressure to be lower than the servocontroller set pressure, which lowered the fuel injector hydrogen flowrate, increased the gas generator mixture ratio, and resulted in an elevated combustion temperature which triggered the overtemperature redline cutoff circuitry. Fuel injection pressure was about 120 N/cm^2 (175 psi) lower than the controller set pressure. The controller was readjusted for the following test using the on-line site data.

Test No. 11: (016-021)

Test Date: 8-3-76

Duration: 16.58 seconds

Objective: Turbopump performance at 6282 rad/s (60,000 rpm) for test stand duration (~50 seconds).

Results: Objectives partially achieved. The maximum rpm attained was 6575 rad/s (62,800 rpm) with steady-state performance until a premature cutoff by the combustion temperature redline.

Analysis: Review of the scaled data revealed that the main fuel valve was operating at about 2.5% open, or in a high-flow gain region. Figure 119 graphically depicts the problem. Note that, in the near-closed position, relatively large fluctuations in flowrate can be expected with small changes in valve position. The result of the fluctuation could cause the noted overtemperature in the combustor due to a sudden increase in the gas generator mixture ratio. A similar problem existed with the main LO_2 valve during the early development testing of the LH_2 turbopump gas generator system. The problem was solved by changing the plug trim to a linear (flow increases proportionally with valve position) design. A main fuel valve plug trim change was not deemed necessary because of the fuel-lead sequence and the normal operating position of the main fuel valve being in the 15% (oxidizer turbopump gas generator) and 50% (hydrogen turbopump gas generator) open position at full 2344 N/cm^2 (3400 psig) chamber pressure. The effective gas combustion discharge flow area (turbine and discharge orifice) for the present oxidizer turbopump, required operating the gas generator at approximately two-thirds power. The net result was that lower fuel injection pressures were required for the lower flowrates. The LH_2 tank pressure for this test had been lowered from 3303 N/cm^2 (440 psig) to 2758 N/cm^2 (4000 psig) (gas generator testing to turbopump testing) to force the main fuel valve to open further and stay outside of the high-flow gain region. For the next test, the LH_2 tank pressure was reduced further to 2413 N/cm^2 (3500 psig). Gas generator performance remained normal, with no damage sustained to either the gas generator or turbopump system.

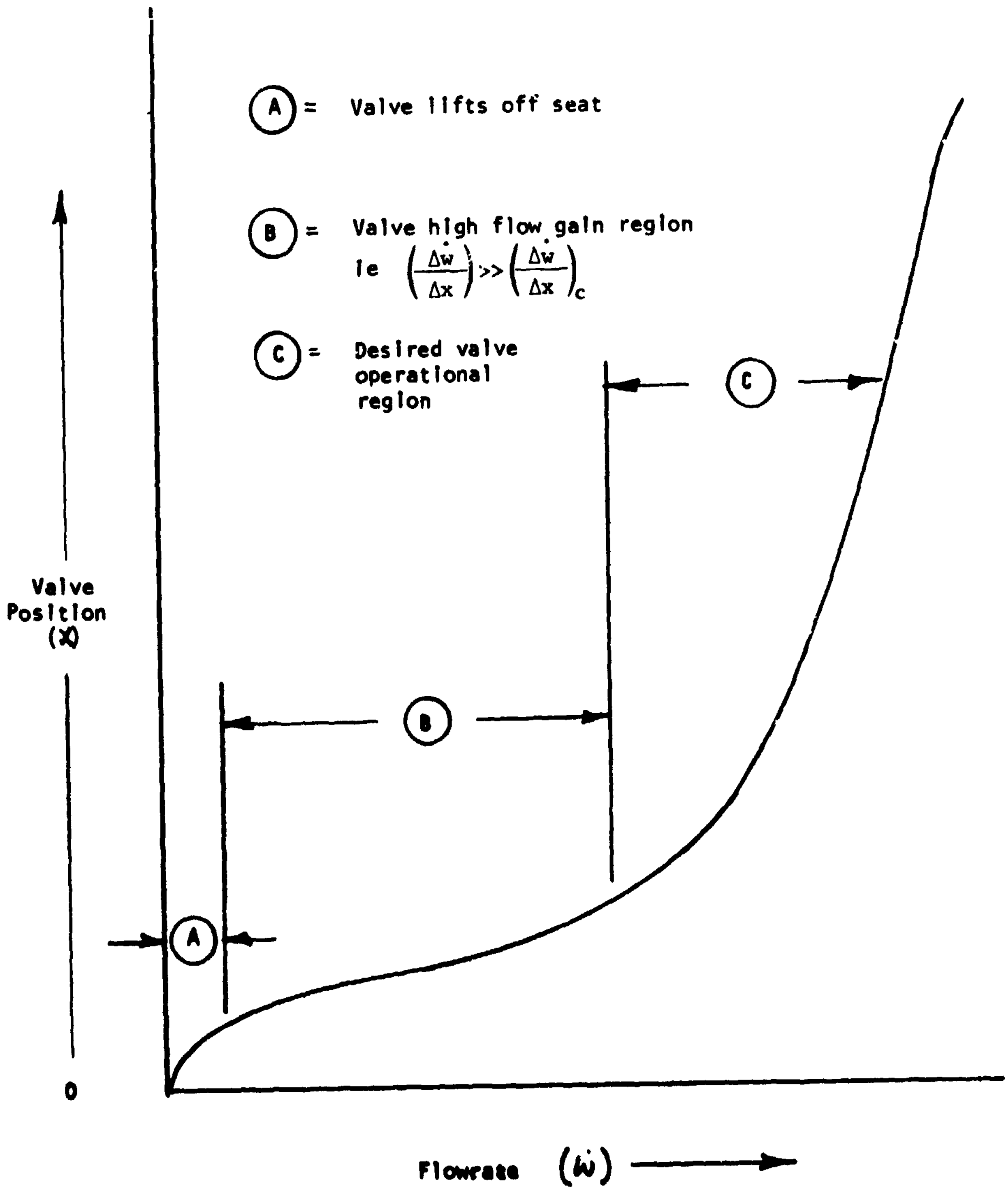

Figure 119. Typical Main Hydrogen Servo Valve Characteristics
Lima Stand - PRA

Test No. 12:	(016-022)
Test Date:	8-9-76
Duration:	0.0 seconds
Objective:	Turbopump performance at 7329 rad/s (70,000 rpm) and duration capability of test stand (~50 seconds).
Results:	Test prematurely terminated by the turbine radial accelerometer VSC cutoff system during the fuel lead stage at 5863 rad/s (56,000 rpm) and 15 g rms.
Analysis:	Gas generator performance during igniter stage and fuel lead was normal. Test terminated near the second critical turbopump speed. No damage noted in either the gas generator or turbopump system.

Test No. 13:	(016-023)
Test Date:	8-9-76
Duration:	0.62 seconds
Objective:	Turbopump performance at 7329 rad/s (70,000 rpm) and duration capability of test stand (~50 seconds).
Results:	The test was prematurely terminated by the turbine radial accelerometer VSC cutoff system at 20 g rms and a maximum speed of 7196 rad/s (68,725 rpm).
Analysis:	All aspects of the test appears normal with the exception of the apparent high g level at 7196 rad/s (68,725 rpm). No damage noted to the hardware.

Test No. 14:	(016-024)
Test Date:	8-9-76
Duration:	1.2 seconds
Objective:	Turbopump performance at 7329 rad/s (70,000 rpm) and duration capability of test stand (~50 seconds).
Results:	Test prematurely terminated by the turbine radial accelerometer VSC cutoff system at 20 g and 7240 rad/s (69,157 rpm).
Analysis:	All test parameters, except the turbine radial accelerometer. g level appeared normal. No hardware damage noted.

Test No. 15: (016-025)

Test Date: 8-9-76

Duration: 2.39 seconds

Objective: Turbopump performance at 7329 rad/s (70,000 rpm) and duration capability of test stand (~50 seconds).

Results: Test prematurely terminated by the turbine inlet overtemperature (1083 K, 1950 R).

Analysis: A review of the records show that the fuel injection pressure was again about 69 N/cm^2 (100 psig) lower than the required set pressure as shown on the controller dial. The resulting higher-than-desired mixture ratio forced the combustion temperature over the redline. Actual targeted combustion temperature was 1033 K (1860 R), with an actual temperature of 1087 K (1957 R) recorded, which was slightly over the redline. For the next test, a slight power increase was planned to ensure that the turbopump speed would be at or above 7329 rad/s (70,000 rpm). Maximum speed for this test was 7140 rad/s (68,199 rpm), and insufficient data were available to ascertain whether the targeted 7329 rad/s (70,000 rpm) would have been attained. The turbine inlet temperature redline was raised to 1089 K (1960 R).

Test No. 16: (016-026)

Test Date: 8-11-76

Duration: 5.82 seconds

Objective: Turbopump performance at 7329 rad/s (70,000 rpm) and duration capability of the test stand (~50 seconds).

Results: Test prematurely terminated by an observer due to a fire in the facility propellant supply system.

Analysis: The fire appeared to be located in the gas generator H_2 system venturi connections. The fasteners were retorqued throughout the immediate area of the H_2 venturi, upstream of the main fuel valve. A review of the records showed the turbopump had achieved 7768 rad/s (74,191 rpm). Evidently, the previous test data, being only 2.39 seconds in duration, had not stabilized; therefore, the targeted power level for this test was too high. Targeted power level for the next test was based on a climbout or a mainstage start to steady state bias of about 314 rad/s (3000 rpm). No damage was sustained to either the turbopump or gas generator system.

Test No. 17: (016-027)

Test Date: 8-11-76

Duration: 3.01 seconds

Objective: Turbopump performance at 7329 rad/s (70,000 rpm) and duration capability of the test stand (~50 seconds).

Results: Test prematurely terminated by turbine inlet overtemperature.

Analysis: Data analysis revealed the fuel injection pressure was again about 69 N/cm^2 (100 psig) lower then the controller dial set pressure requirement. The maximum speed achieved was 6582 rad/s (62,867 rpm). No damage was noted in the turbopump or gas generator systems. For the next test, a site data correction will be applied to the fuel controller to increase the fuel injection pressure by 69 N/cm^2 (100 psig).

Test No. 18: (016-028)

Test Date: 8-11-76

Duration: 40.79 seconds

Objective: Turbopump performance and H-Q excursion at 7329 rad/s (70,000 rpm), and duration capability of the test stand (~50 seconds).

Results: The test was terminated prematurely by the intermediate seal purge supply low-pressure redline circuit.

Analysis: All test objectives, except the demonstration of the test stand propellant duration, was achieved satisfactorily. Maximum speed achieved was 7191 rad/s (68,685 rpm). Figure 120 shows the gas generator chamber pressure profile for the test with the average turbopump speeds indicated during the various phases of the test. As can be noted from Fig. 120, pumped idle-mode operation is nearly achieved during the igniter/main purge start phase of the test. The test proceeded smoothly through main propellant ignition, until after about 10 seconds of mainstage, manual control of the turbopump discharge throttle valve was initiated to first obtain high-head/low-flow conditions. During the planned excursion toward the low-head/high-flow region, cutoff was initiated automatically by the intermediate seal purge supply pressure redline when the pressure dropped below 103 N/cm^2 (150 psig). Normal pressure setting at start was 138 ±7 N/cm^2 (200 ±10 psig). A review of the records show a constant decay in the pressure from start until cutoff. After cutoff, the purge supply pressure recovered to the pretest value. An evaluation of the intermediate seal purge flow during various portions of the test indicates that the purge flow rate increased from about 0.006 kg/s (78.3 ft^3/min; 0.0135 lb/sec) at start to about 0.007 kg/s (89.4 ft^3/min; 0.015 lb/sec at cutoff. These flowrates match the observed changes in the purge system pressure. For the last 10 seconds of mainstage operation, the purge flowrate remained essentially the same, indicating a stabilized condition. Although the comparator setting redline value for the intermediate seal purge pressure was set for 103 N/cm^2 (150 psig), an actual cutoff pressure of 99 N/cm^2 (142 psig) was recorded. A review of the secondary hot-gas seal drain line temperature and primary hot-gas seal drain temperature shows an increase of about 561 K (550 F) and 730 K (855 F) respectively, from the start of the test to cutoff. Figures 121 through 124 show, respectively, the helium purge orifice upstream pressure (supply), the intermediate seal purge pressure (turbopump inlet), the primary hot-gas seal drain line temperature, and the secondary hot-gas seal drain line temperature, all plotted against test reference time. A comparison of these charts indicates that the geometrical effective purge flow area within the secondary hot-gas seal area stabilized after approximately 30 seconds of mainstage, but the purge pressure level of the intermediate seal purge was so near the comparator cutoff value that a small pressure fluctuation below the actual redline valve caused cutoff. Prior to the test series, the intermediate seal purge redline level was selected to ensure that a sufficient margin existed between the LO_2 seal drain line pressure and secondary hot-gas seal pressure, and prevented GO_2 leakage into the secondary hot-gas seal cavity during pretest chilldown. The results of these tests show that the pretest purge level (138 N/cm^2, 200 ±10 psig) is sufficient for start, but the low redline limit of the intermediate seal purge pressure can be reduced below 150 psig.

An intermediate seal purge pressure minimum redline value of 93 N/cm^2 (135 psig) is recommended for future testing. In addition, the purge supply system capacity upstream of the purge flow metering orifice should be enlarged to maintain the required orifice upstream pressure during all phases of the turbopump test. Change in line sizes and/or regulator sizing should be evaluated. An inspection of the gas generator injector revealed it to be in excellent condition (Fig. 125).

To reduce the recorded parameters to a usable form, a computer program was created which received the Beckman data acquisition unit information and converted it to the desired form. To illustrate the output obtained, the printouts for two tests are included in Appendix C: Test No. 017 showing ambient gaseous hydrogen drive data, and Test No. 026 showing hot-gas generator drive data.

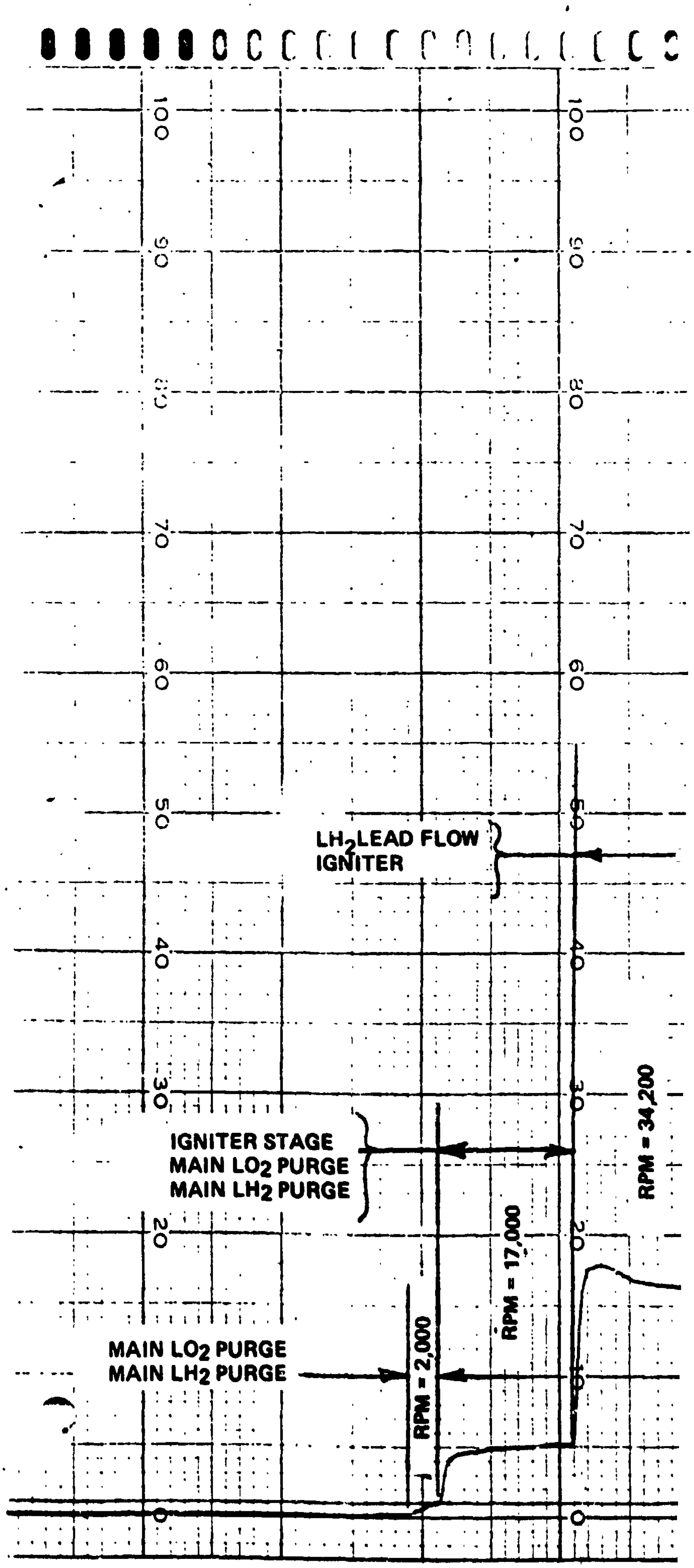

FOLDOUT FRAME 1

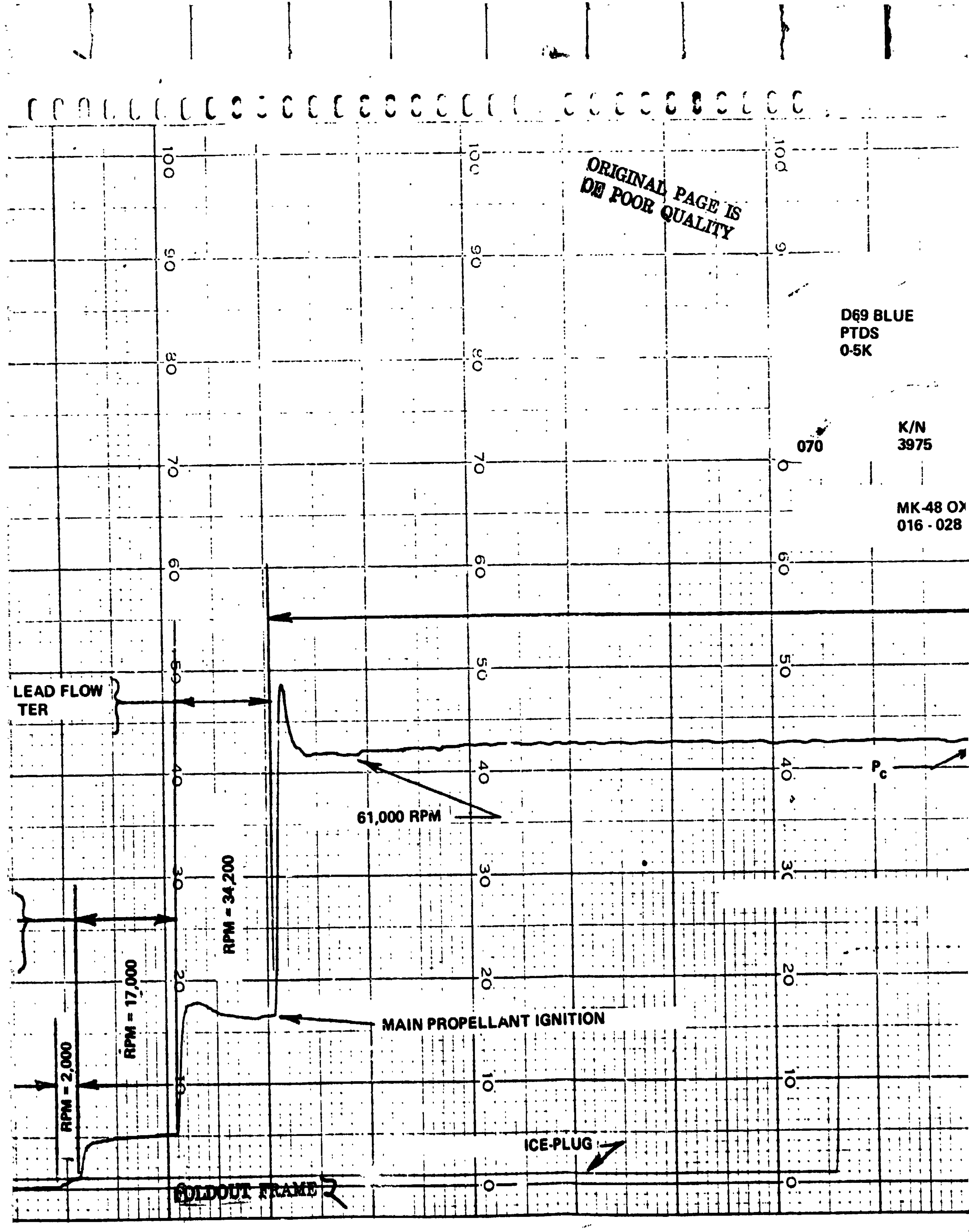
D69 BLUE
PTDS
0-5K
070
K/N
3975
MK-48 OX
016 - 028
LEAD FLOW
TER
RPM = 34,200
61,000 RPM
P_c
MAIN PROPELLANT IGNITION
RPM = 17,000
RPM = 2,000
ICE-PLUG

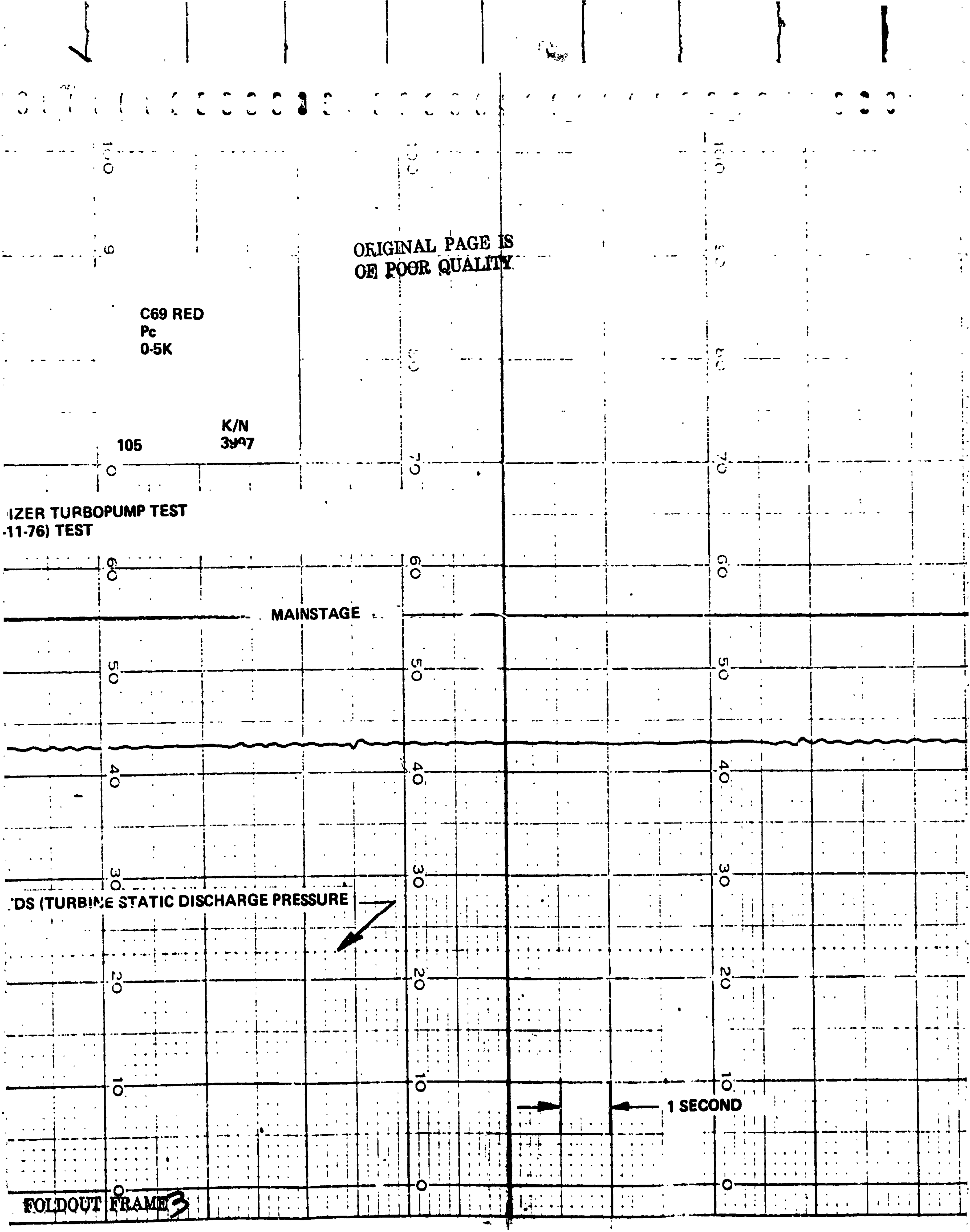

FOLDOUT FRAME 3

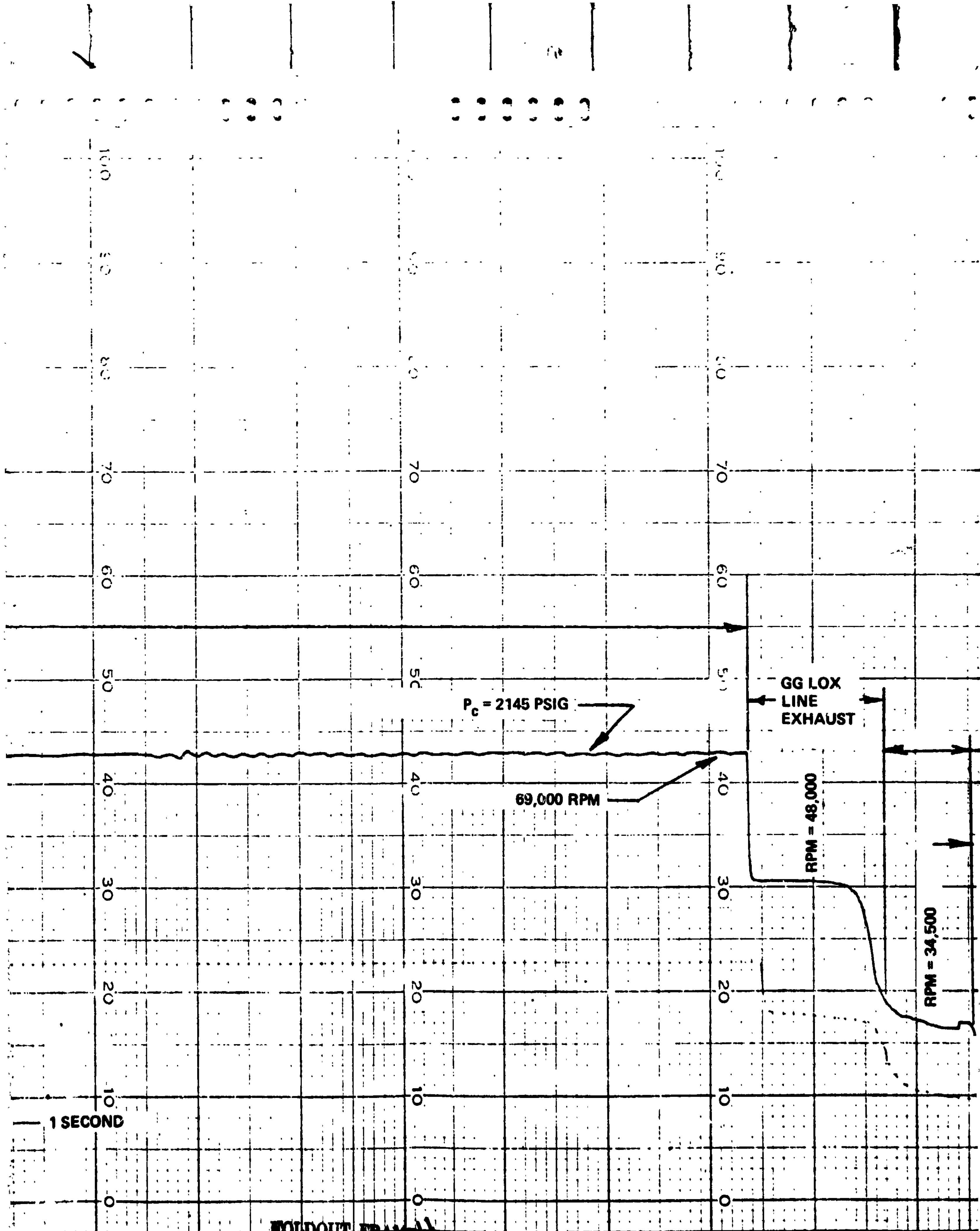

FOLDOUT FRAME

ORIGINAL PAGE IS OF POOR QUALITY

Figure 120. Mark 48-0 Turbopump Start and Cutoff Characteristics Gas Generator Hot-Gas Drive

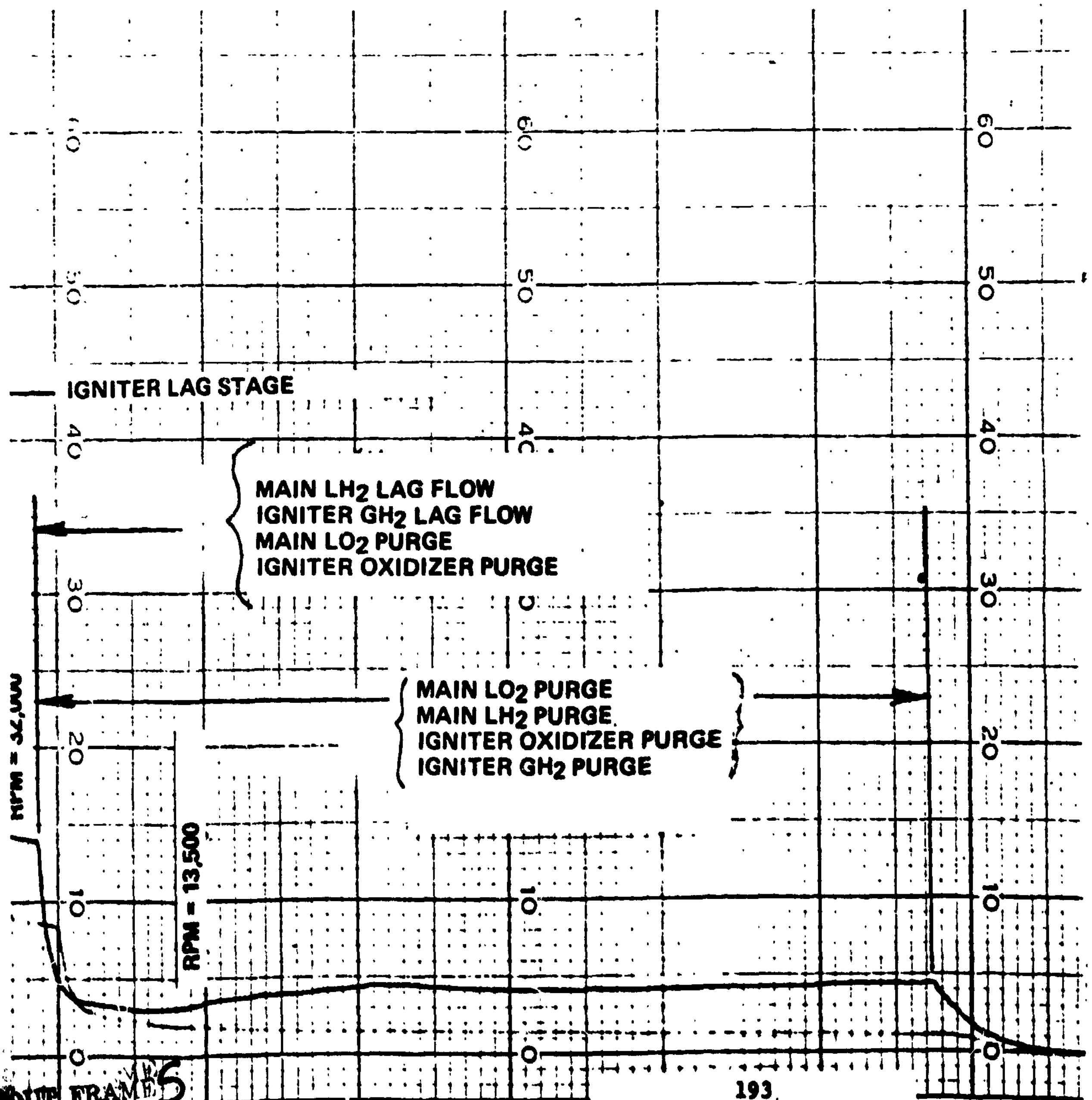

FOLDOUT FRAME 5

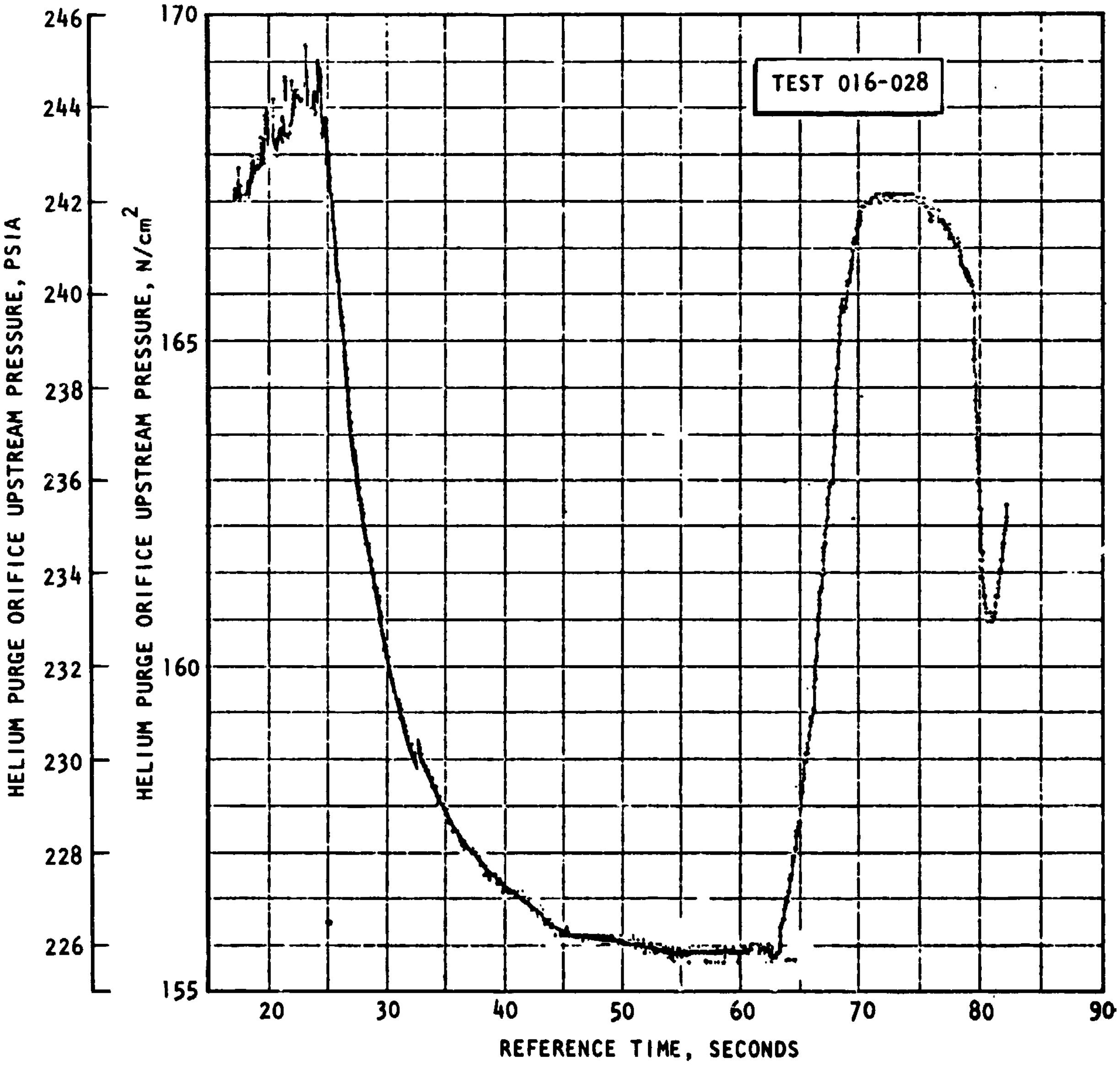

Figure 121. Intermediate Seal Helium Purge Orifice Upstream Pressure

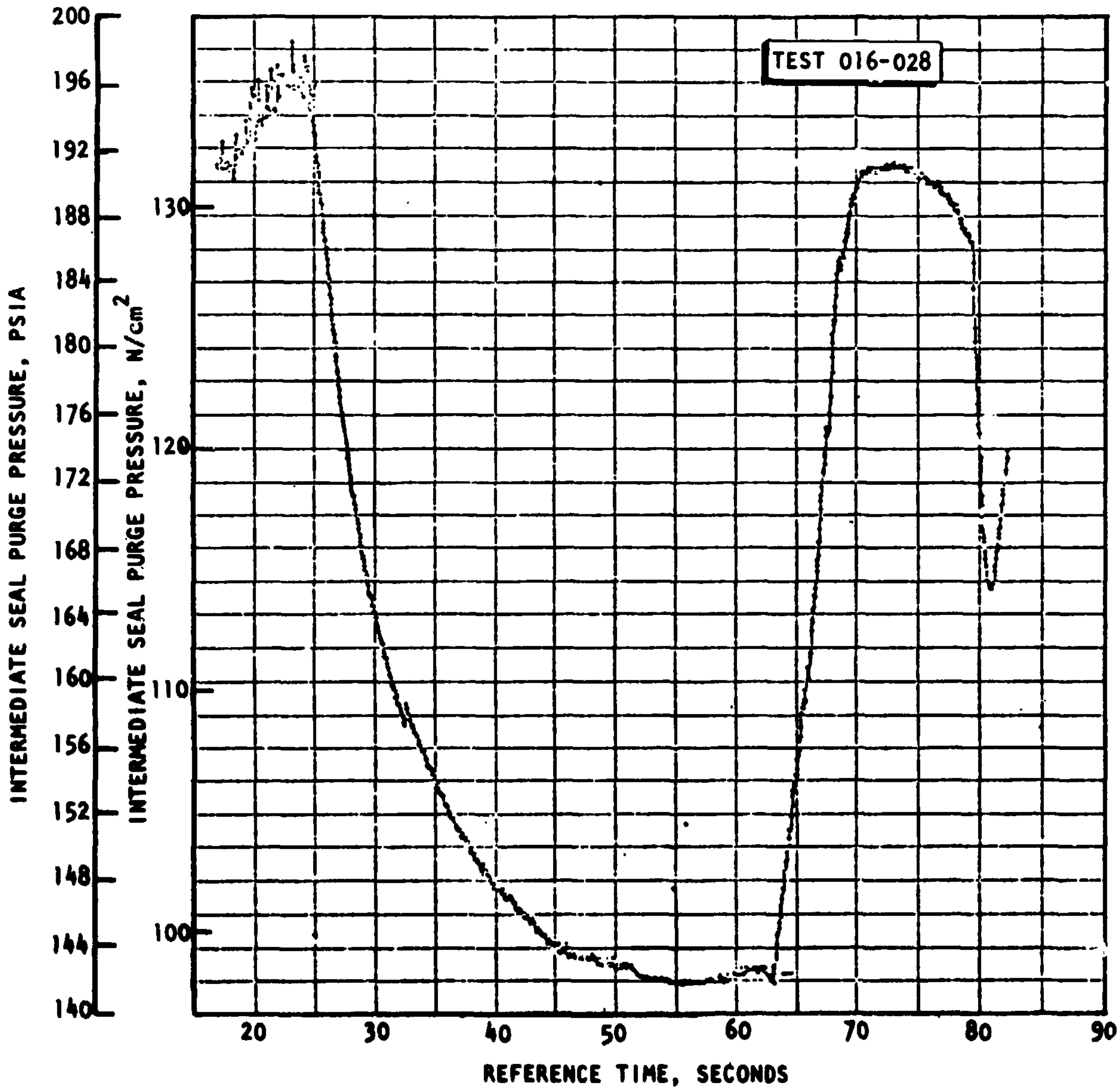

Figure 122. Intermediate Seal Purge Pressure

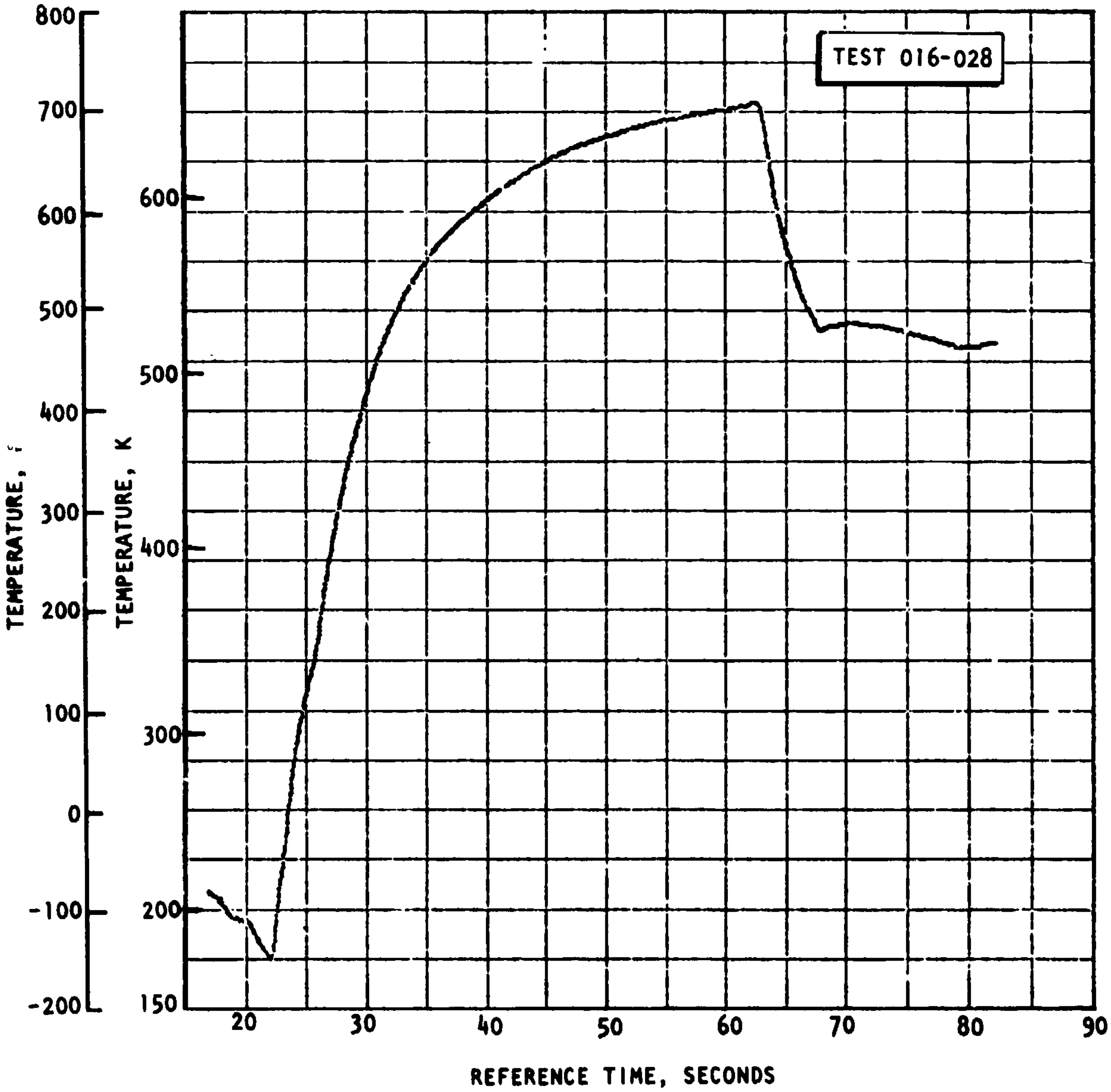

Figure 123. Primary Hot-Gas Seal Drain Temperature

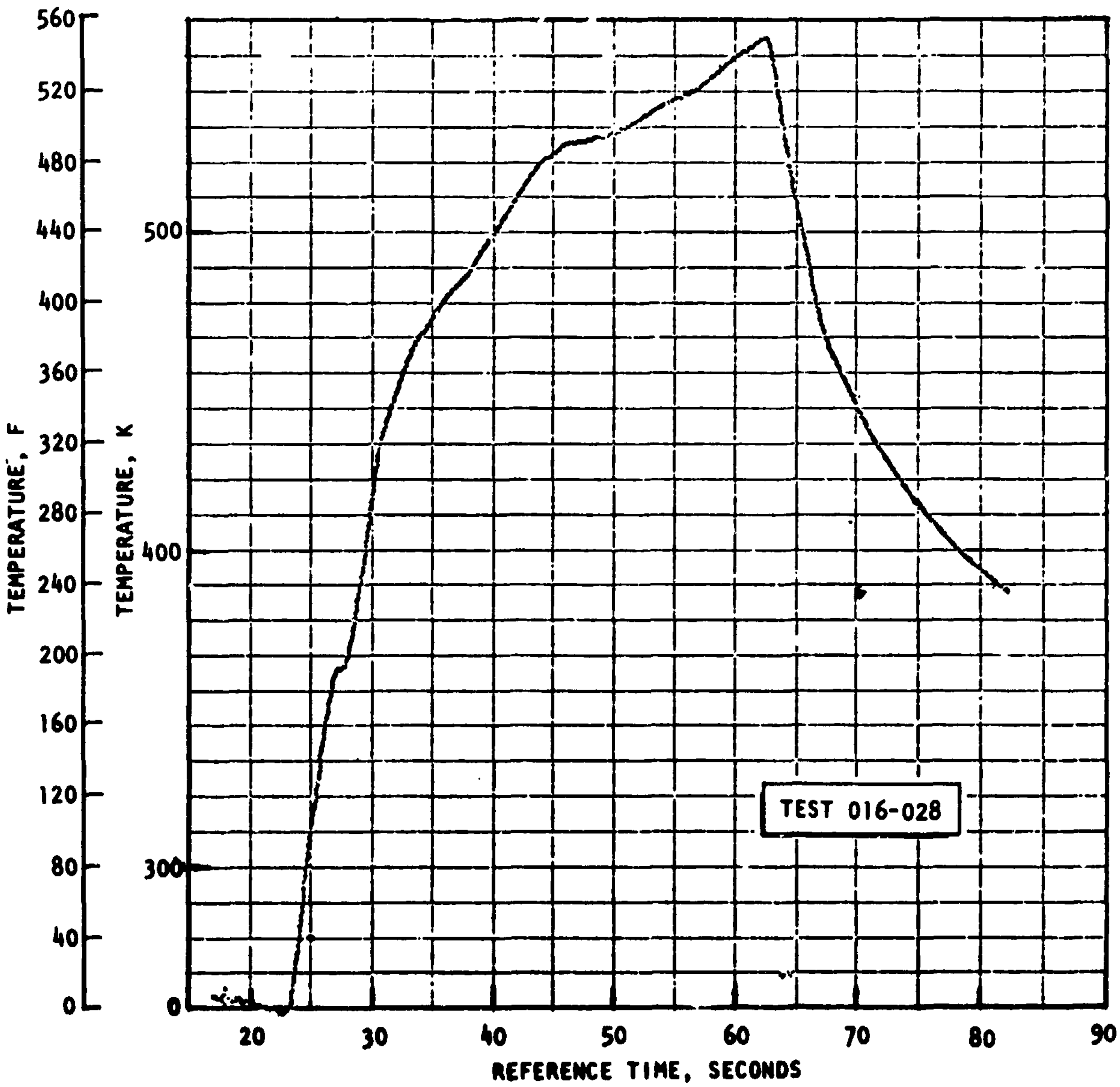

Figure 124. Secondary Hot-Gas Seal Drain Temperature

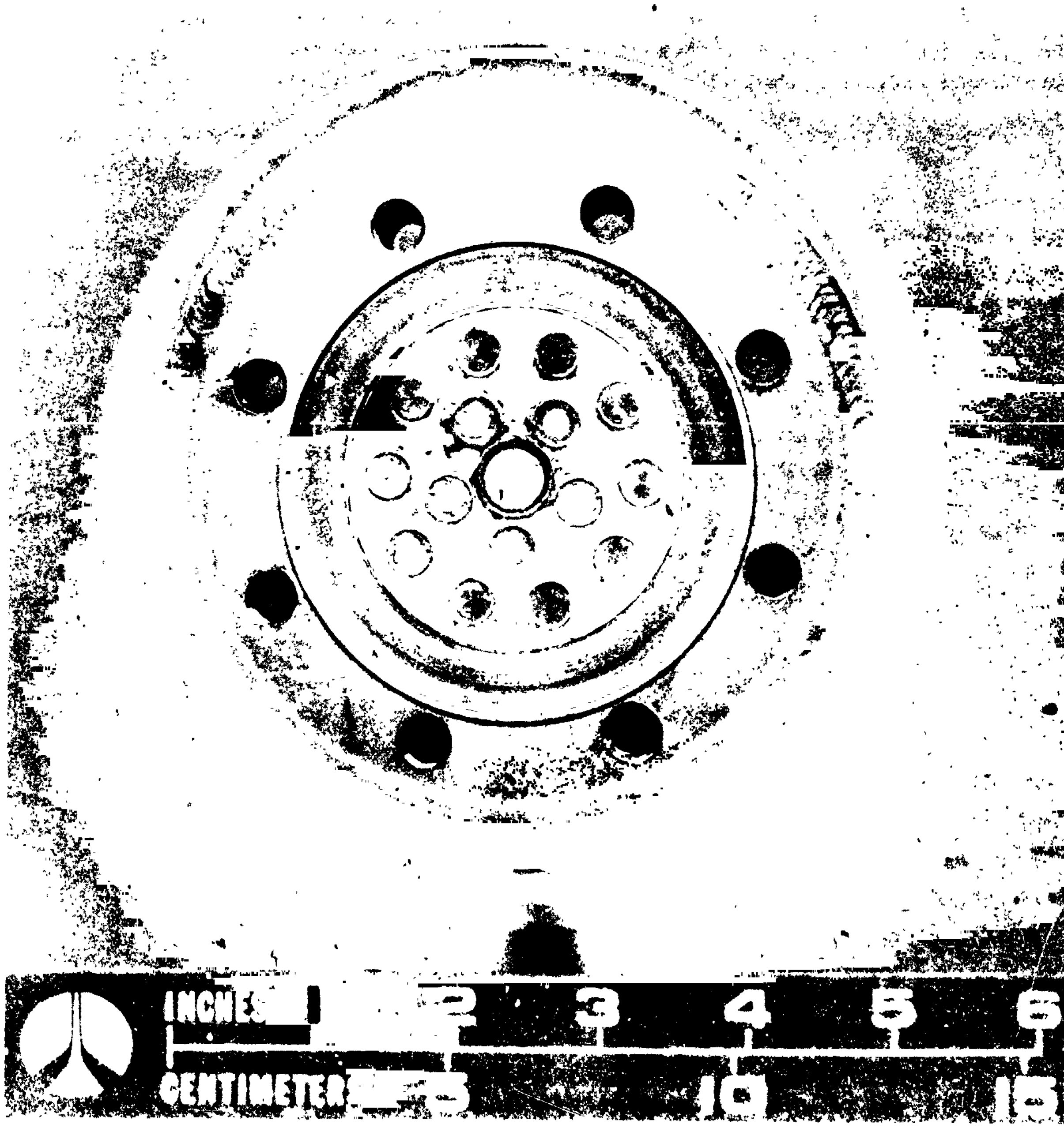

1HS45-8/24/76-C1*

Figure 125. Gas Generator LO_2 Turbopump, P/N RS005024, U/N 2, Posttest Condition

ORIGINAL PAGE IS
OF POOR QUALITY

Pump Hydrodynamic Performance. The following discussion will cover, in order, the pump head rise, pump efficiency, axial thrust, and bearing coolant flow as determined from the test data and compared with the original predictions.

Pump Head Rise. The pump head rise is determined by the relationship

$$H = \frac{144}{\rho} (P_d - P_i) + \frac{V_d^2 - V_i^2}{2g}$$

where P_d and P_i are the measured static pressures at the discharge and inlet of the pump, respectively, and V_d and V_i are the average velocities at the discharge and inlet, respectively. These velocities are not measured but are a function only of the measured flowrate and the geometric diameters of the discharge and inlet ducts. Therefore, the test head rise depends on the two pressures and the flow measurements, all of which are considered to be the more accurate parameters measured in test. The test data were generally sliced to get steady-state performance whenever the test duration was long enough to permit this. The data slices used for evaluating the hydrodynemic parameters were generally approximately 0.23 second in duration and were never less than 0.10 second. This slice time is typical of those generally used at Rocketdyne for steady-state data reduction programs.

Figure 126 is a plot of the pump overall head rise as a function of flow, where both data and the predicted head are scaled to a speed of 7329 rad/s (70,000 rpm). The scaling was accomplished using the affinity laws which have been thoroughly substantiated as applicable for LO_2 and LN_2. The data consist of 66 data points from 15 tests, with test speeds varying from 1628 rad/s (15,550 rpm) to 7768 rad/s (74,190 rpm), and with pumped fluids of both LO_2 and LN_2, primarily the former. The symbols used for the data points distinguish the different operating speed ranges tested. There was no indication that the results were dependent on the pumped fluid medium.

The low-speed data show fairly good agreement with the predicted head rise, but may be indicating a slightly steeper H-Q slope than predicted (this will be discussed more fully at a later point). However, as speed increases, the test data deviate more from the predicted curve, falling short of the curve at the higher flowrates. This type of deviation is typical of that experienced when cavitation is limiting the performance. To investigate this deviation, the ratio ($R_{\Delta H}$) of the test head rise divided by the predicted head rise was calculated and plotted as a function of suction specific speed (N_{ss}) in Fig. 127. The initial plot tended to indicate a great deal of data scatter without clear trend. However, when different symbols were used to represent the different inlet flow coefficients (ϕ_{in}) tested, the data showed a clear trend. For all coefficients, there is a tendency of the head ratio to drop as N_{ss} increases. However, as flow coefficient increases, this dropoff occurs at successively lower values of N_{ss}. To illustrate this trend, the data of Fig. 127 are repeated in Fig. 128, with curves drawn to represent the various flow coefficient ranges tabulated. This trend again is strongly indicative of

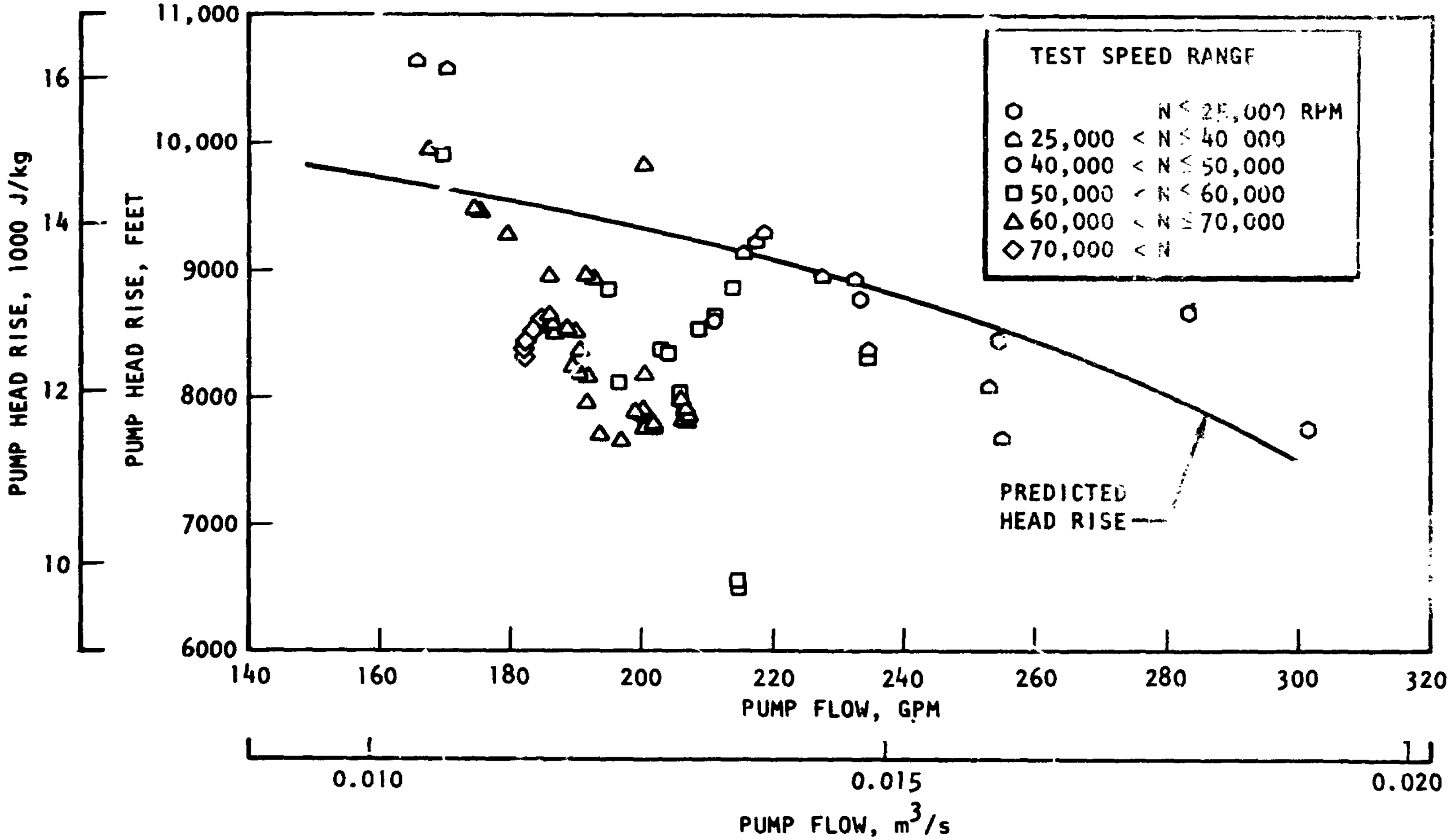

Figure 126. Mark 48 LOX Pump Data and Predicted Head Rise Scaled to 70,000 rpm

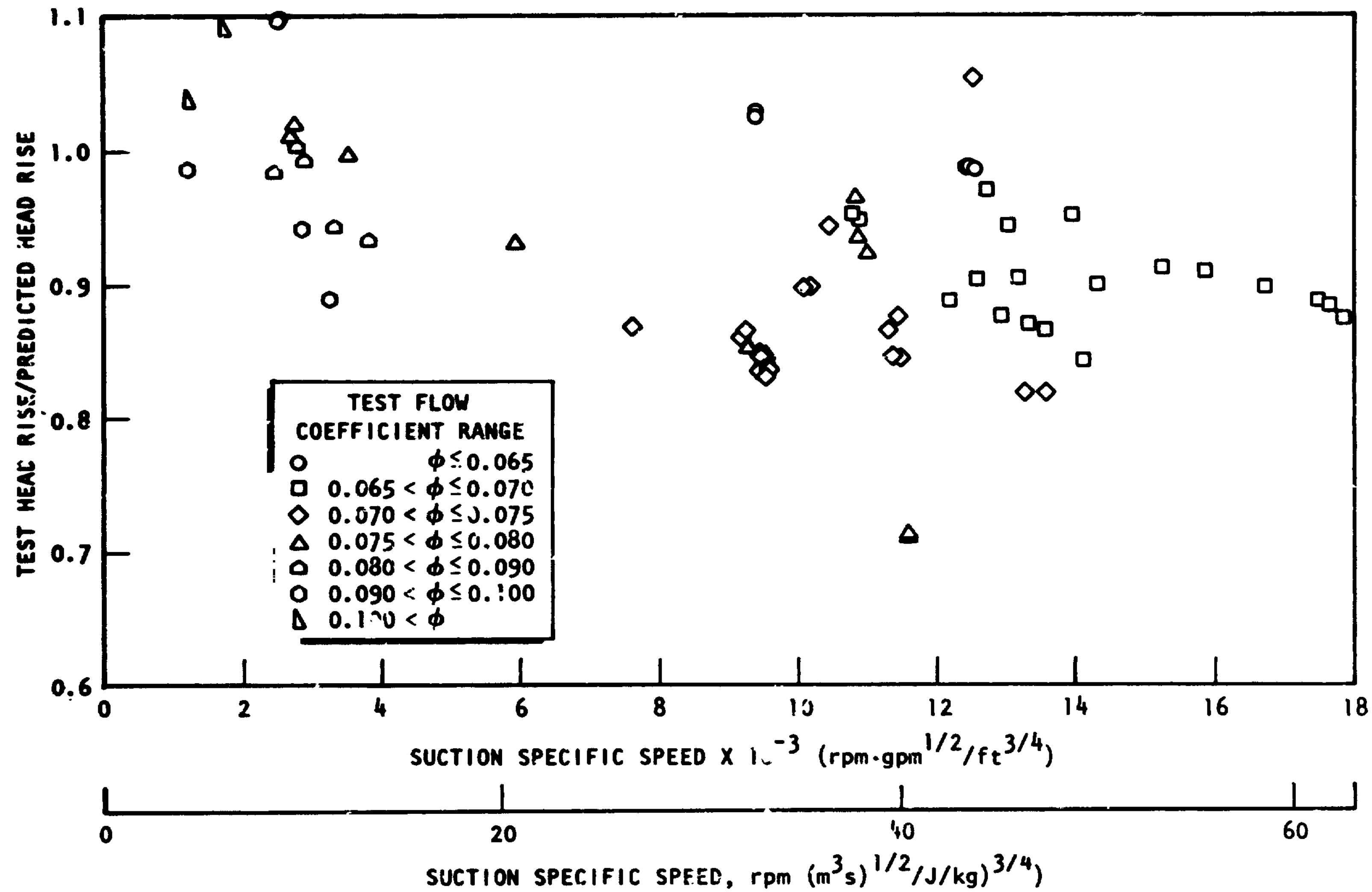

Figure 127. Relative Head Rise as a Function of N_{ss}

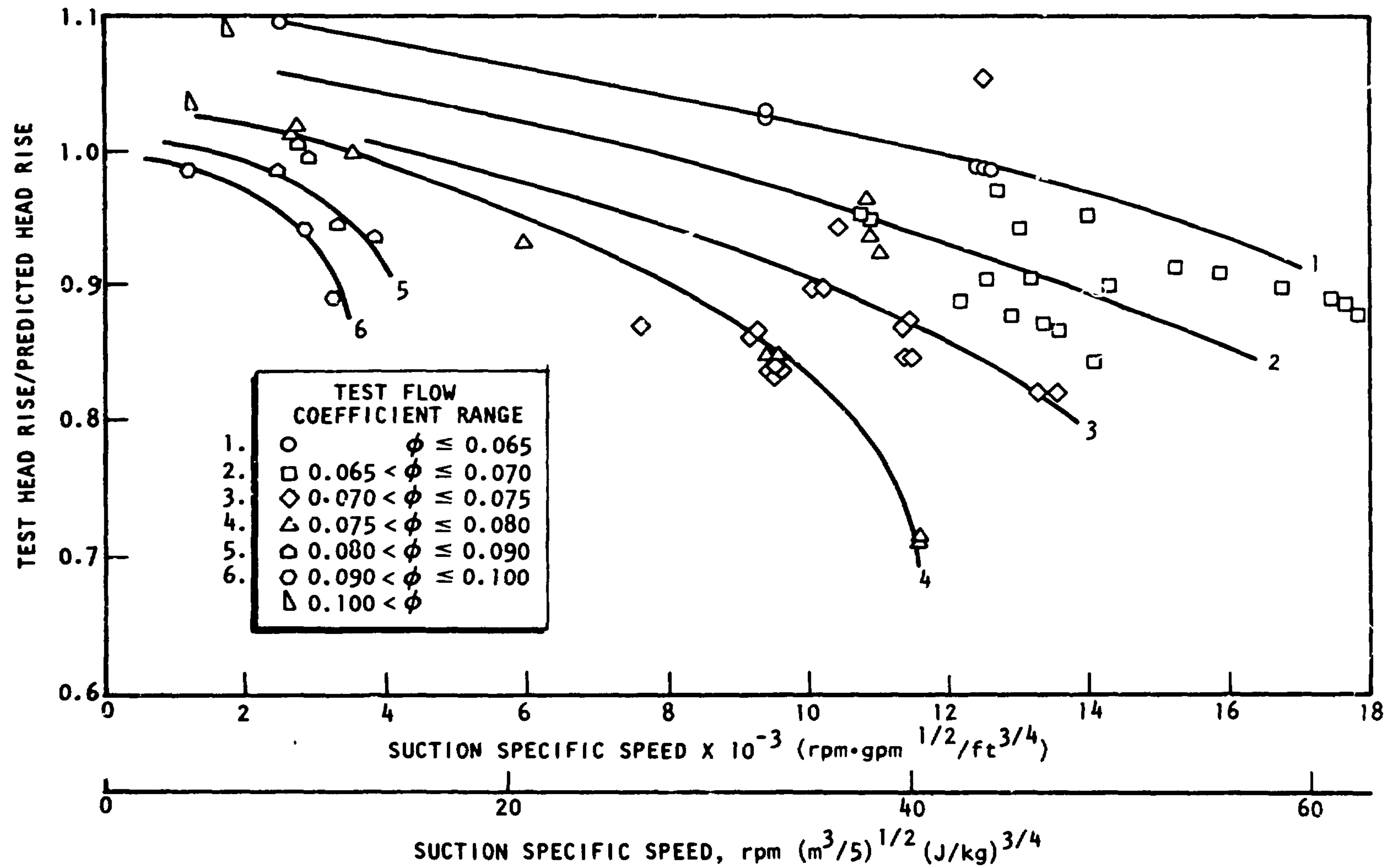

Figure 128. Relative Head Rise as a Function of N_{ss}

cavitation limitations, with the amount of cavitation increasing with either increasing N_{ss} or with increasing flow coefficient at a constant value of N_{ss}.

The cavitation appears to occur at much lower values of N_{ss} than would be expected from the design, considering it does have an inducer designed for good suction performance. This would indicate the more likely possibility that the impeller is cavitating rather than the inducer. This could be caused by:

1. A failure of the inducer to produce its design head rise, which is required to keep the impeller out of cavitation
2. An inadequate impeller design from a cavitation standpoint
3. Too much hot cryogenic being pumped into the impeller eye from the balance piston/bearing area

Arguments will be presented later that there is not a large amount of balance piston flow being returned to the impeller eye. With low circulation, the fluid may be heating up significantly and returning to the impeller eye at much higher temperature than expected. To further define the source of the problem, two further steps of data analysis were attempted:

1. A theoretical inducer head rise curve was used to estimate the inducer performance. This inducer head was added to the inlet NPSH to permit calculation of the impeller NPSH and N_{ss}. (It was assumed in these calculations that there is no fluid entering at the impeller eye except the inducer flow, and that the fluid vapor pressure at the impeller inlet was identical to that upstream of the inducer.)
2. The noncavitating head rise was assumed to be steeper than the predicted noncavitating head. The test data at low speed were used to estimate this new head rise curve, which is shown in Fig. 129.

Figure 130 shows the impeller suction specific speed calculated by the procedure discussed in item (1) above. The data follow a trend typical of cavitation performance. At lower flow coefficients, the data are relatively flat until an N_{ss} of 1.1 rad/s $(m^3/s)^{1/2}/(J/kg)^{3/4}$ 3000 rpm·gpm$^{1/2}$/ft$^{3/4}$ is reached where the head starts to drop. At higher flow coefficients, the head begins to drop at lower N_{ss} values, approximately 1.1 rad/s $(m^3/s)^{1/2}/(J/kg)^{3/4}$ 2200 rpm·gpm$^{1/2}$/ft$^{3/4}$. (Note that an expanded scale is used in Fig. 130 for the abscissa.) These are relatively low values, but if there is much heat added to the flow by the return flow from the front wear ring and from the balance piston area, the actual N_{ss} for each of these points could be significantly higher. However, it must be admitted that one of the key potential technology problems associated with such small-scale hardware is that of achieving a good suction performance.

The results of the procedure outlined in item (2) above are shown in Fig. 131. The approach tended to bring together the data at the lower values of N_{ss} as expected, but the data fall on a sloping line rather than a horizontal line. In fact, the trend of the data is so contrary to the expected trend (as was observed in Fig. 130) that it is concluded that the head rise curve presented

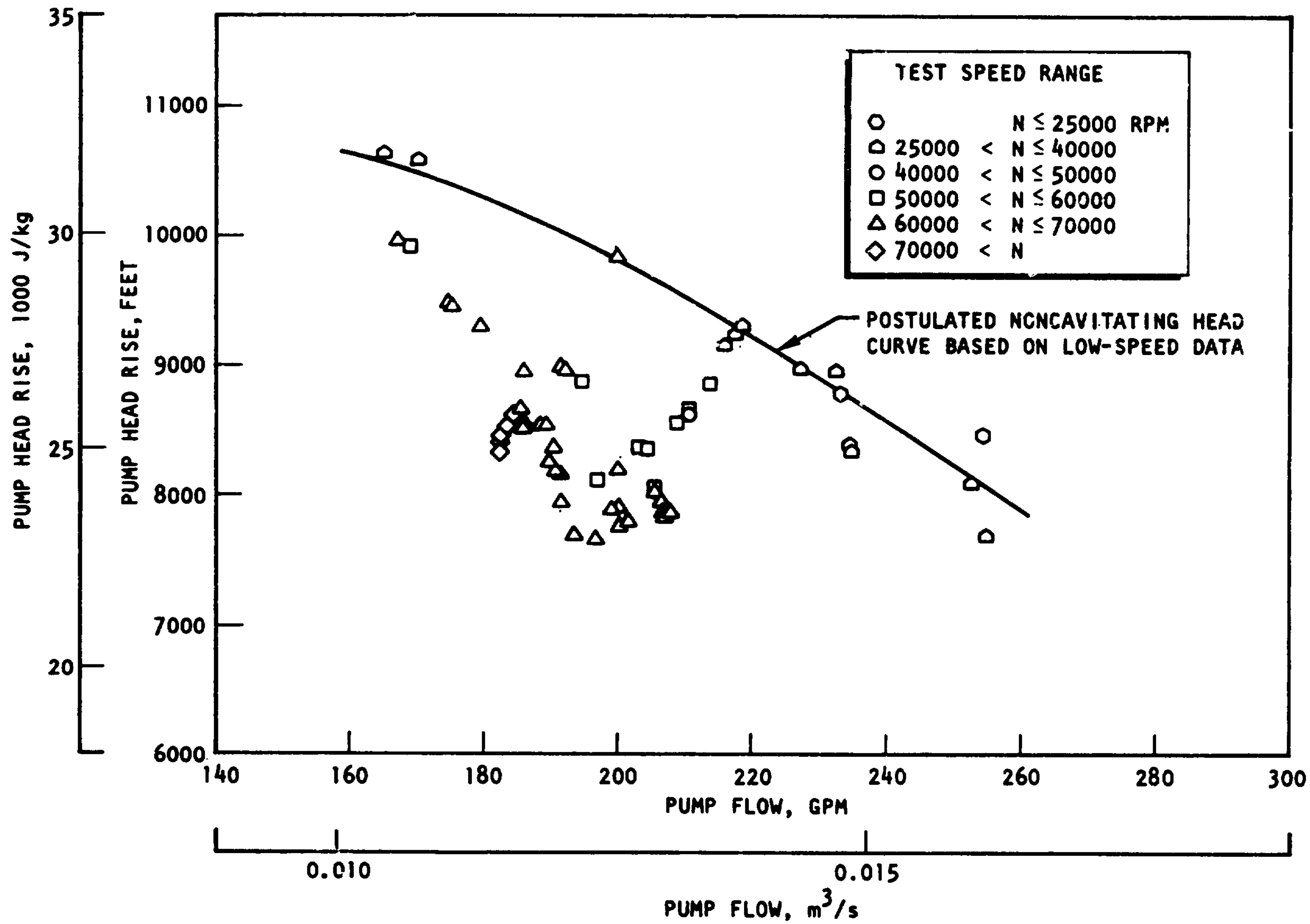

Figure 129. Mark 48 LOX Pump Data Scaled to 70,000 rpm

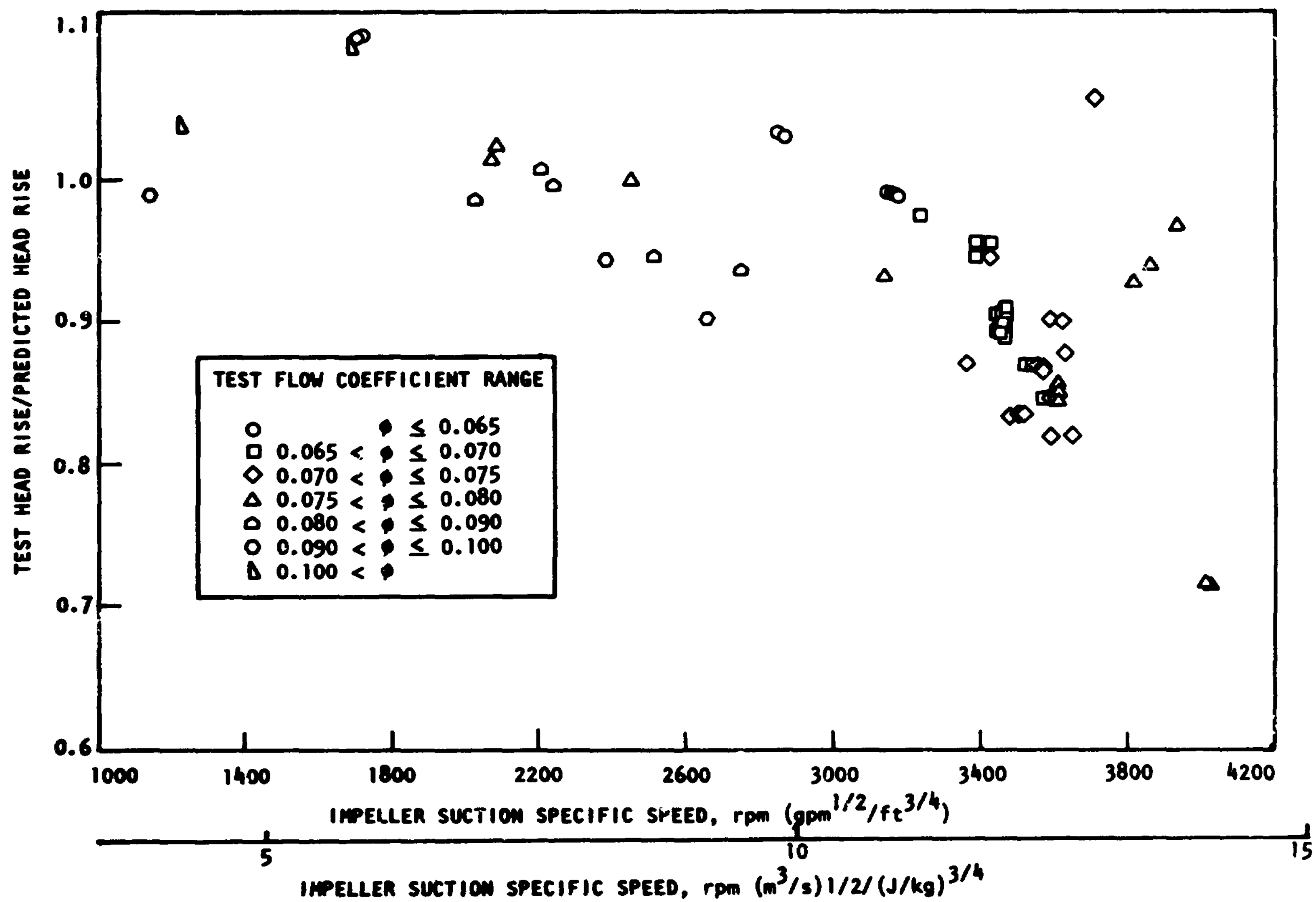

Figure 130. Mark 48-O Turbopump Impeller Section Specific Speed Calculated to Produce Design Head Rise

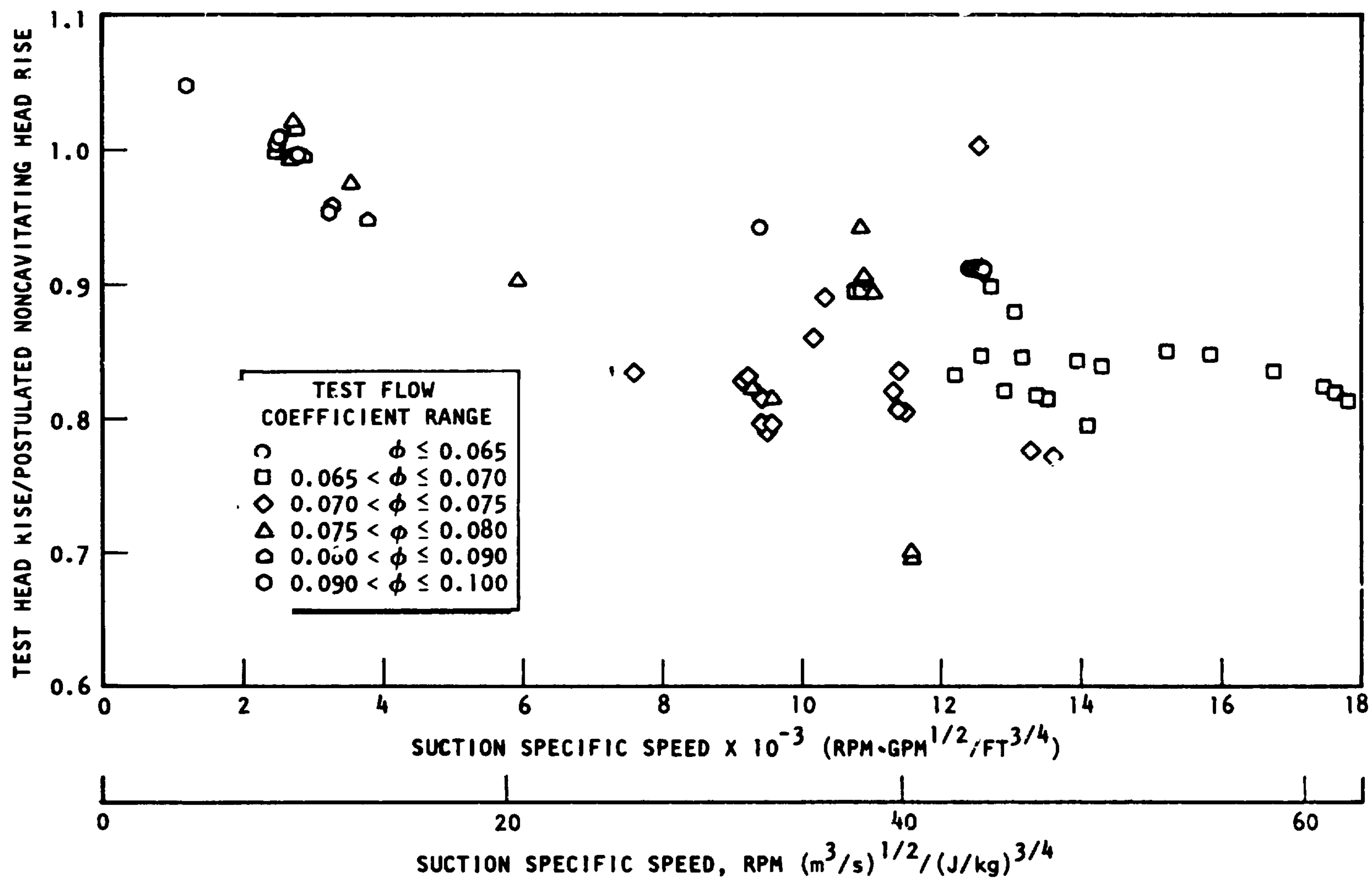

Figure 131. Relative Head Rise as a Function of N_{ss}

in Fig. 129 does not properly reflect the noncavitating head. In all further calculations, the original predicted head rise is used for the theoretical value.

In addition to the overall head rise, internal static pressure measurements were made to aid in distinguishing the hydrodynamic performance of the individual components. Specifically, an impeller and a diffuser discharge pressure was measured. Using these two internal measurements and the pump inlet and discharge pressure, the static pressure rise across the hydrodynamic components could be calculated. This was done for the same data points as presented for the head rise. The results are presented in Fig. 132 through 135 where, in each case, the static pressure rise is plotted as a function of flowrate, and the data are compared with the originally predicted static pressure rise across the same component. Note that the pressure rise of Fig. 135 is a composite of the two pressure rises of Fig. 133 and 134.

It should be pointed out before discussing the significance of these figures, that internal static pressure measurements at positions like the impeller or diffuser discharge are susceptible to large data scatter or even to significant bias from the predicted value. This can result because the instrument is measuring a purely local static wall pressure in an area that is highly susceptible to local gradients in velocity and static pressure. As such, whereas the measurement is taken to achieve an average pressure, it may be measuring either an extreme local value not representative of the average, or a local value in a highly turbulent region that is unstable. The measurements are still of value but always have to be used with the proper care. In the case of the impeller discharge pressure measurement, the data are also affected by the location of the pressure tap on a wall surface at an angle to the throughflow. In such a position, the measurement is reading some component of the velocity head and is not a true static pressure. Thus, this measurement will always read higher than static, and the error will increase as flow increases. However, at 300 gpm, the pressure equivalent of the total meridional component of velocity at the static tap is less than 25 psi, so that this location will not affect any of the conclusions discussed below. In the following discussion, the as-measured pressures are taken as representing average conditions unless otherwise stated.

Figure 132 the first of the four figures, presents the static pressure rise across the impeller and inducer. (There was no static pressure measurement made at the inducer discharge.) The data show the same general trends as the head rise data (Fig. 126); there are some cases, however, where the impeller static pressure rise is higher than design, but the pump head is lower and vice-versa. The data of Fig. 132 actually have more spread than the data of Fig. 126, considering the difference in the scales of the ordinates in the two figures. The data definitely tend to indicate that there is insufficient head being generated by the inducer-impeller combination.

Figure 133 presents the static pressure rise across the vaned diffuser. These data indicate a different potential problem. At low flows the proper diffusion appears to be achieved but, as flow increases, the diffuser performance progressively degrades. This is indicative of a diffuser mismatch which could be caused

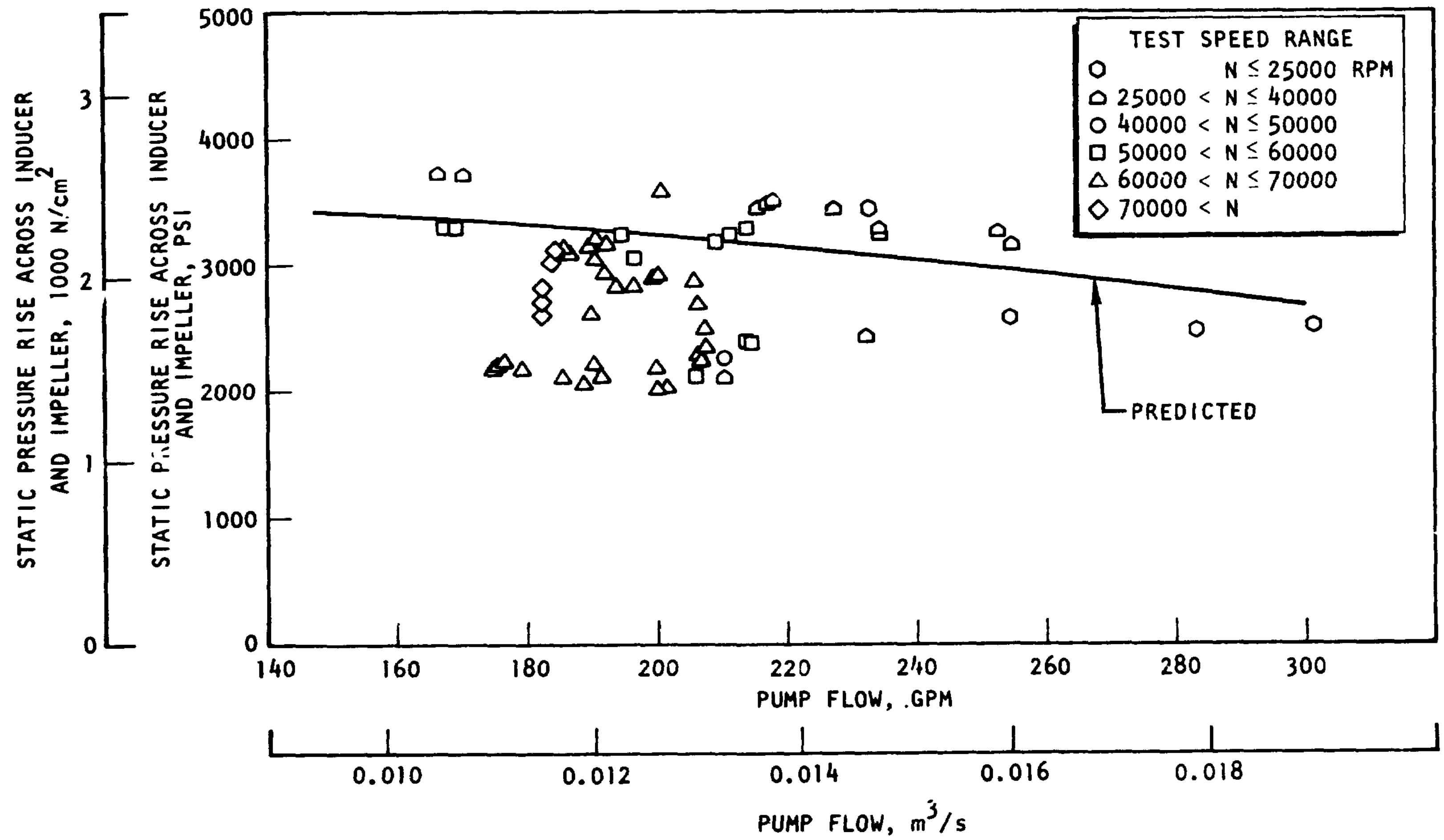

Figure 132. Inducer and Impeller Pressure Rise

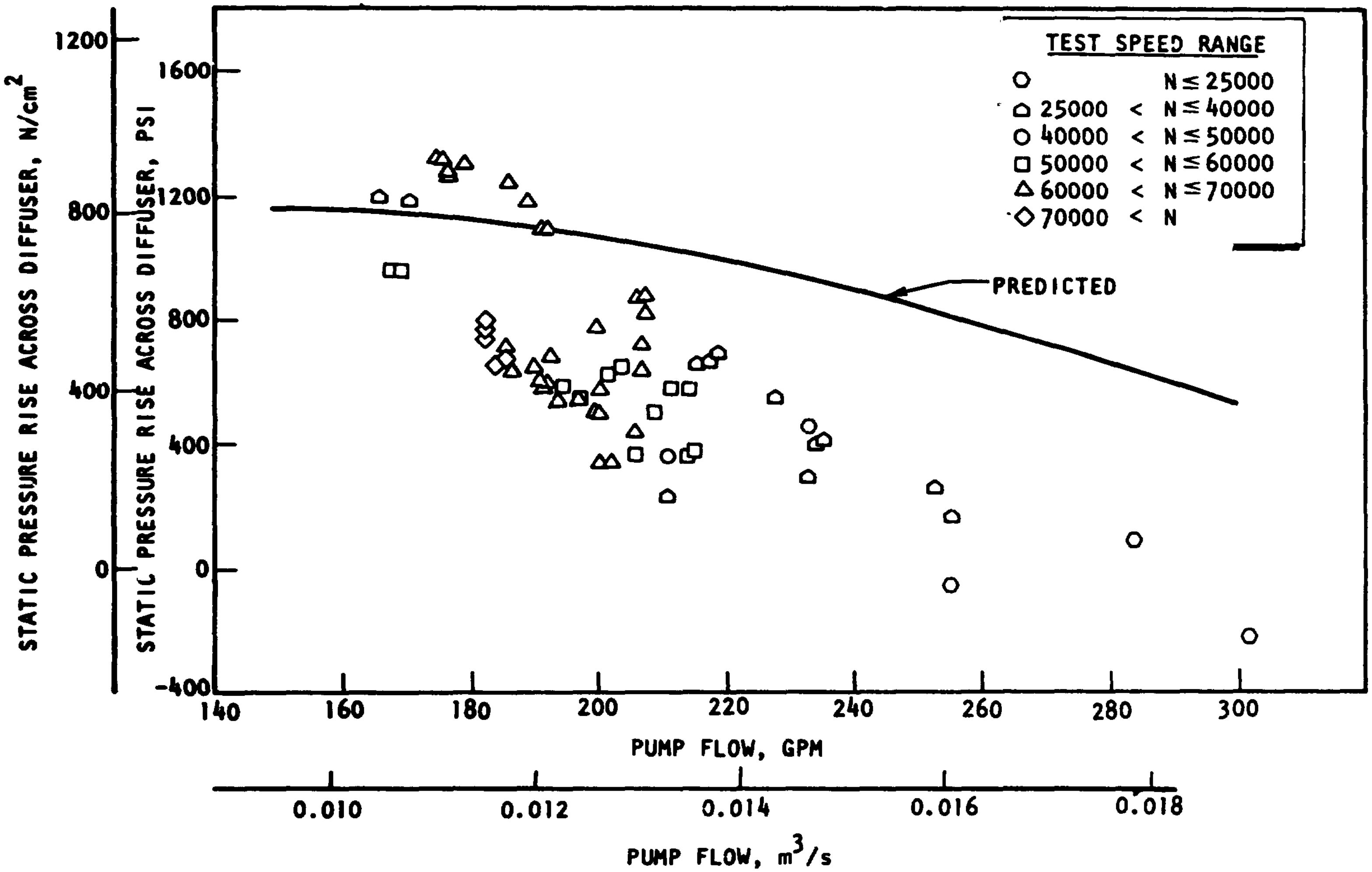

Figure 133. Mark 48 LOX Pump Data and Prediction Scaled to 70,000 rpm

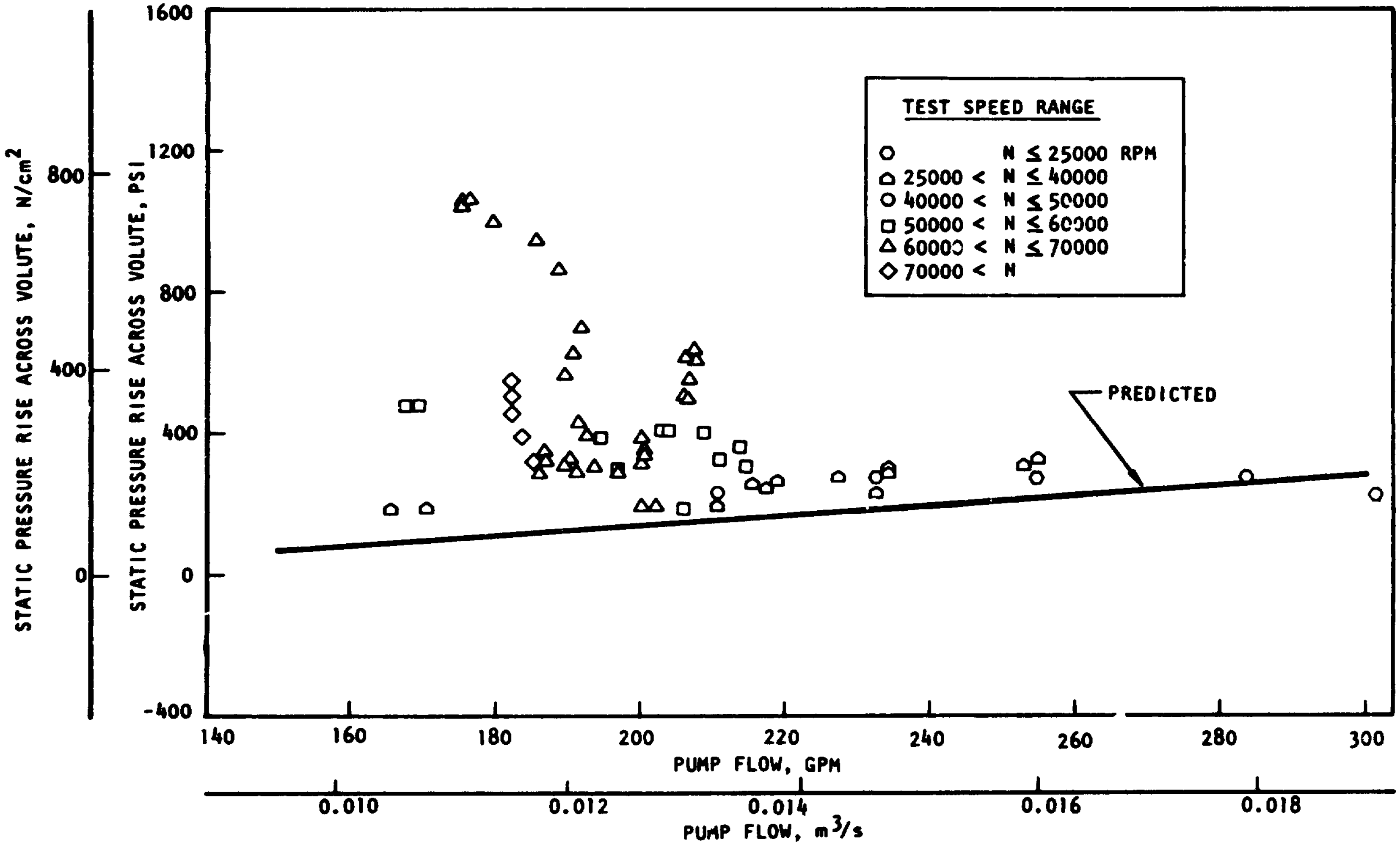

Figure 134. Mark 48-0 Pump Data and Prediction Sealed to 70,000 RPM

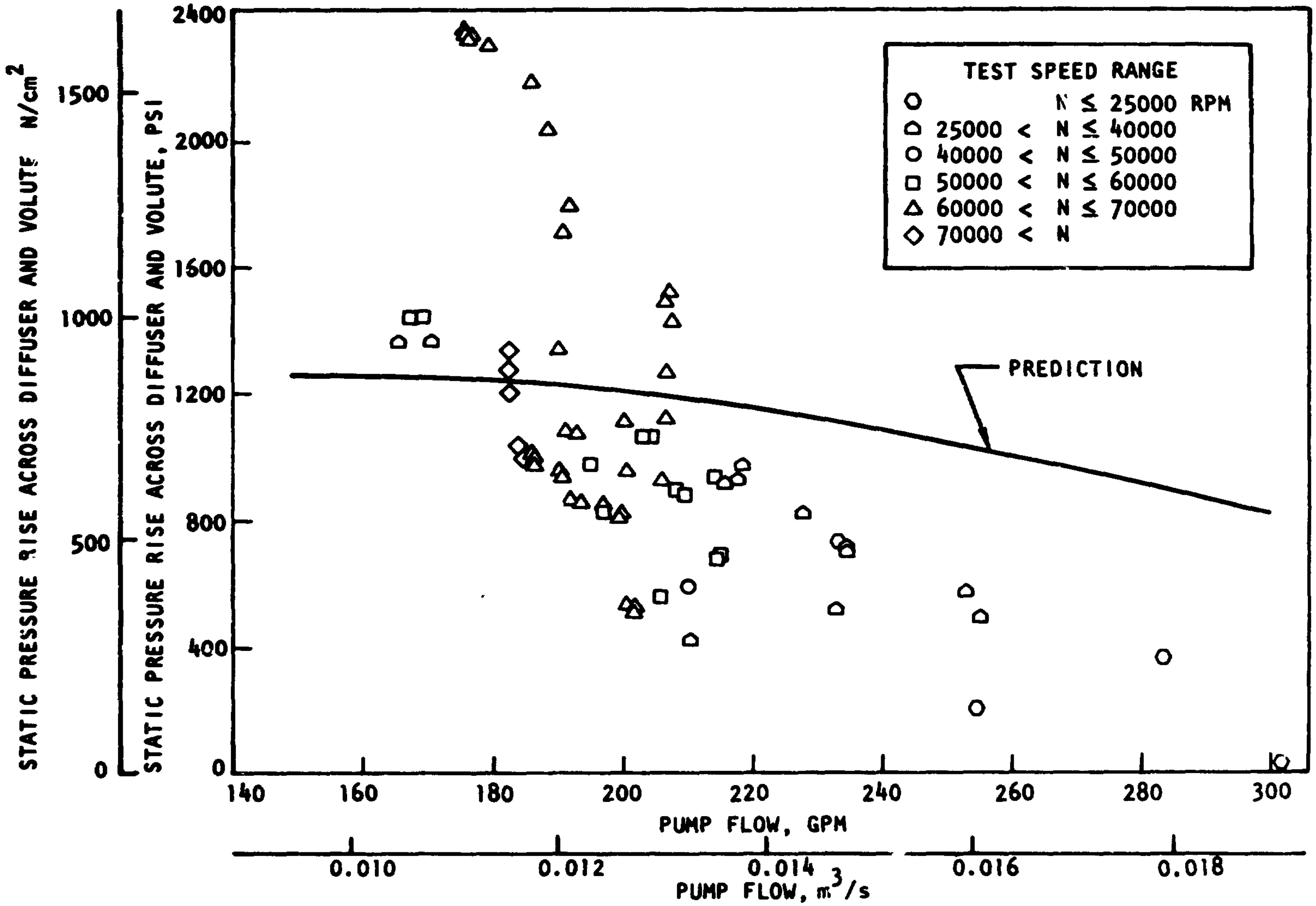

Figure 135. Diffuser and Volute Head Rise

by either a flow angle mismatch at the leading edge, or a flow passage that is too small to pass the flow. The latter appears to be more likely in view of the fact that, for lower-speed data at the real high flows and the real low flows, the impeller pressure rise was in fair agreement with prediction (Fig. 132), yet the diffuser pressure rise is continually dropping as flow increases. Again, this is a typical problem experienced with very small pumps in that boundary layer blockage or blockage due to fabrication mismatch or secondary-flow effects can so easily represent a much larger percentage of the through-flow area than is normally experienced in larger pumps.

Figure 134 presents the pressure recovery through the volute and indicates a larger amount of data scatter, but the data are everywhere equal to or above the design value. Figure 135 is a composite of Fig. 133 and 134, and represents the static pressure rise across the total diffusion system from impeller discharge to pump discharge. This composite shows the same trends as would be expected based on the trends and relative amplitudes of Fig. 133 and 134.

Pump Efficiency. The data reduction program was written to calculate the pump efficiency by assuming a known turbine efficiency based on calibration results (presented in the turbine section) and backing out the pump efficiency from the machine efficiency. This machine efficiency is calculated from test data as the pump delivered horsepower divided by the turbine inlet available energy. The pump efficiency obtained by this procedure is shown in Fig. 136. As can be readily be seen, this calculated efficiency shows very poor agreement with the predicted efficiency, especially at the higher flow coefficients; however, the higher flow coefficient data were obtained from lower-speed tests where the results would be much more susceptible to data inaccuracies. The data are all below the predicted efficiency line even though the head rise did in some cases meet its head objective.

Many of the test slices at higher speeds had a sufficient temperature rise across the pump to permit a calculation of the isentropic efficiency. This calculation has the advantage of using only test data from the pump, specifically pump inlet and discharge pressures and temperatures. These temperatures are much more reliable than the turbine temperatures, but the temperature differentials must be large enough to minimize instrumentation inaccuracy. The data slices with temperature rise of 11 to 17 K (20 to 30 F) were used, and the results are presented in Fig. 137. The data show better efficiency than those calculated from the machine efficiency. These results also would appear much more reasonable in that they are more consistent with the performance degradation noted in the pump head. As such, the isentropic efficiency data are considered to be the most representative, and show the pump running generally about 5 to 10 points low at the lower flow coefficients, the actual amount, however, being rather strongly dependent on flow coefficient.

Achieving a high efficiency in a small pump is difficult. The problems discussed in describing the pump head degradation are primarily responsible for the lower efficiency. It is anticipated that the efficiency can be improved significantly by correcting the conditions that are causing impeller cavitation and low head.

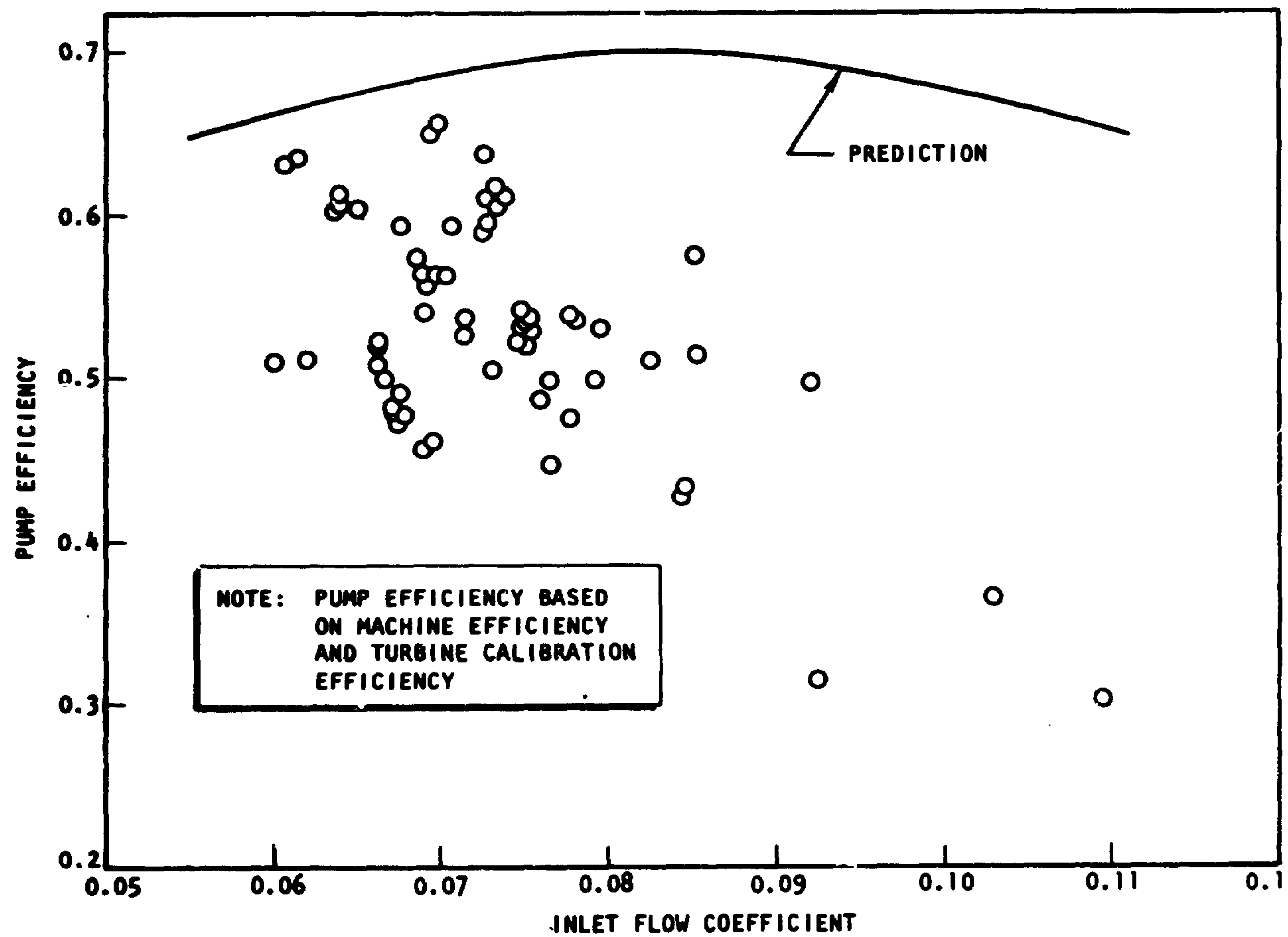

Figure 136. Pump Efficiency

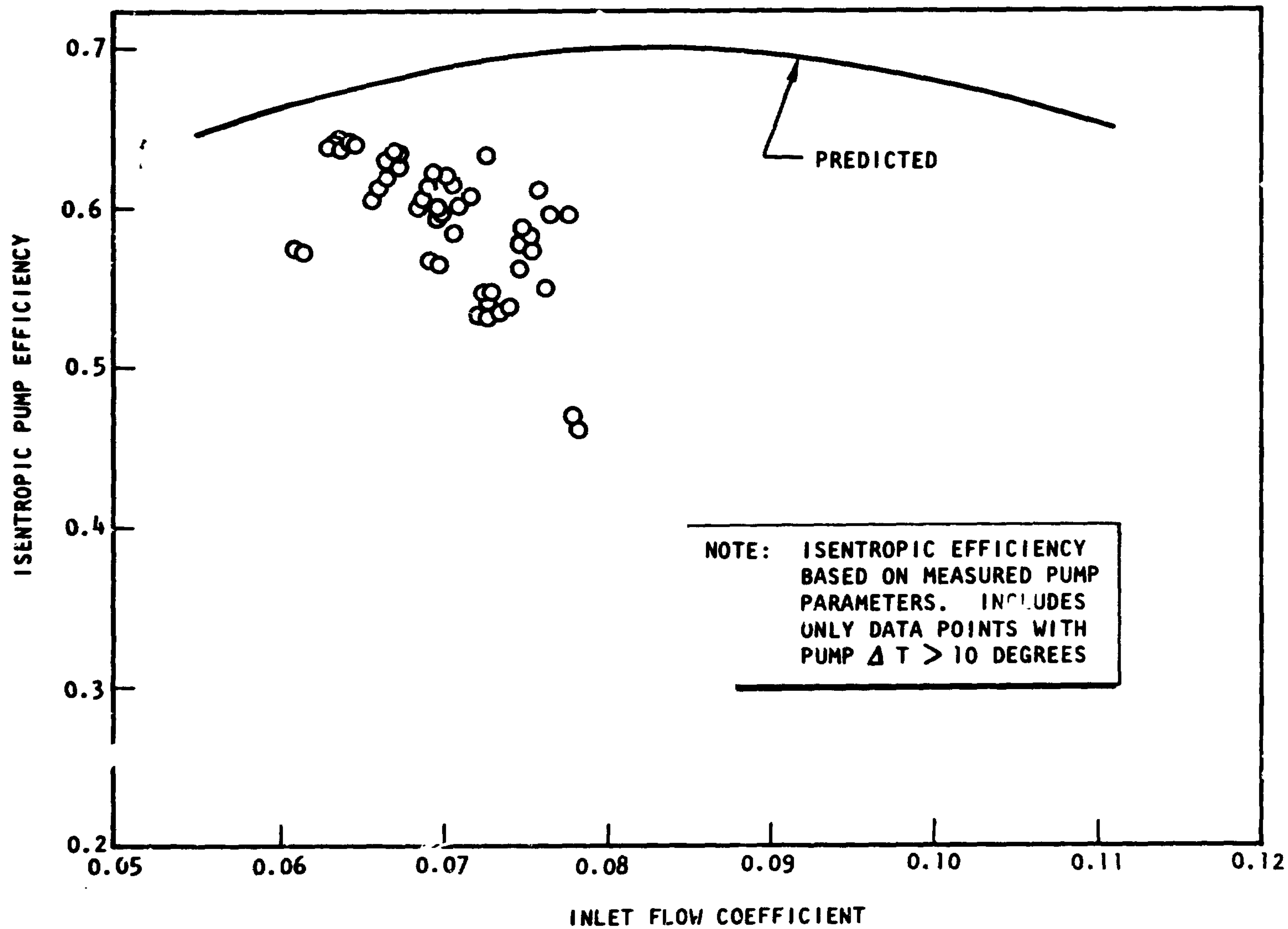

Figure 137. Pump Isentropic Efficiency

Axial Thrust. The turbopump is designed to achieve a balance of axial thrust between the pump and turbine. The pump impeller back side contains a balance piston designed to provide the thrust range as a function of axial position to permit the total turbopump axial thrust to be balanced during all phases of operation, including start and shutdown transients. The balance piston is used to minimize the thrust load-carrying requirements on the bearings, the balance piston using the pressures generated by the pump to achieve the required balancing force.

The balance piston is double acting in the sense that both the high- and low-pressure orifices are sensitive to axial position. A sketch of the balance piston is shown in Fig. 138. Since operation in LO_2 prohibits any significant metal-to-metal contact of rotating and stationary parts, the balance piston is designed to have a radial gap at both orifices at all times. These gaps are a function of speed and, based on calculations from the Stress Department, they the relationships:

$$E_1 = 0.0033 - 0.013\ (N/8061)^2 \text{ mm}$$

$$E_1 = 0.0013 - 0.0005\ (N/77{,}000)^2 \text{ inch}$$

$$E_2 = 0.009 - 0.008\ (N/8061)^2 \text{ mm}$$

$$E_2 = 0.00035 - 0.0003\ (N/77{,}000)^2 \text{ inch}$$

where N is pump speed in rpm. These gaps must be kept as small as practical to avoid a rubbing problem because the axial thrust range is significantly decreased if these gaps are allowed to be too large. Review of the hardware after the complete test series indicated no rubbing occurred in the balance piston area.

The pressure drop across the total balance piston consists of three individual pressure drops:

1. The loss through the high-pressure orifice, which is sensitive to axial position
2. The loss through the low-pressure orifice, which is sensitive to axial position
3. The pressure drop sustained by the rotational (vortex) motion of the fluid within the balance piston. This drop is sensitive to the surface condition in the balance piston and speed.

During the Mark 48-0 testing, the following static pressure measurements were made:

1. Impeller discharge pressure, which is upstream of the balance cavity pressure
2. Balance cavity pressure, which is downstream of the high-pressure orifice but at approximately the same radius

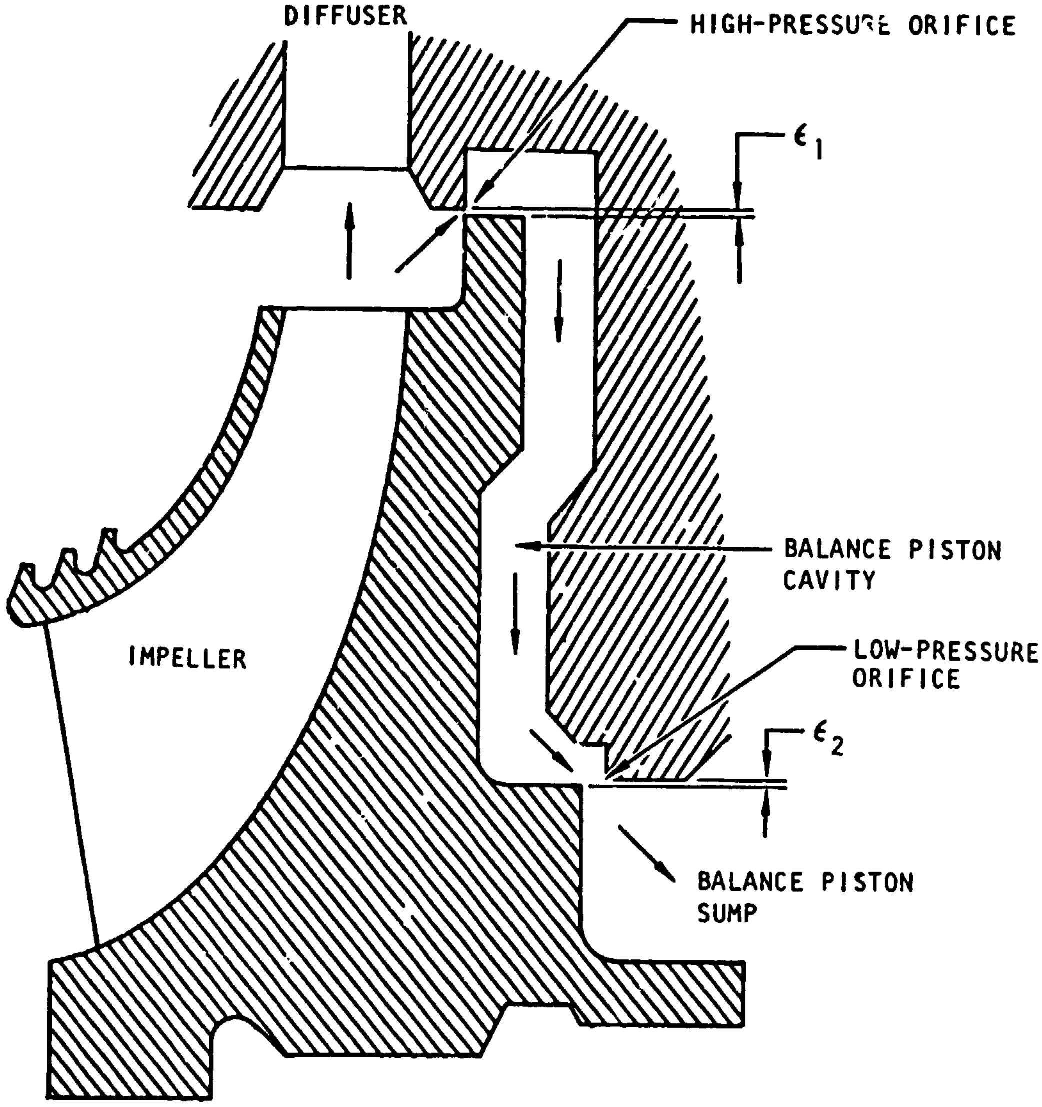

Figure 138. Mark 48-0 Balance Piston

3. Balance piston sump pressure, which is downstream of the low-pressure orifice

4. Balance piston return flow pressure, which is downstream of the bearings and slinger in the return path of the balance piston flow

These pressure measurements and a previous correlation for pressure drop through SSME LO_2 bearings permit analysis of the balance piston performance regarding the fluid average slip coefficient, K. This ratio of fluid-to-impeller speed tangentially was found to be a function of balance piston flow coefficient as well as impeller speed, as can be seen in Fig. 139 and 140. This analysis was done using time slices representative of pressures and speeds that occurred during LO_2 testing.

Analysis of balance piston axial thrust capabilities or range required modification of an existing balance piston computer program. The computer program was modified to accept a split flow downstream of the return cavity, modeling the recirculation holes and overboard bleed line on the Mark 48 oxidizer pump. In addition, a modification was made to the program to accept variable density at each station in the flow path. Once the flowrates through the flow loop had converged and pressures through the system were known, new densities were found from charts for all stations. The computer program was run again, and the process repeated until convergence of the densities was achieved.

The balance piston force was calculated for the full range of the axial travel [i.e., from 0.0 to 0.25 mm, (0.010 inch) gap on the high-pressure orifice], and the axial position at which the measured balance cavity pressure was matched was determined. Because of the time consumption involved in obtaining solutions for a given data slice, five data slices were analyzed which are representative of the testing performed.

The ratio X/δ of high-pressure orifice gap (X) to total balance piston travel (δ) for these cases varied from 0.212 to 0.353. These five cases are summarized in Table 22 showing also the total thrust range. In addition, Table 22 shows the thrust at the point of match, and defines and presents the range factor which varies from 0.52 to 0.78.

Figure 141 presents the thrust range as a function of the pump speed for the cases presented in Table 22. Assuming that the pump pressures vary essentially with speed squared, the thrust range also should vary close to speed squared. (This is an approximation because pump inlet pressure does not vary with speed and the radial gaps of the balance piston are closing with speed, which makes the balance piston more effective at higher speeds.) Lines are drawn on Fig. 141 at a slope of 2 to 1 to represent a speed squared relationship. The parameter K_T is defined in Fig. 141, and four of the cases vary from 81 to 112% of the design value of this parameter. Case 17-8 is found to be 68% of K_T design.

Case 17-8 has an internal recirculation hole and no overboard bleed. It was found during the analysis that the flow in the recirculation passage in this case becomes a two-phase flow with very low density. This causes a higher back pressure in the balance piston sump and, therefore, poorer balance piston performance.

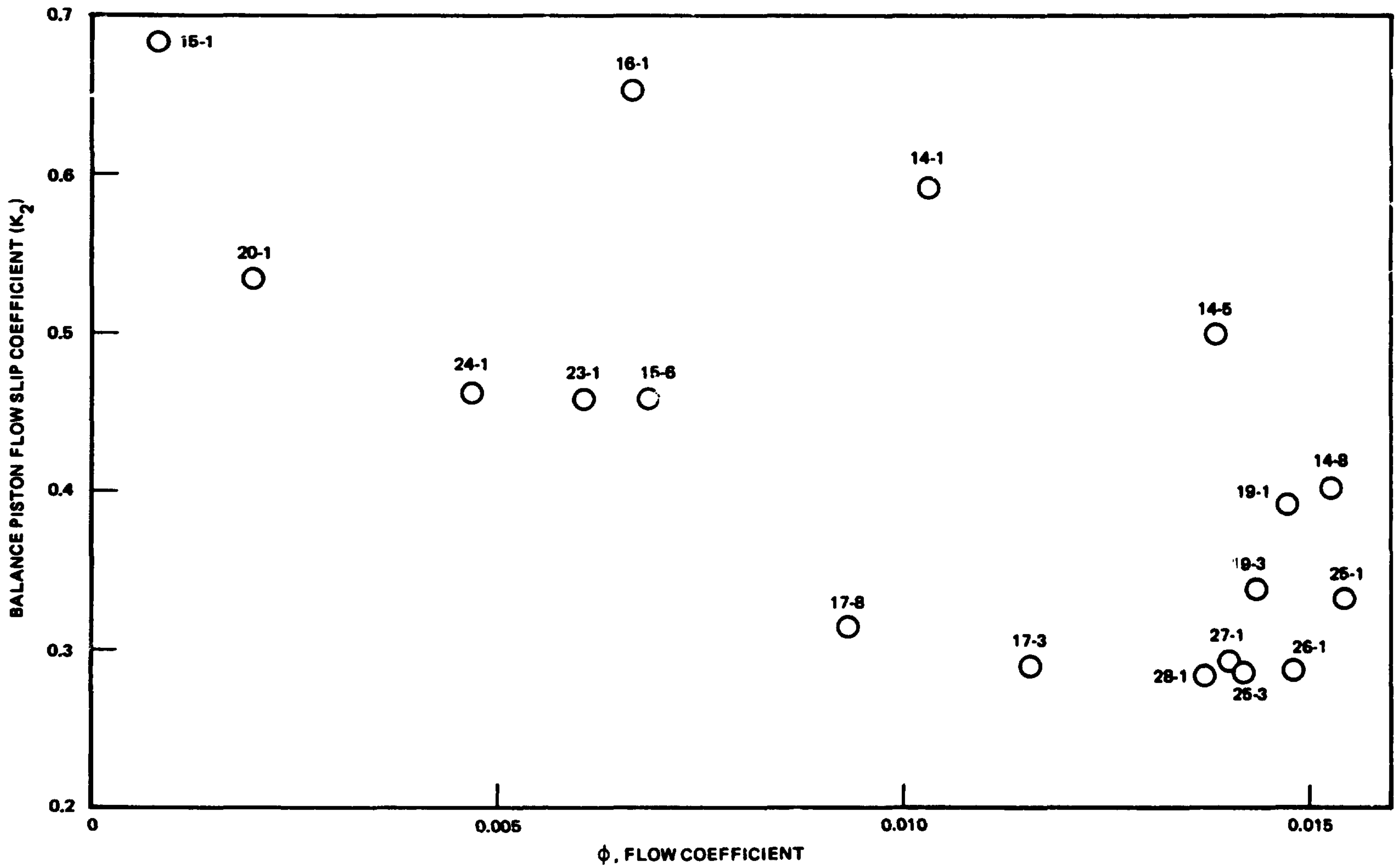

Figure 139. Balance Piston Flow Coefficient Effect on Slip Coefficient

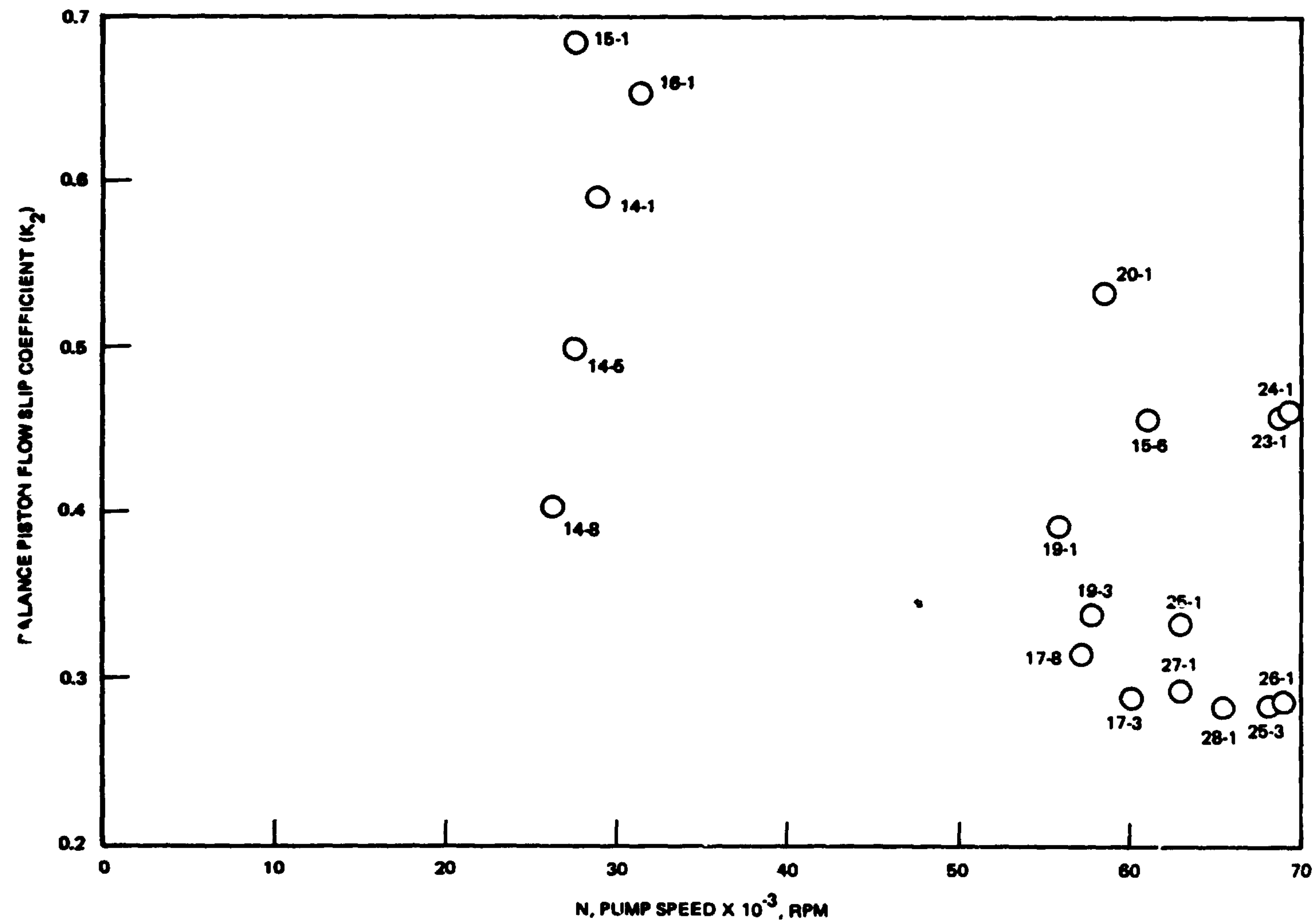

Figure 140. Speed Effect on Balance Piston Slip Coefficient

TABLE 22. MARK 48-0 BALANCE PISTON PARAMETERS

Test No.	Speed		Thrust Range (1)		Thrust at Match Point (2)		Range Factor (3)	X/δ at Match Point (4)
	rad/s	rpm	kN	pounds	kN	pounds		
14-8	2738	26157	4.4	984	10.6	2394	0.78	0.353
17-8	5979	57110	16.6	3732	29.0	6520	0.64	0.212
19-3	6034	57629	26.9	6046	28.0	6289	0.61	0.286
24-1	7241	69157	29.1	6542	31.5	7077	0.52	0.247
25-3	7140	68199	39.2	8803	36.6	8233	0.59	0.277

(1) Thrust Range = maximum balance piston force minus minimum balance piston force

(2) Thrust at Match Point = balance piston force at the position of the balance piston that matches the measured balance cavity pressure

(3) Range Factor = thrust at match point minus minimum balance piston force divided by thrust range

(4) X/δ at Match Point = distance from high-pressure orifice (X) divided by total balance piston travel (δ), with X selected at the position of the balance piston that matches the measured balance cavity pressure

As a general assessment, it can be said that this test series showed the balance piston to be operating in a satisfactory manner, particularly on those tests where part of the flow was bled overboard and, thereby, the return cavity pressure was reduced. To improve the margin in an internal recirculation mode, the size of the return flow passages should be enlarged.

Bearing Coolant Flow. Examination of the bearings posttest showed that the bearings had been overheated. There are two possible explanations:

1. The bearing was overheated during LN_2 tests.
2. The bearing was overheated during the LO_2 tests.

These two possibilities are distinguished because experience with bearings in LN_2 operation. Rocketdyne's experience in this fluid medium has been inconsistent, some tests indicating satisfactory operation, others showing definite signs of bearing distress. The bearings from the Mark 48 had a very similar appearance

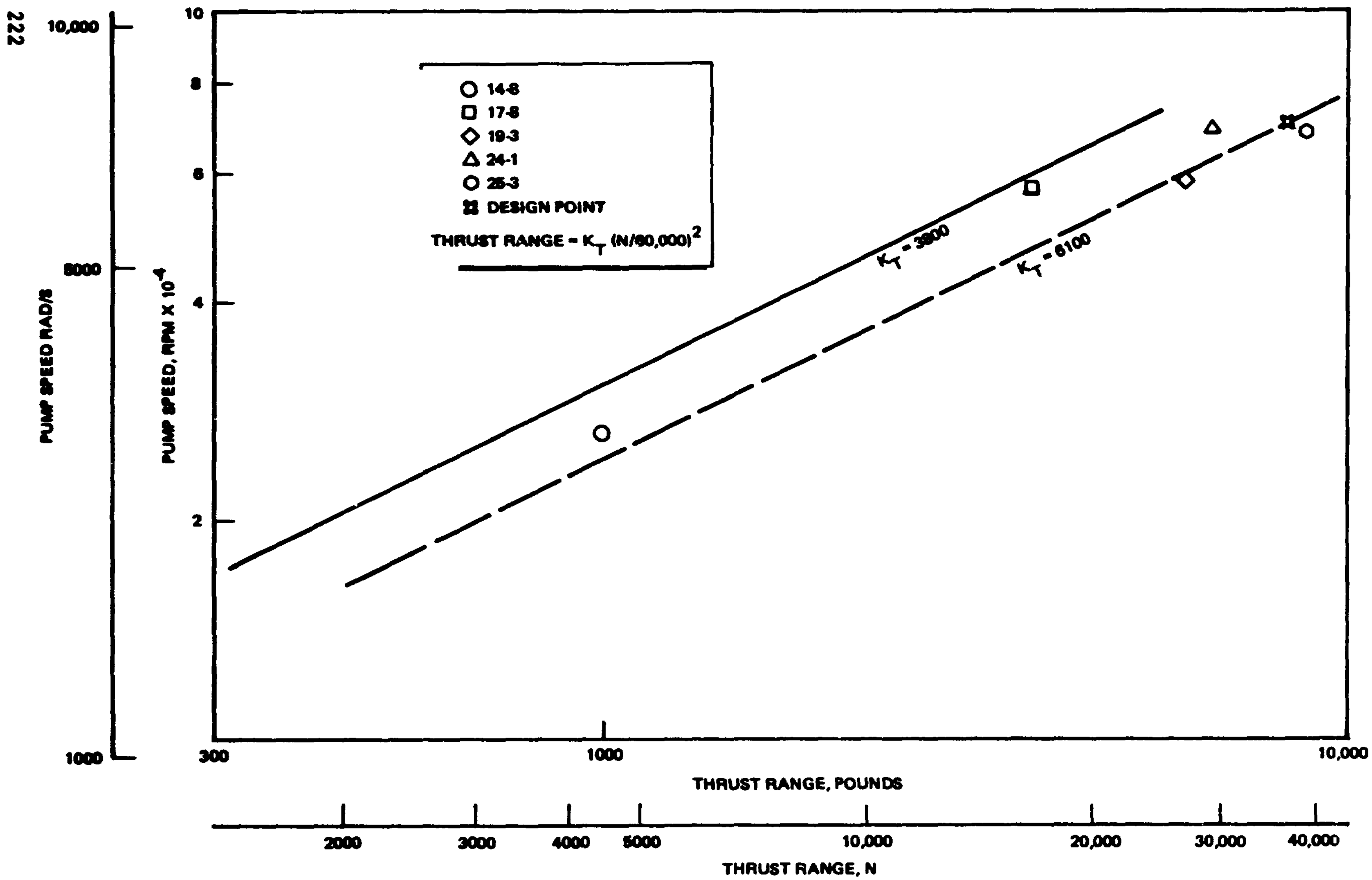

Figure 141. Balance Piston Thrust Range

to others damaged during LN_2 operation. Because of this earlier experience, the total test time in LN_2 was purposely kept to a minimum; three tests were conducted with a total duration of 44 seconds and a maximum rotor speed of 62,000 rpm.

Regardless of the LN_2 operation, however, there are indications that the LO_2 flow through the bearings could be substantially less than was desired and that the temperature of the coolant was potentially higher than expected. The data have already been used to show that the balance piston thrust range in some cases was less than the design range. This limitation was attributed to the higher resistance downstream of the balance piston sump. This same high resistance tends to restrict the coolant flow.

The overheating condition would be made worse by the possible larger loads carried by the bearing due to the inability of the balance piston to develop the thrust range desired in some instances. The load tracks on the bearings were wider than usual, indicating variable loading conditions.

The third factor affecting the bearing temperatures is the temperature of the coolant fluid itself in and around the bearings. Figure 142 shows the temperature in the balance piston return flow area as a function of speed. Many of the temperatures experienced are actually warmer than any encountered previously with LO_2 bearings. It is desirable to keep the temperature down to approximately 110 K (200 R). The data in Fig. 142 show temperatures as high as 160 K (290 R) at speeds of 60,000 rpm. The higher temperatures noted on the earlier tests were a cause of concern that led to the action of opening an instrumentation line as an overboard bleed of the balance piston flow return cavity. This change was made effective on test 19 and subsequent and, even though the return port was small, the data of Fig. 142 show that there was a definite tendency to lower the temperature in this cavity. Subsequent tests were able to get to speeds of 7330 rad/s (70,000 rpm) or higher without exceeding approximately 130 K (235 R). Thus, the overheating initially must be at least partially due to insufficient coolant flowrate out of this cavity area. This same problem leads to a higher back pressure at the balance piston sump, and results in the lower thrust range previously reported.

Further analyses to explore the coolant flow problem should be conducted. These analyses can be expected to cover the effects of the heating due to power disk drag on the back side of the impeller and on the slinger. Preliminary analyses indicate that, at 7330 rad/s (70,000 rpm), the impeller back side power disk drag could easily result in a temperature increase of 17 K (30 R), with the flows calculated in analyzing the balance piston performance. This could explain the temperatures observed during tests.

In conclusion, the bearings show definite signs of overheating. There is no way to determine which tests contributed most to the overheating problem. The whole overheating effect could be due to the tests in LN_2 only, or it could be due to only the tests prior to test 19, where much higher temperatures were experienced. An analysis is required to at least establish sufficient flow through the bearings and return cavity area to keep the temperatures no higher than those experienced on the last tests of the series reported herein.

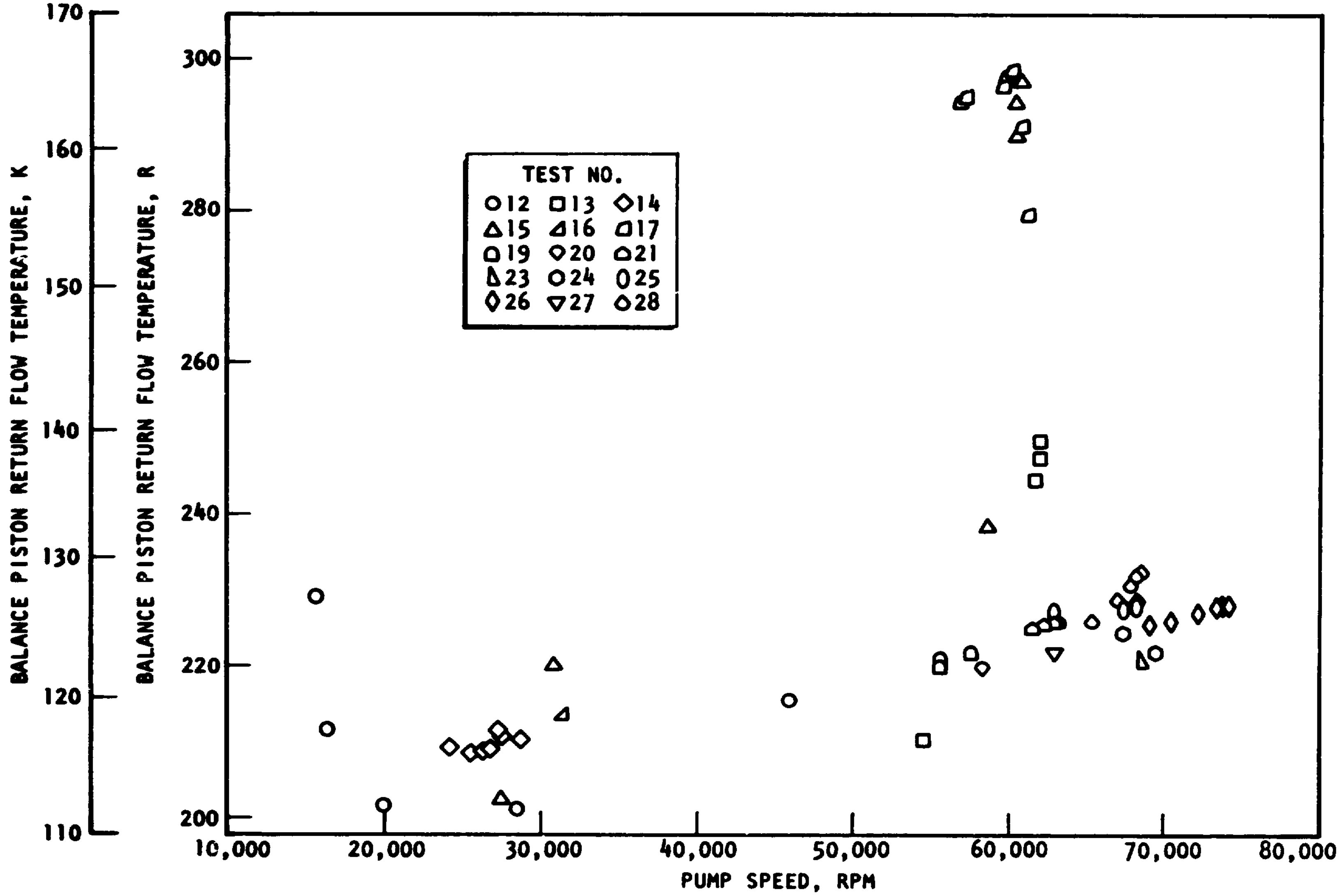

Figure 142. Mark 48-O Turbopump Speed vs Balance Piston Return Flow Temperature

Turbine Performance. Turbine test data for the performance analysis were obtained with instrumentation located as follows:

Turbine Test Parameter	Location
Inlet Static Pressure (P_{s_1}) psia Inlet Total Pressure (P_{t_1}), psia Inlet Total Temperature (T_{t_1}), R	Upstream of the turbine inlet manifold at gas generator interface flange
Exhaust Static Pressure (P_{s_2}), psia Exhaust Total Pressure (P_{t_2}), psia Exhaust Total Temperature (T_{t_2}), R	At the duct downstream of the turbine discharge manifold flange
Speed (N), rpm	Signal obtained at the turbopump shaft
Working Fluid, Mass Flowrate (W_{t_1}), lb/sec	Calculated with gas generator venturi

Tests 11 through 18 were conducted with GH_2 turbine working fluid, and tests 19 through 28 utilized LO_2/LH_2 preburner combustion products to drive the turbine. For the initial tests, 11 through 13, liquid nitrogen was used in the pump, while tests 14 through 28 were run with LO_2 in the pump.

The turbine was tested as an individual component at the Wyle Laboratories for purposes of calibration. These calibration tests were performed with better instrumentation and test operating condition control than is achievable in the turbopump tests. The testing and results from the calibration series have been discussed previously, and the data from those tests are considered to be the best data for defining turbine efficiency. However, the data from the turbopump tests were used in a twofold manner:

1. To determine the turbopump machine efficiency

2. To calculate a turbine efficiency for comparison with the calibration test results

Data from test 24-1 are used as a sample case in the discussions dealing with data reduction procedure and turbine demonstrated performance, because it is the LO_2/LH_2 turbine test with the velocity ratio closest to that of the turbine design (0.345).

Turbine test efficiency is calculated with the following analysis procedure based on turbopump tests:

1. The turbopump machine efficiency is first established by dividing pump delivered fluid horsepower (which is calculated with pump developed head, pump flowrate, and fluid density) by turbine ideal horsepower (evolved with turbine isentropic available energy and mass flowrate).

2. Turbine test efficiency is established by dividing the machine efficiency with pump isentropic efficiency (see Fig. 137 under Pump Hydrodynamic Performance).

At the outset of the turbine analysis, the turbine inlet pressure is adjusted for an estimated 2% pressure loss. The fluid loss starts at the station where the total inlet pressure is measured, and is sustained for the flow distance up to the nozzle entrance plane. The loss assigned to this calculation is based on experience with similar design turbine installations, manifolds, and working fluids, and is charged to the engine system in a staged combustion cycle. Turbine inlet total enthalpy is calculated at the entrance to the nozzle. Thus,

Turbine pressure ratio (total to static), PR (T-S) $= \frac{2460}{1409} = 1.746$

Turbine isentropic enthalpy drop, h_s (T-S), Btu/lb = 384.4

Turbine theoretical spouting velocity, C_o, ft/sec = 4388

Turbine pitch line velocity, U_m, ft/sec = 1418

Turbine velocity ratio, $U_m/C_o = 0.323$

$$\text{Turbopump Machine Efficiency} = \frac{\text{Pump Fluid Horsepower}}{\text{Turbine Ideal Horsepower}} = \eta \text{ T/P Machine} \quad (1)$$

$$\text{where turbine ideal horsepower} = 1.4145\ (\Delta h_s)\ (W_t)$$
$$= 1.4145\ (384.4)\ (2.715) = 1476.6$$

$$\eta \text{ T/P machine} = \frac{415.9}{1476.6} = 0.2817$$

$$\text{Turbine Efficiency} = \frac{\text{T/P machine}}{\text{Pump ideal}} = \frac{0.2817}{0.618} = 0.456 \quad (2)$$

The calculated turbopump machine efficiency versus turbine velocity ratio plot is presented in Fig. 143; the performance data are representative of test speeds ranging from 1623 to 7768 rad/s (15,500 to 74,191 rpm). All the data are below the predicted machine efficiency curves, which was to be expected based on the low pump efficiencies presented in the previous section.

A check of turbopump test data near the turbine design velocity ratio (U_m/C_o = 0.345) indicates the machine efficiency varies from 0.272 to 0.333; this represents an approximate ±10% maximum variation from the average machine efficiency of 0.300. Figure 144 presents the turbine efficiency calculated by dividing the machine efficiency (Fig. 143) by the pump isentropic efficiency (Fig. 137). The data bracket the calibration curve, but show a definite trend of variation with turbine velocity ratio. At the extreme values of U/C_o, the data are off by 10 efficiency points, being 10 points high at high U/C_o and 10 points low at the other end.

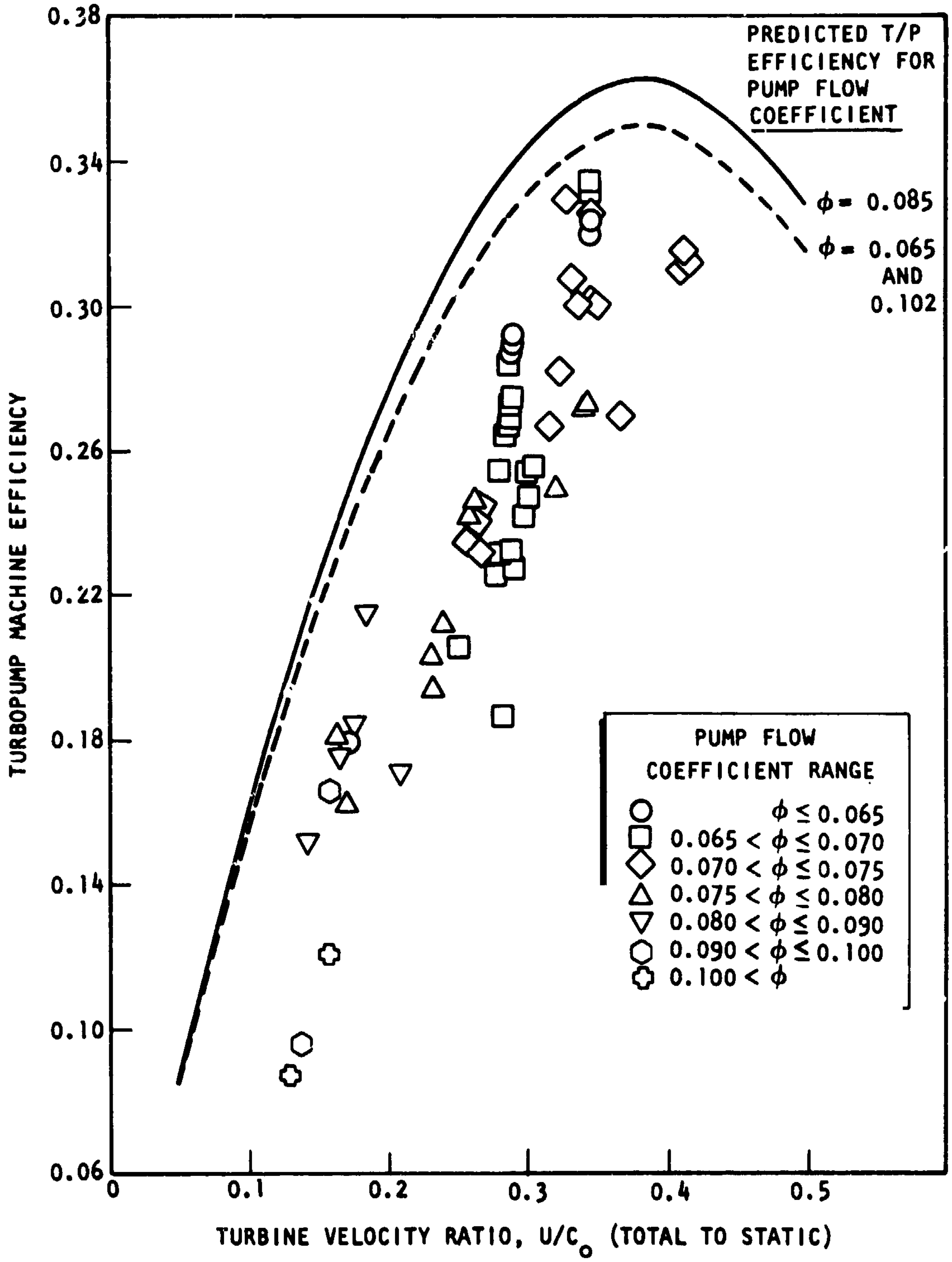

Figure 143. Turbine Velocity Ratio vs Turbopump Machine Efficiency

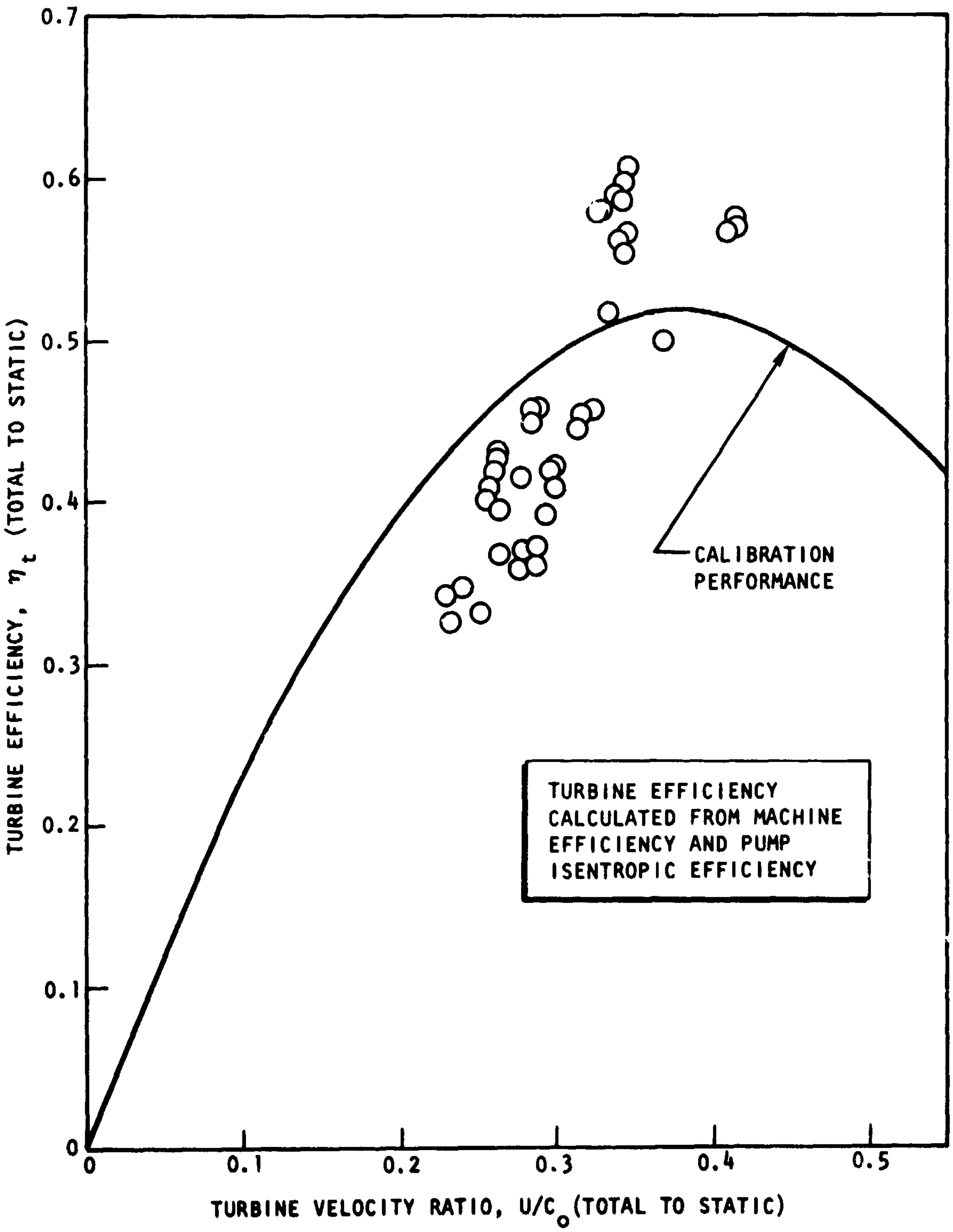

Figure 144. Turbine Velocity Ratio vs Efficiency

Such scatter in turbine efficiency based on the available data is not surprising and, in fact, is the very reason that a more carefully controlled turbine calibration effort was conducted prior to the turbopump testing.

The precision of turbine pressure, temperature, working fluid mass flow, and speed test data affect test results. The plots in Fig. 145 and 146 were made to illustrate quantitatively how turbine inlet temperature and turbine pressure ratio influence turbine performance. With the turbine test parameters from test 24-1 as a reference (and using as an example a calculated turbine efficiency rather than the calibration value), the turbine inlet temperature and pressure ratio were perturbated, i.e., temperature from 814 to 926 K (1467 to 1667 R) and pressure ratio from 1.587 to 1.880 total to static. Estimates of how these data shifts, due to instrumentation error or other causes, can affect turbine performance calculations are tabulated below and plotted in Fig. 145 and 146.

	Variable	Percent Change	Efficiency Change (Points)
(a)	Turbine Inlet Temperature	Minus (1) 2	-0.9
(b)	Turbine Pressure Ratio	Plus (+) 2	-1.8
	Total (a) + (b)		-2.7

No allowance has been made for the precision of the speed and turbine inlet pressure data.

Another factor which influenced the turbine performance is the turbine mass flowrate data. For these tests, the total LO_2/LH_2 turbine W_t was established with four separate oxidizer and fuel venturi meters (LO_2 and LH_2 flow at the preburner, and GO_2-GH_2 flow to the igniter); mass-flow was calculated with flow coefficients at the respective flow stations. Furthermore, problems were experienced with the venturi measurements on several tests, which necessitated calculating flowrates by secondary means. Therefore, if all the above factors are taken into consideration (pump efficiency, instrumentation error, and mass flow precision), the efficiency data point scatter in Fig. 143 and 144 can be readily understood.

A comparison of turbopump test results with turbine calibration data shows that the turbine efficiency is scattered about the turbine calibration data, thereby indicating some substantiation. It should be noted that calibration data were obtained under conditions more suitable to higher precision and, therefore, the turbine efficiency obtained from the calibration tests should be considered most representative of turbine performance.

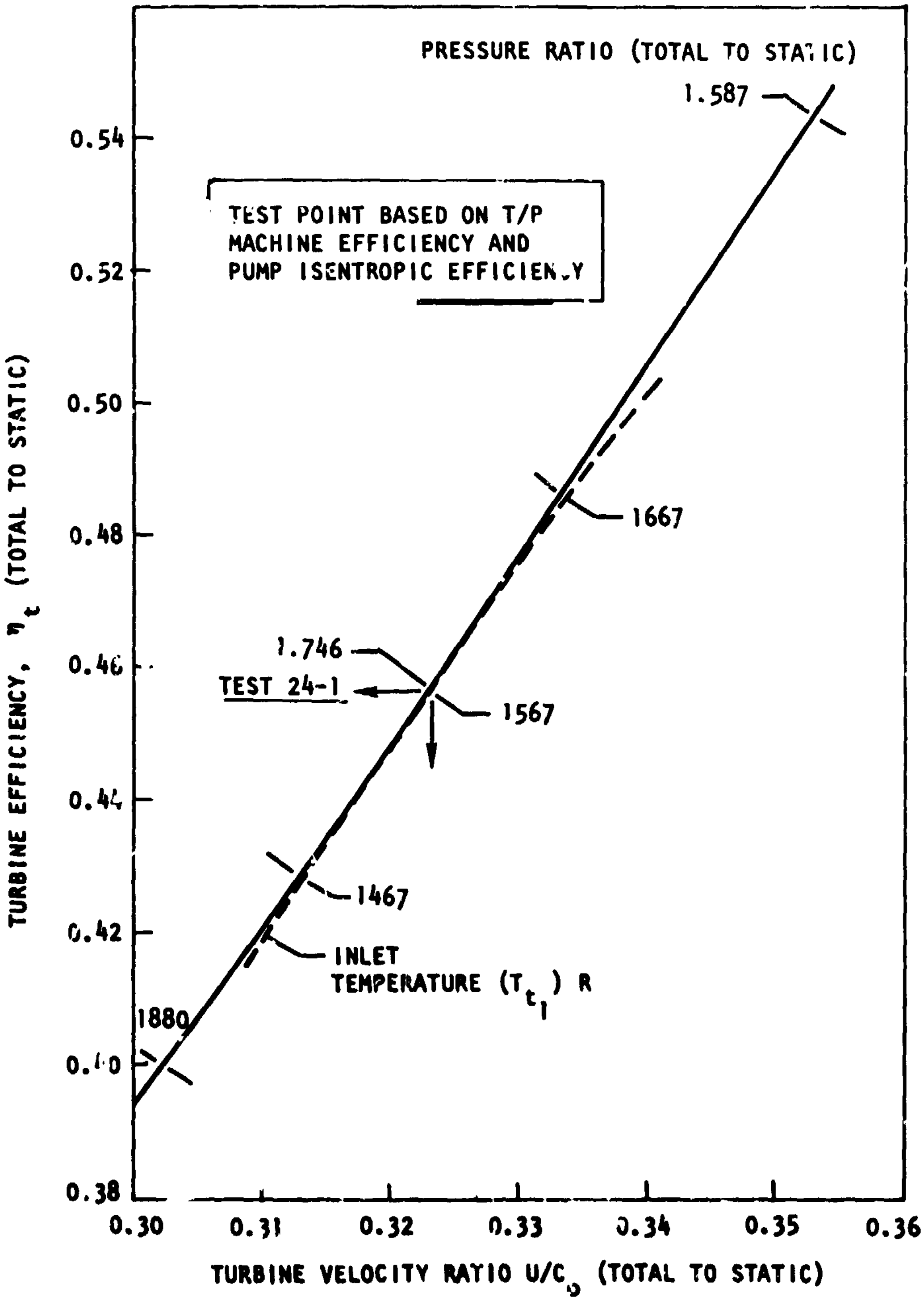

Figure 145. Turbine Velocity Ratio vs Efficiency

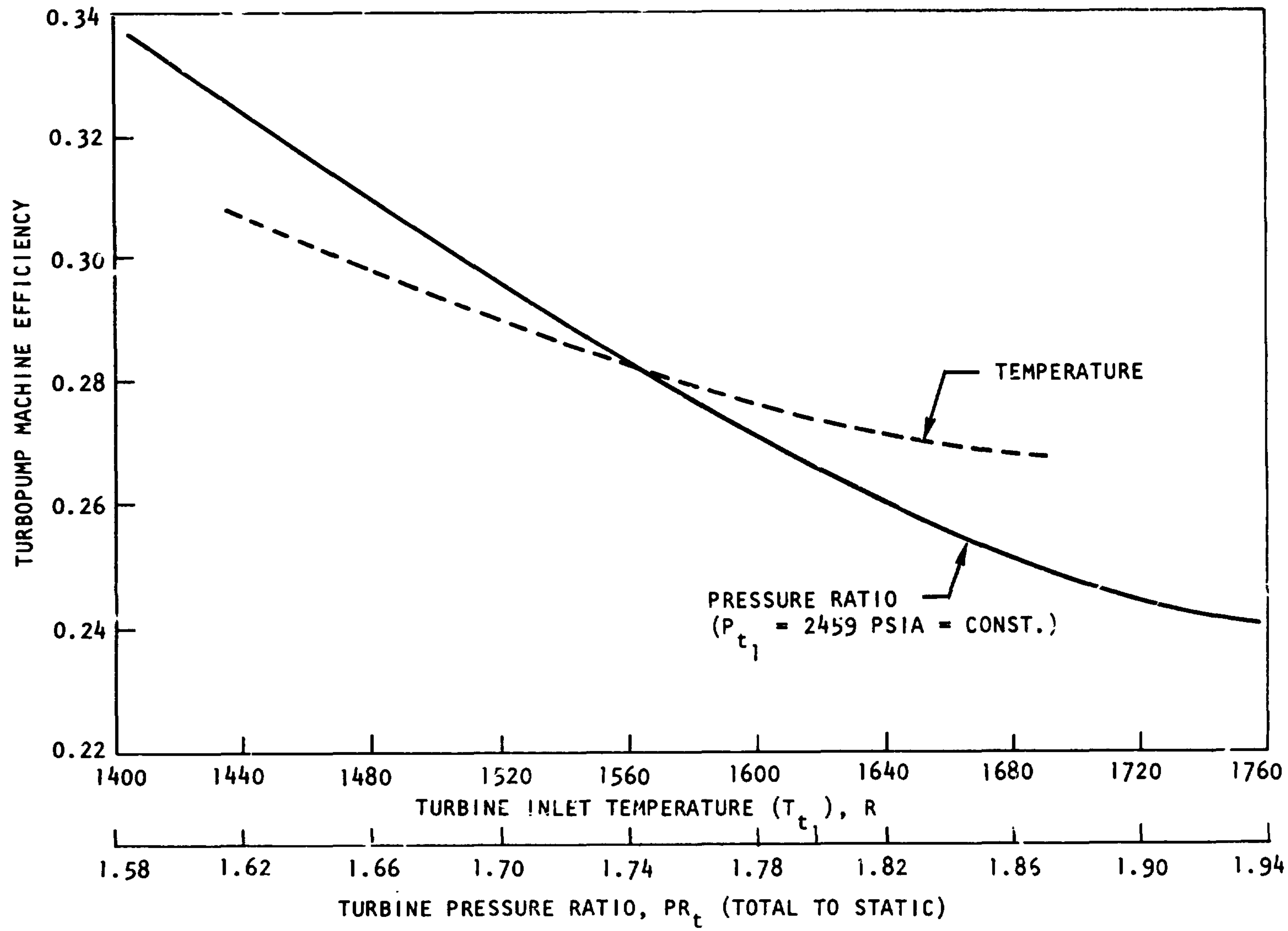

Figure 146. Turbine Pressure Ratio and Inlet Temperature vs. Turbopump Machine Efficiency

Mechanical Performance. Testing of the LO_2 turbopump encompassed 18 starts, with a total accumulated time of 267 seconds. The three initial tests were conducted with LN_2 as the pump fluid; in subsequent tests, LO_2 was used. The first seven tests were performed using ambient-temperature GH_2 to drive the turbine; in the remainder of the test, the combustion product of LH_2 and LO_2 at approximately design temperature was the turbine propellant. The longest test durations conducted were 70 seconds with ambient H_2 drive and 41 seconds with hot-gas drive. The operation covered a rotor speed range of 0 to 7768 rad/s (74,191 rpm); a maximum pump discharge pressure of 3175 N/cm^2 (4606 psia); and a maximum turbine inlet temperature of 1133 K (2040 R).

Several tests were terminated by the vibration sensor device monitoring the output of the accelerometers attached to the turbopump housing. This was caused by a combination of several factors. Normally on a new turbopump several tests are required to establish its vibration signature and thus set the cutoff point at the appropriate levels. It appears that with the Mark 48-0 turbopump, this level is in the 20 to 25 g rms range in conjunction with a 2K Hz low-pass filter. Some of the early runs were terminated because the cutoff redline was set too low. In addition, the manual GH_2 feed control system employed on the first seven runs frequently resulted in slow transition through critical speed zones, with attendant buildup in vibration levels.

Bently data and accelerometer data obtained from high-frequency tapes showed increased synchronous activity at 4115, 5026, and 5528 rad/s (39,300, 48,000, and 52,800 rpm). These compared favorable with the analytically predicted critical speeds of 4723 and 5482 rad/s (45,108 and 52,363 rpm), respectively. No evidence of subsynchronous vibration was present in the data.

The measured seal drain pressures, temperatures, and flowrates were, in general, in good agreement with predicted values, indicating proper functioning of the shaft seals. During chilldown of the pump on the LN_2 tests, it was noted that the secondary hot-gas drain line frosted over. This could occur as a result of heat transfer through conduction, but possibly also as a result of the pump fluid from the primary LO_2 seal drain cavity leaking across the intermediate seal. To prevent a potentially hazardous condition, the purge pressure level in the intermediate seal was raised to 138 N/cm^2 (200 psig). No problem was experienced at this pressure level with mixing of incompatible fluids. It is quite possible that the originally planned purge pressure of 41 N/cm^2 (60 psig) would be adequate. This could be established on future tests by sampling and analyzing the drain fluids during chilldown.

The turbopump was disassembled after the test series to permit visual inspection of the components. Figure 147 show the condition of the more significant parts. The condition of most of the components was excellent; only two discrepancies were apparent: The pump-end bearings showed evidence of overheating, and the chrome plating on the rotor under the primary hot-gas seal ring flaked off.

Figure 148 shows the condition of the inducer and impeller: neither part had any adverse after effects from the testing. As experienced, superficial rubbing contact took place at the tips of the inducer vanes and at the impeller front shroud labyrinths. In Fig. 149 the impeller and the diffuser are included to

1XY55-8/31/76-C1A*

Figure 147. Mark 48-0 Components After Testing

ORIGINAL PAGE IS
OF POOR QUALITY

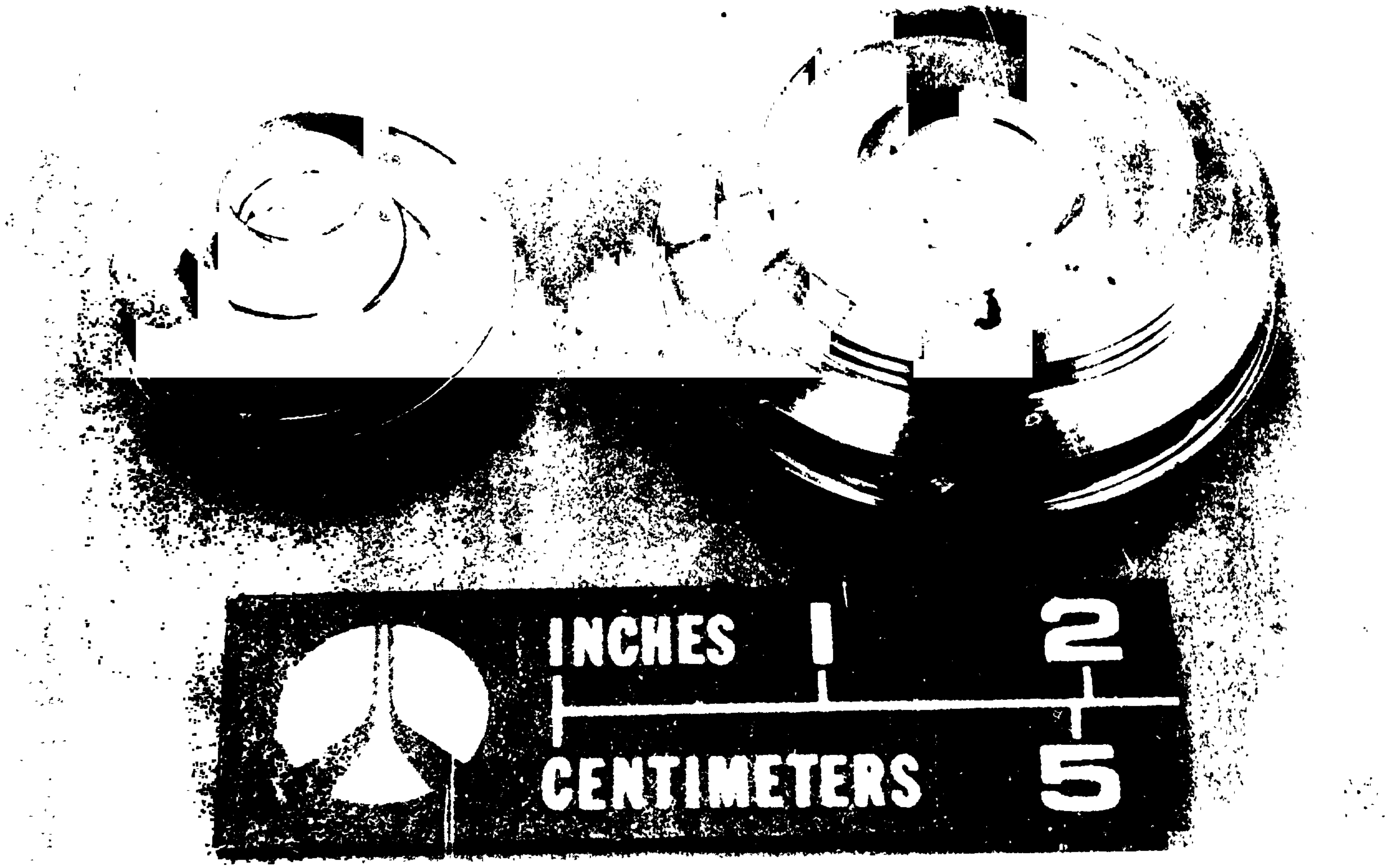

1XY55-8/31/76-C1G*

Figure 148. Mark 48-0 Inducer and Impeller After Testing

1XY55-8/31/76-C1E*

Figure 149. Mark 48-0 Impeller and Diffuser After Testing

illustrate the condition of the balance piston low-pressure orifice elements as well as the stationary land of the high-pressure orifice. There was no sign of contact at either orifice.

Components of the rotating assembly and the shaft dynamic seals are shown in Fig. 150 and 151, respectively. The only discrepancy noted on the seals was a slight roughness on the inner diameter of the turbine-side ring of the primary hot-gas seal, under which the chrome plate flaking occurred. Figure 152 illustrates the appearance of the sealing surfaces on the rotor. The surfaces under the primary LO_2 seal and intermediate seal rings are in excellent condition. On the other hand, some of the chrome plating flaked off under the primary hot-gas seal rings. Difficulty has been experienced during fabrication of the rotor in obtaining a sound plating in this area, but it is anticipated that, with more stringent quality control and engineering surveillance over the process, a satisfactory plating can be achieved.

The turbine-end and pump-end bearings are shown in Fig. 153 and 154, respectively. The condition of the turbine-end bearings was excellent. There was no evidence of overheating or excessive loading. In contrast, the balls of the pump-end bearings were discolored and a piece spalled from one of the balls. The cage pocket which contained the spalled ball was worn. Wear tracks on the races indicated high and varying load levels. The overheating is attributed to insufficient coolant flow caused by high resistance in the balance piston return flow passages. (See discussion under Pump Hydrodynamic Performance).

The remaining components, including the pump and turbine housings and supports, were in excellent condition. There was no sign of structural failure, excessive deflection, or other deterioration.

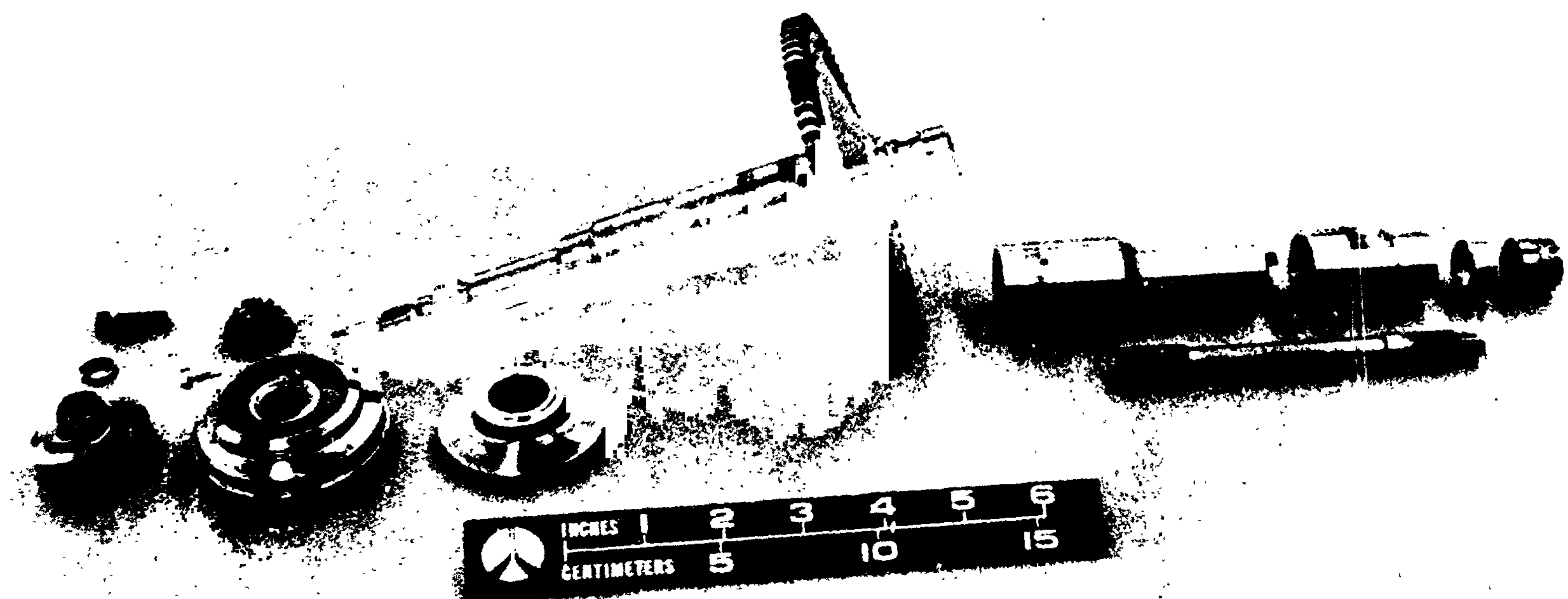

1XY55-8/31/76-C1F*

Figure 150. Mark 48-0 Rotating Parts After Testing

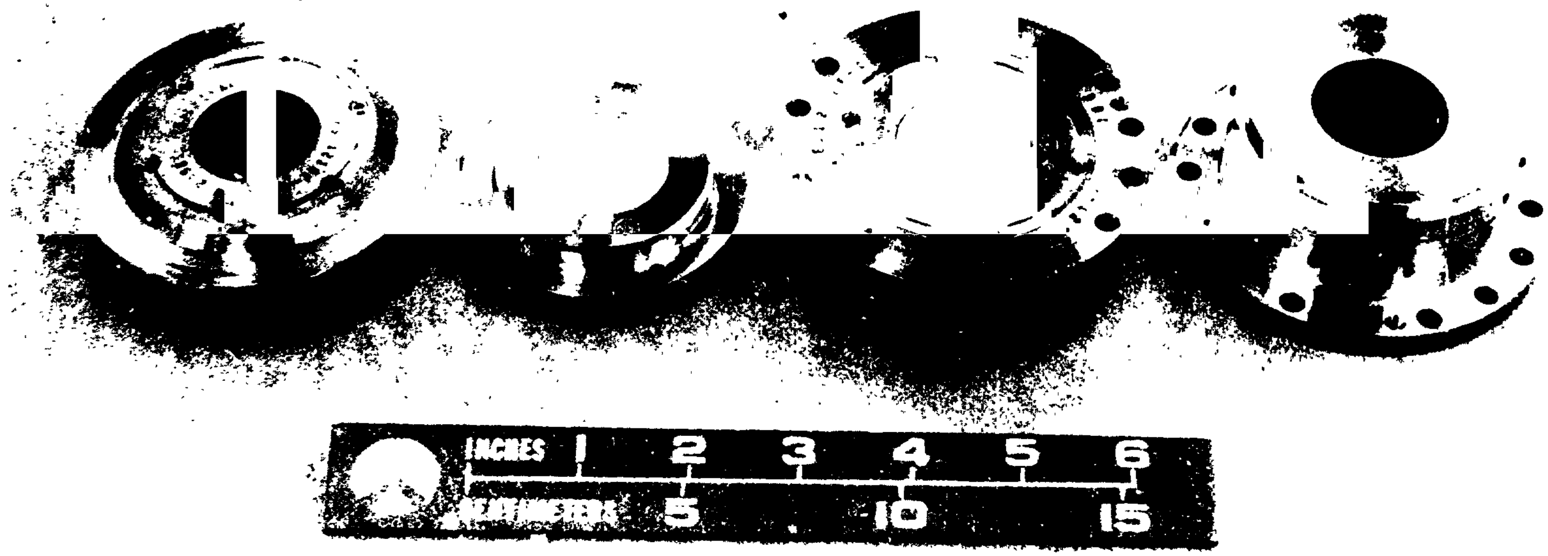

1XY55-8/31/76-C1D*

Figure 151. Mark 48-0 Seals After Testing

ORIGINAL PAGE IS
OF POOR QUALITY

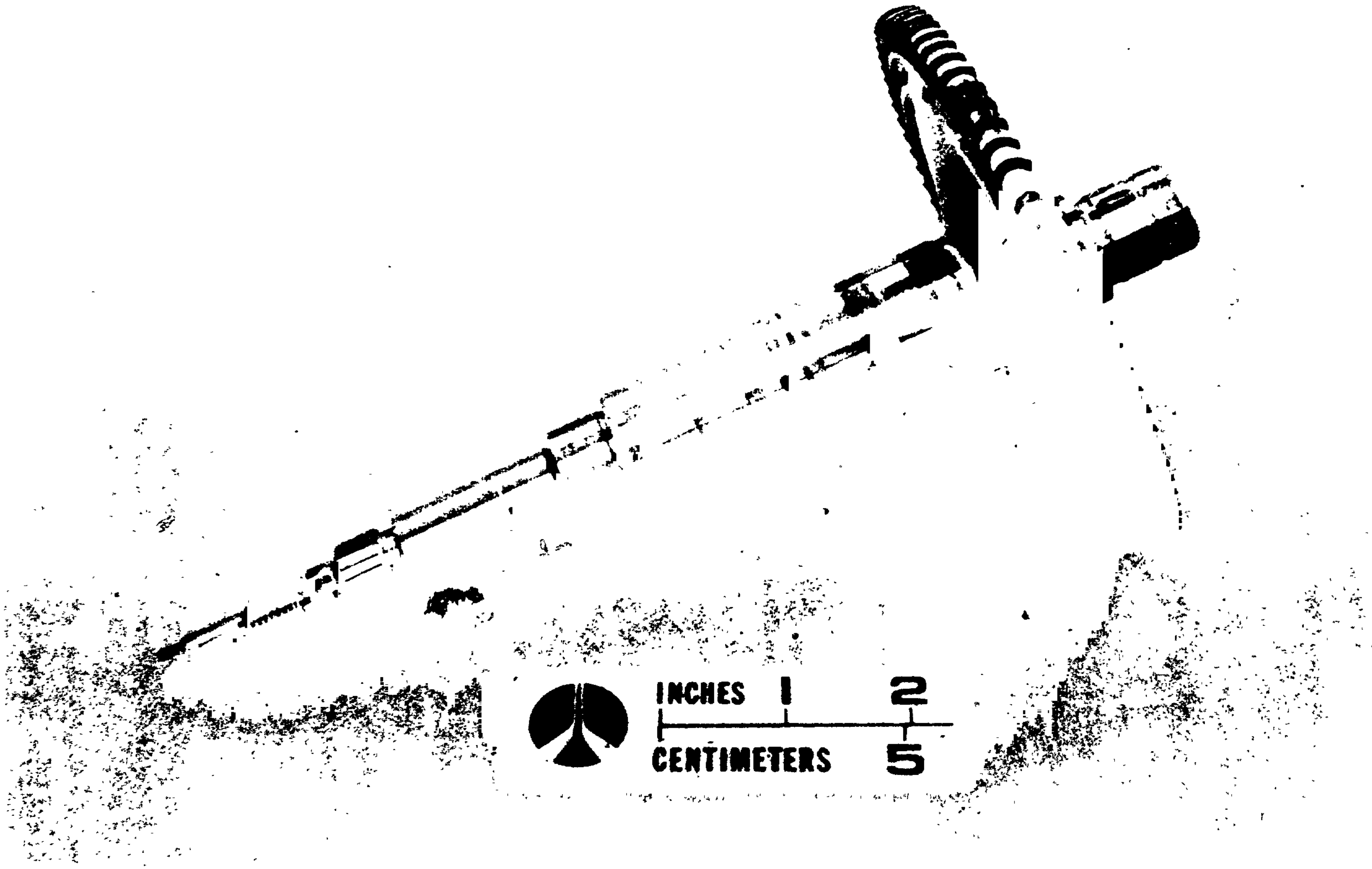

1XY55-8/31/76-C1H*

Figure 152. Mark 48-0 Rotor After Testing

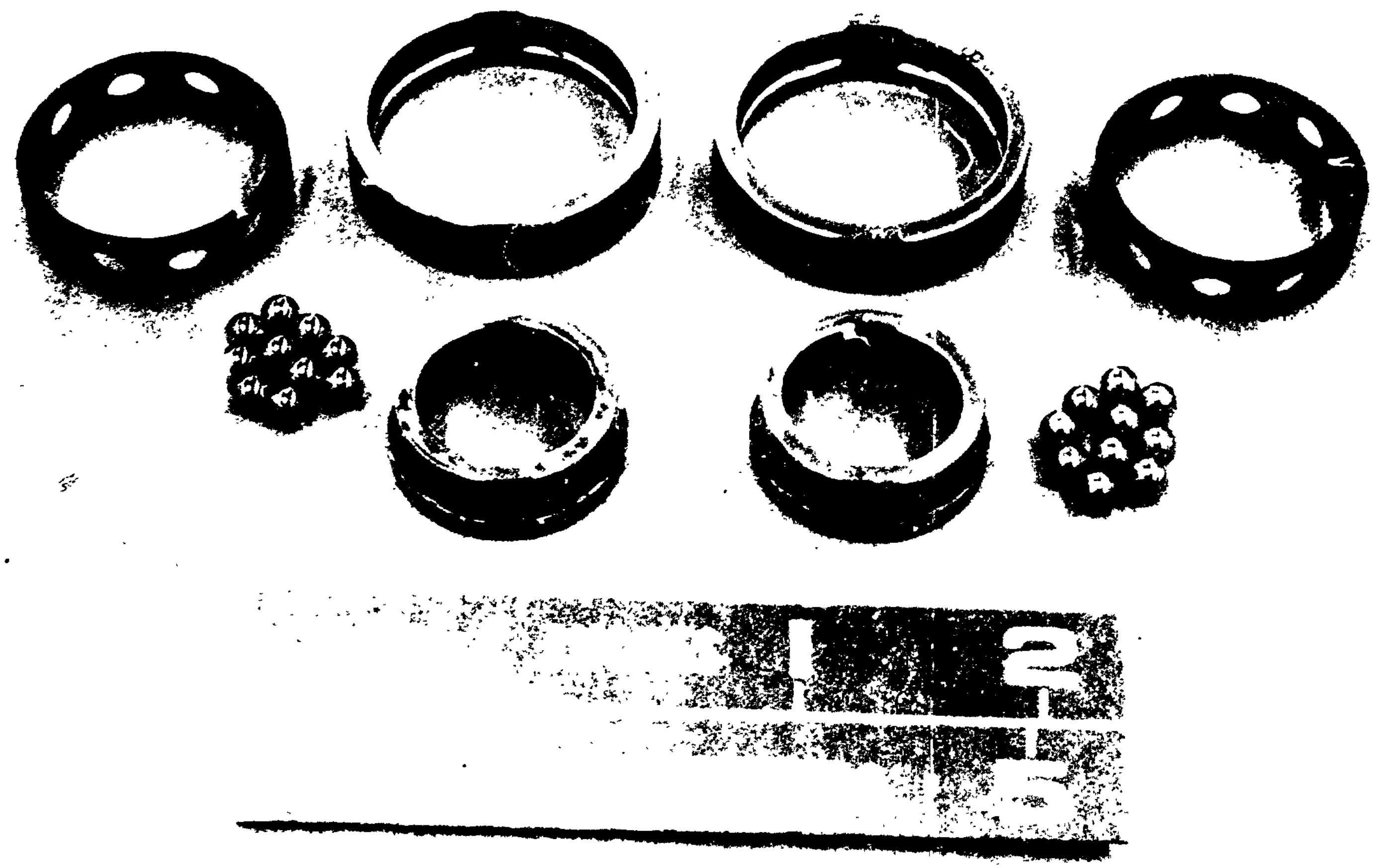

1XY55-8/31/76-C1B*

Figure 153. Turbine-End Bearings After Testing

ORIGINAL PAGE IS
OF POOR QUALITY

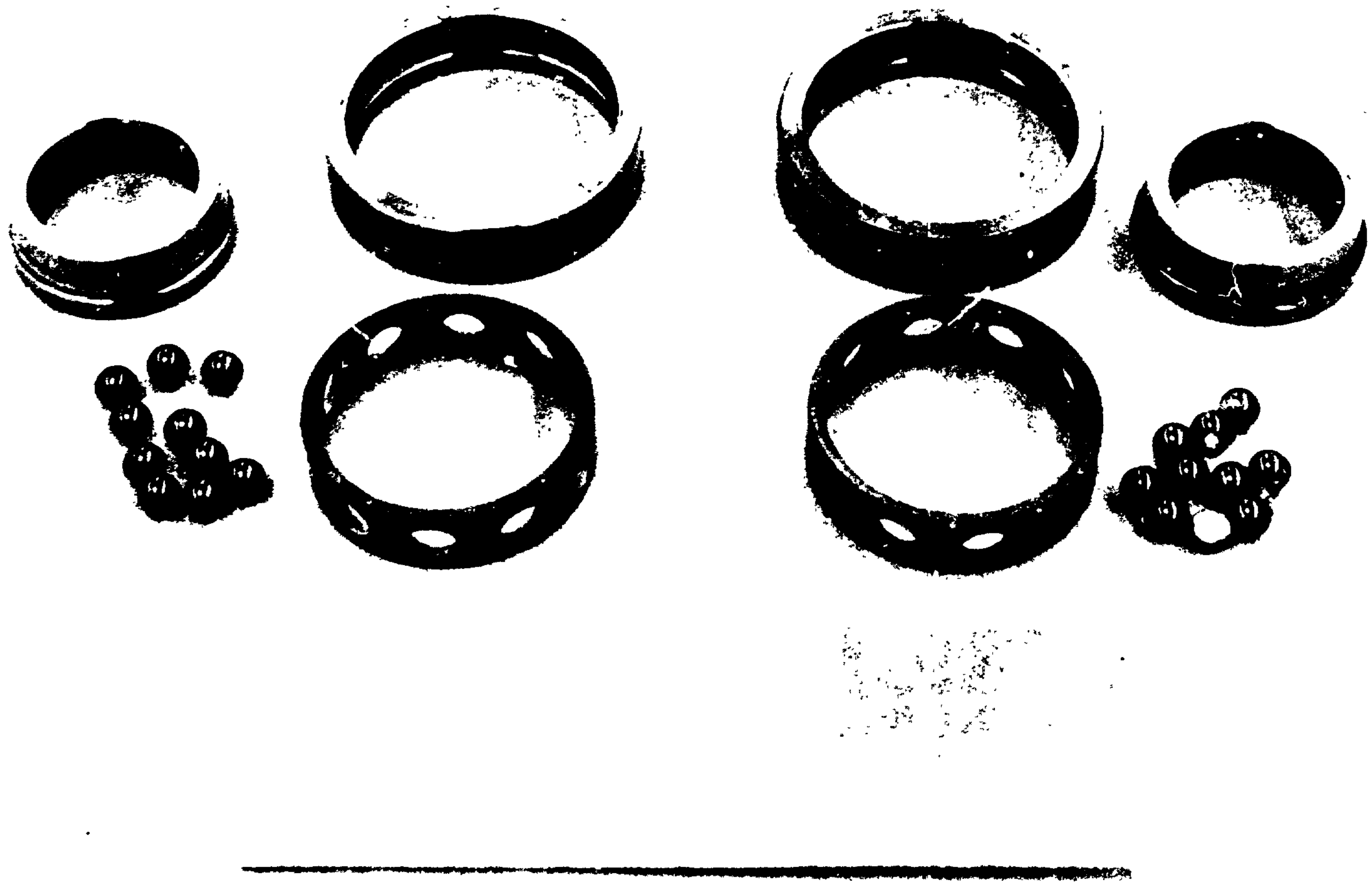

1XY55-8/31/76-C1C*

Figure 154. Pump-End Bearings After Testing

ORIGINAL PAGE IS
OF POOR QUALITY

APPENDIX A

DESIGN GROUND RULES

APPENDIX A

DESIGN GROUND RULES

General

Components which are subject to a low cycle fatigue mode of failure shall be designed for a minimum of 300 cycles times a safety factor of 4.

Components which are subject to a fracture mode of failure shall be designed for a minimum of 300 cycles times a safety factor of 4.

Components which are subject to a high cycle fatigue mode of failure shall be designed within the allowable stress range diagram (based on the material endurance limit). If stress range material property data are not available, modified Goodman diagrams constructed as shown below shall be utilized.

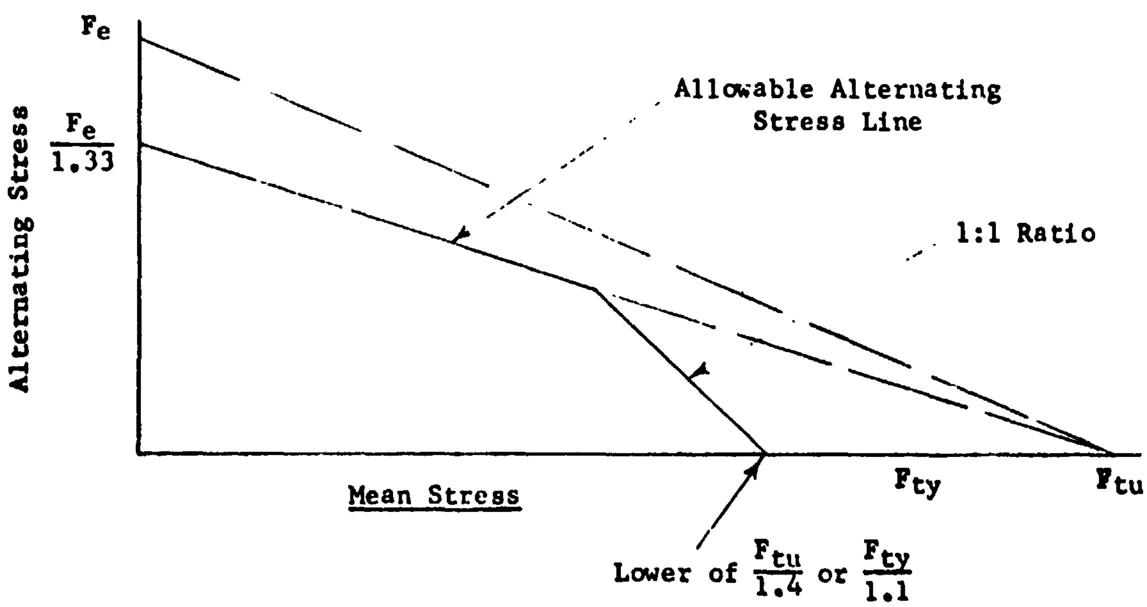

F_e = Material Endurance Limit
F_{ty} = Material Yield Strength (.2% offset)
F_{tu} = Material Ultimate Strength

Effective stress shall be based on the Mises-Hencky constant energy of distortion theory.

Unless otherwise noted under component ground rules specified herein, the following minimum factors of safety shall be utilized:

Factor of Safety (.2% yield) = 1.1 x Limit Load

Factor of Safety (Ultimate) = 1.4 x Limit Load

Limit Load: The maximum predicted load or pressure at the most critical operating condition

Components subject to pressure loading shall be designed to the following minimum proof and burst pressures:

Proof Pressure = 1.2 x Limit Pressure

Burst Pressure = 1.5 x Limit Pressure

Impeller

Inducers and/or impellers utilized in the high pressure pumps shall be designed for operation above incipient cavitation.

Impeller burst speed shall be at least 20% above the maximum operating speed.

Impeller effective stress at 5% above the maximum operating speed shall not exceed the allowable .2% yield stress. (Does not apply to areas in which local yielding is permitted.)

Turbine

Blade root steady-state stress shall not exceed the allowable 1% ten hour creep stress.

Stress state at the blade root as defined by the steady-state stress and an assumed vibratory stress equal to the gas bending stress shall be within the allowable stress range diagram or modified Goodman diagram.

No blade natural frequencies within ±15% of known sources of excitation at steady-state operating speeds.

Disk burst speed shall be at least 20% above the maximum operating speed.

Disk maximum effective stress at 5% above the maximum operating speed shall not exceed the allowable .2% yield stress. (Does not apply to areas in which local yielding is permitted).

Bearings

Turbopump designs shall utilize ball bearings.

Maximum DN: 1.5×10^6

B_{10} life 100 hours

Material:

Rolling Elements	440C
Races	440C

Seals

Turbopump designs shall utilize concentional type seals. However, provision shall be made in the design to permit the incorporation (retrofit) of controlled fluid film (hydrodynamic) face seals. Any rework or modification of the turbopump housing or other component parts in the area of the seals to accommodate the hydrodynamic seals shall be specified. Such modifications should be kept to a minimum.

Face contact seal maximum PV, FV, and P_fV factors:*

	LO_2	H_2+H_2O
PV Factor	25,000	10,000
FV Factor	2,000	800
P_fV Factor	60,000	20,000

*PV = unit load times rubbing velocity (lb/in^2 x ft/sec)
FV = face load per unit length times rubbing velocity (lb/in x ft/sec)
P_fV = fluid pressure differential times rubbing velocity (psig x ft/sec)

Critical Speed

Rotor bending frequency shall be at least 25% above the rotor maximum operating speed.

A minimum margin of 20% shall be maintained between rotor rigid body critical speeds and rotor steady-state operating speeds at full thrust and the pumped-idle thrust condition. Rigid body critical speeds within the throttled-to-full thrust range shall be permitted only if deemed necessary by both the Contractor Program Manager and the NASA Project Engineer.

APPENDIX B

MARK 48-0 TURBOPUMP ASSEMBLY
DRAWING RS009320E

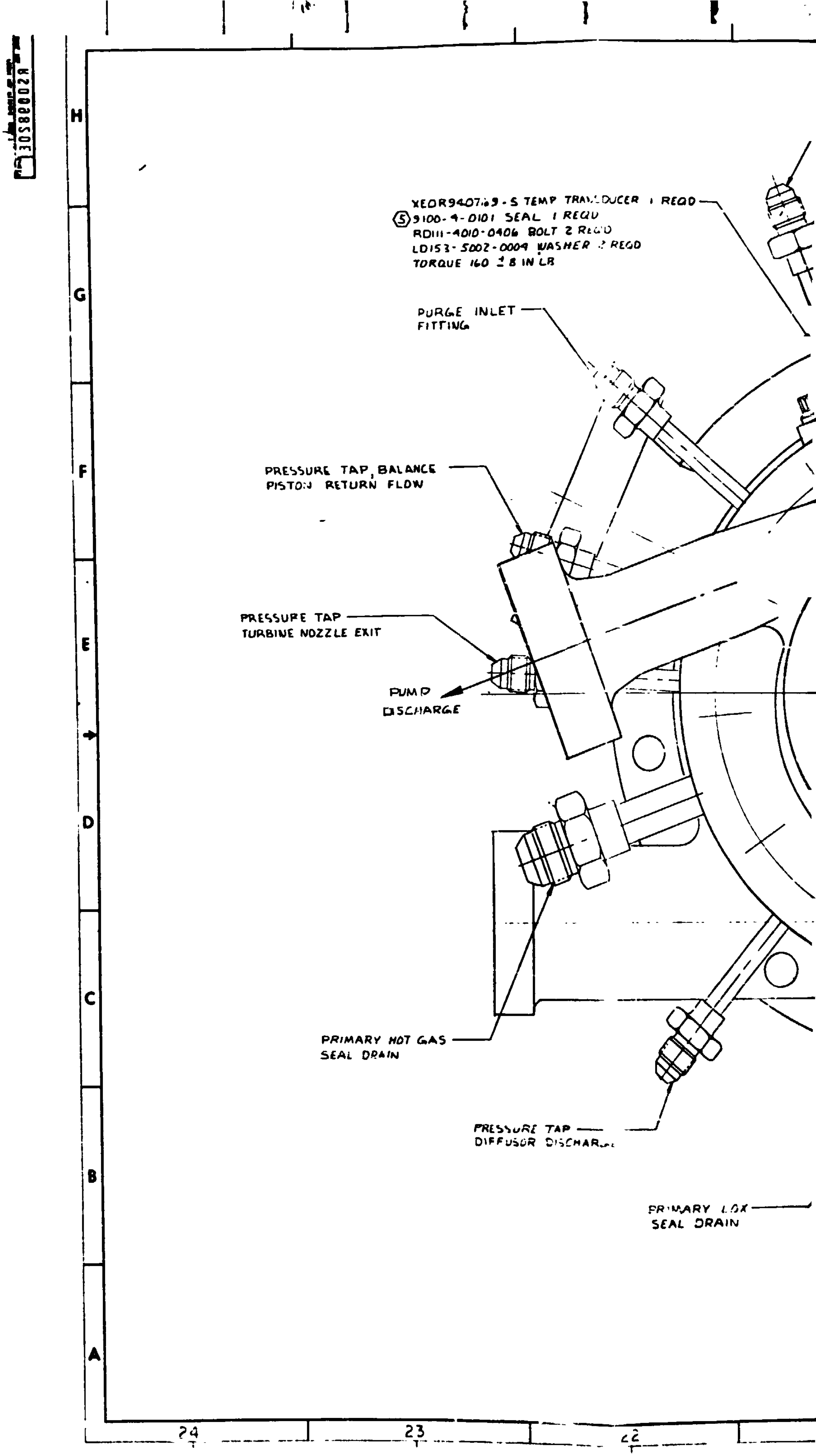

FOLDOUT FRAME 1

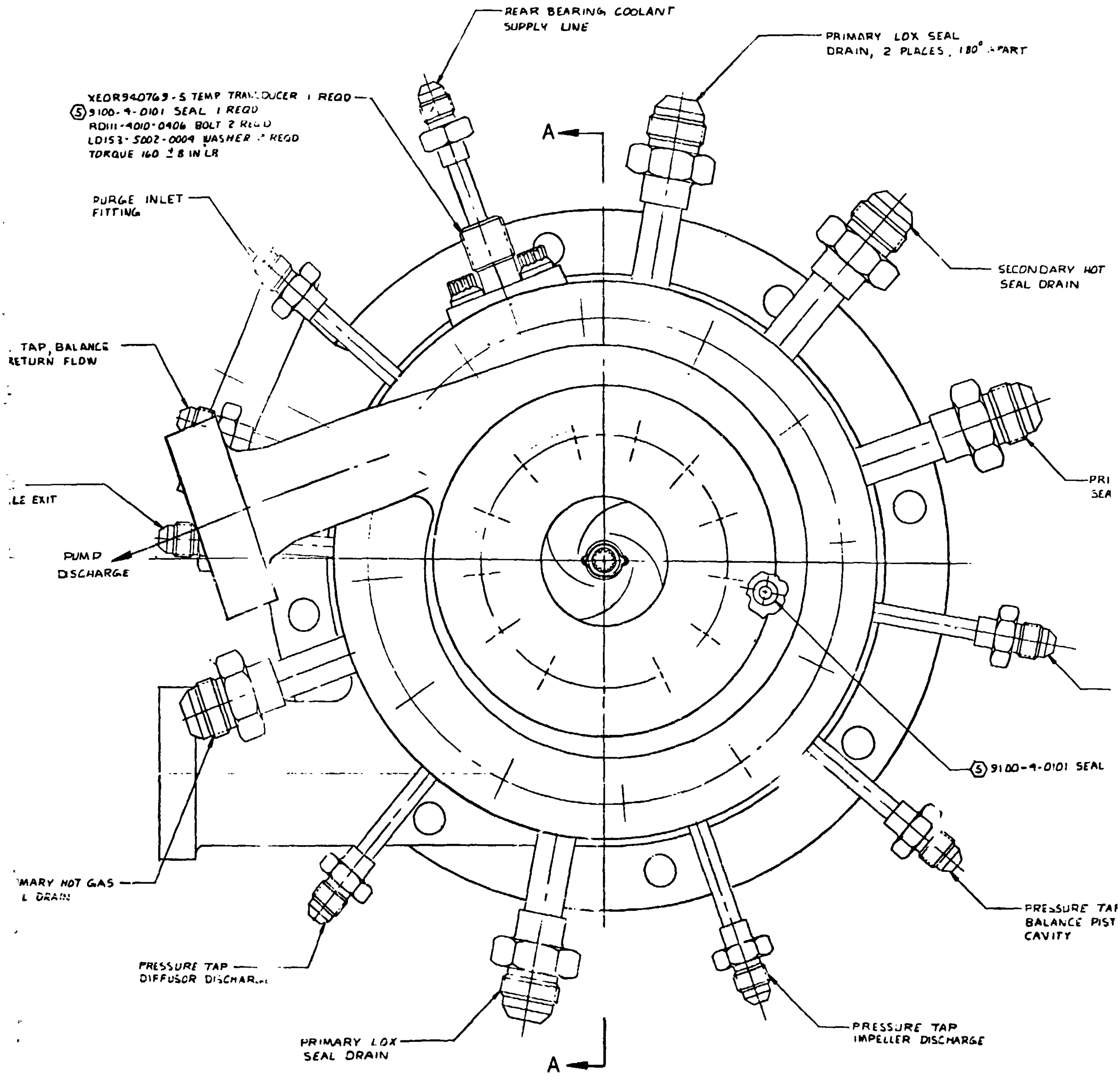

FOLDOUT FRAME 2

23 22 21 20 19

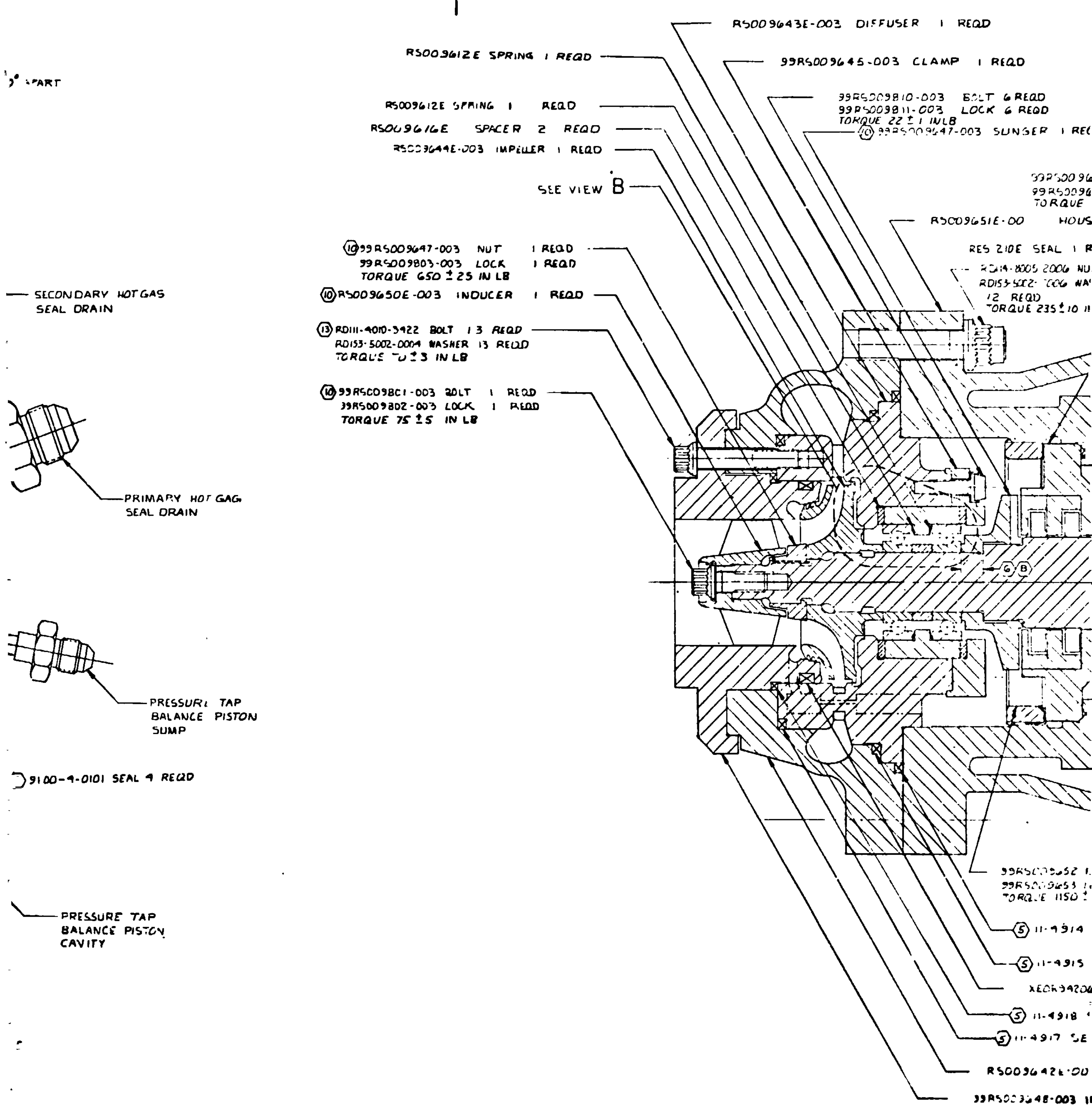

FOLDOUT FRAME 3

Rockwell International Corporation
Rocketdyne Division

RS009820E

18	17	16	15	14

MICROFILM OVERLAP AREA

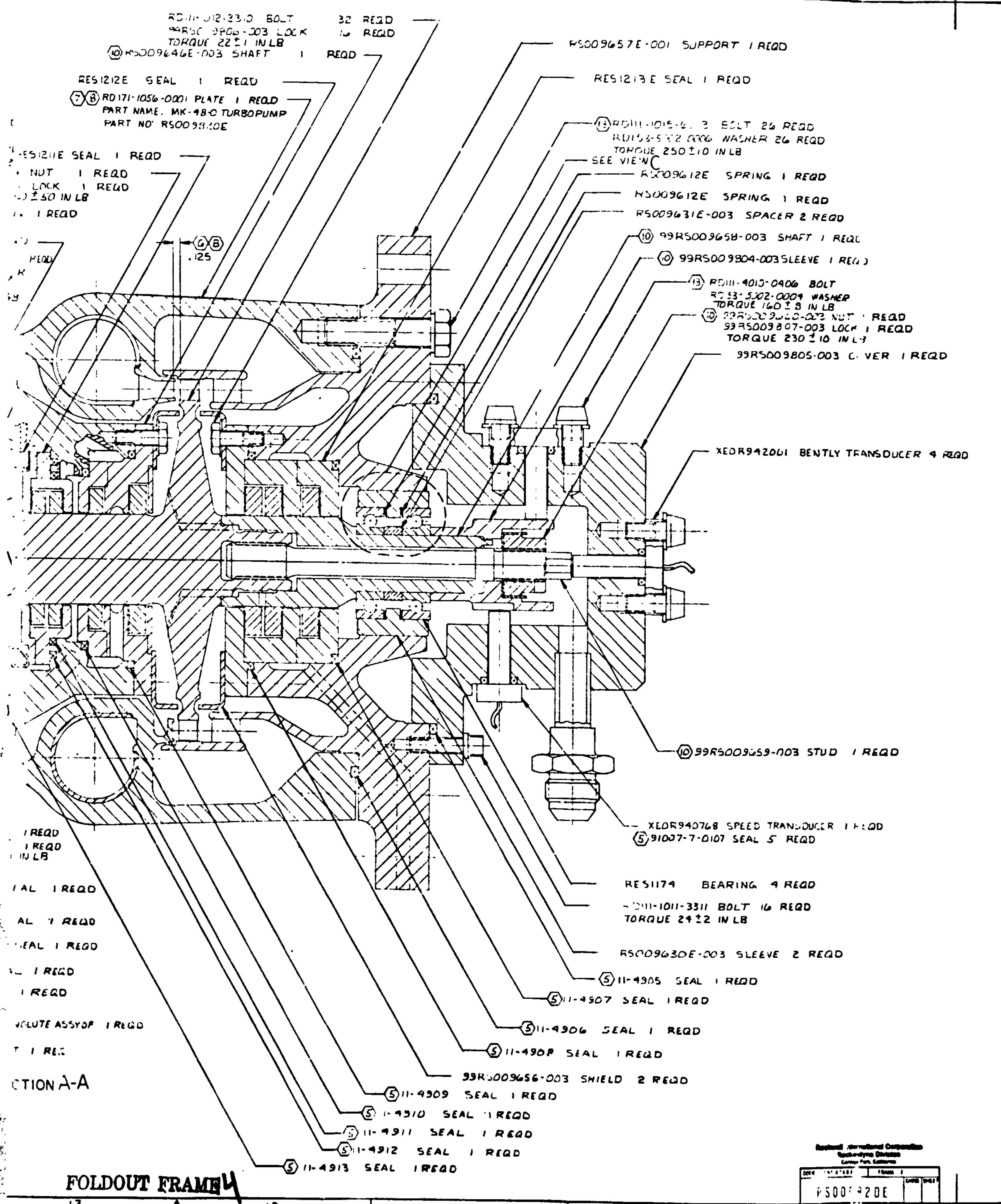

FOLDOUT FRAME 4

MICROFILM OVERLAP AREA

1 SUPPORT 1 REQD

SEAL 1 REQD

15-6613 BOLT 26 REQD
002 0006 WASHER 26 REQD
250 ± 10 IN LB

09612E SPRING 1 REQD

09612E SPRING 1 REQD

9631E-003 SPACER 2 REQD

9RS009658-003 SHAFT 1 REQD

99RS009804-003 SLEEVE 1 REQD

13 RD111-4010-0406 BOLT
RD153-5302-0009 WASHER
TORQUE 160 ± 8 IN LB

10 99RS009660-003 NUT 1 REQD
99RS009807-003 LOCK 1 REQD
TORQUE 230 ± 10 IN LB

99RS009805-003 COVER 1 REQD

XEOR942061 BENTLY TRANSDUCER 4 REQD

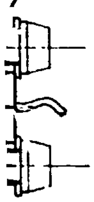

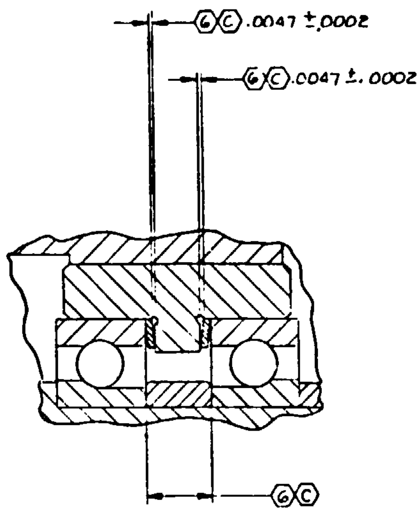

VIEW C

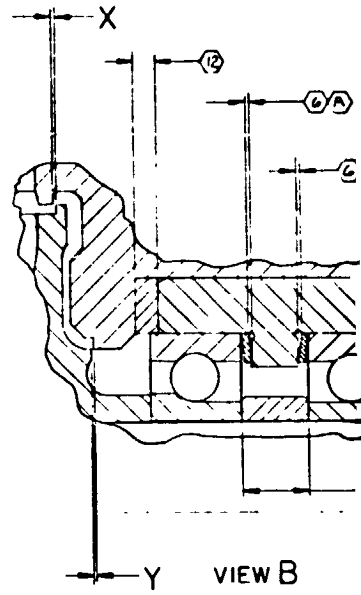

VIEW B

10 99RS009659-003 STUD 1 REQD

IEOR940768 SPEED TRANSDUCER 1 REQD
11007-7-0107 SEAL 2 REQD

174 BEARING 4 REQD

1011-3311 BOLT 16 REQD
UE 24 ± 2 IN LB

9630E-003 SLEEVE 2 REQD

SEAL 1 REQD

1 REQD

REQD

REQD

13 LOCKWI
12 MACHIN
OBTAIN
420 ± 50
11 MACHIN
OBTAIN
470 ±
10 BALANC
MATCH
RA0104-
COMPON
9. INSTALL
8 APPLY
7 IDENTIF
6 MACHII
CODED
5 HYDRO
4. INSTAL
TUBE F
3. LEAK
INSTRU
2 INSTA
1. CLEAN
RA0110-
LOX CL

Rockwell International Corporation
Rocketdyne Division
Canoga Park, California

CODE IDENT 02602 | FRAME 2

RS009420E

FOLDOUT FRAME 5

10 | 8 | 7 | 6 | 5

MICROFILM OVERLAP AREA

REVISIONS

FOLDOUT FRAME

...S PER RA0101-002.
...ER THICKNESS PER DETAIL DRAWING TO
...ID NITROGEN TEMPERATURE A FORCE OF
...THE ROTOR WHEN CLEARANCE X IS ZERO.
...EN THICKNESS PER DETAIL DRAWING TO
...UID NITROGEN TEMPERATURE A FORCE OF
...N THE ROTOR WHEN CLEARANCE Y IS ZERO.
...N ASSEMBLY TO WITHIN .02 GRAM INCHES.
...ALL ROTOR ASSEMBLY COMPONENTS PER
...ELECTRO CHEM ETCH. CODED PARTS ARE
...THE ROTOR ASSEMBLY. ALIGN MATCHMARKS.
...NGS AND TUBE ASSEMBLIES PER RA0102-005.
...0104-010.
...RA0104-008.
...ER PER DETAIL DRAWING TO OBTAIN MATCH
...ION.
...VISION, F.P.I. INC, NORTH HOLLYWOOD, CAL.
...CTIVE COVERS OVER ALL EXPOSED FLANGES,
... & PORTS.
...URBOPUMP PER DETAILED ASSEMBLY
...DED FASTENERS PER RA0101-002.
...ITS PRIOR TO PUMP ASSEMBLY PER
...L INTERNAL SURFACES TO BE MAINTAINED

MARK 48-O Turbopump Assembly
Drawing RS009802E

247

NONE	
NONE	
TURBOPUMP ASSY, OXIDIZER	
02602	RS009820E

MK-48-0

RS009820E

APPENDIX C

MARK 48-0 TURBOPUMP
TEST PRINTOUTS

RUN NUMBER 17
TEST DATE 07-16-76

PROCESSING DATE 07-19-76
TEST DURATION, SEC 37.00

COMMENTS . . .

TURB PR RATIO = NOZ IN TOT PR/TURB EXH STAT PR
PID 61 HAS 0 SHIFT, +1.2

AMBIENT PRESSURE		13.7000
LO2 VENTURI (GG)		
P/N V160248-SGR	UPSTREAM DIAMETER	0.9570
S/N 8871	THROAT DIAMETER	0.2460
	THROAT CD	0.9850
GH2 VENTURI (TURB)		
P/N VP031200-SGR	UPSTREAM DIAMETER	2.3000
S/N 9731	THROAT DIAMETER	1.3065
	THROAT CD	0.9673
LH2 VENTURI (GG)		
P/N V320471-SGR	UPSTREAM DIAMETER	1.6890
S/N 8873	THROAT DIAMETER	0.4710
	THROAT CD	0.9765
LOX VENTURI (PUMP DISCH)		
P/N V321059-SGR	UPSTREAM DIAMETER	1.6890
S/N 8877	THROAT DIAMETER	1.0590
	THROAT CD	0.9820

APPENDIX C (cont'd)

MK48-0
LIQUID OXYGEN TURBOPUMP ASSEMBLY

PAGE 17. 2

RUN NUMBER 17
TEST DATE 07-16-76

PROCESSING DATE 07-19-76
TEST DURATION, SEC 37.00

G A S E O U S   H Y D R O G E N   T U R B I N E   D R I V E   P A R A M E T E R S

TIME SLICE NO	BEGIN TIME (SEC)	END TIME (SEC)	VENTURI U/S PR (PSIA)	VENTURI U/S TEMP (DEG R)	VENTURI DELTA PR (PSID)	SPIN VALVE POSN	SPIN VALVE U/S PR (PSIA)	SPIN VALVE DELTA P (PSID)	TURB GH2 FLOW (LB/SEC)	SPEED (RPM)
1	46.524	46.750	3616.4	538.3	6.59	1.544	3601.8	3588.100	2.65381	61040.
2	48.008	48.235	3583.7	538.3	6.41	1.548	3569.1	3555.400	2.60761	60652.
3	55.515	55.742	3422.9	537.9	6.24	1.548	3408.3	3394.600	2.52151	60019.
4	57.000	57.227	3392.8	537.7	6.20	1.549	3378.2	3364.500	2.50195	59741.
5	63.516	63.743	3264.9	537.1	6.10	1.547	3250.1	3236.400	2.43871	59760.
6	65.537	65.723	3227.3	537.0	6.05	1.549	3212.6	3198.900	2.41747	59450.
7	65.507	68.734	3172.3	536.8	5.67	1.547	3157.1	3143.400	2.36290	57415.
8	65.528	70.755	3135.7	536.5	5.77	1.547	3120.7	3107.000	2.32957	57110.

MK48-O
LIQUID OXYGEN TURBOPUMP ASSEMBLY

RUN NUMBER 17
TEST DATE 07-16-76

PROCESSING DATE 07-19-76
TEST DURATION, SEC 37.00

T U R B I N E P A R A M E T E R S

TIME SLICE NO	BEGIN TIME (SEC)	END TIME (SEC)	SPEED (RPM)	TURB INLET STAT PR (PSIA)	TURB INLET TOT PR (PSIA)	TURB INLET TOT TEMP (DEG R)	TURB NOZZ D/S PR (PSIA)	TURB EXH STAT PR (PSIA)	TURB EXH TOT PR (PSIA)	TURB EXH TOT TEMP (DEG R)	TURB DSCH ORIFICE DELTA P (PSID)
1	46.524	46.750	61040.	2186.4	2197.3	533.7	1312.8	1304.3	1335.7	388.7	1313.4
2	48.008	48.235	60652.	2151.0	2160.5	534.2	1292.0	1283.9	1313.7	388.7	1291.8
3	55.515	55.742	60019.	2058.8	2066.7	534.7	1235.0	1229.5	1258.7	388.9	1237.6
4	57.000	57.227	59741.	2038.6	2046.0	534.6	1224.2	1218.4	1247.1	388.6	1226.0
5	63.516	63.743	59760.	1963.7	1968.9	534.7	1179.3	1174.7	1204.3	388.5	1184.1
6	65.537	65.723	59450.	1940.8	1943.9	534.5	1166.1	1161.1	1190.2	388.1	1170.3
7	65.507	68.734	57415.	1906.1	1908.3	534.3	1148.1	1143.7	1170.6	388.1	1150.9
8	65.528	70.755	57110.	1885.0	1886.3	534.1	1134.7	1130.8	1157.2	388.0	1137.7

APPENDIX C' (cont'd)
MK48-O
LIQUID OXYGEN TURBOPUMP ASSEMBLY

RUN NUMBER 17
TEST DATE 07-16-76

PROCESSING DATE 07-19-76
TEST DURATION, SEC 37.00

T U R B I N E   P A R A M E T E R S (CONTINUED)

TIME SLICE NO	SPEED RPM	FLOW (LB/SEC)	PR RATIO (T-S)	BHP (CALIB) (HP)	BHP (DELTA T) (HP)	TORQUE (FT-LB)	U/C (T-S)	EFF (T-S)	TURB NOZ IN TOT P (PSIA)
1	61040.	2.6538	1.6510	496.3	1981.9	42.69	0.3483	51.25	2153.4
2	60652.	2.6076	1.6491	486.2	1951.7	42.09	0.3464	51.20	2117.3
3	60019.	2.5215	1.6473	468.1	1890.3	40.95	0.3432	51.10	2025.4
4	59741.	2.5019	1.6457	463.1	1877.1	40.69	0.3421	51.07	2005.1
5	59760.	2.4387	1.6426	449.5	1831.0	39.49	0.3429	51.09	1929.5
6	59450.	2.4175	1.6407	444.0	1817.2	39.21	0.3417	51.05	1905.0
7	57415.	2.3629	1.6352	427.5	1773.8	39.09	0.3312	50.66	1870.1
8	57110.	2.3296	1.6347	420.4	1746.9	38.65	0.3296	50.59	1848.6

MK48-O
LIQUID OXYGEN TURBOPUMP ASSEMBLY

RUN NUMBER 17
TEST DATE 07-16-76

PROCESSING DATE 07-19-76
TEST DURATION, SEC 37.00

T U R B I N E   P A R A M E T E R S (CONTINUED)

TIME SLICE NO	SPEED RPM	AVAIL. ENERGY(T-S) BTU/LB)	GAMMA	CP (BTU/LBM-R)	SPEED PARA-METER	FLOW PARA-METER	TORQUE PARA-METER
1	61040.	257.37	1.3970	3.6380	448.7	3.3783	0.0181
2	60652.	257.38	1.3969	3.6364	445.6	3.3774	0.0181
3	60019.	256.74	1.3966	3.6328	440.8	3.4159	0.0164
4	59741.	256.14	1.3965	3.6323	438.8	3.4233	0.0185
5	59760.	254.97	1.3962	3.6298	438.9	3.4677	0.0187
6	59450.	254.23	1.3961	3.6293	436.7	3.4810	0.0188
7	57415.	252.41	1.3960	3.6254	421.8	3.4653	0.0191
8	57110.	252.11	1.3959	3.6260	419.7	3.4556	0.0191

APPENDIX C (cont'd)

MK48-O
LIQUID OXYGEN TURBOPUMP ASSEMBLY

RUN NUMBER 17
TEST DATE 07-16-76

PROCESSING DATE 07-19-76
TEST DURATION, SEC 37.00

S E A L A N D B E A R I N G D A T A

TIME SLICE NO	PRIM LOX SEAL DR PR (PSIA)	PRIM LOX SEAL DR TEMP (DEG R)	I/S PURGE PR (PSIA)	I/S PURGE TEMP (DEG R)	PRIM HG SEAL ORIF U/S PR (PSIA)	PRIM HG SEAL ORIF U/S TEMP (DEG R)	PRIM HG SEAL DR FLOW (LB/SEC)	SEC HG SEAL DR PR (PSIA)	SEC HG SEAL DR TEMP (DEG R)	SEC HG SEAL ORIF U/S PR (PSIA)	SEC HG SEAL ORIF U/S TEMP (DEG R)
1	18.74	167.20	220.30	548.25	19.98	393.41	0.0559	18.9	448.56	13.94	451.22
2	18.70	171.00	219.67	548.28	20.03	416.96	0.0545	19.0	453.06	13.94	452.54
3	22.23	157.90	222.45	549.28	20.03	452.28	0.0525	19.2	465.76	13.94	462.37
4	22.48	157.90	221.59	549.70	19.63	454.14	0.0517	19.1	466.83	13.93	463.92
5	18.97	193.20	215.51	550.68	19.15	459.20	0.0490	18.4	469.83	13.89	469.14
6	19.02	196.70	215.38	550.68	18.96	460.15	0.0482	18.4	470.82	13.89	470.54
7	19.61	186.50	215.71	550.96	18.75	460.15	0.0474	18.3	471.70	13.89	472.10
8	19.67	18[illegible].60	215.67	551.28	18.61	459.73	0.0469	18.3	472.06	13.89	472.93

MK48-O
LIQUID OXYGEN TURBOPUMP ASSEMBLY

RUN NUMBER 17
TEST DATE 07-16-76

PROCESSING DATE 07-19-76
TEST DURATION, SEC 37.00

SEAL AND BEARING DATA (CONTINUED)

TIME SLICE NO	SEC HG SEAL DR FLOW (LB/SEC)	RR BRG COOLANT SUPPL.PR (PSIA)	RR BRG COOLANT SUPPL,TEMP (DEG R)	RR BRG DRAIN PR (PSIA)	RR BRG DRAIN TEMP (DEG R)	RR BRG COOL.ORIF U/S PR (PSIA)	RR BRG COOL.ORIF U/S TEMP (DEG R)	RR BRG COOLANT FLOW (LB/SEC)
1	0.0	3024.0	85.40	155.8	52.10	30.2	54.90	0.1676
2	0.0	3024.1	85.50	155.7	52.10	30.1	53.80	0.1694
3	0.0	3025.1	85.60	155.6	52.10	29.8	53.40	0.1659
4	0.0	3025.0	85.50	155.5	52.10	29.7	53.40	0.1626
5	0.0	3024.7	85.50	155.3	51.20	29.6	52.30	0.1628
6	0.0	3024.5	85.30	154.8	49.60	29.6	52.20	0.1629
7	0.0	3022.6	85.60	155.2	48.60	29.6	52.20	0.1628
8	0.0	3017.5	85.80	155.8	49.70	29.6	52.20	0.1627

APPENDIX C (cont'd)

MK48-0

LIQUID OXYGEN TURBOPUMP ASSEMBLY

PAGE 17. 8

RUN NUMBER 17
TEST DATE 07-16-76

PROCESSING DATE 07-19-76
TEST DURATION, SEC 37.00

PUMP PRESSURES

TIME SLICE NO	SUPPLY TANK PR (PSIA)	PUMP INLET PR (PSIA)	IMPELLER DISCH PR (PSIA)	DIFFUSER DISCH PR (PSIA)	PUMP DISCH PR (PSIA)	BAL PIST CAV PR (PSIA)	BAL PIST SUMP PR (PSIA)	BAL PIST RETURN PR (PSIA)
1	213.8	165.2	2382.4	2765.1	3005.8	2160.4	1331.7	1340.7
2	213.7	165.3	2353.5	2726.6	2972.2	2109.7	1327.3	1336.5
3	214.4	183.0	2606.2	3314.5	3662.1	2253.6	1768.9	1085.7
4	214.5	182.6	2570.9	3271.8	3620.4	2218.1	1757.2	1072.0
5	213.7	164.3	1909.7	2181.7	2407.9	1565.5	1159.5	1179.2
6	213.6	163.3	1878.0	2150.7	2374.7	1540.3	1149.4	1168.5
7	213.7	172.2	2117.1	2563.6	2833.8	1776.1	1397.0	1354.1
8	213.8	172.8	2088.9	2527.3	2797.9	1752.0	1382.7	1339.3

/APPENDIX C (cont'd)

MK48-0

LIQUID OXYGEN TURBOPUMP ASSEMBLY

RUN NUMBER 17
TEST DATE 07-16-76

PROCESSING DATE 07-19-76
TEST DURATION, SEC 37.00

P U M P   P R E S S U R E S   A N D   T E M P E R A T U R E S

TIME SLICE NO	PUMP INLET TEMP (DEG R)	PUMP DISCH TEMP (DEG R)	BAL PIST RETURN TEMP (DEG R)	PUMP DISCH VENT U/S TEMP (DEG R)	PUMP DISCH VENT U/S PR (PSIA)	PUMP DISCH VENT DELTA PR (PSI)
1	174.40	199.00	279.70	196.30	2994.1	26.56
2	174.40	198.90	290.70	196.30	2959.3	26.38
3	174.40	201.40	297.20	196.30	3654.8	18.23
4	174.30	201.10	297.20	196.30	3613.1	18.44
5	174.50	198.00	297.20	196.30	2397.1	29.13
6	174.50	198.00	296.90	196.30	2363.1	28.91
7	174.50	197.70	294.30	196.30	2823.8	24.19
8	174.50	197.30	294.40	196.30	2787.9	24.26

ORIGINAL PAGE IS
OF POOR QUALITY

APPENDIX C (cont'd)

MK48-U

LIQUID OXYGEN TURBOPUMP ASSEMBLY

PAGE 17.10

RUN NUMBER 17
TEST DATE 07-16-76

PROCESSING DATE 07-19-76
TEST DURATION, SEC 37.00

C A L C U L A T E D   P U M P   P A R A M E T E R S

TIME SLICE NO	TEST SPEED (RPM)	PUMP FLOW GPM	PUMP FLOW (LB/SEC)	HEAD FT	PRESS RISE (PSI)	FLUID HP (HP)	TURB HP (HP)	EFF (%)	OVERALL EFF (%)	SPECIFIC SPEED
1	61040.	173.91	26.6030	6005.3	2840.6	290.5	496.30	58.55	58.53	1180.
2	60652.	173.39	26.5083	5935.3	2806.9	286.1	486.24	58.85	58.83	1181.
3	60019.	143.41	22.1476	7306.6	3479.1	294.2	468.13	62.88	62.85	909.
4	59741.	144.26	22.2659	7219.7	3437.8	292.3	463.05	63.14	63.12	916.
5	59760.	182.99	27.7316	4778.7	2243.5	240.9	449.54	53.62	53.60	1407.
6	59450.	182.35	27.6201	4712.1	2211.4	236.6	443.98	53.32	53.30	1412.
7	57415.	166.20	25.3574	5625.2	2661.6	259.3	427.51	60.69	60.66	1140.
8	57110.	166.49	25.3876	5547.9	2625.0	256.1	420.42	60.94	60.91	1146.

APPENDIX C (cont'd)

MK48-O

LIQUID OXYGEN TURBOPUMP ASSEMBLY

RUN NUMBER 17
TEST DATE 07-16-76

PROCESSING DATE 07-19-76
TEST DURATION, SEC 37.00

CALCULATED PUMP PARAMETERS

TIME SLICE NO	TEST SPEED (RPM)	NPSH (FT)	SUCTION SPECIFIC SPEED	INLET FLOW COEFF	HEAD COEFF	PUMP DELTA T (DEG R)	(Q/N) OVER (Q/N)DES
1	61040.	288.92	11486.70	0.07242	0.41888	24.60	0.8597
2	60652.	288.98	11394.57	0.07266	0.41932	24.50	0.8625
3	60019.	324.52	9400.48	0.06073	0.52714	27.00	0.7209
4	59741.	323.66	9403.28	0.06138	0.52573	26.80	0.7286
5	59760.	287.59	11575.61	0.07783	0.34776	23.50	0.9239
6	59450.	285.30	11564.75	0.07796	0.34649	23.50	0.9255
7	57415.	303.16	10167.91	0.07357	0.44348	23.20	0.8734
8	57110.	304.48	10109.63	0.07410	0.44207	22.80	0.8796

APPENDIX C (cont'd)
MK48-O
LIQUID OXYGEN TURBOPUMP ASSEMBLY

RUN NUMBER 17
TEST DATE 07-16-76

PROCESSING DATE 07-19-76
TEST DURATION, SEC 37.00

SCALED TO TARGET SPEED = 60000. RPM

TIME SLICE NO	FLOW (GPM)	FLOW (#/SEC)	HEAD (FT)	PRESS RISE (PSI)	HORSE POWER (BHP)	NPSH (FT)
1	170.95	26.14971	5802.39	2744.60	275.87	279.16
2	171.52	26.22331	5808.43	2746.91	276.94	282.80
3	143.36	22.14063	7301.98	3476.90	293.95	324.31
4	144.59	22.36246	7282.47	3467.66	296.10	326.47
5	183.73	27.84298	4817.14	2261.61	243.86	289.91
6	184.04	27.87559	4799.64	2252.55	243.26	290.60
7	173.68	26.49911	6143.11	2906.64	295.98	331.07
8	174.91	26.67233	6123.58	2897.45	296.96	336.07

ORIGINAL PAGE IS
OF POOR QUALITY

APPENDIX C (cont'd)

4K48-G

LIQUID OXYGEN TURBOPUMP ASSEMBLY

PAGE 17.13

RUN NUMBER 17
TEST DATE 07-16-76

PROCESSING DATE 07-19-76
TEST DURATION, SEC 37.00

SCALED TO DESIGN SPEED = 70,000. RPM

TIME SLICE NO	FLOW (GPM)	FLOW (#/SEC)	HEAD (FT)	PRESS RISE (PSI)	HORSE POWER (BHP)	NPSH (FT)
1	199.44	30.50799	7897.69	3735.70	438.08	379.97
2	200.11	30.59386	7905.91	3738.84	439.77	384.93
3	167.26	25.83073	9938.81	4732.44	466.78	441.43
4	169.03	26.08954	9912.25	4719.87	470.19	444.36
5	214.35	32.48348	6556.66	3078.30	387.24	394.59
6	214.72	32.52152	6532.85	3065.97	386.29	395.54
7	202.63	30.91563	8361.46	3956.26	470.00	450.52
8	204.06	31.11772	8334.67	3943.75	471.57	457.43

AT= 0.222600+00

AT= 0.223480+00

AT= 0.223540+00

APPENDIX C (cont'd)
MK48-O
LIQUID OXYGEN TURBOPUMP ASSEMBLY

RUN NUMBER 28
TEST DATE 08-11-76

PROCESSING DATE 08-16-76
TEST DURATION, SEC 40.79

COMMENTS . . .

SLICES 2,3,4,8,9,10,AND 11 ARE STEADY STATE VALUES.
PID 25,29,46,51,52,AND 77 ARE ENGINEERING ADJUSTED VALUES.
TURB PR RATIO = NOZ IN TOT PR/TURB EXH STAT PR

AMBIENT PRESSURE		13.7000
LO2 VENTURI (GG) P/N V160248-SGR S/N 8871	UPSTREAM DIAMETER	0.9570
	THROAT DIAMETER	0.2480
	THROAT CD	0.9850
GH2 VENTURI (TURB) P/N VP031200-SGR S/N 9731	UPSTREAM DIAMETER	2.3000
	THROAT DIAMETER	1.3085
	THROAT CD	0.9873
LH2 VENTURI (GG) P/N V320471-SGR S/N 8873	UPSTREAM DIAMETER	1.6890
	THROAT DIAMETER	0.4710
	THROAT CD	0.9765
LOX VENTURI (PUMP DISCH) P/N V321059-SGR S/N 8877	UPSTREAM DIAMETER	1.6890
	THROAT DIAMETER	1.0590
	THROAT CD	0.9820

APPENDIX C (cont'd)

MK48-O
LIQUID OXYGEN TURBOPUMP ASSEMBLY

PAGE 28. 2

RUN NUMBER 28
TEST DATE 08-11-76

PROCESSING DATE 08-16-76
TEST DURATION, SEC 40.79

TURBINE PARAMETERS

TIME SLICE NO	BEGIN TIME (SEC)	END TIME (SEC)	SPEED (RPM)	TURB INLET STAT PR (PSIA)	TURB INLET TOT PR (PSIA)	TURB INLET TOT TEMP (DEG R)	TURB NOZZ D/S PR (PSIA)	TURB EXH STAT PR (PSIA)	TURB EXH TOT PR (PSIA)	TURB EXH TOT TEMP (DEG R)	TURB DSCH ORIFICE DELTA P (PSID)
1	25.860	26.046	65262.	2148.7	2157.7	1692.3	1196.3	1191.3	1196.2	1179.1	1173.6
2	30.067	30.253	67031.	2148.8	2157.1	1717.1	1196.1	1191.1	1195.7	1182.3	1172.8
3	35.058	35.243	67920.	2146.0	2154.3	1730.0	1171.7	1166.7	1194.9	1182.3	1171.7
4	38.069	38.254	68239.	2157.0	2164.6	1729.6	1176.2	1171.2	1200.1	1182.3	1176.6
5	43.059	43.245	67742.	2144.3	2152.5	1696.9	1174.7	1169.7	1198.8	1182.3	1175.0
6	46.070	46.256	67799.	2151.0	2160.0	1734.9	1177.2	1172.2	1202.3	1182.3	1178.4
7	49.040	49.225	68338.	2156.6	2163.7	1740.7	1178.2	1173.2	1203.0	1182.3	1178.9
8	54.278	54.422	68489.	2148.6	2156.6	1749.1	1175.5	1170.5	1200.1	1182.3	1175.8
9	56.258	56.443	68435.	2150.4	2159.6	1760.4	1176.8	1171.8	1202.4	1182.3	1178.1
10	60.052	60.238	68685.	2164.6	2171.7	1755.1	1181.9	1176.9	1206.6	1182.3	1182.1
11	61.042	61.227	68630.	2152.2	2162.3	1768.9	1177.6	1172.6	1202.3	1182.3	1177.8

APPENDIX C (cont'd)

MK48-L
LIQUID OXYGEN TURBOPUMP ASSEMBLY

RUN NUMBER 28
TEST DATE 08-11-76

PROCESSING DATE 08-16-76
TEST DURATION, SEC 40.79

T U R B I N E P A R A M E T E R S (CONTINUED)

TIME SLICE NO	SPEED RPM	FLOW (LB/SEC)	PR RATIO (T-S)	BHP (CALIB) (HP)	BHP (DELTA T) (HP)	TORQUE (FT-LB)	U/C (T-S)	EFF (T-S)	TURB NOZ IN TOT P (PSIA)
1	65262.	2.1859	1.7750	676.1	3092.7	54.39	0.2782	47.30	2114.5
2	67131.	2.2018	1.7748	694.5	3234.8	54.40	0.2844	47.81	2114.0
3	67920.	2.2186	1.8096	723.6	3331.6	55.93	0.2831	47.70	2111.2
4	68239.	2.2188	1.8112	721.5	3304.8	55.51	0.2854	47.88	2121.3
5	67742.	2.2292	1.8034	715.5	3160.1	55.53	0.2849	47.84	2109.4
6	67799.	2.2198	1.8058	719.6	3343.6	55.72	0.2836	47.74	2116.8
7	68338.	2.2260	1.8074	724.4	3375.7	55.65	0.2858	47.91	2120.4
8	68489.	2.2168	1.8056	725.6	3423.2	55.62	0.2656	47.90	2113.5
9	68435.	2.2190	1.8061	730.1	3398.6	56.01	0.2843	47.80	2116.4
10	68685.	2.2317	1.8084	730.0	3457.0	55.79	0.2868	47.99	2128.3
11	68630.	2.2269	1.8071	735.1	3554.1	56.23	0.2848	47.83	2119.1

MK48-O

LIQUID OXYGEN TURBOPUMP ASSEMBLY

PAGE 26. 4

RUN NUMBER 28
TEST DATE 08-11-76

PROCESSING DATE 08-16-76
TEST DURATION, SEC 40.79

T U R B I N E P A R A M E T E R S (CONTINUED)

TIME SLICE NO	SPEED RPM	AVAIL. ENERGY(T-S) (BTU/LB)	GAMMA	CP (BTU/LBM-R)	SPEED PARA-METER	FLOW PARA-METER	TORQUE PARA-METER
1	65262.	462.11	1.3572	1.9482	373.3	3.6419	0.0235
2	67031.	466.51	1.3563	1.9417	381.6	3.6860	0.0235
3	67920.	483.20	1.3559	1.9373	385.8	3.7276	0.0242
4	68239.	479.94	1.3556	1.9230	389.2	3.6952	0.0239
5	67742.	4[illegible]4.81	1.3571	1.9467	387.1	3.7264	0.0240
6	67799.	479.85	1.3555	1.9262	385.8	3.7129	0.0240
7	68338.	479.98	1.3552	1.9189	389.1	3.7149	0.0239
8	68489.	482.93	1.3550	1.9250	388.5	3.7260	0.0240
9	68435.	486.50	1.3546	1.9273	386.9	3.7[illegible]71	0.0241
10	68685.	481.71	1.3545	1.9109	390.6	3.7155	0.0239
11	68630.	487.72	1.3542	1.9226	387.7	3.7488	0.0242

APPENDIX C (cont'd)
4K48-0
LIQUID OXYGEN TURBOPUMP ASSEMBLY

RUN NUMBER 28
TEST DATE 08-11-76

PROCESSING DATE 08-16-76
TEST DURATION, SEC 40.79

SEAL AND BEARING DATA

TIME SLICE NO	PRIM LOX SEAL DR PR (PSIA)	PRIM LOX SEAL DR TEMP (DEG R)	I/S PURGE PR (PSIA)	I/S PURGE TEMP (DEG R)	PRIM HG SEAL ORIF U/S PR (PSIA)	PRIM HG SEAL ORIF U/S TEMP (DEG R)	PRIM HG SEAL DR FLOW (LB/SEC)	SEC HG SEAL DR PR (PSIA)	SEC HG SEAL DR TEMP (DEG R)	SEC HG SEAL ORIF U/S PR (PSIA)	SEC HG SEAL ORIF U/S TEMP (DEG R)
1	17.05	163.20	199.64	543.87	30.21	625.63	0.0946	26.1	607.85	13.92	547.56
2	18.59	189.30	177.29	543.96	33.13	883.23	0.0879	30.9	757.79	14.11	658.65
3	20.15	221.90	167.33	544.13	34.09	1013.27	0.0854	28.6	853.49	14.21	784.14
4	20.75	248.80	163.21	543.80	33.90	1053.24	0.0835	28.3	879.59	14.20	824.91
5	21.41	252.40	159.01	542.33	33.20	1097.94	0.0794	29.0	932.87	14.24	880.21
6	21.69	256.00	157.27	541.58	33.36	1117.96	0.0796	26.9	950.53	14.06	905.55
7	22.42	262.30	156.67	541.34	33.00	1131.57	0.0784	26.2	954.75	14.04	917.20
8	22.97	265.10	155.62	541.07	32.53	1149.65	0.0766	26.0	973.33	14.03	933.14
9	23.33	266.50	155.62	540.83	32.35	1154.47	0.0759	26.0	979.42	14.02	939.04
10	23.51	274.90	156.10	540.31	31.32	1162.44	0.0736	28.5	999.79	14.14	955.46
11	23.50	276.70	156.26	540.31	31.24	1164.86	0.0731	28.2	1003.98	14.11	960.65

APPENDIX C (cont'd)

MK48-O

LIQUID OXYGEN TURBOPUMP ASSEMBLY

PAGE 28. 6

RUN NUMBER 28
TEST DATE 08-11-76

PROCESSING DATE 08-16-76
TEST DURATION, SEC 40.79

S E A L A N D B E A R I N G D A T A (CONTINUED)

TIME SLICE NO	SEC HG SEAL DR FLOW (LB/SEC)	RR BRG COOLANT SUPPL.PR (PSIA)	RR BRG COOLANT SUPPL,TEMP (DEG R)	RR BRG DRAIN PR (PSIA)	RR BRG DRAIN TEMP (DEG R)	RR BR COOL.ORIF U/S PR (PSIA)	FR BRG COOL.ORIF U/S TEMP (DEG R)	RR BRG COOLANT FLOW (LB/SEC)
1	0.0	3354.9	76.10	123.0	225.80	24.6	40.40	0.0207
2	0.0	3354.[illegible]	76.00	125.7	225.40	24.5	43.30	0.0
3	0.0	3349.2	75.50	127.1	226.60	24.1	40.90	0.0
4	0.0	3348.6	75.50	129.4	226.70	24.1	43.30	0.0
5	0.0	3346.4	77.00	135.4	228.90	24.3	48.40	0.0
6	0.0	3344.7	78.60	137.7	230.60	24.3	51.80	0.0
7	0.0	3346.1	77.20	133.7	231.[illegible]	24.0	48.60	0.0
8	0.0	3344.6	77.10	131.6	232.10	24.0	48.50	0.0
9	0.0	3343.9	76.40	121.0	232.10	24.0	46.60	0.0
10	0.0	3343.7	76.50	131.8	232.10	24.0	47.40	0.0
11	0.0	3344.3	76.70	132.3	232.30	23.9	47.90	0.0

ORIGINAL PAGE IS OF POOR QUALITY

C-4

APPENDIX C (cont'd)

RK48-0

LIQUID OXYGEN TURBOPUMP ASSEMBLY

RUN NUMBER 28
TEST DATE 08-11-76

PROCESSING DATE 08-16-76
TEST DURATION, SEC 40.79

P U M P   P R E S S U R E S

TIME SLICE NO	SUPPLY TANK PR (PSIA)	PUMP INLET PR (PSIA)	IMPELLER DISCH PR (PSIA)	DIFFUSER DISCH PR (PSIA)	PUMP DISCH PR (PSIA)	BAL PIST CAV PR (PSIA)	BAL PIST SUMP PR (PSIA)	BAL PIST RETURN PR (PSIA)
1	226.0	165.1	2834.1	3363.2	3657.8	1988.6	1348.2	1196.8
2	224.8	161.7	2555.3	3283.0	3796.9	2023.0	1492.7	1290.2
3	224.0	159.2	2247.6	3269.8	3657.2	1985.5	1561.6	1325.9
4	223.8	158.2	2168.2	3206.7	3871.6	1980.9	1579.1	1336.1
5	223.3	160.3	2037.4	3190.7	3998.2	1984.0	1609.7	1353.7
6	223.3	161.1	2144.6	3314.8	4197.4	2074.0	1665.5	1393.0
7	223.3	164.7	2231.1	3470.8	4423.5	2164.8	1736.7	1446.8
8	223.4	166.9	2272.7	3533.9	4534.4	2208.6	1782.9	1467.6
9	223.5	167.4	2279.2	3525.4	4527.5	2215.2	1795.3	1471.0
10	223.6	166.3	2286.3	3518.9	4547.0	2224.3	1805.8	1469.7
11	223.6	166.8	2287.7	3510.6	4538.5	2225.8	1807.4	1468.9

ORIGINAL PAGE IS
OF POOR QUALITY

MK48-U
LIQUID OXYGEN TURBOPUMP ASSEMBLY

RUN NUMBER 28
TEST DATE 08-11-76

PROCESSING DATE 08-16-76
TEST DURATION, SEC 40.79

P U M P   P R E S S U R E S   A N D   T E M P E R A T U R E S

TIME SLICE NO	PUMP INLET TEMP (DEG R)	PUMP DISCH TEMP (DEG R)	BAL PIST RETURN TEMP (DEG R)	PUMP DISCH VENT U/S TEMP (DEG R)	PUMP DISCH VENT U/S PR (PSIA)	PUMP DISCH VENT DELTA PR (PSI)
1	171.00	195.10	225.80	195.10	3672.0	27.94
2	170.90	196.90	228.40	196.90	3806.9	29.31
3	171.00	198.00	228.60	198.00	3869.8	30.31
4	171.10	198.00	223.70	198.00	3883.6	30.87
5	171.10	198.10	228.90	198.10	4010.1	29.47
6	171.20	198.10	230.60	198.10	4209.8	28.62
7	171.30	198.70	231.70	198.70	4436.3	27.26
8	171.30	199.30	232.10	199.30	4548.3	26.10
9	171.40	199.30	232.10	199.30	4541.3	26.20
10	171.50	199.50	232.10	199.50	4561.5	26.66
11	171.50	199.60	232.30	199.60	4552.2	26.57

APPENDIX C (cont'd)

MK48-O

LIQUID OXYGEN TURBOPUMP ASSEMBLY

RUN NUMBER 28
TEST DATE 08-11-76

PROCESSING DATE 08-16-76
TEST DURATION, SEC 40.79

CALCULATED PUMP PARAMETERS

TIME SLICE NO	TEST SPEED (RPM)	PUMP FLOW GPM	PUMP FLOW (LB/SEC)	HEAD FT	PRESS RISE (PSI)	FLUID HP (HP)	TURB HP (HP)	EFF (%)	OVERALL EFF (%)	SPECIFIC SPEED
1	65262.	177.27	27.4504	7276.4	3492.7	363.2	676.07	53.74	53.72	1103.
2	67031.	181.76	28.0927	7580.1	3635.2	387.2	694.53	55.77	55.75	1112.
3	67920.	185.02	28.5536	7718.9	3698.0	400.7	723.60	55.40	55.38	1122.
4	68239.	186.67	28.8150	7752.3	3713.4	406.2	721.51	56.31	56.29	1128.
5	67742.	182.26	28.1770	8000.8	3837.9	409.9	716.51	57.23	57.21	1061.
6	67799.	180.01	27.9037	8399.3	4036.2	426.1	719.55	59.24	59.22	1037.
7	68338.	174.93	27.1646	8848.9	4258.8	437.0	724.40	60.36	60.33	991.
8	68469.	171.15	26.5641	9069.4	4367.5	438.4	725.56	60.44	60.42	964.
9	68435.	171.48	26.6327	9055.9	4360.1	438.5	730.09	60.09	60.06	965.
10	68685.	173.01	26.8671	9101.4	4380.7	444.6	729.96	60.93	60.91	970.
11	68630.	172.73	26.8151	9083.9	4371.7	442.9	735.09	60.27	60.25	969.

MK48-O
LIQUID OXYGEN TURBOPUMP ASSEMBLY

RUN NUMBER 28
TEST DATE 08-11-76

PROCESSING DATE 08-16-76
TEST DURATION, SEC 40.79

CALCULATED PUMP PARAMETERS

TIME SLICE NO	TEST SPEED (RPM)	NPSH (FT)	SUCTION SPECIFIC SPEED	INLET FLOW COEFF	HEAD COEFF	PUMP DELTA T (DEG R)	(Q/N) OVER (Q/N)DES
1	65262.	295.51	12191.10	0.06904	0.44400	24.10	0.8196
2	67031.	288.76	12900.93	0.06892	0.43844	26.00	0.8182
3	67920.	283.89	13357.94	0.06924	0.43486	27.00	0.8219
4	68239.	281.84	13554.24	0.06953	0.43267	26.90	0.8254
5	67742.	285.99	13150.63	0.06839	0.45311	27.00	0.8118
6	67799.	287.74	13020.30	0.06746	0.47488	26.90	0.8011
7	68338.	294.82	12703.60	0.06506	0.49244	27.40	0.7724
8	68489.	299.32	12450.94	0.06351	0.50249	28.00	0.7540
9	68435.	300.34	12421.48	0.06369	0.50254	27.90	0.7560
10	68685.	298.17	12590.54	0.06402	0.50139	28.00	0.7600
11	68630.	299.31	12534.36	0.06397	0.50123	28.10	0.7594

APPENDIX C' (cont'd)

MK48-O

LIQUID OXYGEN TURBOPUMP ASSEMBLY

PAGE 28.11

RUN NUMBER 28
TEST DATE 08-11-76

PROCESSING DATE 08-16-76
TEST DURATION, SEC 40.79

SCALED TO TARGET SPEED = 70000. RPM

TIME SLICE NO	FLOW (GPM)	FLOW (#/SEC)	HEAD (FT)	PRESS RISE (PSI)	HORSE POWER (BHP)	NPSH (FT)
1	190.14	29.44328	8371.28	4018.29	448.14	339.98
2	189.81	29.33702	8266.43	3964.35	440.93	314.91
3	190.68	29.42802	8198.90	3927.93	438.69	301.54
4	191.49	29.55865	8157.63	3907.57	438.42	296.57
5	188.34	29.11620	8543.06	4098.04	452.26	305.37
6	185.85	28.80956	8953.51	4302.57	468.99	306.73
7	179.19	27.82523	9284.50	4468.50	469.72	309.34
8	174.92	27.17055	9473.98	4562.30	468.02	312.67
9	175.40	27.24173	9474.87	4561.81	469.29	314.23
10	176.32	27.38150	9453.22	4550.08	470.62	309.70
11	176.18	27.35044	9450.16	4547.95	469.94	311.38

APPENDIX C (cont'd)

MK48-0

LIQUID OXYGEN TURBOPUMP ASSEMBLY

PAGE 26.12

RUN NUMBER 28
TEST DATE 08-11-76

PROCESSING DATE 08-16-76
TEST DURATION, SEC 40.79

SCALED TO DESIGN SPEED = 70,000. RPM

TIME SLICE NO	FLOW (GPM)	FLOW (#/SEC)	HEAD (FT)	PRESS RISE (PSI)	HORSE POWER (BHP)	NPSH (FT)
1	190.14	29.44328	8371.28	4018.29	448.14	339.98
2	189.81	29.33702	8266.43	3964.35	440.93	314.91
3	190.68	29.42802	8198.90	3927.93	438.65	301.54
4	191.49	29.55865	8157.63	3907.57	438.42	296.57
5	188.34	29.11620	8543.06	4098.04	452.26	305.37
6	185.85	28.60956	8953.51	4302.57	468.99	306.73
7	179.19	27.82523	9284.50	4468.50	469.72	309.34
8	174.92	27.17055	947[illegible].98	4562.30	468.02	312.67
9	175.40	27.24173	9474.67	4561.81	469.29	314.23
10	176.32	27.38150	9453.22	4550.08	470.62	309.70
11	176.18	27.35044	9450.16	4547.95	469.94	311.38

APPENDIX C (cont'd)
MK48-O
LIQUID OXYGEN TURBOPUMP ASSEMBLY

RUN NUMBER 28
TEST DATE 08-11-76

PROCESSING DATE 08-16-76
TEST DURATION, SEC 40.79

G G P A R A M E T E R S

TIME SLICE NO	GG LOX TANK PR (PSIA)	GG LOX VENTURI TEMP (DEG R)	GG LOX INJECT TEMP (DEG R)	GG LOX INJECT PR (PSIA)	GG MLV POSN	GG LH2 TANK PR (PSIA)	GG LH2 VENTURI TEMP (DEG R)	GG LH2 INJECT TEMP (DEG R)	GG LH2 INJECT PR (PSIA)	GG MFV POSN
1	3855.7	296.70	235.30	2443.2	0.0	3431.5	67.90	90.60	2558.9	0.0
2	3855.3	284.20	218.80	2436.3	0.0	3427.2	66.00	87.40	2553.2	0.0
3	3853.7	258.80	210.10	2433.6	0.0	3421.6	68.30	85.40	2548.3	0.0
4	3853.2	252.90	205.90	2448.9	0.0	3420.1	68.50	84.70	2553.6	0.0
5	3852.0	235.30	200.60	2425.9	0.0	3417.7	68.80	83.30	2553.8	0.0
6	3851.6	223.90	198.30	2436.3	0.0	3416.1	68.90	83.50	2546.2	0.0
7	3851.6	221.50	195.30	2443.5	0.0	3414.9	69.10	83.50	2549.8	0.0
8	3851.2	219.60	192.20	2430.1	0.0	3413.7	69.70	83.10	2540.9	0.0
9	3851.3	218.90	191.60	2431.6	0.0	3412.5	69.70	83.00	2543.5	0.0
10	3851.6	218.30	190.20	2453.0	0.0	3412.4	70.80	83.40	2555.7	0.0
11	3851.8	218.70	190.30	2436.3	0.0	3412.1	71.70	84.10	2548.1	0.0

4K48-0

PAGE 28.14

LIQUID OXYGEN TURBOPUMP ASSEMBLY

RUN NUMBER 28
TEST DATE 08-11-76

PROCESSING DATE 08-16-76
TEST DURATION, SEC 40.79

G G P A R A M E T E R S

TIME SLICE NO	IGNITER GOX INJ. PR (PSIA)	IGNITER GOX INJ.TEMP (DEG R)	IGNITER GH2 INJ. PR (PSIA)	IGNITER GH2 INJ.TEMP (DEG R)	GG PC (PSIA)	COMB TEMP #1 (DEG R)	COMB TEMP #2 (DEG R)	TURB INLET STAT PR (PSIA)	TURB INLET TOT PR (PSIA)
1	2155.40	499.60	2219.50	524.96	2169.0	1691.20	1693.40	2148.70	2157.70
2	2155.80	497.32	2218.20	526.45	2169.1	1726.50	1707.70	2148.80	2157.10
3	2151.20	494.84	2214.20	527.15	2164.5	1744.90	1715.20	2146.00	2154.30
4	2163.20	493.71	2224.00	527.55	2177.8	1749.10	1710.20	2157.00	2164.60
5	2150.90	491.67	2211.40	527.73	2164.8	1721.60	1672.20	2144.30	2152.50
6	2156.90	489.86	2217.80	527.81	2170.9	1755.60	1714.20	2151.00	2160.00
7	2162.50	488.44	2221.80	527.80	2175.8	1767.40	1714.10	2156.60	2163.70
8	2154.00	486.23	2213.30	527.72	2168.2	1784.40	1713.90	2148.60	2156.60
9	2155.40	485.46	2216.30	527.67	2169.9	1793.80	1727.00	2150.40	2159.60
10	2169.80	484.34	2228.40	527.66	2183.9	1781.70	1728.60	2164.60	2171.70
11	2156.90	484.04	2217.80	527.64	2171.6	1800.70	1737.10	2152.20	2162.30

APPENDIX C (cont'd)

MK48-O

LIQUID OXYGEN TURBOPUMP ASSEMBLY

PAGE 28.15

RUN NUMBER 28
TEST DATE 08-11-76

PROCESSING DATE 08-16-76
TEST DURATION, SEC 40.79

C A L C U L A T E D   G G   P A R A M E T E R S

TIME SLICE NO	GG LOX FLOW (#/SEC)	IGNITER GOX FLOW (#/SEC)	GG LH2 FLOW (#/SEC)	IGNITER GH2 FLOW (#/SEC)	GG TOTAL FLOW (#/SEC)	GG INJECTOR FLOW (#/SEC)	IGNITER TOTAL FLOW (#/SEC)	GG OVERALL MIXTURE RATIO	GG INJECTOR MIXTURE RATIO	IGNITER OVERALL MIXTURE RATIO
1	0.9937	0.0542	1.0763	0.0617	2.1859	2.0700	0.1159	0.92067	0.92525	0.87928
2	1.0074	0.0544	1.0788	0.0612	2.2018	2.0861	0.1157	0.93141	0.93382	0.88890
3	1.0185	0.0546	1.0846	0.0607	2.2186	2.1033	0.1153	0.93673	0.93888	0.89852
4	1.0278	0.0546	1.0760	0.0605	2.2188	2.1038	0.1150	0.95235	0.95513	0.90274
5	1.0149	0.0548	1.0995	0.0600	2.2292	2.1144	0.1148	0.92257	0.92310	0.91288
6	1.0261	0.0550	1.0789	0.0598	2.2198	2.1050	0.1148	0.94955	0.95113	0.92102
7	1.0343	0.0551	1.0772	0.0595	2.2260	2.1115	0.1146	0.95835	0.96016	0.92544
8	1.0266	0.0550	1.0761	0.0591	2.2168	2.1027	0.1141	0.95281	0.95396	0.93154
9	1.0269	0.0552	1.0779	0.0589	2.2190	2.1048	0.1141	0.95193	0.95269	0.93803
10	1.0432	0.0553	1.0747	0.0583	2.2317	2.1178	0.1138	0.96932	0.97069	0.94417
11	1.0344	0.0554	1.0787	0.0585	2.2269	2.1131	0.1139	0.95832	0.95889	0.94763

RUN NUMBER 28
TEST DATE 08-11-76

PROCESSING DATE 08-16-76
TEST DURATION, SEC 40.79

CALCULATED GG PARAMETERS

TIME SLICE NO	GG INJ.END PC TOT PR (PSIA)	GG COMB TEMP (DEG R)	GG INJECTOR C* (FT/SEC)	GG INJECTOR C* THEOR (FT/SEC)	GG INJECTOR C* EFF (%)	IGNITER GH2 CORE FLOW (#/SEC)	IGNITER CORE MIXTURE RATIO	IGNITER GH2 COOLANT FLOW (#/SEC)	IGNITER CORE PC STATIC (PSIA)
1	2169.0	1692.3	6808.1	6832.3	99.65	0.0027	19.9845	0.0590	2151.1
2	2169.1	1717.1	6839.1	6847.0	99.88	0.0027	20.3381	0.0586	2151.5
3	2164.5	1730.0	6855.4	6854.0	100.02	0.0027	20.3445	0.0581	2146.9
4	2177.6	1729.6	6827.2	6880.3	99.23	0.0026	20.6397	0.0578	2158.9
5	2164.8	1696.9	6814.4	6826.2	99.83	0.0026	20.8404	0.0574	2146.6
6	2170.9	1734.9	6842.4	6874.1	99.54	0.0026	20.8371	0.0571	2152.6
7	2175.8	1740.7	6838.5	6889.3	99.26	0.0026	21.0827	0.0569	2158.2
8	2168.2	1749.1	6864.7	6879.3	99.79	0.0026	21.1181	0.0565	2149.7
9	2169.9	1760.4	6888.3	6877.6	100.16	0.0026	20.9250	0.0563	2151.1
10	2183.9	1755.1	6847.6	6907.8	99.13	0.0026	21.2476	0.0559	2165.5
11	2171.6	1768.9	6893.7	6889.9	100.05	0.0026	20.9812	0.0558	2152.6

APPENDIX D

REFERENCES

REFERENCES

1. Advanced Space Engine Preliminary Design Report, NASA CR 121236, R-9269, Rocketdyne Division of Rockwell International, Canoga Park, California.

2. Liquid Rocket Engine Centrifugal Flow Turbopumps, NASA SP 8109.

3. Klassen, H. A.: Cold-Air Investigation of Effects of Partial Admission on Performance of 3.75-Inch Mean-Diameter Single-Stage Axial-Flow Turbine, NASA TN D-4700, August 1968.

4. NASA SP-110, Liquid Rocket Engine Turbines, S. B. Macaluso of Rocketdyne, January 1974.

5. Cordes, G.: Fluid Mechanics of the Axial Flow Gas Turbine, With Special Consideration of the Jet Engine Turbine, Springer-Veriag, Berlin, 1963.

6. Horlock, J. H.: Axial Flow Turbines, Butterworth & Co., Ltd. (London), 1966.

7. Geising, J.: Extension of Douglas-Newmann Program to Problems of Lifting Infinite Cascades, Contract NONR 4308(00), 2 July 1964.

APPENDIX E

DISTRIBUTION LIST